AD Number	Date 4/25/2007	DTIC ACCESSION NOTICE
1. Report Identifying Information		
A. Originating Agency USAMRMC		
B. Report Title and/or Number MOHAN		
C. Monitor Report Number ANNUAL (OCT 2005)		
D. Prepared Under Contract Number DAMD17-03-2-0021		
2. Distribution Statement DISTRIBUTION STATEMENT A Approved for public release; distribution unlimited		

SEND REPORT AS ATTACHMENT

AD_____

Award Number: DAMD17-03-2-0021

TITLE: Molecular Genetic and Gene Therapy Studies of the Musculoskeletal System

PRINCIPAL INVESTIGATOR: Subburaman Mohan, Ph.D.

CONTRACTING ORGANIZATION: Loma Linda Veterans Association
for Research and Education
Loma Linda, CA 92357-1000

REPORT DATE: October 2005

TYPE OF REPORT: Annual

PREPARED FOR: U.S. Army Medical Research and Materiel Command
Fort Detrick, Maryland 21702-5012

REPORT DOCUMENTATION PAGE

Form Approved
OMB No. 0704-0188

1. REPORT DATE *(DD-MM-YYYY)*	2. REPORT TYPE	3. DATES COVERED *(From - To)*
01-10-2005	Annual	9 Sep 04 – 8 Sep 05

4. TITLE AND SUBTITLE
Molecular Genetic and Gene Therapy Studies of the Musculoskeletal System

5a. CONTRACT NUMBER

5b. GRANT NUMBER
DAMD17-03-2-0021

5c. PROGRAM ELEMENT NUMBER

6. AUTHOR(S)
Subburaman Mohan, Ph.D.

E-Mail: subburaman.mohan@med.va.gov

5d. PROJECT NUMBER

5e. TASK NUMBER

5f. WORK UNIT NUMBER

7. PERFORMING ORGANIZATION NAME(S) AND ADDRESS(ES)

Loma Linda Veterans Association for Research and Education
Loma Linda, CA 92357-1000

8. PERFORMING ORGANIZATION REPORT NUMBER

9. SPONSORING / MONITORING AGENCY NAME(S) AND ADDRESS(ES)
U.S. Army Medical Research and Materiel Command
Fort Detrick, Maryland 21702-5012

10. SPONSOR/MONITOR'S ACRONYM(S)

11. SPONSOR/MONITOR'S REPORT NUMBER(S)

12. DISTRIBUTION / AVAILABILITY STATEMENT
Approved for Public Release; Distribution Unlimited

13. SUPPLEMENTARY NOTES
Original contains color plates: All DTIC reproductions will be in black and white.

14. ABSTRACT

No abstract provided.

15. SUBJECT TERMS
No subject terms provided.

16. SECURITY CLASSIFICATION OF:			17. LIMITATION OF ABSTRACT	18. NUMBER OF PAGES	19a. NAME OF RESPONSIBLE PERSON
a. REPORT	b. ABSTRACT	c. THIS PAGE			USAMRMC
U	U	U	UU	264	19b. TELEPHONE NUMBER *(include area code)*

Table of Contents

	Page
SF 298	
Table of Contents	
General Introduction	4
A. Molecular Genetics Projects	
Project 1	
Introduction	4
Body	4
Key Research Accomplishments	12
Reportable Outcomes	13
Conclusions	13
References	14
Project 2	
Introduction	16
Body	16
Key Research Accomplishments	32
Reportable Outcomes	32
Conclusions	32
References	33
Project 3	
Introduction	34
Body	34
Key Research Accomplishments	40
Reportable Outcomes	40
Conclusions	40
References	41
Project 4	
Introduction	43
Body	43
Key Research Accomplishments	73
Reportable Outcomes	74
Conclusions	74
References	75
B. Gene Therapy Projects	
Project 6	
Introduction	77
Body	77
Key Research Accomplishments	86
Reportable Outcomes	86
Conclusions	86
Project 7	

Introduction 87
Body 87
Key Research Accomplishments 100
Reportable Outcomes 101
Conclusions 101
References 101
Project 8
Introduction 103
Body 103
Key Research Accomplishments 119
Reportable Outcomes 119
Conclusions 119
References 120
Appendix – Proj 8 121
C. Support Services Projects
Project 9
Introduction 127
Body 127
Project 10
Introduction 133
Body 133
Development of New technologies 136
Project 11
Introduction 138
Body 138
Additional Progress 141
Key Research Accomplishments 143
Reportable Outcomes 143
Conclusions 143
References 143
Project 12
Introduction 151
Body 151
Key Research Accomplishments 159
Reportable Outcomes 159
Conclusions 159
Appendices 160

I. GENERAL INTRODUCTION

This proposal is divided into three sections: A) Molecular Genetic Projects, of which there are four projects. In our initial proposal, our final Molecular Genetic project was a fifth project involving a large human clinical trial, but work on this project has not been initiated at this time due to the Army suspension of human related activities and thus there is no progress to report; B) Gene Therapy Projects, of which there are three projects; and C) Support Service Facilities, of which there are four projects. Each of the above projects has an introduction.

Our goals for the second 12-months of this funding period for each of the technical objectives, as well as our progress for each of the technical objectives, are described below. The progress report for each project is organized according to the outline provided by the office of the U.S. Army Medical Research and Material Command.

A. MOLECULAR GENETICS PROJECTS

Project 1: Studies on Genetic Regulation of Digit Tip Regeneration

Introduction

Experiments with amphibian limbs, first undertaken in the 18th century, demonstrate that limb regeneration in vertebrates is possible (1, 2). In amphibians, the first stages of regeneration are initial wound healing by formation of an epidermal layer over the wound, followed by dedifferentiation of cells that cluster under this epidermal layer (3). These dedifferentiated cells (blastema cells), similar to stem cells, redifferentiate into other cell types including bone, cartilage and epithelial cells. The genes and genetic pathways that determine how the cells dedifferentiate and redifferentiate into other cell types are not completely understood.

Higher mammals also have marginal abilities to regenerate. One example of regeneration in mammals is the healing of ear holes in rabbits without scarring (4, 5). Recently, we and others have demonstrated that the MRL inbred strain of mouse shows greater regeneration and healing of earhole punches as opposed to several other inbred strains of mice (6, 7). Among inbred mouse strains, the MRL mouse was found to completely heal earhole punches, the DBA strain was found to be an intermediate regenerator, and the B6 strain found to be a poor regenerator of earhole punches (6). Other studies have found that the MRL mouse is also capable of cardiac muscle regeneration (8). Thus, the MRL mouse is a unique model to study the genetic mechanisms that regulate wound healing and tissue regeneration. However, to date, the MRL mouse has not been investigated extensively for its abilities to regenerate more complex biological structures, such as digit tips. This project examined digit tip regeneration in the MRL inbred strain of mice in order to determine if MRL mouse strains have similar regeneration capabilities of digit tips as in earhole punches. We also undertook global RNA expression profiling in those strains to identify the genes and genetic mechanisms responsible for wound healing and digit tip regeneration. Candidate genes that were found to be differentially expressed in MRL mice were further investigated by in vivo studies of knockout mice.

Body

1. Technical Objectives

The following are our Specific Objectives for the second 12 months of this project.

1) Extend the histological studies to additional time points (days 4, 7, 14, 21) to further characterize cells involved in blastema formation and digit regeneration.

2) Do additional microarray and real-time PCR expression studies at these times points to determine the genes and genetic pathways involved in the digit tip regeneration at each time point.
3) Use immunohistochemistry of a selected subset of differentially expressed genes to determine what cellular types express those genes involved in digit tip regeneration.
4) Examine knockout mice of differentially expressed genes (if they are available from Jackson Laboratories) to further characterize the function of genes involved in digit tip regeneration.

2. Progress on Technical Objectives

Specific Objective 1: Extend the histological studies to additional time points (days 4, 7, 14, 21) to further characterize cells involved in blastema formation and digit regeneration.

Studies undertaken in axolotls have documented the stages in amphibian limb regeneration. In axolotls, the first stage after amputation involves the formation of wound epithelial cells to cover the wound (http://www.uoguelph.ca/zoology/devobio/210labs/regen1.html). After two days, beneath this epithelial layer, cells begin to dedifferentiate and form a blastema. These blastema cells redifferentiate and completely regenerate the amphibian limb within six weeks post amputation.

Studies undertaken in the first year of subproject 1 only examined a single time point, namely at day 1 post dissection, for determination of blastema formation in MRL, DBA, B6, C3H and 129Sv inbred mice. These studies found that day 1 was too early for a blastema to form. In the last year, we examined mice for blastema formation at additional time points by sacrificing mice at 1, 4, 14 and 21 and 28 days post digit tip dissection. Dissected paw tissues were stored in 10% formalin until processing. The tissues were fixed in paraffin and five micron tissue sections were mounted on to microscope slides. Following hematoxylin and eosin (H&E) staining, the tissues were examined under a microscope. In these studies, our histology studies find that the early stages of digit tip regeneration are partially similar to that of axolotls (Figure 1). Within one day of digit tip amputation epithelial cells have formed over the wound in MRL mice. At four days, epithelial cells have completely covered the wound and undifferentiated cells beneath the wound epithelium begin to proliferate. At 7-days osteoblasts are present and have begun to form bone. At 14-days post dissection the cells beneath the wound epithelium are not as de-differentiated and the bone marrow cavity has begun forming above the third phalange's joint. By 21-days post dissection, the cells have redifferentiated, the nail has begun reforming and the digit tip has almost completely regenerated. It is interesting that when de- and re- differentiation of cells beneath the wound epithelium is occurring is also when the MRL mouse shows the greatest regenerative capacity. This suggests possible links between the enhanced healing and regeneration capabilities of MRL mice and the molecular causes of de- and re-differentiation of cells.

Figure 1. Regeneration Histology. At 1-day post dissection a wound epithelial layer has begun to form. By 4-days post dissection the wound epithelial layer has completely covered the tip and beneath this dedifferentiated and proliferating cells are present. At 7-days post dissection, bone has begun to form and by day 14 the marrow cavity is forming above the 3rd phalange's joint. By 21 days, the digit has nearly completed regenerated and the nail has begun reforming. In Figure 31A all images are at 4X, in Figure 1B images are 10X or 20X.

Figure 1A.

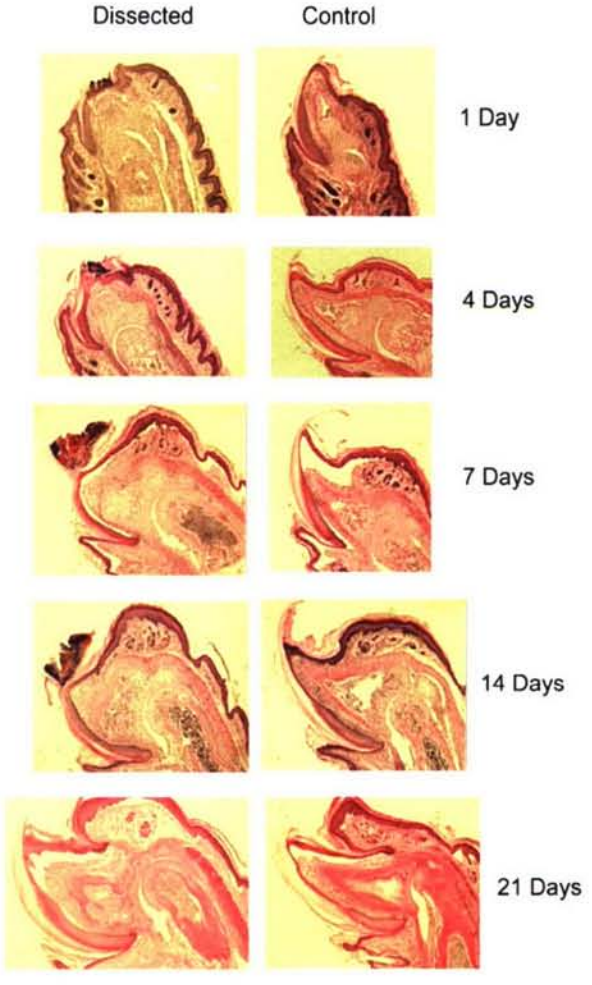

Figure 1B.

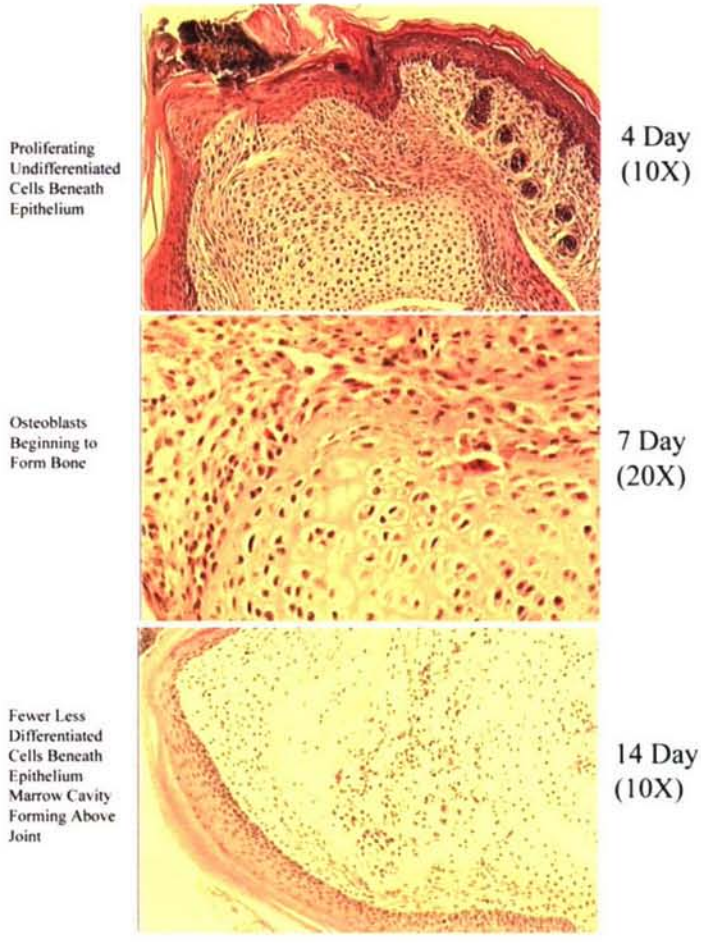

Specific Objective 2: Do additional microarray and real-time PCR expression studies at these times points to determine the genes and genetic pathways involved in the digit tip regeneration at each time point.

Microarray Expression Analysis. Total RNA was isolated from dissected tissues at days 4, 7, 14, 21 and 28 days post surgery using the Agilent Total RNA Isolation Kit (Agilent Technologies). For control RNA samples, tissue was collected from uncut paw tissue at these same time points. Tissues were lysed using a Polytron Generator (Kinemalica AG), and then processed following the manufacturer's protocol (Agilent). The total RNA concentration was determined by NanoDrop spectrophotometer and RNA quality was determined by 18S/28S ribosomal peak intensity on an Agilent Bioanalyzer. For microarray expression profiling and real-time PCR, RNA samples were used only if they showed little to no degradation. Oligonucleotides were spotted on to slides using a Q-Array2 robot (Genetix). A total of 250 ng RNA was used to synthesize double stranded cDNA using the Low RNA Input Fluorescent Linear Application Kit

(Agilent). First strand cDNA synthesis was primed with T7-(dT24) promoter primer. From the purified cDNA, cRNA was synthesized using transcription master mix and purified. 250 ng of purified cRNA was used to reverse transcribe to fluorescent cDNA. Cyanine-3-dCTP and cyanine-5-dCTP were used to label experimental samples and control samples. Samples were hybridized at 60°C for 17 hours. The slides were then washed with Solution I (6X SSC, 0.005% Triton X-102) for 10 min. in the dark and then with Solution II (0.1X SSC, 0.005% Triton X-102) for 5 min. in the dark. The slides were dried with pressurized nitrogen and immediately scanned using a Axon Genepix 4200 scanner. The signal intensity of all microarray images was determined using Imagene 6.0 software. Expression analysis of microarray experiments was performed with GeneSpring 7.2 (Silicon Genetics) using the raw intensity data generated by the ImaGene software. Local background-subtracted median signal intensities were used as intensity measures, and the data was normalized using per spot and per chip LOWESS normalization. The transcripts were then further analyzed by utilizing a one-sample Student's t-test to test whether the mean normalized expression level for the gene is statistically different from 1.0.

Microarray Expression Results. A particularly interesting gene was found to be differentially expressed in MRL mice in comparison to DBA and B6 mice at 4 days post dissection (Figure 2). Formin 2 (FMN 2) is related to Formin 1 which is differentially expressed in the mouse embryo and is required for normal expression of fibroblast growth factor 4 (FGF-4) and sonic hedgehog (SHH) in the limb bud (12, 13). Thus, we focused on the FMN2 gene for further investigations. Confirmation of microarray results was done by real-time PCR of 20 genes. RT-PCR results for these genes were consistent with the microarray results and gave correlation coefficients of 0.62, 0.91 and 0.40 for MRL, DBA and B6 expression results. Additionally, FMN2 was found to be expressed in osteoblast cell line MC3T3 by RT-PCR. FMN2 was also found to be increased 2 fold in expression in WNT3A treated MC3T3 cell lines in comparison to control MC3T3 cell lines by realtime PCR ($p = 0.01$).

Time points at 7, 14, 21 and 28 days were also examined by microarray expression analysis. This data is currently in the process of being analyzed. However, preliminary analysis finds that at the 7 day time point, FMN2 is also differentially expressed in only MRL digit tips. Later time points do not show differential expression of FMN2, suggesting that it is important in the initial regenerative response. At 4 days post surgery, Table 1 shows a list of genes differentially expressed only in MRL mice.

Table 1. Genes significantly differentially expressed in MRL mouse regenerating digit tips but not DBA and B6 mice. Many of these genes are ESTs of unknown function.

Name	Ratio	p-value	Ratio	Ratio	Name	Description	Biological Process
H3001C06	0.40	0.04	0.74 *	0.87	5730436H21Rik	UNKNOWN: Similar to clone MGC:37386 IMAGE:4977054	
H3002E06	1.91	0.01	0.95	absent	Dbt	Dihydrolipoamide branched chain transacylase (Dbt)	metabolism(GO:0008152)
H3002G06	1.80	0.04	0.91	1.22	AA410130	UNKNOWN	
H3002H12	1.96	0.01	0.90	absent			
H3003A01	2.23	0.04	0.83	absent		Mus musculus similar to LOC264166 mRNA	
H3004G07	1.71	0.04	0.77	0.91	Tmod3	Tropomodulin 3 (Tmod3), mRNA	actin filament organization(GO:0007015)
H3005D06	1.65	0.04	1.24	0.96			
H3008E02	0.63	0.03	0.90	1.21		UNKNOWN	
H3010G07	3.77	0.01	2.81	1.29	Ak4	Adenylate kinase 4 (Ak4), mRNA	
H3011G06	1.88	0.02	1.23	0.59		Ferritin light chain 1 (Ftl1), mRNA	
H3017B10	0.68	0.04	1.01	1.01			
H3019B02	1.70	0.05	1.01	1.06	Nfat5	UNKNOWN	transcription, DNA-dependent(GO:0006351);regulation of transcription
H3024A05	1.73	0.01	0.87	1.09	Sparc	Secreted acidic cysteine rich glycoprotein (Sparc), mRNA	
H3028F03	1.96	0.00	0.96	1.12	Ctsl	Cathepsin L (Ctsl), mRNA	proteolysis and peptidolysis(GO:0006508)
H3028F04	1.98	0.00	1.34	1.01	Ctsl	Cathepsin L (Ctsl), mRNA	proteolysis and peptidolysis(GO:0006508)
H3029B01	1.69	0.02	1.04	absent	Slc11a2	Natural resistance macrophage protein-2 (Nramp2) mRNA	transport(GO:0006810);iron ion transport(GO:0006826)
H3031D07	1.59	0.04	0.68	absent	Psmd1	Proteasome, non-ATPase, 1 (Psmd1), mRNA	
H3034F02	1.63	0.01	1.04	0.97	Hel308-pending	UNKNOWN	DNA metabolism(GO:0006259)
H3037C05	1.52	0.02	0.80	0.89		UNKNOWN	
H3037D01	0.64	0.04	0.99	0.90		UNKNOWN	
H3037D07	1.99	0.04	1.05	1.12		UNKNOWN	
H3038C05	1.52	0.04	0.62	0.39 *		UNKNOWN	
H3039A12	1.53	0.02	1.08	absent		UNKNOWN	
H3041F03	1.53	0.05	0.86 *	1.01		UNKNOWN	
H3042B01	1.57	0.01	1.15	0.95		UNKNOWN	
H3042F06	1.53	0.02	1.38	absent		UNKNOWN	
H3050A02	2.25	0.04	1.08	absent		UNKNOWN	
H3051D04	1.54	0.03	0.81	1.07	Mdm2	Double minute 2 (Mdm2) gene, 3' untranslated region	cell growth and/or maintenance(GO:0008151)
H3053D05	1.54	0.01	0.89	0.91		UNKNOWN	
H3054F02	1.81	0.04	0.93	1.09		UNKNOWN	
H3054G08	1.71	0.04	0.94	absent		UNKNOWN	
H3056C01	1.53	0.01	1.42 *	0.94	Fmn2	Formin 2 (Fmn2)	development(GO:0007275)
H3060H01	1.59	0.04	0.98	0.98		UNKNOWN	
H3061D03	1.68	0.00	1.02	absent	Pcsk5	Clone MGC:18501 IMAGE:4036159, mRNA	electron transport(GO:0006118);proteolysis and peptidolysis(GO:0006508)
H3062G12	1.68	0.03	1.03	0.95		UNKNOWN	
H3065B10	1.63	0.02	1.07	0.78		UNKNOWN	
H3065D02	1.58	0.04	1.10	0.96		UNKNOWN	
H3065F05	0.65	0.02	0.97	1.04		UNKNOWN	
H3067C07	1.55	0.05	0.88	absent		UNKNOWN	
H3067E04	0.70	0.03	1.00	1.14		UNKNOWN	
H3069H05	0.69	0.04	1.02	0.95	2310015A05Rik	RIKEN cDNA 2310015A05 gene (2310015A05Rik), mRNA	
H3070E09	1.77	0.00	1.06	1.00		UNKNOWN	
H3071H07	1.85	0.04	0.96	absent		UNKNOWN	
H3072D01	1.50	0.03	0.92	1.29		UNKNOWN	
H3075D02	1.51	0.01	0.98	absent		UNKNOWN	
H3079B08	1.80	0.02	1.08	1.33	6030466N05Rik	dCMP deaminase, IMAGE:3672932, mRNA	pyrimidine nucleotide metabolism(GO:0006220);nucleotide biosynthesis(GO:0009165)
H3081F06	1.51	0.01	0.76	0.82		UNKNOWN	
H3083B04	1.66	0.04	0.85	1.03		UNKNOWN	
H3084F04	1.55	0.02	0.87	1.26		UNKNOWN	
H3087A08	1.59	0.03	0.94	0.98		UNKNOWN	
H3097G06	1.54	0.04	0.96	1.03	5730530J16Rik	UNKNOWN	
H3097H10	0.70	0.05	1.03	1.00		UNKNOWN	
H3098G02	1.82	0.04	0.73	absent		UNKNOWN	
H3104G06	1.57	0.05	0.71 *	0.53 *		UNKNOWN	
H3106A02	1.71	0.02	1.29	absent	2210409E12Rik	RIKEN cDNA 2210409E12 gene (2210409E12Rik), mRNA	
H3114A12	1.58	0.04	0.87	absent	3010021M21Rik	UNKNOWN	ubiquitin cycle(GO:0006512);protein modification(GO:0006464)
H3119H03	1.94	0.03	1.10	1.12	Col1a1	Collagen alpha 1(I) chain precursor (LOC217123), mRNA	cell adhesion(GO:0007155)
H3121E06	2.29	0.04	0.96	0.99	2900057D21Rik	RIKEN cDNA 2900057D21 gene (2900057D21Rik), mRNA	intracellular signaling cascade(GO:0007242)
H3123G08	0.64	0.04	1.07	0.99		UNKNOWN	
H3124H10	2.42	0.00	1.48	1.44	Col3a1	Procollagen, type III, alpha 1 (Col3a1), mRNA	cell adhesion(GO:0007155)
H3128B02	0.69	0.01	0.94	0.80		UNKNOWN	
H3134H07	1.55	0.00	0.96	1.49	Birc6	Inhibitor of apoptosis mRNA (LOC210168)	apoptosis(GO:0006915)
H3143F07	1.55	0.03	0.95	0.92		UNKNOWN	
H3144F02	2.00	0.05	1.27	0.88	A230053O16Rik	Similar to hypothetical protein FLJ12547	
H3146G03	1.92	0.04	0.91	2.05		UNKNOWN	
H3146H05	0.69	0.01	1.08	0.92		UNKNOWN	
H3150H02	1.53	0.00	0.17	absent		UNKNOWN	
H3152F07	1.54	0.03	0.47	1.10		UNKNOWN	
H3156C06	1.61	0.02	1.17	absent		UNKNOWN	
H3159A06	0.70	0.02	1.00	0.97		UNKNOWN	
H3159B04	0.49	0.05	0.80	1.00		UNKNOWN	

Specific Objective 3: Use immunohistochemistry of a selected subset of differentially expressed genes to determine what cellular types express those genes involved in digit tip regeneration.

Immunohistochemistry of FMN2 was done using antibodies obtained from Santa Cruz Biotechnology. Five micron paraffin sections were mounted on poly-L-lysine coated slides. Antigen retrieval was done using pH 6.0 Citrate buffer followed by incubation at 80°C and 70°C for ten minutes each. The sections were blocked in 20% Horse serum at 37°C for 1 hour. Primary antibodies were diluted at both 1:50 and 1:200 and incubated for 60' at 37°C. The sections were rinsed extensively and incubated with the secondary anti-goat antibody for 12 minutes at 37°C. The sections were reacted with diaminobenzidine and hydrogen peroxide, counter-stained with Methyl Green and cover-slipped.

Immunohistochemistry of FMN2 with MRL digit tip tissue shows that FMN2 is highly expressed in the nuclei of these regenerating dedifferentiated cells and chondrocytes at day 4 (Figure 2). Specificity of the primary FMN2 antibody is demonstrated by co-hybridization of FMN2 antibodies and FMN2 blocking peptide.

Figure 2. Immunohistochemistry of Formin-2 expression in MRL mice 4-days post digit tip dissection. Note that that formin-2 is primarily expressed in the nuclei of regenerating dedifferentiated cells beneath the wound epithelial layer and in the nuclei of chondrocytes. Specificity of the anti-Formin-2 IgG is demonstrated by repeating the hybridizations with the addition of formin-2 blocking peptide (right panel).

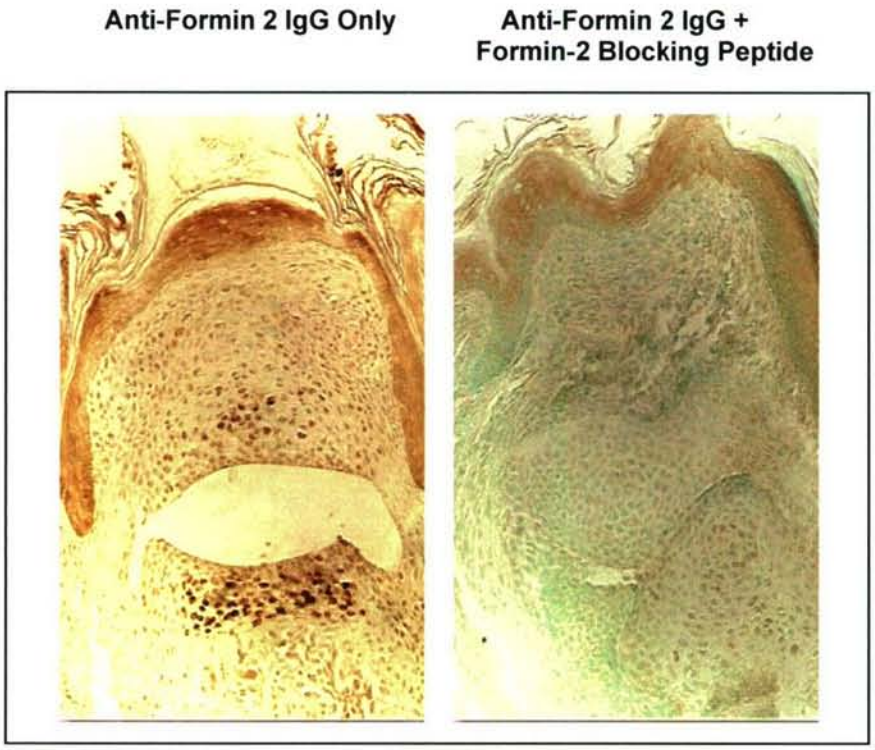

Specific Objective 4: Examine knockout mice of differentially expressed genes (if they are available from Jackson Laboratories) to further characterize the function of genes involved in digit tip regeneration.

FMN2 Knockout Mice. FMN2 knockout mice were obtained from Dr. Philip Leder (Department of Human Genetics, Harvard Medical School, Howard Hughes Medical Institute, Boston, MA). The mice were originally generated in inbred 129Sv mice by homologous recombination of a targeting vector with 1300 bp of the FH1 domain of FMN2 deleted and replaced by 1257 bp containing the PGK-Neo gene followed by stop codons in all three reading frames (10). Two heterozygote FMN2 (+/-) male/female pairs were bred to generate wildtype (+/+), and knockout (-/-) pups for subsequent bone density, bone size and bone volume studies.

Bone Measurements. Volumetric bone mineral density (vBMD) and geometric parameters of femurs were determined by peripheral quantitative computed tomography (pQCT) (Norland Medical Sytems). The resolution limit of this instrument is approximately 70 microns. Calibration of pQCT was performed daily with a defined cone phantom standard. Analysis of the pQCT scans was performed using Bone Density Software version 5.40 (Norland Medical Systems). Total bone mineral density (total BMD) and geometric parameters were estimated with Loop analysis. The threshold was set at 230-630 mg/cm^3. Femur bone parameters were measured and averaged for three scans at mid-diaphysis. The longitudinal lengths of femurs were measured with a caliper. Statistical analyses of bone parameters were done using Statistica software (Statsoft Inc). Since total and cortical bone mineral content (BMC), total bone area, endosteal and periosteal circumference and cortical thickness are size dependent, these bone parameters were normalized with body weight (11).

FMN2 Knockout Mouse Phenotypes. Knockout (-/-) and wildtype (+/+) FMN2 mice were measured for bone size and volumetric BMD at 12 weeks by peripheral quantitative computed tomography (pQCT) (Table 4). FMN2 (-/-) mice were found to have significantly lower femur cortical thickness ($p = 0.0004$) and total bone mineral density ($p = 0.03$) (Figure 3). Also, knockout mice have increased femur endosteal circumference ($p = 0.0002$) (Figure 3). Volumetric BMD was also reduced in FMN2 (-/-) mice, although it did not reach statistical significance ($p = 0.09$).

Table 2. Bone Phenotypes Measured by pQCT. Shown are mean total weight and bone size and density measurements for FMN2 knockout and wildtype mice. Bone periosteal and endosteal circumferences and bone cortical thickness are influenced by animal size. Since FMN2 knockout mice were on average smaller than FMN2 wildtype mice, these bone parameters were adjusted by the method of Srivastava et al (11) (Figure 3).

Unadjusted Phenotypes	**FMN2 (+/+) (n = 9)**	**FMN2 (-/-) (n = 7)**
Body weight (g)	24.1 +/- 1.7	21.1 +/- 1.4
Length (mm)	14.2 +/- 0.93	14.5 +/- 0.90
vBMD (mg/cm3)	884.5 +/- 44.3	850.0 +/- 27.8
Periosteal Circumference (mm)	4.28 +/- 0.23	4.04 +/- 0.29
Endosteal Circumference (mm)	2.29 +/- 0.35	2.44 +/- 0.16
Cortical Thickness (mm)	0.32 +/- 0.06	0.25 +/- 0.02

The studies of knockout FMN2 mice find that they have decreased femur cortical thickness and total bone density and increased endosteal circumference of femurs in comparison to wildtype FMN2 mice (Figure 3). The mechanisms that cause these phenotypes could be

either increased bone resorption and/or decreased bone formation. However, histology studies show that FMN2 is expressed in the nuclei of chondrocytes and expression studies find that FMN2 is highly expressed in osteoblast cell line MC3T3. This indicates that FMN2 likely acts by inducing bone formation. Since both bone formation and resorption are due to multiple genes and genetic pathways, it is striking that the deletion of a single gene in an inbred mouse strain reduces bone cortical thickness by over 20%.

Mutations in a related formin gene, formin-1, lead to developmental defects in limb formation due to a reduction in the number of bony elements in the fore and hind limbs (12). Formin-1 is thought to act in limb bud polarization through establishment of a SHH/FGF-4 feedback loop (13). Also, studies in a yeast homologue of formin, forp1, have found that its mutation leads to asymmetric patterns of cell growth (16). This suggests that formins are critical signaling components of pattern formation and directing cellular fate. Our previous microarray studies of mouse ear punch wound healing found that formin-binding protein 21 is differentially expressed in healing ear tissue (17). Thus, the formin family of genes is involved in both soft tissue wound healing and digit tip regeneration. This indicates that there are common genetic mechanisms influencing soft tissue wound healing and digit tip regeneration in the MRL super-healer mouse. Members of the formin gene family have been implicated in the WNT signaling pathway (18, 19). The WNT signaling pathway initiates outgrowth, controls patterning, and regulates cell differentiation in a number of tissues (19). During vertebrate embryogenesis, secreted WNT molecules regulate cell differentiation by signal transduction that is mediated by disheveled (DSH) (18) DSH is a WNT signal transducer that functions in all known WNT signaling pathways (19). Also, bone formation has been shown to be activated by WNT signaling in osteoblast stem cells by promoting osteoblastic differentiation (20, 21). Recently, a member of the formin family, Daam (Dishevelled-associated activator of morphogenesis), has been shown to regulate gastrulation in a WNT-dependent manner through interactions with DSH (22). FMN2 has been reported to be highly expressed in both developing and adult central nervous systems (23). This is intriguing since denervation of has been shown to eliminate regeneration capabilities in amphibians (24). We have demonstrated that FMN2 is highly expressed in both MRL regenerating digit tip cells and in osteoblast cell line MC3T3. This suggests roles of FMN2 and the WNT signaling pathway in both regeneration and bone formation.

Figure 3. Periosteal and endosteal circumference and cortical thickness measurements are dependent on mouse size so these measurements were weight normalized. Calculations of normalizations as a ratio of observed to body weight-normalized wildtype value were done for female and male mice separately before combining the data (11). Mean femur adjusted cortical thickness was reduced by 27% in FMN2 knockout mice ($p = 0.0004$). Mean femur normalized endosteal circumferences was increased by 24% ($p = 0.0002$). Also, mean femur total bone density was decreased by 5% in FMN2 knockout mice ($p = 0.03$).

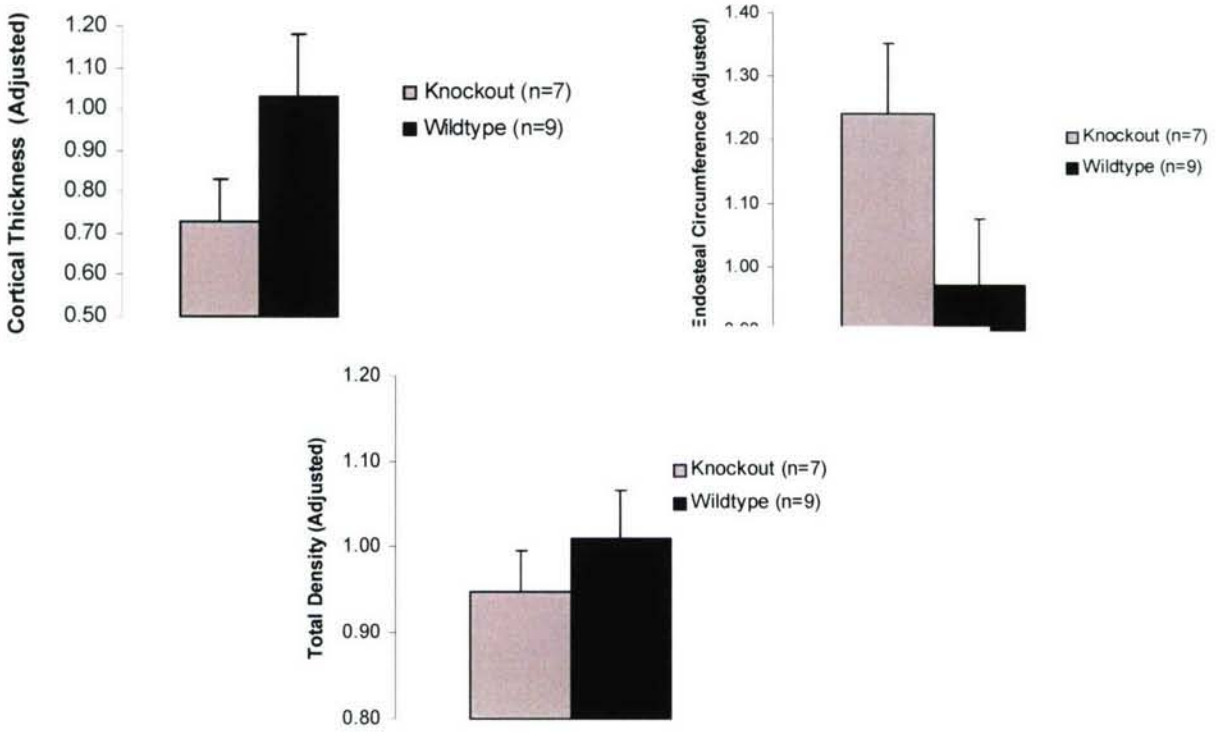

Key Research Accomplishments

1) Histology studies were undertaken at time points of 1, 4, 7, 14, and 21 days post dissection. These studies find that by 4-days post dissection wound epithelium has completely covered the tip and beneath this dedifferentiated and proliferating cells are present. At 7-days post dissection, bone has begun to form and by 21 days the digit tip has nearly completely regenerated.

2) Additional microarray expression experiments were undertaken at days 7, 14, 21 and 28 post dissection. These experiments (and previous 4 day experiments) find that the FMN2 gene is differentially expressed in MRL digit tips at days 4 and 7 post dissection.

3) FMN2 was found to be highly expressed in the nuclei of chondrocytes in regenerating digit tips by immunohistochemistry.

4) FMN2 was found to be increased in expression in Wnt3A treated MCT3T osteoblast cell line, suggesting that FMN2 is in the Wnt signaling pathway.

5) Formin-2 (FMN2) knockout mice have significantly reduced femur cortical thickness and total bone mineral density and significantly increased femur endosteal circumference.

6) These studies suggest that there are common genetic mechanisms influencing soft tissue wound healing, digit tip regeneration and bone formation.

Reportable Outcomes

Chadwick R.B., Bu L.M., Yu H., Hu Y., Sachdev R., Tan Q.W., Wergedal J.E., Mohan S., and Baylink D.J. Digit Tip Regeneration and Differential Expression Profiling in the MRL Super-Healer Mouse. Wound Healing and Regeneration, Chicago, Illinois, May 2005.

Chadwick R.B., Bu L.M., Yu H., Sachdev R., Tan Q.W., Wergedal J.E., Mohan S., and Baylink D.J. Digit Tip Regeneration and Global Gene Expression Profiling in the MRL Super-Healer Mouse. 26th Annual Meeting American Society of Bone and Mineral Research, Seattle, Washington, October 1-5, 2004

Conclusions

In conclusion, our histology studies find that the early stages of digit tip regeneration parallel that of amphibians. In axolotls (salamanders), the first stage after amputation involves the formation of wound epithelial cells to cover the wound. After two days, beneath this epithelial layer, cells begin to dedifferentiate and form a blastema. These blastema cells redifferentiate and completely regenerate the amphibian limb within six weeks post amputation. In our MRL mouse histology studies, within one day of digit tip amputation epithelial cells have formed over the wound. At four days, epithelial cells have completely covered the wound and undifferentiated cells beneath the wound epithelium begin to proliferate. At 7-days osteoblasts are present and have begun to form bone. At 14-days post dissection the cells beneath the wound epithelium are not as de-differentiated and the bone marrow cavity has begun forming above the third phalange's joint. By 21-days post dissection, the cells have redifferentiated, the nail has begun reforming and the digit tip has almost completely regenerated.

Our microarray expression experiments find that the FMN2 gene is differentially expressed in MRL digit tips at days 4 and 7 post dissection. Mutations in a related formin gene, formin-1, have been reported to lead to developmental defects in limb formation. The immunohistochemistry studies of FMN2 that we undertook find that FMN2 is highly expressed in the nuclei of chondrocytes in regenerating digit tips. Also, FMN2 was found to be increased in expression in Wnt3A treated MCT3T osteoblast cell line, suggesting that FMN2 is in the Wnt signaling pathway. Formin-2 (FMN2) knockout mice have been found to have significantly reduced femur cortical thickness and total bone mineral density and significantly increased femur endosteal circumference. Members of the formin gene family have been implicated in the WNT signaling pathway which is known to initiate outgrowth, control patterning, and regulate cell differentiation in a number of tissues (18, 19). Also, bone formation has been shown to be activated by WNT signaling in osteoblast stem cells by promoting osteoblastic differentiation (20, 21). This suggests that formins are critical signaling components of digit tip regeneration and bone formation or resorption.

Our previous microarray studies of mouse ear punch wound healing found that formin-binding protein 21 is differentially expressed in healing ear tissue. Thus, the formin family of genes is involved in both soft tissue wound healing, digit tip regeneration and bone formation/resorption. Future studies will further clarify the functions and molecular pathways of

FMN2 as well as discover additional genes and genetic pathways that contribute to soft tissue wound healing, digit tip regeneration and bone formation.

References

1. Muller TL, Ngo-Muller V, Reginelli A, Taylor G, Anderson R, Muneoka K. Regeneration in higher vertebrates: limb buds and digit tips. Semin Cell Dev Biol 1999; 10(4):405-413.
2. Brockes JP. Amphibian limb regeneration: rebuilding a complex structure. Science, 1997; 276(5309): 81-87.
3. Endo T, Bryant SV, Gardiner DM. A stepwise model system for limb regeneration. Developmental Biology 2004; 270(1): 135-45.
4. Goss RJ, Grimes LN. Epidermal downgrowths in regenerating rabbit ear holes. J Morphol, 1975; 146(4):533-542.
5. Joseph J, Dyson M. Effect of anabolic androgens on tissue replacement in the ear of the rabbit. Nature 1966; 211(45): 193-194.
6. Li X, Gu W, Masinde G, Hamilton-Ulland M, Xu S, Mohan S, Baylink DJ. Genetic control of the rate of wound healing in mice. Heredity 2001; 86(Pt 6): 668-674.
7. Clark LD, Clark RK, Heber-Katz E. A new murine model for mammalian wound repair and regeneration. Clin Immunol Immunopathol, 1998; 88(1):35-45.
8. Leferovich JM, Bedelbaeva K, Samulewicz S, Zhang XM, Zwas D, Lankford EB, Heber-Katz E. Heart regeneration in adult MRL mice. Proc Natl Acad Sci U S A, 2001; 98(17):9830-9835.
9. Tanaka TS, Jaradat SA, Lim MK, Kargul GJ, Wang X, Grahovac MJ, Pantano S, Sano Y, Piao Y, Nagaraja R, Doi H, Wood WH 3rd, Becker KG, Ko MS. Genome-wide expression profiling of mid-gestation placenta and embryo using a 15,000 mouse developmental cDNA microarray. Proc Natl Acad Sci U S A, 2000; 97(16): 9127-9132.
10. Leader B, Lim H, Carabatsos MJ, Harrington A, Ecsedy J, Pellman D, Maas R, Leder P. Formin-2, polyploidy, hypofertility and positioning of the meiotic spindle in mouse oocytes. Nat Cell Biol. 2002;4(12):921-8.
11. Srivastava AK, Mohan S, Wergedal JE, Baylink DJ. A genomewide screening of N-ethyl-N-nitrosourea-mutagenized mice for musculoskeletal phenotypes. Bone. 2003; 33(2):179-91.
12. Zeller R, Haramis AG, Zuniga A, McGuigan C, Dono R, Davidson G, Chabanis S, Gibson T. Formin defines a large family of morphoregulatory genes and functions in establishment of the polarising region. Cell Tissue Res. 1999 Apr;296(1):85-93.
13. Zuniga A, Haramis AP, McMahon AP, Zeller R. Signal relay by BMP antagonism controls the SHH/FGF4 feedback loop in vertebrate limb buds. Nature. 1999 Oct 7;401(6753):598-602.
14. Cho TJ, Gerstenfeld LC, Einhorn TA. Differential temporal expression of members of the transforming growth factor beta superfamily during murine fracture healing. J Bone Miner Res. 2002 Mar;17(3):513-20.
15. Dickinson ME, Kobrin MS, Silan CM, Kingsley DM, Justice MJ, Miller DA, Ceci JD, Lock LF, Lee A, Buchberg AM, Siracusa, LD, Lyons KM, Derync R, Hogan BLM, Copeland NG, Jenkins NA. Chromosomal localization of seven members of the murine TGF-beta

superfamily suggests close linkage to several morphogenetic mutant loci. Genomics. 1990 6(3):505-20.
16. Sawin KE. Cell polarity: following formin function. Curr Biol. 2002; 12(1):6-8.
17. Li X, Mohan S, Gu W, Baylink DJ. Analysis of gene expression in the wound repair/regeneration process. Mamm Genome. 2001; 12(1):52-9.
18. Habas R, Kato Y, He X. WNT/Frizzled activation of Rho regulates vertebrate gastrulation and requires a novel Formin homology protein Daam1. Cell. 2000; 107(7):843-54.
19. Church VL, Francis-West P. WNT signalling during limb development. Int. J. Dev. Biol. 2002; 46: 927-936.
20. Gong Y, Slee RB, Fukai N, Rawadi G, Roman-Roman S, Reginato AM, Wang H, Cundy T, Glorieux FH, Lev D, Zacharin M, Oexle K, Marcelino J, Suwairi W, Heeger S, Sabatakos G, Apte S, Adkins WN, Allgrove J, Arslan-Kirchner M, Batch JA, Beighton P, Black GC, Boles RG, Boon LM, Borrone C, Brunner HG, Carle GF, Dallapiccola B, De Paepe A, Floege B, Halfhide ML, Hall B, Hennekam RC, Hirose T, Jans A, Juppner H, Kim CA, Keppler-Noreuil K, Kohlschuetter A, LaCombe D, Lambert M, Lemyre E, Letteboer T, Peltonen L, Ramesar RS, Romanengo M, Somer H, Steichen-Gersdorf E, Steinmann B, Sullivan B, Superti-Furga A, Swoboda W, van den Boogaard MJ, Van Hul W, Vikkula M, Votruba M, Zabel B, Garcia T, Baron R, Olsen BR, Warman ML; Osteoporosis-Pseudoglioma Syndrome Collaborative Group. LDL receptor-related protein 5 (LRP5) affects bone accrual and eye development. Cell 2001; 107: 513-523.
21. Bain G, Muller T, Wang X, Papkoff, J. Activated beta-catenin induces osteoblast differentiation of C3H10T1/2 cells and participates in BMP2 mediated signal transduction. Biochem. Biophys. Res. Commun. 2003; 301: 84-91.

Project 2: Sensitizer Screening to Enhance Detection of ENU-Induced Mutant Phenotypes

Introduction

In the present study, we propose to employ mouse models in which genes that have been previously implicated to play a critical role in the development and maintenance of musculoskeletal tissues have been knocked out. By using mice with mutation in a gene known to affect musculoskeletal phenotypes, we propose to sensitize a classical ENU mutagenesis screening system (1), and thereby increase the recovery of mutants by discovering genes that have subtle effects on musculoskeletal phenotype. The principle for increased sensitivity of recognition is synergism between the unknown ENU mutation and the known knock out gene (2-4). One of the important requirements for the success of our approach involving a sensitizer screen to identify novel mouse mutants for musculoskeletal phenotypes relates to which knockout mouse models are selected for ENU mutagenesis screens. In this regard, it is now widely accepted that IGF-I (5) and TGF β (6) are two critical regulatory molecules that regulate growth and development of musculoskeletal tissues and that deficiencies in these two growth factors contribute to impaired growth and maintenance. Furthermore, IGF-I and TGF β have been implicated in mediating the effects of many systemic and local factors that regulate musculoskeletal system. Therefore, we employed a *lit/lit* mouse model where the *lit* allele results in a nonfunctional growth hormone related hormone receptor (GHRHR). These mice are IGF-I deficient. The Smad2 is a key molecule for the TGF β signaling pathway in bone cells, the homozygous smad2 knockout mice are lethal but heterozygous smad2 mice survive and appear to have a normal musculoskeletal phenotype. We have used these models to screen for musculoskeletal phenotypes based on the hypothesis that ENU-induced mutation will exhibit greater effect on the musculoskeletal phenotype under reduced dosage of IGF-I and TGF-β.

Body

1. Technical Objectives

To identify the mouse mutants with musculoskeletal phenotypes in the F1 progeny of ENU treated male mice mated with IGF-I deficient *lit/lit* and TGF β deficient Smad2 knockout female mice compared to their respective wild type female mice.

To achieve the above technical objective, we have proposed the following specific objectives during second 12 months of this study.

1) Breed knockout females with wild type ENU treated males to generate approximately 100 F1 progeny for each lit/lit and Smad2 mutant. Breed wild type females with ENU treated males to produce 100 F1 control progeny.

2) Perform musculoskeletal screens at 10 weeks of age in the F1 progeny to measure bone mineral content, bone density, bone size, muscle size and fat content using PIXImus and pQCT instruments. Perform biochemical measurements of bone turnover in the serum samples.

3) Begin to confirm the mutant phenotypes by backcrossing the mutant mice with lit/lit or Smad2 knockout mice, as appropriate.

2. Progress on Technical Objectives

Specific Objective 1: Breed knockout females with wild type ENU treated males to generate approximately 100 F1 progeny for each lit/lit and Smad2 mutant. Breed wild type females with ENU treated males to produce 100 F1 control progeny.

Generation of Knock-out Mice for Breeding with ENU Injected Males. To achieve the objective of generating 200 F1 progeny from breeding ENU injected males with lit/lit or smad2/+ mice, we generated breeding pairs of *lit/lit* mice from our previous studies. We bred heterozygous (*lit*/+) male mice with either homozygous (*lit/lit*) or heterozygous (*lit*/+) females to produce approximately 80 *lit/lit*, *lit*/+, or +/+ male and female progeny. Both *lit*/+ and Smad2/+ progeny were identified by PCR based genotyping assays developed in previous grant period. The little (*lit/lit*) mouse has an autosomal recessive mutation in the growth hormone-releasing hormone receptor (GHRHR) gene. The mutation affects only one nucleotide, an A to G mutation, at base number 112 in the GHRHR gene. The PCR based genotype assay identifies this single nucleotide polymorphism (SNP) to verify the heterozygote (*lit*/+) mice that have only one mutated copy of the gene.

To establish our Smad2 breeding colony, we bred male and female heterozygous smad2\+ mice obtained from our collaborator Dr. Michael Weinstein, Molecular Genetics Division, Ohio State University. For reporting purpose, the 'Smad2' sign indicates a disabled copy of 'Smad2' gene while the '+' sign indicates the presence of a normal Smad2 gene. The homozygous (Smad2/Smad2) KO mice die during embryonic development, whereas, heterozygous (Smad2/+) mice survive and live normally. We generated 113 smad2/+ or +/+ mice from breeding heterozygous smad2/+ male and females. To determine which mice have the 'Smad2' allele, we genotyped all smad2 progeny with an assay developed previously and is based on detection of the PCR product corresponding to the neomycin sequence. For the genotyping assay, DNA was extracted using the DNeasy 96 kit and the Smad2 sequence was amplified using primer pairs specific for 'smad2' and 'neomycin' gene. The PCR products were separated on 6% polyacrylamide gel, stained with ethidium bromide and visualized by Chemilmager 4400 Low Light Imaging system.

Normative data on musculoskeletal phenotypes in lit/lit and Smad2 knockout mice. In order to identify outlier (phenodeviant) mice, it is important to obtain reliable cut-off values from control mice. To obtain control data we bred heterozygous *lit*/+ or Smad2/+ mice with wild type B6 males and females to generate approximately 53 F1 progeny each from *lit*/+ and Smad2/+ strain (see details in Table-1). These mice were genotyped at 10-week age when blood collection, DEXA, and pQCT measurements were performed as described below in Specific Objective 2 (age varied by ±2days). The phenotype measurements were repeated at 16-weeks age to establish reference values for the 16-week old mice. The availability of normative data is essential for identification of outlier mice based on quantitative differences.

Production of ENU mutagenized male. To generate F1 mice for sensitized screen our screening strategy requires that we inject ENU to wild type male mice fro breeding with lit/+ or smad2/+ mice. We injected three batches of 8-10 week old C57BL/6J mice with 3x100 mg/kg of ENU. Previous studies by our group have shown that B6 mice can tolerate this dose and regain fertility within 12-20 weeks post ENU injection. These three batches of ENU injected males were spaced at a 3-month period to allow us a continuous supply of ENU mutagenized B6 males for breeding with *lit/lit* or Smad2/+ mice. After 10-12 weeks, each ENU injected B6 male was bred with two 8-20 week old *lit/lit* or Smad2/+ females. The B6 ENU injected male mice typically

recovered in 14-15 weeks and produced litters with 2-6 pups/litter. However, the fertile period was brief and lasted between 10-14 weeks. Females are checked routinely for pregnancy, and the pregnant mice are removed from mating cages and replaced by fresh females.

The generation and screenings of B6 mice were initially attempted as proposed in Figure-1A. However, we observed that *lit/lit* female mice (which have 30-40% lower body weight) were difficult to breed and took considerable amount of time to even produce a relatively few litters. The breeding with ENU injected males was especially slow because of small period of time (fertility window) during which ENU injected males are fertile. To overcome this difficulty, we changed our strategy to breed *lit*/+ female mice, which have normal body weight and produce litters more frequently with ENU injected males (this new breeding scheme is described in Figure 1B). Due to the change in breeding strategy, we generated additional animals that have the +/+ genotype, which are not useful for our sensitized screen. However, this strategy eliminates the need for additional breeding of wild type B6 with ENU injected males to produce about 100 pups for calculating and comparing mutation frequency rate between sensitized and non-sensitized ENU screen as proposed in Specific Objective-2. It may be possible to use the mice that have been generated from breeding *lit*/+ with ENU injected males and have +/+ genotype for non-sensitized screen. During this reporting period, we have produced a total of 109 mice for dominant screen in *lit*/+ or Smad2/+, +/+ background. Out of these, 49 mice had the +/+ genotype and 21 mice are yet to be genotyped.

The total number of mice screened for sensitized mutations in the current reporting period was lower than the 200 proposed in the current grant period. However, the number of phenodeviants identified in previous year exceeded our expectations. Once we observed a higher number of phenodeviants from previous screens, we thought it is necessary to confirm these phenodeviants by backcrossing them with lit/+ or smad2/+ that would require 300-400 additional mice. Consequently, we focused on confirming the interesting phenodeviants in backcross to lit/+ or smad2/+ mice. We produced approximately 448 F1 mice from these backcross breeding to confirm several phenodeviants. Out of these 448 F1 backcross mice, approximately 100 mice were produced in previous year screen but not reported earlier. Details of the backcross progeny are described below under 'Inheritance Testing' under Specific Objective 3.

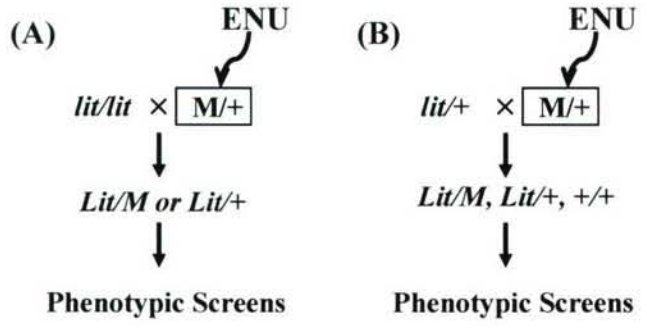

Figure 1. **(A)** Breeding scheme proposed in the Technical Objectives using lit/lit mice. **(B)** Alternate breeding strategy employed for sensitized screen using lit/+ mice.

Specific Objective 2: Perform musculoskeletal screens at 10 weeks of age in the F1 progeny to measure bone mineral content, bone density, bone size, muscle size and fat content using PIXImus and pQCT instruments. Perform biochemical measurements of bone turnover in the serum samples.

Musculoskeletal screening of 10 week old F1 progeny from lit/+ or Smad2/+. All sensitized screen mice and control mice were first screened for visible phenotypes at weaning when their body weights were also recorded. After weaning, mice were kept in groups of 2-3 males/cage

and 3-4 females/cage until 10-week old. At 10-weeks, mice were screened for: a) visible abnormalities, b) body weight; c) total body bone density determined by DEXA instrument PIXImus (excluding skull area); d) total body bone mineral content by DEXA; e) total body bone area by DEXA; f) total body fat mass; g) lean mass; h) volumetric bone density at tibia determined by peripheral quantitative computed tomography; i) IGF-I levels in *lit*/+ mice; j) skeletal alkaline phosphatase; k) serum calcium; and l) lipid profile. An abnormality is usually recognized if a phenotype differs by 2-3 standard deviations (SD) units as compared to values obtained from age and sex matched non-mutagenized control mice. Measurements that are found to be outside the cutoff range are repeated at 16-weeks to confirm the phenotype. For this purpose, we have obtained additional baseline values for age and sex matched *lit*/+ and Smad2/+ mice at 16-week of age. Some phenotype measurements, such as BMC, bone area, femur BMD are size-dependent and show strong correlation with body weight. Therefore, these measurements were normalized with body weight for identifying phenodeviants. Those phenodeviants that are confirmed after repeat testing are introduced to inheritance-test (IT) or backcross with wild type *lit/lit* or Smad2/+ mice. A mutation is considered inheritable if the phenotype is recovered in backcross progeny.

Since the TGF-β pathway has been implicated in the tissue regeneration, we also screened smad2/+ mice for 'soft-tissue regeneration' (STR). To screen mice, we punched a 2 mm hole in both ears and tissue regeneration was monitored by measuring hole size after 14-day and 21-day period using a magnifying glass (4x) with an embedded measuring scale (reading capabi*lit*y of ±0.1 mm). We observed that healing is normally slow in Smad2/+ background with mean hole size after 3-weeks of 1.8±0.2. Therefore, we anticipate hypomorphic mutation could be easier to identify.

Screening of Control Mice. We have generated 193 mice from breeding of *lit/lit* or *lit*/+ mice (n=80) or Smad2/+ mice (n=113) with wild type B6 mice. About 40% mice carried *lit*/+ or Smad2/+ genotype. Out of the 193 mice generated, we screened 53 mice for generating normative data at 10-week and 16-week as described above for phenotype screening of mutant mice.

Phenodeviants Identified in Sensitized ENU Screening. We have screened 109 F1 progeny (Table 2) for phenotypes listed above in screening procedure. We observed one phenodeviant in smad2/+ background in our primary screening performed at 10-weeks and confirmed this quantitative phenodeviant in 16-weeks repeat testing. The mutant identified as 1874DF has body weight Z-score of –3, BMD Z-score of –1.9, BMC Z-score of –3.2, bone area Z-score of –2.8, and lean body mass Z-score of –3.8. The body weight adjusted BMD and BMC was 10-14% lower as compared to smad2/+ control mice. The phenotype appears to be growth related and was anticipated because mutations in Smad2 gene are involved in developmental type phenotypes.

Specific Objective 3: Begin to confirm the mutant phenotypes by backcrossing the mutant mice with lit/lit or Smad2 knockout mice, as appropriate.

Those phenotypes that are confirmed after repeat testing at 16-week are subjected to inheritance-test (IT) or backcross with lit/+ or smad2/+ mice. Because of the significant efforts involved in progeny testing, we have focused on those phenodeviants that had highest differences in

phenotypes. A mutation is considered inheritable if the phenotype is recovered in backcross progeny (a minimum of 20 mice).

In the current reporting period, we introduced 10 phenodeviant mice (including mutant mice from both lit/+ & smad2/+ background) into inheritance testing (Table-2) by mating affected male and female mice with wild type lit/+ or smad2/+ mice. Each phenodeviant is mated with 1-2 normal wild type male or female mice. Once the mating is successful, pregnant mice are separated and placed separately to give birth to backcross littermates. If an F1-affected mouse is a female, it is reintroduced for mating to produce 3-5 litters totaling about 20-25 backcross pups. If the affected mouse is male, 3-5 female mice were mated simultaneously. The inheritance testing (IT) F2 offspring were screened at 10-week and 16-weeks of age. The animals are genotyped to identify the background alleles such as lit/+ or smad2/+ genotype. To differentiate mutant from non-mutant genotypes, 2SD cut-off was used for separating the mutants from their unaffected littermates. To avoid potential breeding of an un-affected progeny, we bred only extreme scoring mice for generating affected progeny in subsequent breeding. All phenodeviant mice that are under inheritance testing are listed in Table-2. In addition to the phenodeviants bred in the current reporting period, we also continued breeding phenodeviants from the previous year's screens; these phenodeviants are only reported in current grant period.

Detailed Phenotypic Characterization of Selective Phenodeviants Identified in Previous Screens

Mutant Line 14104 – Mutant male mouse 14104AM was identified in the lit/+ strain of mice. The phenodeviant had 18% high volumetric bone density measured by pQCT. As compared to control mice, the periosteal circumference at midshaft tibia was 17% lower but endosteal circumference was 38% lower, thus, the increased BMD was mainly due to increased bone at endosteal surface. The cortical thickness was increased by 5%. We bred the 14104 phenodeviant with lit/+ females and generated about 42 progeny in this grant period. Out of 25 screened, 23 were with lit/+ genotype and approximately 13 pups from IT or about 50% appear to be affected. As shown in Figure 2, the pQCT scan of tibia midshaft shows the increased endocortical bone phenotype was recovered in the 10-week old affected 14104 progeny. The decreased periosteal and endosteal circumference correlated significantly with increased BMD (Figure 3). The increased BMD phenotype and decreased endosteal and periosteal circumference phenotypes at 16-week (Figure 4) were similar to 10-week old mice, indicating that changes in BMD occurs early and phenotype was maintained during peak bone mass growth. Currently more mutant progeny is generated for more invasive characterization and mapping the chromosomal location of the mutation.

Mutant Line 1665CM – Mutant male mouse 1665CM was identified in the smad2/+ strain of mice. The phenodeviant had 18% high body weight and 13% higher total body bone density measured by DEXA (Dual Energy X-ray Absortiometry), as compared to control smad2/+ mice. The body weight adjusted bone density was not significantly higher in mutant mice. The lean body mass was increased by 19%. Since TGF-b is implicated in growth, we believe the mutant mouse has a high growth phenotype. We bred the 1665CM phenodeviant with smad2/+ females and generated about 120 progeny. Out of 86 mice screened, 55 mice with smad2/+ background have been screened at 10-week and 37 mice screened at 16-week. At 16-week, approximately 16 pups from inheritance testing backcross or about 43% appear to be affected (Figure 5). Currently

more mutant progeny is generated for more invasive characterization and mapping the chromosomal location of the mutation.

Mutant Line 1665DF – Mutant female mouse 1665DF was identified in the smad2/+ strain of mice. The phenodeviant had 23% high body weight and 17% higher total body bone density measured by DEXA (Dual Energy X-ray Absortiometry), as compared to control smad2/+ mice. The body weight adjusted bone density was 4-8% higher in 16-week old 1665DF mutant mice ($p<0.05$ vs control smad2/+ mice). The lean body mass was 25% higher in 1665DF. We believe the mutant mouse has a high growth as well as high BMD phenotype. We bred the 1665DF phenodeviant with smad2/+ male mice and generated about 146 progeny. Out of 107 mice screened, 65 mice with smad2/+ background have been screened at 10-week and 45 mice were screened at 16-week age. At 16-week, approximately 13 pups from inheritance testing backcross or about 29% appear to be affected (Figure 6). The 1665DF mutant appears to be similar to 1665CM described above, however, the body weight adjusted total body BMD was 4-8% higher ($p<0.05$) in 1665DF indicating that increase in BMD was greater than that explained by increased body weight. Therefore, the 1665DF mutation also affects BMD. Currently more mutant progeny is generated for more invasive characterization and mapping the chromosomal location of the mutation.

Soft Tissue Regeneration Mutations: (Mutant Lines 1617EF and 1617EF) – Two mutants 1617EF and 1617DF were identified in the smad2/+ strain of mice, both these mutants were littermates and could represent same mutation. Therefore, we have combined data from these two mutants. The phenodeviants 1617EF and 1617DF had 20% more healing as compared to WT control mice (smad2/+). The healing phenotype was measured by punching a 2 mm hole and measuring the hole size after 3-5 weeks. We bred the 1617EF and 1617DF phenodeviant with smad2/+ male and generated about 31 progeny (including those mice that had +/+ genotype). Out of 31 mice generated, approximately 4 pups from inheritance testing backcross appear to be affected (Figure 7A & B). The mutation appears to be inheritable but not confirmed. We currently plan to breed the affected mice further to confirm inheritance.

Table 1. Number of mice generated, mice screened for various phenotypes, and number of mice introduced to inheritance testing.

Procedure	Number of *lit*/+ Mice	Number of Smad2/+ Mice
Control Mice Screened for Dominant Mode of Inheritance (F1)	28	25
Sensitized ENU Mice Screened for Dominant Mode of Inheritance (F1)	26*	83*
Abnormal Phenotypes Identified in Primary Screen (in *lit*/+ or Smad2/+ background and excluding +/+ background)	0	1
Abnormal Phenotypes Confirmed in Secondary Screen (in *lit*/+ or Smad2/+ background and excluding +/+ background)	0	1
Phenotypes Introduced to Progeny Testing	0	1

*Includes mice with genotype +/+ and mice that are not yet genotyped.

Table 2. List of phenodeviants identified previously and introduced to inheritance testing.

Phenotype (Mice ID)	Description of 16-Week Repeat Phenotype	Background Strain	Mice Produced in IT*	No of Affected Mice IT	Mutation Confirmed in IT
14.9.8.EM	BMD Z-Score=3.0 BMC Z-Score=3.3 (Body weight adjusted BMC 20% High)	Lit/+	44	0	Not Confirmed
14.10.4.AM	pQCT BMD Z-Score=5	Lit/+	42	13	**Confirmed**
15.2.3.BM	Body Weight Z-Score=3.2 BMD Z-Score=3.6 BMC Z-Score=3.8	Lit/+	0	0	Not Confirmed
15.12.7.FF	Body Weight Z-Score=-5.7 BMD Z-Score=-6.1 BMC Z-Score=-5.5	Lit/+	0	0	Not Confirmed
14.10.6.AF	Body Weight Z-Score=-2.3 BMD Z-Score=-2.6 BMC Z-Score=-2.6	Lit/+	0	0	Not Confirmed
14.10.12	High IGF-I, Z-Score=-2.3	Lit/+	65	0	Not Confirmed
16.1.7.EF	20% Higher Tissue Healing	Smad2/+	31		Under Testing
16.6.5.CM	Body Weight Z-Score=2.2 BMD Z-Score=3.8 BMC Z-Score=3.7	Smad2/+	120	21	**Confirmed**
16.6.5.DF	Body Weight Z-Score=2.4 BMD Z-Score=4.9 BMC Z-Score=4.1	Smad2/+	146	17	**Confirmed**
16.16.8.CM	Body Weight Z-Score=4.4 Lean Mass Z-Score=1.5 BMD Z-Score=3.3 BMC Z-Score=2.1	Smad2/+	0	0	Not Confirmed

*The mice produced also include mice that have +/+ genotype, and therefore, are not informative.
BMD= Bone Mineral Density, BMC= Bone Mineral Content, STR= Soft tissue regeneration
Z-Score indicates differences in a particular phenotype in terms of SD units from non-mutagenized control mice.

Table 3. Phenotype of affected 14104AM mutant measured by pQCT at tibia midshaft expressed as percent difference from lit/+ control mice (n=20-25).

Mice		Endosteal Circumference	Periosteal Circumference	Total BMD	Cortical Thickness
10-Wek (n=8)	Female	-49.5	-22.8	12.2	6.3
10-Week (n=5)	Male	-40.1	-23.5	7.0	-6.6
16-Week (n=7)	Female	-55.6	-22.2	10.6	10.3
16-Week (n=4)	male	-42.2	-22.1	5.3	-0.8

Table 4. Phenotype of affected 1665CM mutant measured by total body DEXA scan expressed as percent difference from smad2/+ control mice (n=25-30).

Mice (n=No of Affected Mice)*		Body Weight	Total Body BMD	Total Body BMC	Femur BMD
10-Wek (n=13)	Female	10.3	6.6	10.2	5.8
10-Week (n=8)	Male	17.3	10.6	18.1	11.0
16-Week (n=10)	Female	16.2	11.4	15.8	10.7
16-Week (n=7)	male	20.9	10.7	17.4	16.0

All values were statistically significant from smad2/+ control mice ($p<0.01$)
*Total number of 1665CM smad2/+ mice screened was 55.

Table 5. Phenotype of affected 1665DF mutant measured by total body DEXA scan expressed as percent difference from smad2/+ control mice (n=25-30).

Mice (n=No of Affected Mice)*	Body Weight	Total Body BMD	Total Body BMC	Femur BMD
10-Wek Female (n=10)	21.5	11.7	20.3	15.2
10-Week Male (n=7)	20.1	12.2	20.8	12.8
16-Week Female (n=9)	22.1	14.0	24.3	15.7
16-Week male (n=7)	24.6	12.7	20.2	15.2

All values were statistically significant from smad2/+ control mice ($p<0.01$)
*Total number of 1665DF smad2/+ mice screened was 65.

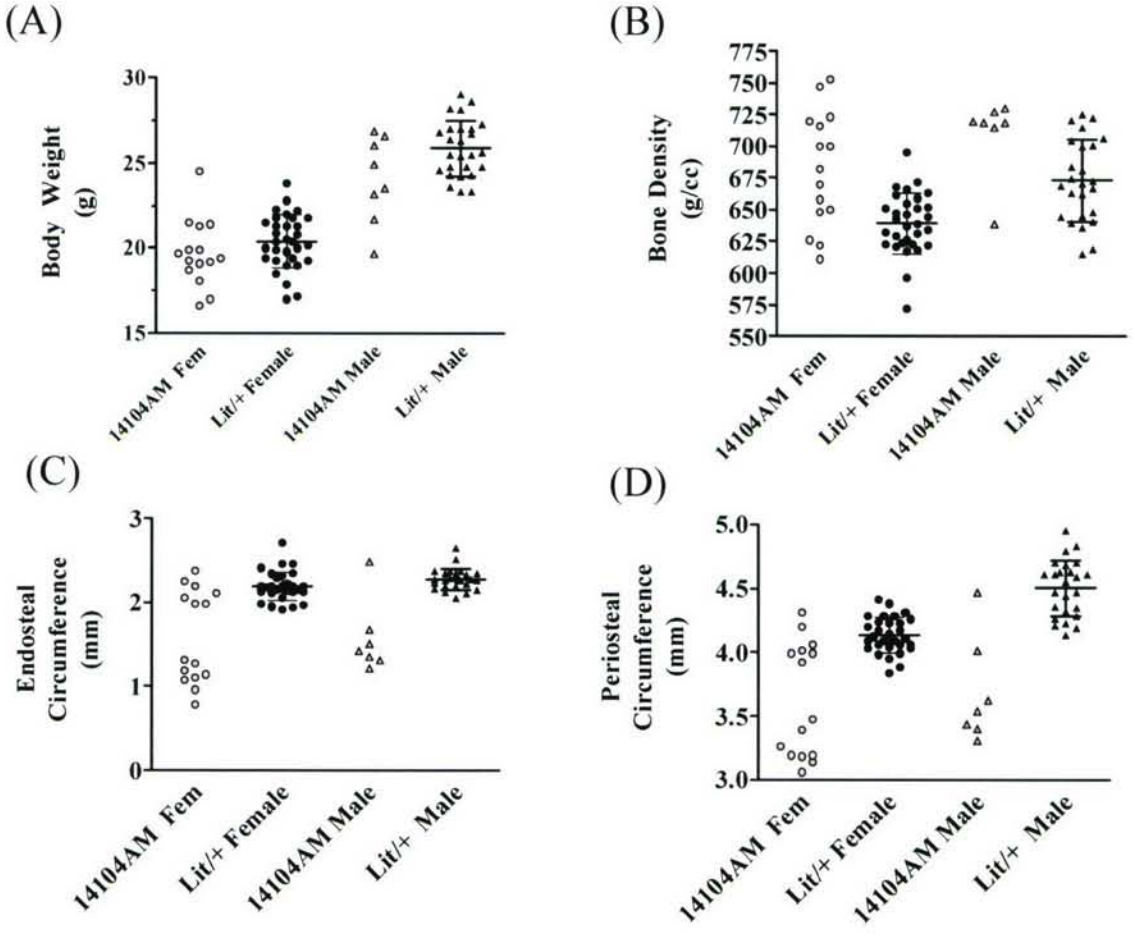

Figure 2. Phenotype data from 10-week old mutant progeny generated from backcross of a mutant mouse, 14104AM, identified in sensitized screening using lit/+ mice. A. The body weight of the male and female 14104AM progeny appears to be similar to age and sex matched lit/+ mice. B. The volumetric BMD was 10-12% higher ($p<0.01$) as compared to control mice. C & D. The increased BMD appears to be due to increased endosteal bone. Each data point represents one mouse and both affected and non-affected littermates are shown under 14104AM progeny. BW=Body weight, BMD=Total body bone mineral density, BMC=Total body bone mineral content, Lit/+= WT mice with one 'lit' allele (data shown as Mean±SD).

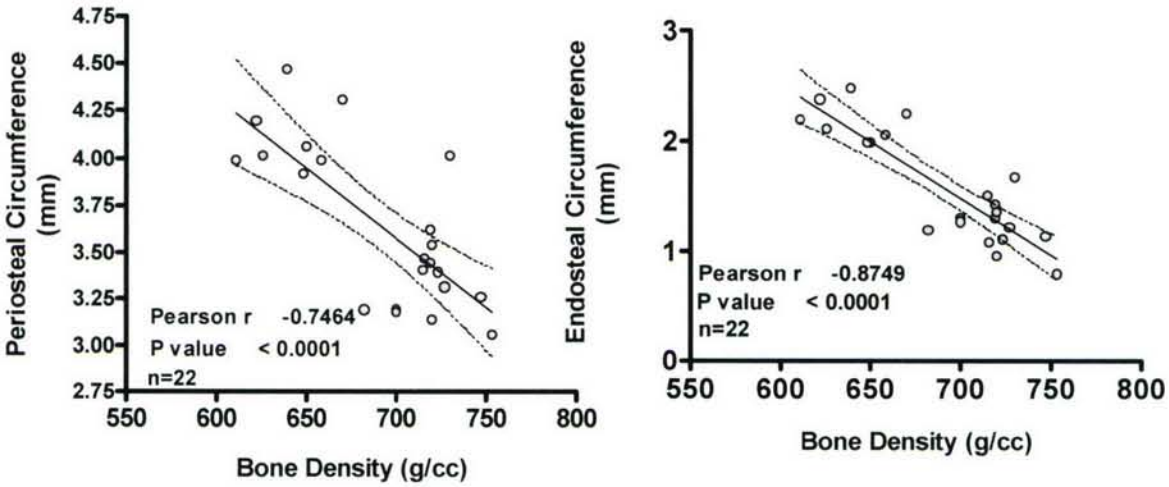

Figure 3. Correlation between endosteal and periosteal circumference and volumetric bone density in 14104AM mutant mice. A significant correlation between endosteal circumference and BMD indicates that probably a higher rate of endocortical bone formation contributes to higher bone density in 14104AM mutant mice.

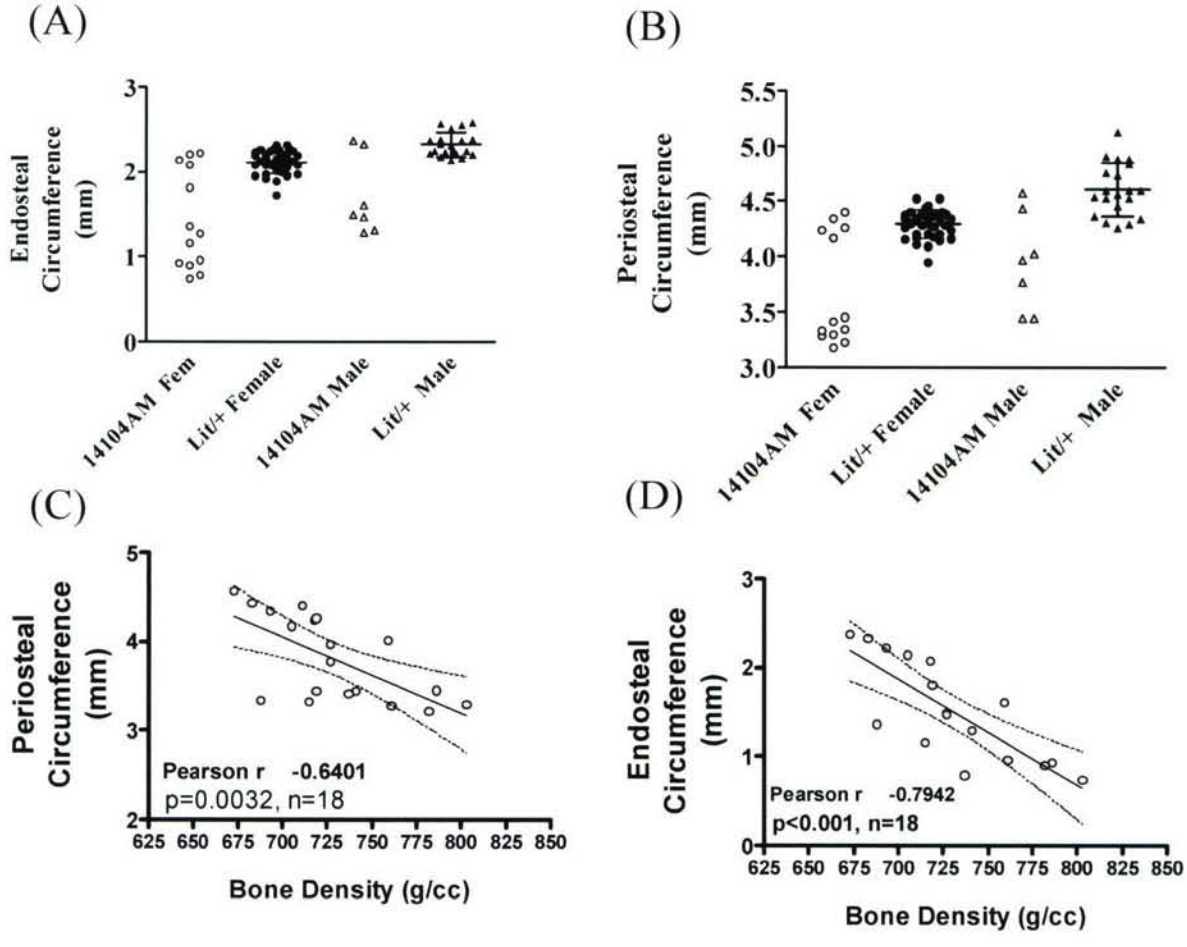

Figure 4. Phenotype data from 16-week old mutant progeny generated from backcross of 14104AM mutant. A & B. The endosteal circumference in 16-week old mice was 40-50% lower and periosteal circumference was 22% lower. C & D. Both periosteal and endosteal circumference negatively correlated with volumetric BMD. These data suggests that mutation causes more endocortical bone resulting in increased BMD in mutant mice as compared to control mice. Each data point represents one mouse and both affected and non-affected littermates are shown under 14104 progeny. BW=Body weight, BMD=Total body bone mineral density, BMC=Total body bone mineral content, Lit/+= WT mice with one 'lit' allele (data shown as Mean±SD).

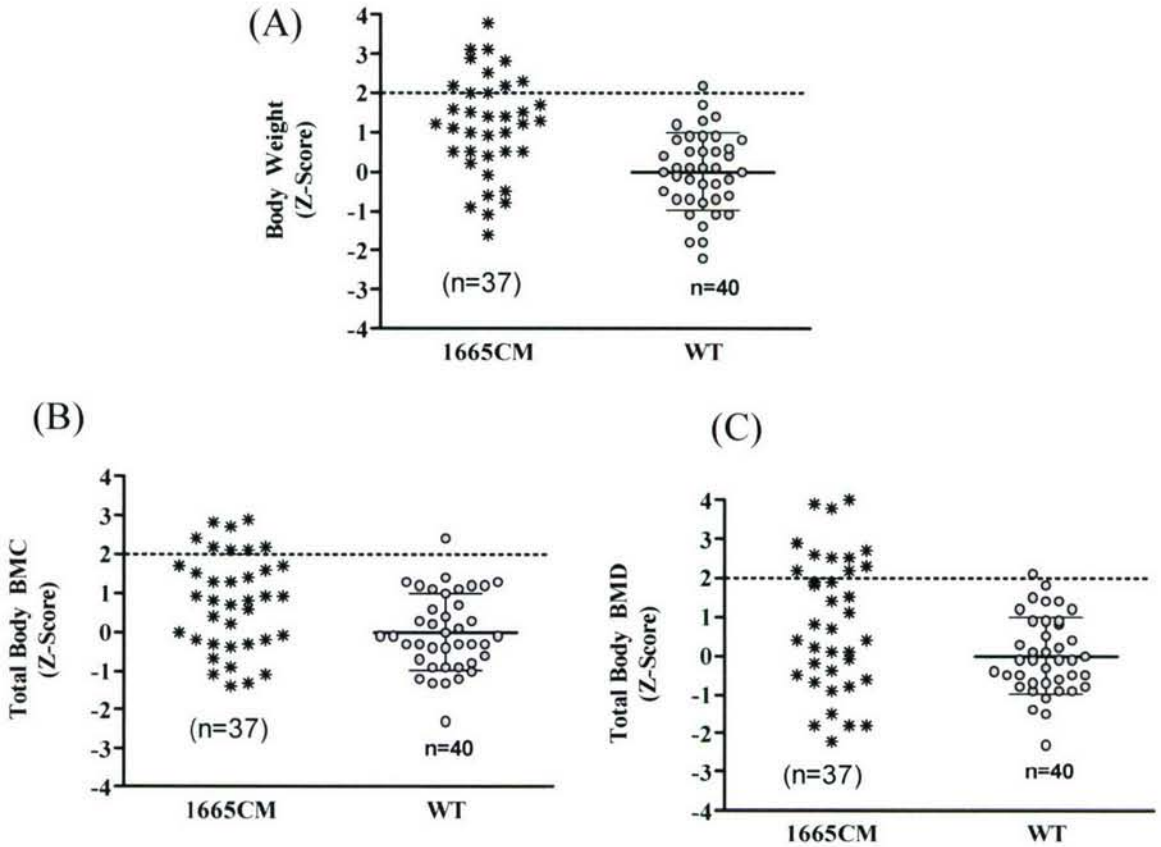

Figure 5. Phenotype data from 16-week old mutant progeny generated from backcross of a mutant mouse, 1665CM, identified in sensitized screening in Smad2/+ background. The progeny from 1665CM mutant shows 10-17% higher body weight (A) phenotype. In addition to body weight, the mutant progeny has 10-18% higher total body BMC (B) and 7-10% higher total body BMD (C). Each data point represents one mouse and both affected and non-affected littermates are shown under 1665CM progeny. The horizontal line indicates 2SD cut-off for identifying mutant mice from non-affected littermates. WT=Wild Type (smad2/+) (data shown as Mean±SD).

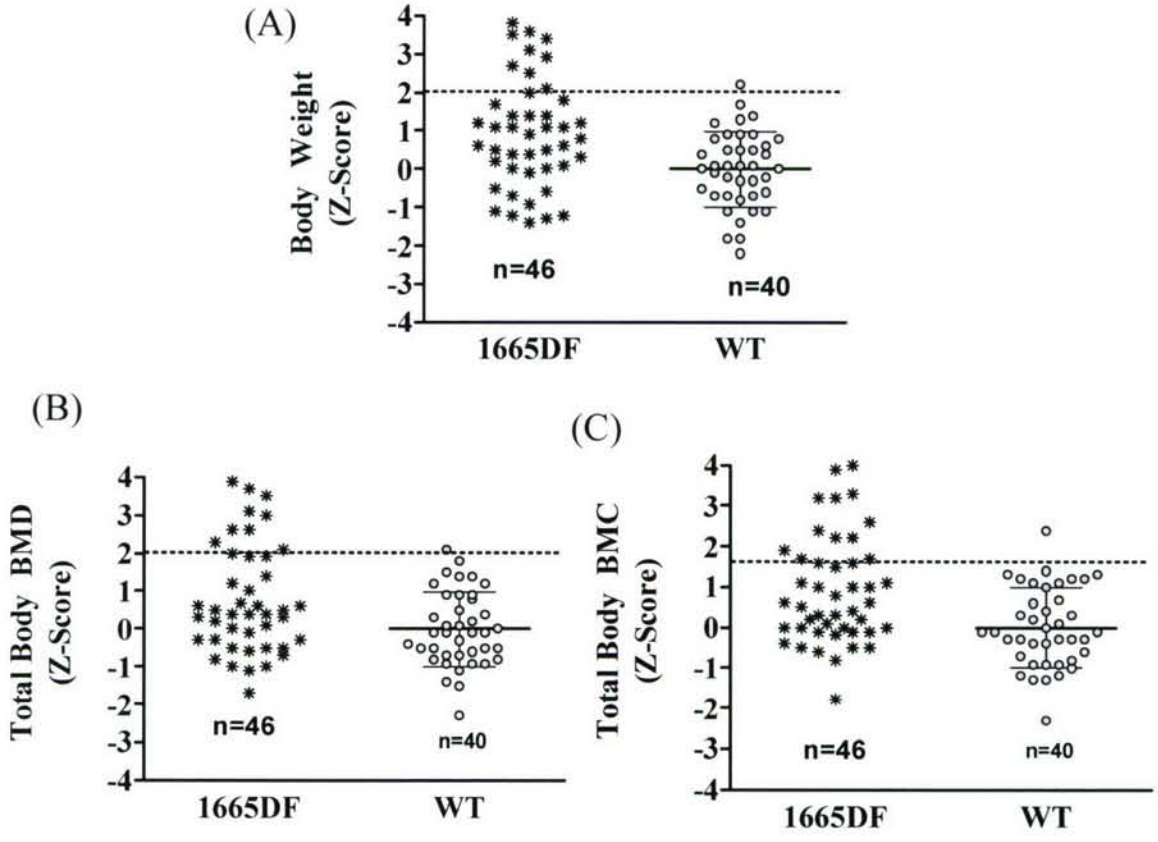

Figure 6. Phenotype data from 16-week old mutant progeny generated from backcross of a mutant mouse, 1665DF, identified in sensitized screening in Smad2/+ background. The progeny from 1665CM mutant shows 20% high body weight (A) phenotype. In addition to body weight, the mutant progeny have 15-16% higher total body BMD (B) and 20-25% higher total body BMC (C). Each data point represents one mouse and both affected and non-affected littermates are shown under 1665DF progeny. The horizontal line indicates 2SD cut-off for identifying mutant mice from non-affected littermates. WT=Wild Type (smad2/+) (data shown as Mean±SD).

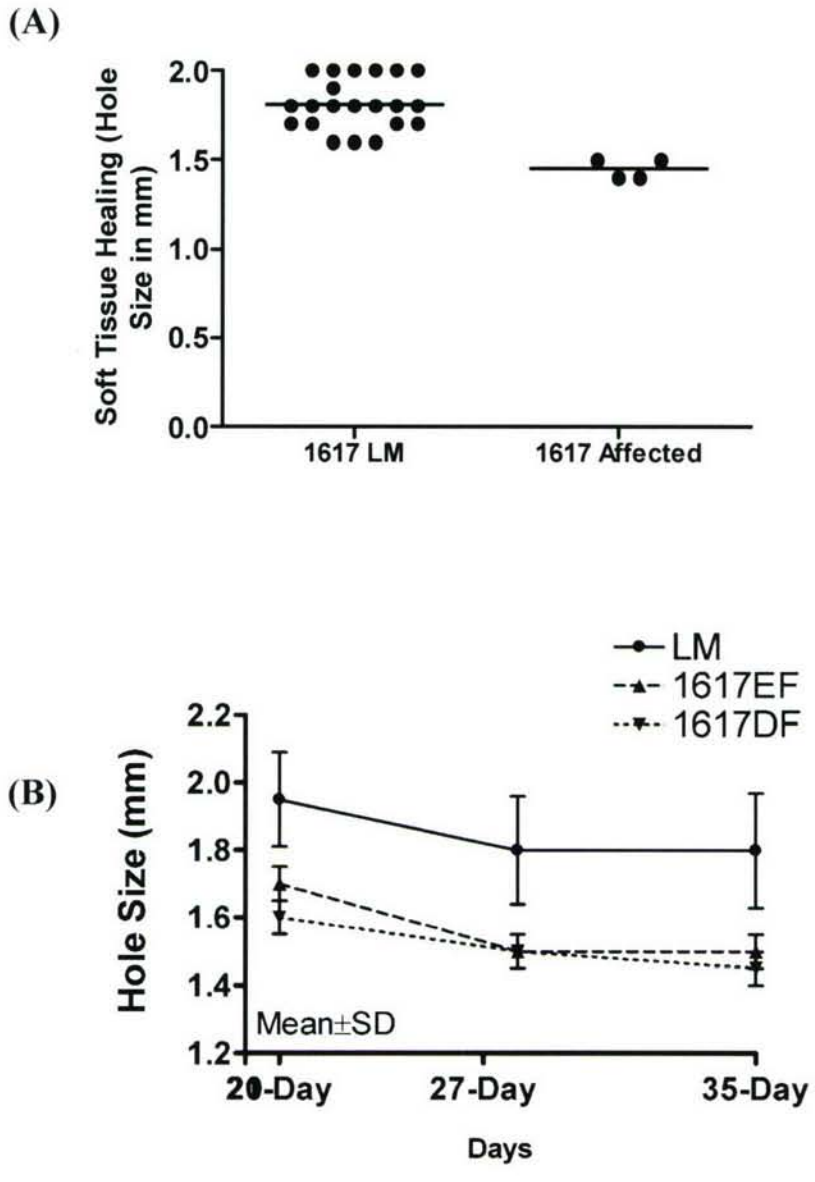

Figure 7. Soft tissue regeneration phenotype data from 6-week-old mutant progeny (A) generated from backcross of mutant mice identified in sensitized screening in Smad2/+ background. The bottom figure shows the tissue healing capacity of mutant mice measured at 3-, 4-, and 5-weeks after a 2 mm hole punched in ear lobe (B). The affected mice have approximately 20% more healing as compared to non-affected littermates or WT control.

Key Research Accomplishments

1) We maintained a breeding colony of *lit/lit* mice and Smad2/+ mice to have a continuous supply of *lit*/+ and Smad2/+ mice for breeding with ENU injected B6 males.
2) We injected three batches of B6 males with a 3 X 100 mg/kg dose of ENU and bred them with *lit*/+, and Smad2/+ mice.
3) To obtain control data, we bred wild type B6 mice with *lit*/+, and Smad2/+ mice.
4) We have screened 53 F1 control mice generated from breeding wild type B6 mice with *lit*/+ or Smad2/+ mice.
5) We have screened 109 F1 sensitized screen mice generated from breeding ENU injected B6 males mice with *lit*/+ or Smad2/+ mice.
6) We have identified one new phenodeviant in current year 10-week sensitized screen and confirmed this phenodeviant in 16-week repeat testing.
7) We bred 10 phenodeviant mice from previous year screen for inheritance testing. We generated 448 mice from inheritance testing of phenodeviants.
8) We confirmed three phenodeviants in inheritance testing. Two phenodeviants were in smad2/+ background genotype and exhibit higher growth and high total body bone density phenotype. One phenodeviant was in lit/+ background and represents high volumetric bone density phenotype that is related to higher endosteal bone volume.
9) The inheritable phenodeviants are single gene mutations, and therefore, provide interesting mouse model to identify genes that are involved in the genetic regulation of growth and musculoskeletal phenotypes.

Reportable Outcomes

None at the present time

Conclusions

1) We have used two key pathways involving IGF-I growth hormone axis and TGF-β signaling pathway to perform a sensitized ENU screening for musculoskeletal phenodeviants.
2) We bred *lit/lit* mice and heterozygous Smad2 knockout mice to generate *lit*/+ and smad2/+ mice for breeding with ENU injected males.
3) We have injected three batches of C57BL/6J males with ENU dose of 3 X 100 mg/kg to generate ENU founder males. We bred the ENU injected males in a breeding scheme to generate about 53 F1 mice for dominant screening. Our aim was to generate about 200 F1 animals. However, due to higher number of phenodeviants observed in previous year we considered that follow-up of these phenodeviants was more important. In the follow-up backcross we have generated and screened more than 400 mice, therefore, we have partially accomplished our main goal of the Specific Objective 1. The resources proposed in Specific Objective 1 were diverted to extra efforts required in accomplishing the Specific Objective 3, which involved higher than expected number of follow-ups.
4) We have generated 193 F1 mice by breeding lit/+ and smad2/+ mice with WT B6 mice and screened 53 mice with lit/+ or samd2/+ genotype to generate normative data for identification of mutants.
5) We have performed musculoskeletal screens at 10 weeks of age in the F1 progeny to measure bone mineral content, bone density, bone size, muscle size and fat content using PIXImus and pQCT instruments. We identified one growth related phenodeviant in the 10-week screen and

confirmed this in repeat testing at 16-week screen. Therefore, we have accomplished our main goal of the Specific Objective 2.

6) We bred 10 phenodeviants identified in previous year screen in backcross to test inheritability of the mutations. We generated more than 400 progeny from backcross and confirmed three phenodeviants to be inheritable. We have partially confirmed one soft tissue regeneration mutant in the backcross. The number of mice generated in backcross far exceeded those proposed in the current grant period. Therefore, we exceeded our goals for final objective Specific Objective 3.

References

1. Srivastava AK, Mohan, S, Wergedal JE, Baylink DJ. A Genome-wide Screening of N-Ethyl-N-nitrosourea Mutagenized Mice for Musculoskeletal Phenotypes. Bone, 33, 179-191, 2003.
2. Go MJ and Tsakonas SA. A genetic screen for novel components of the Notch signaling pathway during Drosophila bristle development. Genetics 150:211-220, 1998.
3. Carrera P, Abrell S, Kerber B, Walldorf U, Preiss A, Hoch M, Jackle H. A modifier screen in the eye reveals control genes for Kuüppel activity in the Drosophila embryo. Proc. Natl. Acad. Sci. 95:10779-10784, 1998.
4. Satterthwaite AB, Willis F, Kanchanastit P, Fruman D, Cantley LC, Helgason, Humphries RK, Lowell CA, Simon M, Leitges M, Tarakhovsky A, Tedder TF, Lesche R, Wu H, and Witte ON. A sensitized genetic system for the analysis of murine B lymphocyte signal transduction pathways dependent on Bruton's tyrosine kinase. Proc. Natl. Acad. Sci. 97: 6687-6692, 2000
5. Attisano, L. and J.L. Wrana, Signal transduction by the TGF-beta superfamily. Science, 296(5573): 1646-7, 2002.
6. Donahue, L.R. and W.G. Beamer, Growth hormone deficiency in 'little' mice results in aberrant body composition, reduced insulin-like growth factor-I and insulin-like growth factor-binding protein-3 (IGFBP-3), but does not affect IGFBP-2, -1 or -4. J Endocrinol, 136(1): 91-104,1993.

Project 3: Development of Transgenic Approaches Using BAC Clones to identify Candidate Genes for Musculoskeletal Phenotypes

Introduction

The primary goal of our studies is to localize chromosomal regions and subsequently identify genes responsible for various musculoskeletal phenotypes including bone density, fracture repair and soft tissue regeneration, and evaluate the molecular function of these genes. We have been using two main strategies to identify these genes for musculoskeletal system. They are: 1) Ethylnitrosourea (ENU) chemical mutagenesis to generate mutant mice with significant musculoskeletal alteration and 2) Genetic linkage analysis to discover genetic components of quantitaive trait loci (QTL) that contribute to phenotypic changes. In our previous studies, we have made significant progress with both ENU and QTL approaches, and identified several mutant mouse strains and genetic loci that are associated with phenotypes of small bone size, high bone density and soft tissue regeneration. However, these regions contain dozens of intact genes with a large piece of genomic DNA in several overlapping bacterial artificial chromosomes (BACs) and need to be further tested for their functions. The aim of this project is to develop a gene transfer system of BAC to deliver candidate genes as large as 150-kb into bone cells for functional studies. In the first 12 months of this grant, we have successfully developed an approach using herpes simplex virus type 1 (HSV-1)-amplicon system to transfer of BAC genomic locus into bone cells, and established that the candidate gene is expressed at high level and is functional.

Body

1. Technical Objectives

Our specific objective during the second 12 months of this grant period is to begin to evaluate the utility of BAC clone transgenesis for identification of ENU mutant that contributes to decreased bone size as described below:

1) Begin to retrofit one or more BAC clones for chemical or viral transfer.
2) Isolate periosteal cells from mutant mice and transfect with one or more BAC clones.
3) Begin to evaluate the phenotypic change (cell proliferation/ differentiation/ apoptosis) in cells transfected with one or more BAC clones.

Our progress in each of the specific objective is given below.

2. Progress on Specific Objectives

Specific Objective 1: To begin to retrofit one ore more BAC clones for chemical or viral transfer.

To achieve our objective of developing an optimal protocol for efficient transfer of candidate genes into mouse cells in vitro for functional evaluation, we also undertook studies to clone the complete coding sequence of candidate genes into the HSV amplicon-based expression vector and package them into infectious viral particles to deliver the transgene into bone cells (4, 9). We established this gene transfer approach for the following reasons. 1) Some of our test genes may contain large introns (>100 kb) such that the size of intact gene including introns and exons could be beyond limitation of HSV packaging capacity (e.g. >150 kb). 2) The BAC clone containing candidate gene may be not available in the mouse genome databases. 3) The BAC

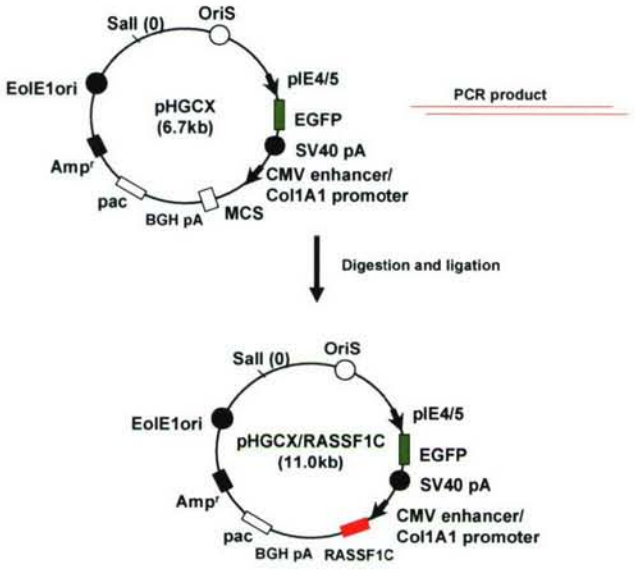

Figure 1. Schematic diagram of infectious HSV-1/RASSF1C construct. The PCR product of RASSF1C coding sequence is inserted into HSV amplicon-based expression vector, pHGCX to generate an expression vector of pHGCX/RASSF1C.

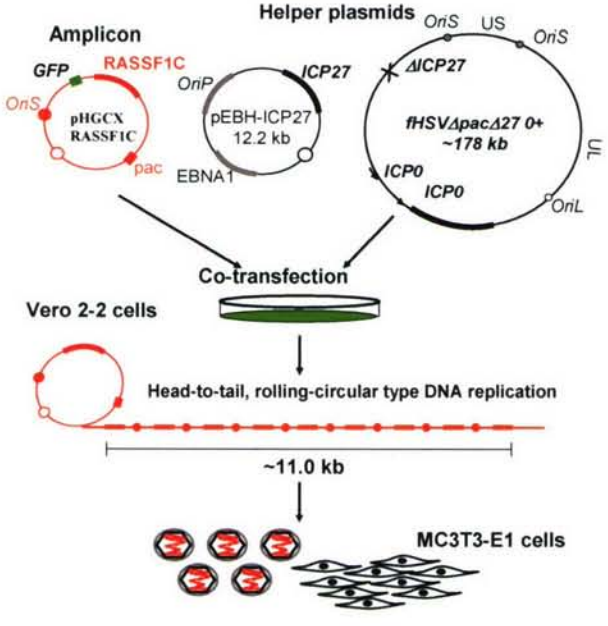

Figure 2. Schematic diagram of gene transfer by infectious HSV-1 amplicon. The HSV expression vector, pHGCX containing RASSF1C coding sequence is packaged into infectious HSV amplicon to infect MC3T3E1 cells.

clone may encode multiple alternatively spliced variants with diverse functions from a single gene. In addition, we also developed an optimal protocol of non-viral transfection technique by utilizing a modified form of "Nucleoporation" to make the delivery system safer and more feasible (5). We believe that either viral transduction or non-viral transfection of the complete coding sequence of candidate genes offers a rapid, simple alternative method of gene transfer for functional studies.

One of the test genes that we selected for evaluation using HSV based amplicon system is an alternatively spliced form of ras-association domain family 1 protein, RASSF1C. There are four variants encoded from the same gene in mouse, and the RASSF1C is believed to be involved in regulating osteoblast cell number (2). In order to test the RASSF1C's function, we amplified the coding sequence from c-DNA libraries by PCR with specific primers to RASSF1C, tagged it with Flag synthetic sequence and cloned Flag/RASSF1C into pHGCX expression vector that contains CMV enhancer/collagen 1A1/rabbit beta-globin intron heterogeneous promoter, HSV amplicon and GFP reporter gene (Figure 1). We then carried out co-transfection, and packaged pHGCX/RASSF1C into HSV viral particles to transduct MC3T3-E1 cells (Figure 2). We modified our expression vector, and inserted a 2.3 kb Collagen 1A1 to drive transgenes to boost the expression level specifically in osteoblast cells. Our experiments revealed that the transduction efficiency of HSV-based amplicon bearing coding sequence of RASSF1C variant was approximately 85% in MC3T3-E1 cells (Figure 3A & B). The high level

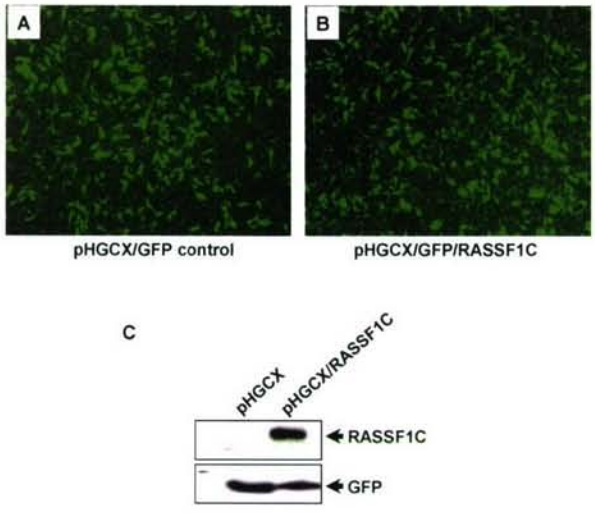

Figure 3. Transgene expression in HSV amplicon infected MC3T3-E1 cells. A: GFP expression in MC3T3-E1 cells transducted with pHGCX/GFP control amplicon. B: GFP expression in MC3T3-E1 cells transducted with pHGCX/GFP/RASSF1C amplicon. C: RASSF1C and GFP protein expression in MC3T3-E1 cells detected by Western blots.

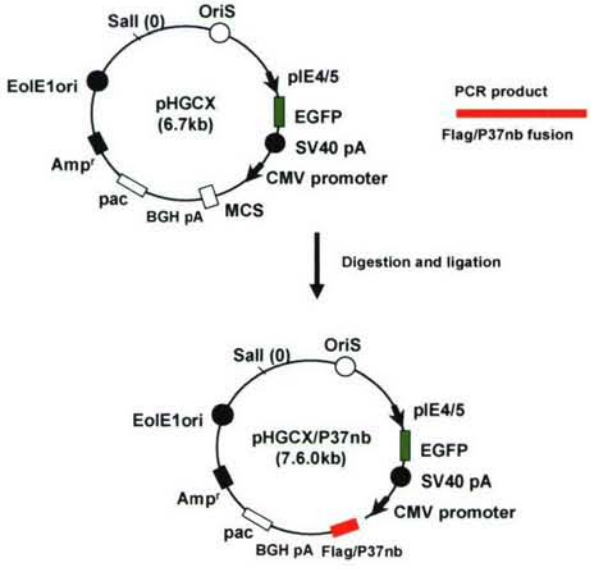

Figure 4. Schematic diagram of infectious HSV-1/P37nb construct. The PCR product of P37nb coding sequence is inserted into HSV amplicon-based expression vector, pHGCX to generate an expression vector of pHGCX/P37nb

expression of transgene, Flag-RASSF1C, driven by CMV enhancer/Collagen 1A1 promoter was detected by Western blot with antibody against Flag 24 hours after transduction (Figure 3C). Experiments are in progress to evaluate the consequence of RASSF1C overexpression on osteoblast cell function.

We also have begun to test the function of a novel expressed sequence tag (EST) named as P37nb with leucine-rich repeats (LRR), a known functional domain present in a number of proteins with diverse functions and cellular locations (8). In our previous studies, we have demonstrated that the expression of P37nb gene in bone was significantly induced by mechanical loading in mice. The high level expression of P37nb was consistent with the robust anabolic response, increased bone size and bone mineral density. In addition, one recent study found evidence that one of the LRR proteins, CMF608, a mechanical strain-induced bone-specific protein, is involved in promoting osteochondroprogenitor proliferation (7). Based on these data, we believe that further studies are needed to evaluate whether the expressed sequence of P37nb with an important functional domain is involved in regulating osteoblast cell proliferation leading to bone formation (10). Since the BAC clone containing P37nb is not available, we amplified the complete coding sequence by PCR, and inserted the transgene into pHGCX expression vector with Flag tag at its amino terminus. Therefore, the fusion protein of Flag/P37nb driven by CMV promoter in pHGCX vector can be expressed in osteoblast or bone marrow stromal cells for functional testing (Figure 4).

In addition to the two genes mentioned above, we have started functional testing of a signaling molecule,

Ephrin B2 receptor (EphB2). It has been previously established that the EphB2 is localized within the QTL region of mouse chromosome 4 which is believed to contain mechanosensitive gene(s) (6). The Eph receptor and its membrane-anchored ephrin ligands (Eprin B1, B2 and B3) direct both reverse and forward signaling by cell-cell interactions regulating cell proliferaction, differentiation and migration (1). Targeted disruption of the Eph receptor ligand ephrinB1 in mice has also been reported to cause abnormal cartilage segmentation and the formation of additional skeletal elements, suggesting that ephrinB1 signaling is required for normal morphogenesis of skeletal elements (3). Our previous study provided evidence that mechanical loading increased Eph receptor B2 expression in bone cells, and established the groundwork for further examination of the Eph receptor signaling pathway's role in regulating bone formation. To test the function of EphB2, we searched the BAC clones from the mouse genome databases, and found that the EphB2 gene contains 16 introns, two of which are greater than 50 kb. The size of intact gene in a single BAC clone is greater than 200 kb, which is far beyond the limitation of HSV amplicon packaging system. Thus, we engineered the complete coding sequence of EphB2 into pHGCX expression vector as describle in figure 4. The 3.0 kb length of the coding sequence of EphB2 gene driven by CMV promoter in pHGCX can be either packaged into infectious HSV viron to deliver the transgene into osteoblast cells or directly transfected into bone cells by utilizing non-viral transfection technique (see below).

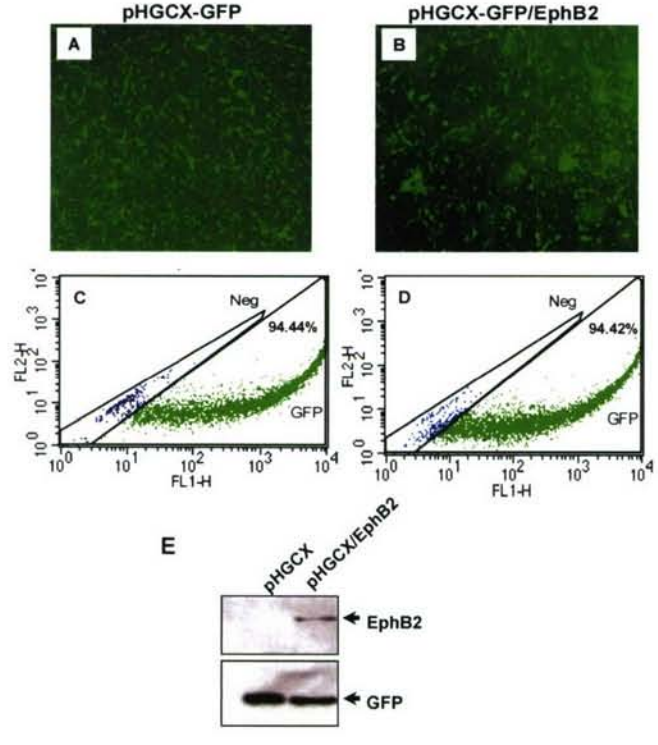

Figure 5. Transgene expression in MC3T3-E1 cells transfected. A & B: GPF expression in MC3T3-E1 cells transfected with pHGCX and pHGCX/EphB2 by Nucleoporation; C: Representive data of flow cytometric analysis in the cells transfected with pHGCX; D: Representive data of flow cytometric analysis in the cells transfected with pHGCX/EphB2; E: EphB2 and GFP expression in transfected cells, detected by Western blot.

In addition to the HSV amplicon-based viral gene transfer, we also established a non-viral gene transfer system for the constructs less than 12 kb in length. We believe that unlike BAC clone, plasmid DNA can be transferred into bone cells by chemical transfection or electroporation. Therefore, we optimized a protocol of "Nucleoporation" technique to deliver the transgenes into nuclei of MC3T3-E1 cells, by utilizing a commercial "Nucleofection buffer" (Amaxa Inc) and "Gene Pulser" (Biorad). Briefly, 10^6 MC3T3-E1 cells were resuspended in 100 µl of nucleofector buffer T containing 5 µg of pHGCX/EphB2 plasmid DNA. The cells were then transferred into a 2-mm gap width electroporation cuvette, and electroporated at 160 V for 20 milliseconds, using a Gene

Pulser. After electroporation, the cells were transferred into prewarmed αMEM medium containing 10 % fetal bovine serum, 2 mM L-glutamine, 100 units/ml penicillin and 100 μg/ml streptomycin in 6-well plate, and cultured in a humidified 37 ^{0}C incubator with 5% CO_2. Twenty-four hours after transfection, the green fluorescent protein (GFP) reporter gene was expressed in most of MC3T3-E1 cells transfected with either control plasmid pHGCX or pHGCX/EphB2 (Figure 5A & B). Flow cytometry analyses revealed that 94.44% of the cells transduced with pHGCX and 94.42% of the cells transfected with pHGCX/EphB2 were GFP-positive (Figure 5C & D). We have repeated this experiment, and found that the efficiency of Nucleoporation was reliable. The transgene expression of EphB2 was easily detected by Western blot using specific antibody against mouse EphB2 (Figure 5E) 24 hours after transfection. The green fluorescent protein exprssed in transfected cells was visible 5 days after transfection.

In the proposal for the second 12 months, specific objective (i), we had developed simple protocols described above for efficient transfer of the complete coding seqnece of candidate genes into osteoblast cells in vitro for functional evaluation. We have demonstrated that clonging cDNA and packaging of the HSV-1 amplicon into infectious virion can be accomplished within short period of time (2 weeks). However, cloning cDNA and transfection by "Nucleoporation" can be finished in a week of work. By utilizing cDNA cloning strategy for the genes for which infectious BAC technique is not appropriate, we are able to search and test candidate genes in a QTL region. In addtion, a non-viral gene transfer provides a rapid, cost-effective and more efficient and safer cell-based model of high-thoughput screening of candidate genes.

Specific Objective 2: To isolate periosteal cells from mutant mice and transfect with one or more BAC clones.

In our previous studies, we have screened mutant mice generated by ENU, and identified a mouse line (12137M) with a phenotype of high bone density. To further test the candidate genes in bone cells in vitro, we have isolated periosteal cells from mutant mice. Briefly, 10 weeks-old 12137M mutant B6 mice were sacrificed, and the femur and tibias were removed. The bones were dissected free of soft tissue, and digested with 1 mg/ml collagenase in DMEM for 90 minutes at 37°C to isolate periosteal osteoblasts. The cells were then plated at a density of 10^5 per well in 6-well-plates and cultured in DMEM supplemented with 10% fetal bovine serum (FBS), 100 units/ml penicillin and 100 μg/ml streptomycin in a humidified 37 ^{0}C incubator with 5% CO_2. The control cells were isolated in identical manner from age-and sex-matched wild-type B6 mice. The cells were confirmed as osteoblasts by alkaline phosphatase (ALP) staining after vitamin D-induced differentiation. The periosteal osteoblasts at passages 2-3 were used for cell proliferation, differentiation, and apoptosis assays

In our initial studies, we used alamarBlue assay to examine the cell proliferation and viability. Briefly, 2 x 10^3 osteoblast cells per well in 96-well plates were incubated in DMEM supplemented with 10% calf serum (CS), 100 units/ml penicillin and 100 μg/ml streptomycin for 24 hours, followed by starvation in serum-free media for another 24 hours. The same number of cells in two paired wells were then cultured in the media supplemented with 10% CS and in serum-free media respectively for 48 hours at 37 ^{0}C. The cells were washed once in phosphate buffered saline (PBS), followed by 2-4 hours incubation at 37 ^{0}C in fresh culture media containing 10% alamarBlue. The plates were read on a fluorescent plate reader with excitation at 544 nm and emission at 590 nm. The proliferation rate was evaluated by comparing the uptake of alamar blue in the cells grown in the presence of 10% CS to the cells cultured in serum free media. Our experiments demonstrated that the proliferation of periosteal osteoblasts from mutant

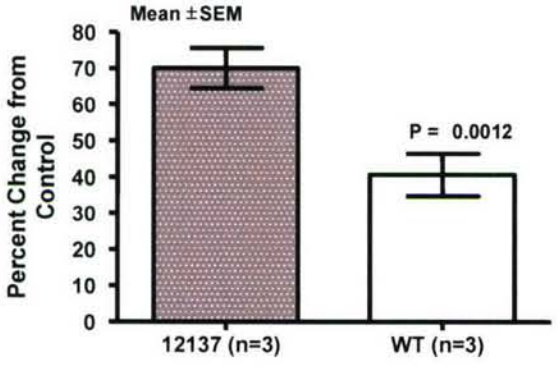

Figure 6. Proliferation rate determined by uptake of almarBlue dye in periosteal osteoblasts isolated from femur and tibia of 10-week 12137 mutant and WT mice. Equal number of cells was seeded at a density of 2000 cells/well in a 96 well plate and grown in presence of 10%FCS for 48 hours. Each column represents mean of 9 replicates including three from each animal. The differences between groups were analyzed by TTEST.

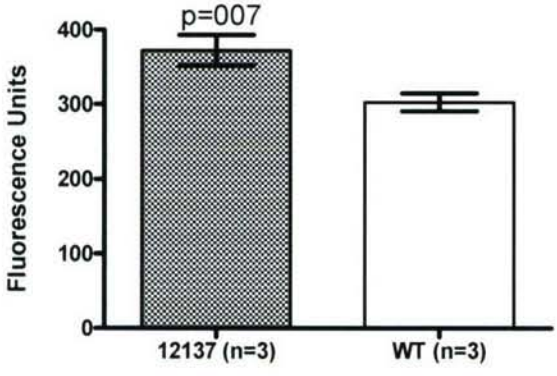

Figure 7. Caspase activity in periosteal osteoblasts isolated from 12137 and wild type mice. Equal number of cells was seeded at a density of 2000 cells/well in a 96 well plate and grown under serum-depleted conditions for 48 hours. Each column represents mean of 9 replicates including three from each animal. The differences between groups were analyzed by TTEST. WT=wild type

mice with high bone density was increased by 70% in the presence of serum whereas the proliferation of osteoblasts from wild-type mice was stimulated by 40% in the same culture conditions (P=0.0012) (Figure 6). In addtion to alamarBlue assay, we are currently comparing the cell proliferation in these two lines of mice by using [^{3}H] thymidine incorporation assay.

We have also compared apoptosis rate of the osteoblasts from mutant and wild-type mice by utilizing Homogeneous Caspase Assay. We quantified the activity of caspases 2, 3, 6, 7, 8, 9 and 10 to cleave fluorogenic tetrapeptide in isolated bone cells in vitro. Briefly, 2 x 10^3 osteoblast cells per well in 96-well plates were incubated in DMEM supplemented with 10% calf serum (CS), 100 units/ml penicillin and 100 µg/ml streptomycin for 24 hours. The cells were then washed once, and starved in serum-free media for 48 hours. The starved osteoblasts were then incubated in the culture media supplemented with 100 µl fluorogenic tetrapeptide for 1-24 hours at 37 ^{0}C. The fluorescence of the released Rhodamine was measured with an excitation filter 470-500 and emission filter 500-560. Our experiments have found that caspase activity in periosteal osteoblasts from mutant mice was significantly higher than the cells from wild-type mice (Figure 7). Our data indicate that increased osteoblast proliferation may contribute to the high bone density in mutant mice.

In conclusion, we have successfully isolated periosteal osteoblasts from mutant mice, and expended them in vitro for cell

proliferation, differentiation and apoptosis studies. We believe that the approaches of isolating periosteal cells, cell proliferation and apoptosis are useful for testing candidate genes in our future functional studies.

Specific Objective 3: To begin to evaluate the phenotypic change (cell proliferation/ differentiation/ apoptosis) in cells transfected with one or more BAC clones.

We have constructed three pHGCX-based cDNA expression vectors, and demonstrated that test genes were expressed in bone cells after viral or non-viral gene transfer. Since the endogenous EphB2 expression was undetectable in MC3T3-E1 cells by Western blot, we have begun to transfect the cells with pHGCX/EphB2, treated the cells with recombinant Ephrin B2 (0, 0.01, 0.1, 1 and 2 μg/ml), and examined the effect of EphB2 forward signaling on alkaline phosphotase (ALP) activity and cell proliferation (thymidine incorporation assay). In addition, we have planned to over-express Ephrin B2 MC3T3-E1 cells, and treat the cells with recombinant EphB2 extracellular domain (0, 0.01, 0.1, 1 and 2 μg/ml) to activate the Ephrin B2 reverse signaling, and test the cell differentiation and proliferation. We are also planning to carry out a co-culture of the mesenchymal stem cells (MSC) expressing Ephrin B2 and the osteoblast cells expression EphB2, and examine the cell migration.

In addition to the EphB2 gene, we are currently testing P37nb and RASSF1C genes in bone cells, and investigate their functions on the cell proliferation, differentiation and apoptosis.

Key Research Accomplishments

1) Have begun to test three candidate genes on cell proliferation, differentiation, migration and apoptosis in bone cells using viral and non-viral deliver approaches, and established that the expression of coding sequences of candidate gene can compensate for the limitation of infectious BAC gene transfer.
2) Have established in vitro functional assay using periosteal cells from mutant mice for in vitro testing of candidate genes.
3) Periosteal osteoblasts derived from high bone density mutant mice exhibited increased proliferation compared to control mice.

Reportable Outcomes

Xing W., Baylink D.J., Kesavan C., and Mohan S. Transfer of 128-kb BMP-2 Genomic Locus by HSV-Based Infectious BAC Stimulates Osteoblast Differentiation: A Platform for Functional Genomic Studies. ASBMR-2004, 19 suppl 1: S150, 2004

Xing W., Baylink D.J., Kesavan C., and Mohan S. HSV-1 Amplicon-Mediated Transfer of 128 kb BMP-2 Genomic Locus Stimulates Osteoblast Differentiation in vitro. Biochem Biophys Res Commun 319(3): 781-6, 2004

Conclusions

1) We have successfully cloned the complete coding sequence of candidate genes into pHGCX expression vector, and deliver the transgenes into osteoblast cells with high efficiency by utilizing either viral HSV amplicon system or non-viral "Nucleoporation" approach.

2) The osteoblast cells containing transgenes express high level of proteins for functional studies.

3) Transfer of the coding sequence of candidate genes into bone cells provides an alternative approach for functional studies when the infectious BAC technique is not applicable.

4) We have successfully isolated periosteal cells from mutant mice, and established the cell proliferation and apoptosis methods for future studies.

References

1. Adams, R. H., Diella, F., Hennig, S., Helmbacher, F., Deutsch, U., and Klein, R. The cytoplasmic domain of the ligand ephrinB2 is required for vascular morphogenesis but not cranial neural crest migration. Cell 104:57-69; 2001.
2. Amaar, Y. G., Baylink, D. J., and Mohan, S. Ras-Association Domain Family 1 Protein, RASSF1C, Is an IGFBP-5 Binding Partner and a Potential Regulator of Osteoblast Cell Proliferation. J Bone Miner Res 20:1430-9; 2005.
3. Compagni, A., Logan, M., Klein, R., and Adams, R. H. Control of skeletal patterning by ephrinB1-EphB interactions. Dev Cell 5:217-30; 2003.
4. Cortes, M. L., Bakkenist, C. J., Di Maria, M. V., Kastan, M. B., and Breakefield, X. O. HSV-1 amplicon vector-mediated expression of ATM cDNA and correction of the ataxia-telangiectasia cellular phenotype. Gene Ther 10:1321-7; 2003.
5. Lenz, P., Bacot, S. M., Frazier-Jessen, M. R., and Feldman, G. M. Nucleoporation of dendritic cells: efficient gene transfer by electroporation into human monocyte-derived dendritic cells. FEBS Lett 538:149-54; 2003.
6. Robling, A. G., Li, J., Shultz, K. L., Beamer, W. G., and Turner, C. H. Evidence for a skeletal mechanosensitivity gene on mouse chromosome 4. Faseb J 17:324-6; 2003.
7. Segev, O., Samach, A., Faerman, A., Kalinski, H., Beiman, M., Gelfand, A., Turam, H., Boguslavsky, S., Moshayov, A., Gottlieb, H., Kazanov, E., Nevo, Z., Robinson, D., Skaliter, R., Einat, P., Binderman, I., and Feinstein, E. CMF608-a novel mechanical strain-induced bone-specific protein expressed in early osteochondroprogenitor cells. Bone 34:246-60; 2004.
8. Strausberg, R. L., Feingold, E. A., Grouse, L. H., Derge, J. G., Klausner, R. D., Collins, F. S., Wagner, L., Shenmen, C. M., Schuler, G. D., Altschul, S. F., Zeeberg, B., Buetow, K. H., Schaefer, C. F., Bhat, N. K., Hopkins, R. F., Jordan, H., Moore, T., Max, S. I., Wang, J., Hsieh, F., Diatchenko, L., Marusina, K., Farmer, A. A., Rubin, G. M., Hong, L., Stapleton, M., Soares, M. B., Bonaldo, M. F., Casavant, T. L., Scheetz, T. E., Brownstein, M. J., Usdin, T. B., Toshiyuki, S., Carninci, P., Prange, C., Raha, S. S., Loquellano, N. A., Peters, G. J., Abramson, R. D., Mullahy, S. J., Bosak, S. A., McEwan, P. J., McKernan, K. J., Malek, J. A., Gunaratne, P. H., Richards, S., Worley, K. C., Hale, S., Garcia, A. M., Gay, L. J., Hulyk, S. W., Villalon, D. K., Muzny, D. M., Sodergren, E. J., Lu, X., Gibbs, R. A., Fahey, J., Helton, E., Ketteman, M., Madan, A., Rodrigues, S., Sanchez, A., Whiting, M., Young, A. C., Shevchenko, Y., Bouffard, G. G., Blakesley, R. W., Touchman, J. W., Green, E. D., Dickson, M. C., Rodriguez, A. C., Grimwood, J., Schmutz, J., Myers, R. M., Butterfield, Y. S., Krzywinski, M. I., Skalska, U., Smailus, D. E., Schnerch, A., Schein, J. E., Jones, S. J., and Marra, M. A. Generation and initial analysis of more than 15,000 full-length human and mouse cDNA sequences. Proc Natl Acad Sci U S A 99:16899-903; 2002.
9. Wade-Martins, R., Saeki, Y., and Antonio Chiocca, E. Infectious delivery of a 135-kb LDLR genomic locus leads to regulated complementation of low-density lipoprotein receptor deficiency in human cells. Mol Ther 7:604-12; 2003.

10. Xing, W. B., D.; Kesava, C.; Hu, Y.; Chadwick, R.; Kapoor, S.; Mohan, S. Global gene expression analysis in the bones reveals involvement of several novel genes and pathways in mediating an anabolic response of mechanical loading in mice. Journal of Cellular Biochemistry In press; 2005.

Project 4: The Application Of Transgenic Mice To Assess Gene Function In Mechanical Loading And In Bone Fracture Healing Models

Introduction

Bone formation in response to exercise or injury requires the coordinated interactions of a number of molecular pathways of gene expression. However, a more complete understanding of gene expression in bone formation and fracture repair requires definitive proof of the functional significance of the genes that regulate the molecular pathways. In this regard, the analysis of mice engineered to be deficient in the expression of a particular gene-of-interest (i.e., knockout mice) is especially valuable. The study of knockout mice provides conclusive evidence of the functional significance of particular genes in the development and repair of bone. The use of knockout mice in studies of bone development and repair will eventually help to elucidate the regulation of their molecular regulatory pathways, and suggest therapeutic strategies and gene candidates to augment or accelerate bone formation and repair.

We have utilized commercially available knockout mice to determine what effect the absence of expression a particular gene of interest has on bone formation in response to mechanical loading and in fracture repair. Not only will the examination of bone formation and repair characterize the functional effects of the knockout gene deficiency in each case, but subsequent examination of the expression of other genes in knockout mouse tissues will help to define the regulatory networks that modulate the observed knockout phenotype. Ultimately, this approach will suggest additional gene candidates for therapeutic alternatives in bone formation and healing.

Body

1. Technical Objectives

Our Technical Objectives were as follows:

Technical Objective 1: The functional significance of a gene of interest on bone formation will be identified by characterizing the skeletal phenotype in mice deficient in that gene (i.e., knockout mice) in response to mechanical loading of the bone by exercise.

Our Specific Objectives during the second 12 months of this grant period were as follows:

1) To complete the identification of phenotypic differences between 3 strains of knockout mice and wild-type control mice by peripheral quantitative computed tomography (pQCT), micro-CT measurements, histological examination and molecular marker expression of the bone response to mechanical loading. This Specific Objective began in the first year of the study.

2) To apply microarray technology to study gene expression in the loaded bones of the one strain of knockout mice that exhibited the greatest phenotypic differences in bone response to mechanical loading.

Technical Objective 2: The functional significance of a gene of interest on bone formation in response to injury will be identified by characterizing the skeletal phenotype in mice deficient in that gene (i.e., knockout mice) during fracture healing.

Our Specific Objectives for fracture repair during the second 12 months of this grant period were as follows:

1) To complete the identification of phenotypic differences between 3 strains of knockout mice and wild-type control mice by X-ray examination, pQCT measurements, micro-CT measurements and histological examination of the fracture callus tissues. This Specific Objective began in the first year of the study.
2) To apply microarray technology to study gene expression in the fracture tissues of the one strain of knockout mice that exhibited the greatest phenotypic differences in fracture healing.

Knockout Mouse Strains

Table 1. Knockout Mice with Phenotypes for Mechanical Loading and Fracture Studies

Gene	JAX[1] Stock #	Genotype[2]	Phenotype
Leptin	0632	B6-*Lep* ^{ob}	NIDDM, obese, delayed wound healing
Bax	2994	B6.129X1-*bax* ^{tm1Sjk}	delayed apoptosis, organ defects (gonads)
Serpine	2507	B6.129S2-Serpine1^{tm1Mlg}/J	enhanced wound healing

1: JAX, The Jackson Labs
2: The wild-type control strain genotype is C57BL/6 (B6) for "Leptin", "Bax" and "Serpine" knockout mice.

a) Leptin Knockout (Obese) Mice:

Leptin, a 16 kDa protein, expressed predominantly in adipose tissue, functions as a hormone that keeps the brain apprised of the amount of body fat and regulates carbohydrate metabolism (3). This mouse is also a model for non-insulin dependent (NIDDM, Type 2) diabetes (Table 1). Other functions related to bone formation include:

i) Stimulating osteoblastic differentiation and mineralization of bone matrix (4).
ii) Stimulating the development of the periosteal envelope in growing bone (5).
iii) Bone formation increases by peripheral leptin administration and decreases by third ventricle leptin infusion in *ob/ob* mice (6). The systemic versus local effects of leptin on the fat and bone cell lineages are not well characterized, though osteoblasts do have leptin-specific receptors (7).

The heterozygous ob/ob knockout breeder mice were purchased from the Jackson Labs and bred in our animal facility. Because of the character of recessive inheritance, only ¼ of pups were expected to be homozygous. The homozygous mice were identified by both the obese phenotype and PCR-based genotyping for the ob mutation.

b) Bax Knockout Mice:

Bax, the Bcl-2-associated X protein and a member of the Bcl-2 protein family, binds to Bcl-2 to form a heterodimeric complex. It functions to oppose Bcl-2 and promote apoptosis (8). The Bax/Bcl-2 ratio controls the apoptosis frequency in each cell. Both genes are expressed in cartilage and bone cells in the rat (9). Apoptosis has a major impact on skeletal development and remodeling, and is essential for the elimination of osteoblasts during skeletal development

(reviewed in 10). The frequency of osteoblast apoptosis controls osteoblast lifespan and bone formation during the postnatal life (reviewed in 11).

Heterozygous breeder mice were purchased from the Jackson Labs and inbred in our animal facility. Only ¼ of all pups were expected to be homozygous mice, and all mice were identified by PCR-based genotyping for the Bax gene deletion. There is no obvious Bax mouse phenotype.

c) Serpine Knockout Mice:

The fibrinolytic system has been claimed to play a very important role in a variety of biological phenomena, such as maintenance of vascular patency, inflammation, embryogenesis, angiogenesis and tissue remodeling processes. Activation of plasminogen by tissue-type plasminogen activator (t-PA) is believed to be required for these functions. However, specific plasminogen activator inhibitor (PAI; Protease Nexin-1, PN-1) appears to be the primary physiological inhibitor for this fibrinolytic system. Theoretically, the removal of PAI should result in more or faster plasminogen activation and enhance the process of fibrin-specific clot lysis, promoting healing after fracture or other tissue injury (reviewed in 12).

Homozygous breeder mice (PAI-1 deficiency), in which the Serpine-1 gene is disrupted (13), were purchased from the Jackson Labs and bred in our animal facility. The homozygous mutants have a mild hyperfibrinolytic state but normal hemostasis. There is no obvious serpine knockout mouse phenotype. The genotype of all breeders and pups was identified by PCR-based genotyping for the serpine-1 gene deletion.

The homozygous Npr3 (Natriuretic peptide receptor-3, "Longjohn") knockout mouse (14) was originally intended as one of the knockout mouse strains for studies on bone formation and repair (15), and was purchased from the Jackson Labs. However, the pups bred in our animal facility failed to show the described phenotype, and we suspected that the genotype of the supplied breeder pairs had been misidentified. Sequence analysis failed to identify the Npr3 point mutation and confirmed that the genotype of the mice acquired from the Jackson Labs was in fact wild-type DBA, and not the knockout Longjohn mice. Unfortunately, considerable effort was expended to establish this colony and begin the studies during the first year of this project before our suspicions were confirmed. We therefore acquired the serpine (Protease Nexin-1, PN-1) as the third knockout mouse strain for the proposed studies.

2. Progress on Technical Objectives

Technical Objective 1:

Mechanical loading determines both the mechanical density and the architecture of bone. Previous studies have established changes in bone mineral content and bone mineral density in response to exercise among boys (1), and our own studies have demonstrated that mechanical loading by exercise increased bone formation in mice (2). In this study, we used knockout mice to identify and characterize the functional effects of exercise-induced bone formation in mice deficient for a gene-of-interest previously implicated in bone growth or development, or in wound healing (Table 1, "Leptin", "Bax" and "Serpine" mice). The phenotypic response to mechanical loading in the particular strain of knockout mouse was correlated to pQCT and molecular measurements of bone formation.

Specific Objective 1: to complete the identification of phenotypic differences between 3 strains of knockout mice and wild-type control mice by peripheral quantitative computed tomography

(pQCT), micro-CT measurements, histological examination and molecular marker expression of the bone response to mechanical loading.

Leptin Knockout Mice

Findings

A four-point bending mechanical loading procedure that approximates exercise was developed. It consisted of a 12-day four-point bending routine of a 9 Newton (N) force applied at 2 Hertz (Hz) and 36 cycles to the right tibia. This routine was developed from a load response trial that tested bone formation in response to loads of 6N through 9N, with the 9N load established as producing the optimal bone response, as measured by pQCT analysis and the expression of molecular markers of bone formation.

Microstrain gauge test:

For an accurate comparison of bone response after loading between two strains of mice, the larger tibias encountered in the leptin mice must be normalized to their wild-type control bones through force-induced strain. Thus, we measured the tibial Moment of Inertia (MOI) and periosteal circumference (PC) by pQCT and calculated the strains by different loading forces using the formula: Strain = F x L x C/(2 x I x E), I = moment of inertia, C = bone radius, E = 38 Gpa, a coefficient, L = a distance between loading parts. We established the theoretical linear relationship of loading force and strain in B6 and leptin mice (Figure 1). To demonstrate the accuracy of theoretical calculation curve, actual strain was measured using strain gauges for several different loading forces in male, female B6 and Leptin KO mice.

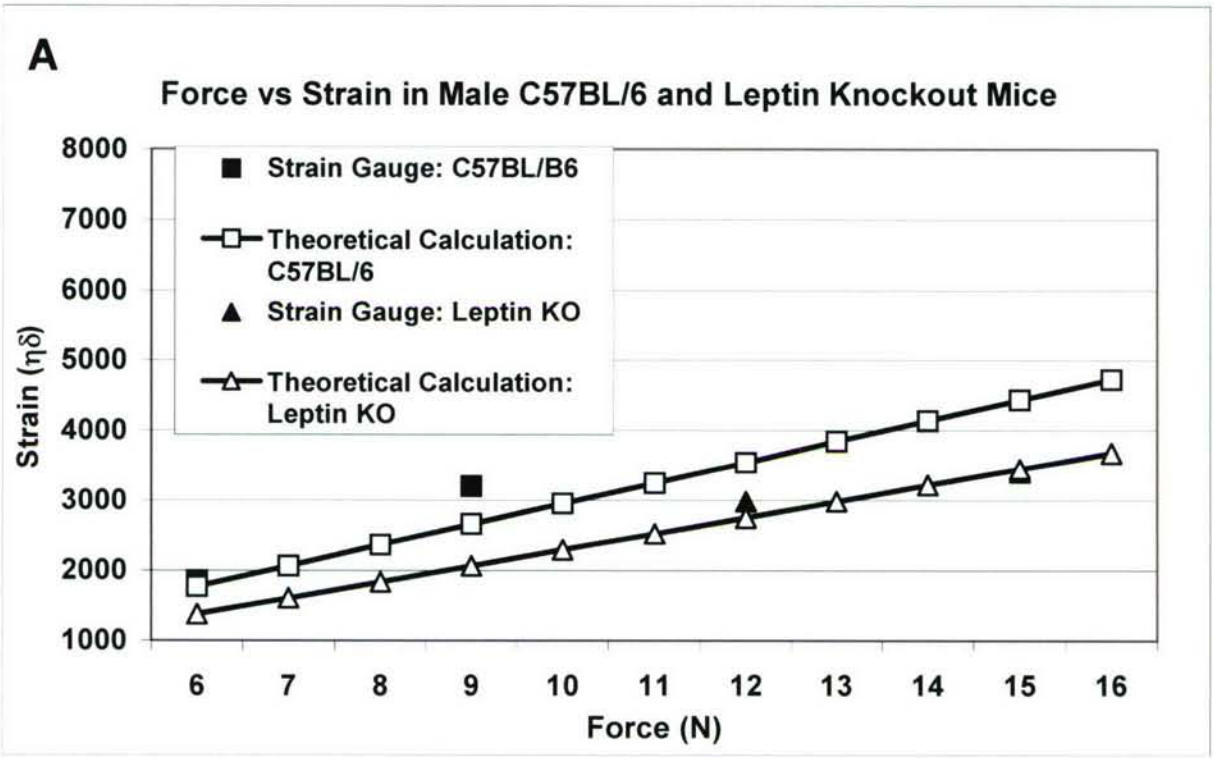

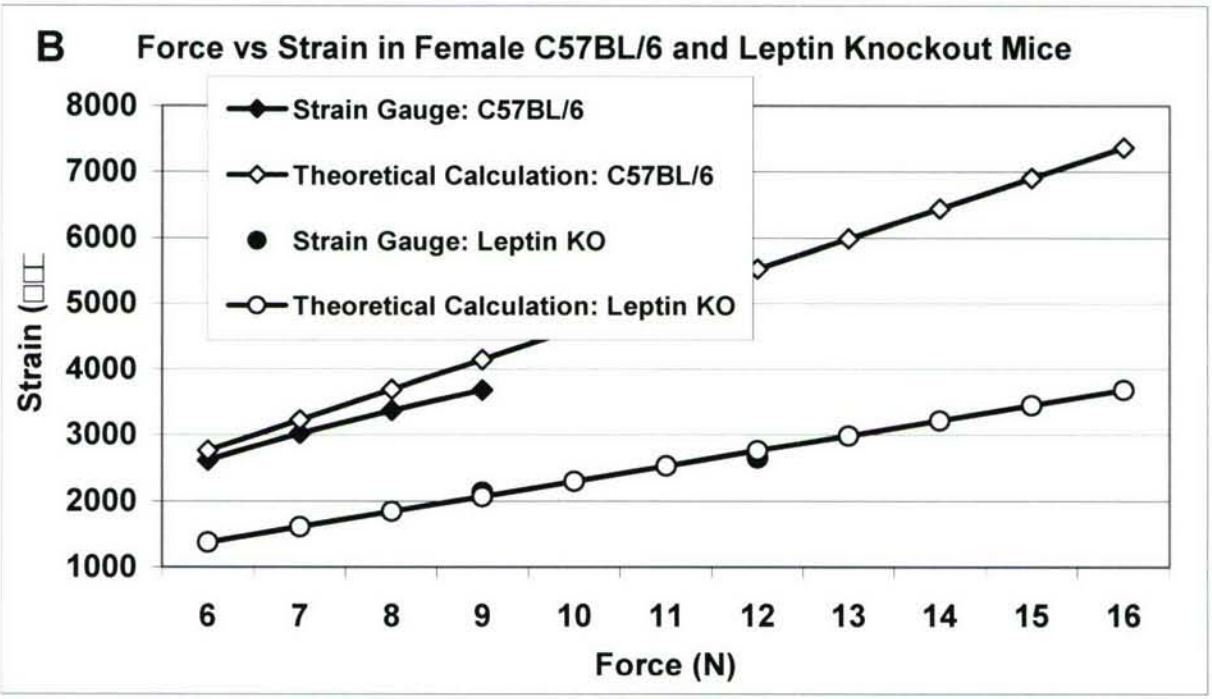

Figure 1. Microstrain analysis of mechanical loading forces in male (A) and female (B) leptin knockout (KO) and C57BL/6 wild-type control mice. Theoretical calculations of strain were compared with strain gauge measurements at different forces. Strain gauge measurements in (A) at 6N in the

C57BL/6 mice and 12N in the leptin knockout mice are so close to theoretical calculations that the data points are barely visible under the theoretical data points at these forces. This is also true of the 9N and 12N strain gauge measurements of the leptin knockout female mice in (B).

Findings from the microstrain gauge test:

1. From our theoretical calculation curve, leptin knockout male and female mice share a same force-strain relationship curve, as they share the same bone PC and MOI. However, the strain is much higher in female C57BL/6 than in male C57BL/6 mice under identical loading force. This is because female mice have a smaller PC than male mice, resulting in a higher loading force/area unit. The strain in leptin male and female knockout mice is lower than that in female and male C57BL/6 mice under the same loading force. For example, at a force of 9N, we observe a strain 4145 με in female C57BL/6, 2659 με in male C57BL/6, and 2067 με in male and female leptin knockout mice.
2. From the strain gauge test results (Figure 1), we found that the leptin knockout mice displayed a much lower microstrain (2129) in response to 9N load, as we expected, than the control C57BL/6 mice displayed for the same 9N load (3600 microstrain). In both cases, several of the parameters measured in the loaded bone displayed significant changes ($p<0.05$) as compared to the unloaded bone.
3. C57BL/6 mice were then tested for their mechanical response at a load of 6N, a load found to produce a microstrain of 2500, close to the 9N, 2129 microstrain produced by the bone size differences in the leptin knockout mice (Figure 1). Based on our strain gauge data in control mice tibia at 2500 microstrain, we did not find any significant change ($p<0.05$) in the bone parameters in the loaded bone as compared to the unloaded bone. This observation at 6N loading contrasts with the 9N loading routine, and confirms that microstrain normalization is important to accurately measure differences in bone of different sizes.

This mechanical loading routine was then performed on the right tibia of 6 female and 6 male leptin knockout mice and 12 female and 9 male B6 control mice at 10 weeks of age. For the desired equivalent microstrain, a 9N load was applied at 2 Hertz (Hz) for 36 cycles for 12 consecutive days to the leptin knockout mice, and compared with an identical approach using 6N for the B6 mice. pQCT measurements on both tibias were performed after the final loading on the 12^{th} day and the data were collected and analyzed. The pQCT thresholds were 180-730, designed to detect the low-density bone that might be produced by mechanical loading by this time. Statistical analysis was performed by t-test and the results were deemed significant at $P<0.05$.

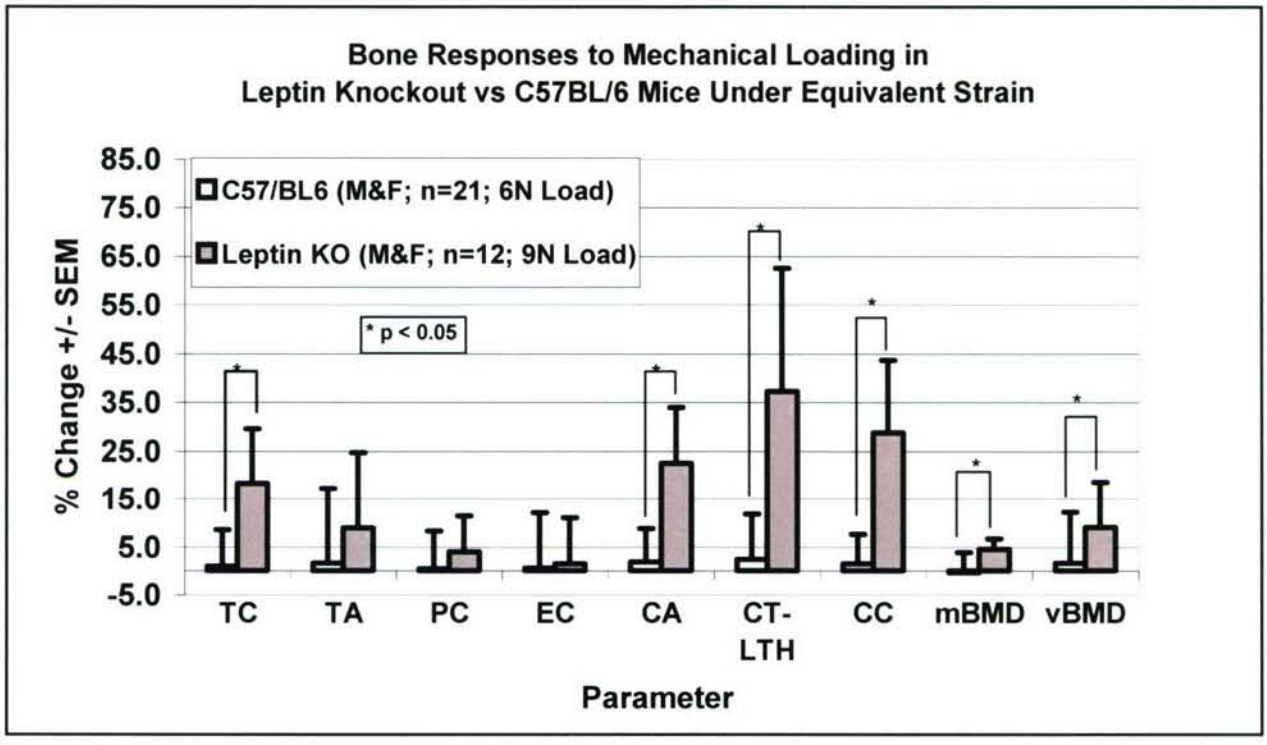

Figure 2. Bone responses to mechanical loading in leptin knockout (KO) and C57BL/6 wild-type control mice under forces providing equivalent strain. The loaded and unloaded contralateral tibias were compared for bone formation by pQCT following the final loading. Males and females were combined for analysis. The bone parameters examined in knockout and C57BL/6 wild-type control mice were total bone mineral content (TC), total bone area (TA), periosteal circumference (PC), endosteal circumference (EC), cortical area (CA), lower pQCT threshold cortical thickness (CT-LTH), cortical ontent (CC), total bone mineral density (mBMD), and volumetric bone mineral density (vBMD).

Findings from the four-point mechanical loading test in the leptin knockout mice:

There were statistically significant differences in the response of the bone parameters to the 9N mechanical loading routine in the leptin knockout mice as compared to the wild-type control mice applied to 6N loading. By measures of trabecular bone mineral content, cortical area, cortical thickness, cortical bone mineral content, total and volumetric bone mineral density, leptin knockout mice show more sensitivity of loading response than C57BL/6 mice at an equivalent microstrain (Figure 2).

These results confirm that, when the loading routine is normalized for bone size, the absence of leptin expression does indeed affect the cortical and total bone mineral content and bone mineral density in response to mechanical loading. These differences were too subtle to be observed by an examination of the bone histology. Measurements by histomorphometry were therefore not pursued. The increase in these parameters must reflect leptin effects on bone formation and deserves further study in this regard, in addition to the obvious involvement of obesity in skeletal loading. Micro-CT measurements were not attempted, both because of the success of the pQCT measurements (Figure 2) and the availability of the micro-CT instrument, which was undergoing repair at the institution where it is housed. Confirmation of bone formation by measurement of molecular markers of bone formation is underway on total RNA purified from loaded leptin knockout bones. The primers for bone marker genes (mouse collagen-1 and osteocalcin) and housekeeping control genes (mouse cyclophilin) have been

successfully developed, and real-time PCR conducted indicate that these molecular markers of bone formation can be used to identify differences in bone formation between wild-type and knockout mice.

Bax Knockout Mice

The mechanical loading routine was then performed on the right tibias of 5 Bax knockout mice and 7 male C57BL/6 control mice at 10 weeks of age. Because the bone sizes of these strains were very similar, both received a 6N load applied at 2 Hertz (Hz) for 36 cycles for 12 consecutive days. pQCT measurements on both tibias were performed after the final loading on the 12th day and the data were collected and analyzed. Statistical analysis was performed by t-test and the results were deemed significant at $P<0.05$.

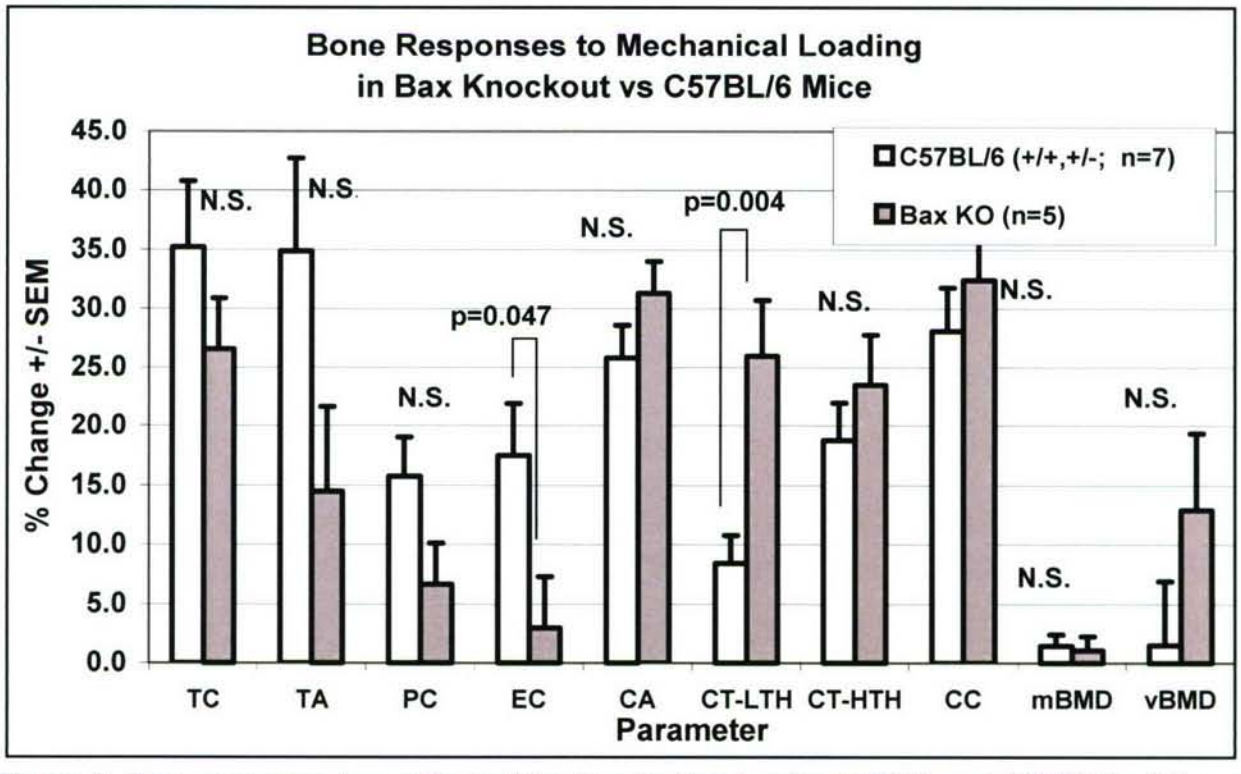

Figure 3. Bone responses to mechanical loading in Bax knockout (KO) and C57BL/6 wild-type control mice under equivalent force (6N). The loaded and unloaded contralateral tibias were analyzed for bone formation by pQCT following the final loading. Only male mice were examined. A comparison of Bax heterozygous littermates (+/-) revealed no significant differences from the C57BL/6 wild-type (+/+); they were combined for the analysis. The bone parameters examined in knockout and C57BL/6 wild-type control mice were total bone mineral content (TC), total bone area (TA), periosteal circumference (PC), endosteal circumference (EC), cortical area (CA), lower pQCT threshold cortical thickness (CT-LTH), higher pQCT threshold cortical thickness (CT-LTH), cortical content (CC), total bone mineral density (mBMD), and volumetric bone mineral density (vBMD).

Findings from the four-point mechanical loading test in the Bax knockout mice:

There were statistically significant differences in the response of only very few of the bone parameters in the Bax knockout mice as compared to the wild-type control mice applied at 6N loading (Figure 3). Bax knockout mice did display significant differences in the responses of the

endosteal circumference and the cortical thickness, when the latter was measured at a lower threshold (Figure 3, CT-LTH) to identify lower density cortical bone. These differences were subtle in effect and could not be observed in an examination of the bone histology, so measurements by histomorphometry were not possible. Determination of the expression of two molecular markers of bone formation from the RNA repertoire of Bax knockout and control mice was undertaken; real-time PCR analysis of osteocalcin and collagen-1 gene expression with gene-specific primers also revealed no significant differences in Bax knockout bone response to mechanical loading (Figure 4). Micro-CT measurements were not attempted, both because of the success of the pQCT measurements and the availability of the micro-CT instrument, which was undergoing repair. By pQCT measurements, however, the leptin knockout mice produced a more dramatic response to mechanical loading and were at this point the choice for microarray analysis of gene expression induced by mechanical loading.

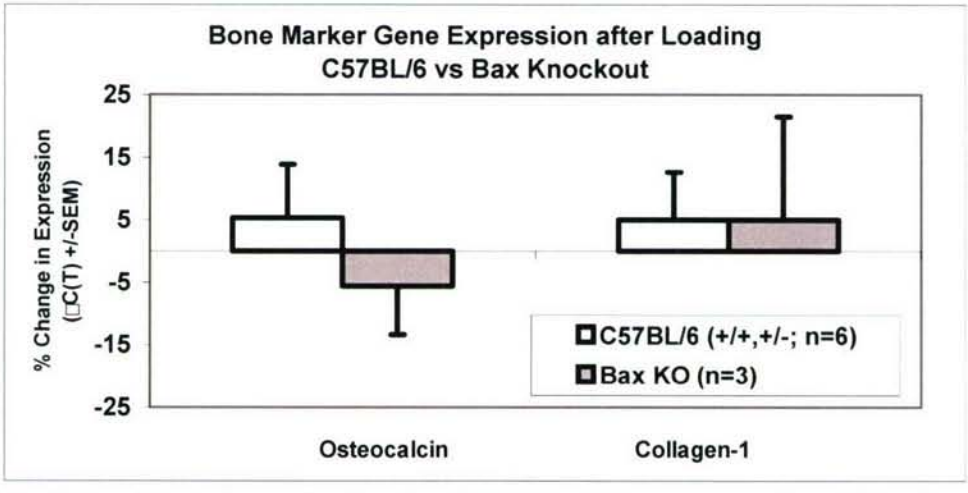

Figure 4. Real-time PCR determination in C57BL/6 wild-type control and Bax knockout (KO) bones after mechanical loading. Six control mice (homozygotes and heterozygotes) were compared with 3 Bax knockout mice. Expression was determined through the change in PCR cycle number on osteocalcin and collagen-1 gene expression in total RNA isolated from tibias subjected to mechanical loading. No significant changes in gene expression were observed.

Serpine Knockout Mice

The serpine mouse mechanical loading study has suffered from delayed purchasing and breeding, but several litters of pups are approaching the appropriate 10-week age for analysis, which is expected to be conducted during the next two months.

Specific Objective 2: to apply microarray technology to study gene expression in the loaded bones of the one strain of knockout mice that exhibited the greatest phenotypic differences in bone response to mechanical loading.

RNA has been isolated from 6 leptin knockout and 6 C57BL/6 wild-type control tibias that underwent the leptin-designed mechanical loading routine. Microarray analysis using our in-house mouse gene chip with 28,000 unique targets is set to begin immediately and should be completed in one month.

This Specific Objective was not completed, largely due to difficulties in acquiring sufficient numbers of leptin knockout mice through our breeding program, as well as technical difficulties

with the strain gauge measurements that were necessary for accurate measurements of the response to mechanical loading. These mice were also variably sensitive to the gas anesthesia used to immobilize them for the loading routine, which often produced a high mortality.

Technical Objective 2:

During the first twelve months of the study, the functional significance of a knockout gene of interest in fracture repair was initiated by a comparison of femur fracture healing in knockout mice deficient in that gene with wild-type control mice.

The three knockout mouse strains used in the exercise study (Technical Objective 1) were also used in this study (Table 1, "Leptin", "Bax" and "Serpine" mice). A description of each knockout mouse, the relevance of the phenotype to bone formation in mechanical loading and fracture repair and the results of our breeding program are provided (above).

Bone formation was measured following healing intervals that have been determined to provide characteristic landmarks of fracture callus maturation in our pilot experiments in wild-type mice. The phenotypic response to fracture healing in the particular strain of knockout mouse was correlated to X-ray and molecular measurements of bone formation and histologic examination of the fracture tissues. These measurements were used to determine whether the knockout gene-of-interest was functionally significant in fracture healing, and which fracture tissues were affected by the absence of its expression.

Specific Objective 1: to complete the identification of phenotypic differences between 3 strains of knockout mice and wild-type control mice by X-ray examination, pQCT measurements, micro-CT measurements and histological examination of the fracture callus tissues.

The femur fracture model was developed in the first year of this study and was applied to all 3 knockout mouse strains and the C357BL/6 wild-type control strain. Briefly, an intramedullary pin was surgically implanted in the femur prior to fracture and the skin incision closed. A diaphyseal fracture was produced by the three-point bending technique (16). This procedure produced fractures that were consistently transverse and midshaft, and provided a uniform basis for the comparison of the differences in fracture healing between wild-type and knockout mice.

The development of the fracture callus during healing was examined by X-ray, pQCT and histology. For the analysis of callus development, it was necessary to adapt the pQCT analysis to quantify soft and hard tissues of the maturing fracture callus. We therefore scanned the bone at high resolution 1 mm intervals along the length of the fracture callus. The thresholds of the pQCT analysis were adjusted so that only the lower density (noncortical) bone or soft tissue was measured. The values at each 1 mm scan interval were added together to quantify the bone mineral content of the entire fracture callus. In this way, we used pQCT data to analyze the development of the soft and hard callus and identify differences between wild-type (normal) and knockout (altered) healing in mice. The pQCT parameters and their threshold settings used to quantify the fracture callus were the:

1) bone mineral content of the lower density fracture callus and intramedullary bone, at threshold 214-570, a measurement of the bone in the fracture callus, excluding the cortical bone.
2) cross-sectional area of the lower density fracture callus and intramedullary bone, at threshold 214-570, a measurement of the cross-sectional area of the bony fracture callus, excluding the cortical bone.

3) cross-sectional area of the soft tissue and lower density fracture callus and intramedullary bone, at threshold 0-570, a measurement of the cross-sectional area of all bony and soft tissue of the fracture callus, excluding the cortical bone.

Because the C57BL/6 is the background strain on which all 3 knockout mouse strains have been developed, the same C57BL/6 mice served as controls for the X-ray and pQCT analysis of all 3 knockout mouse strains. Statistical analysis was performed by least significant analysis test, and deemed significant at $p<0.05$. Micro-CT measurements were not attempted because of the unavailability of the micro-CT instrument, which was undergoing repair.

Findings

Leptin Knockout Mice

An initial examination of the fracture calluses by X-rays revealed that the healing was very similar in leptin knockout and control mice throughout healing (Figure 5). Because differences were difficult to quantify visually, pQCT measurements of the fracture bone mineral content, bony cross-sectional area and total callus hard and soft tissue area were undertaken for all samples (Figures 6, 7, 8).

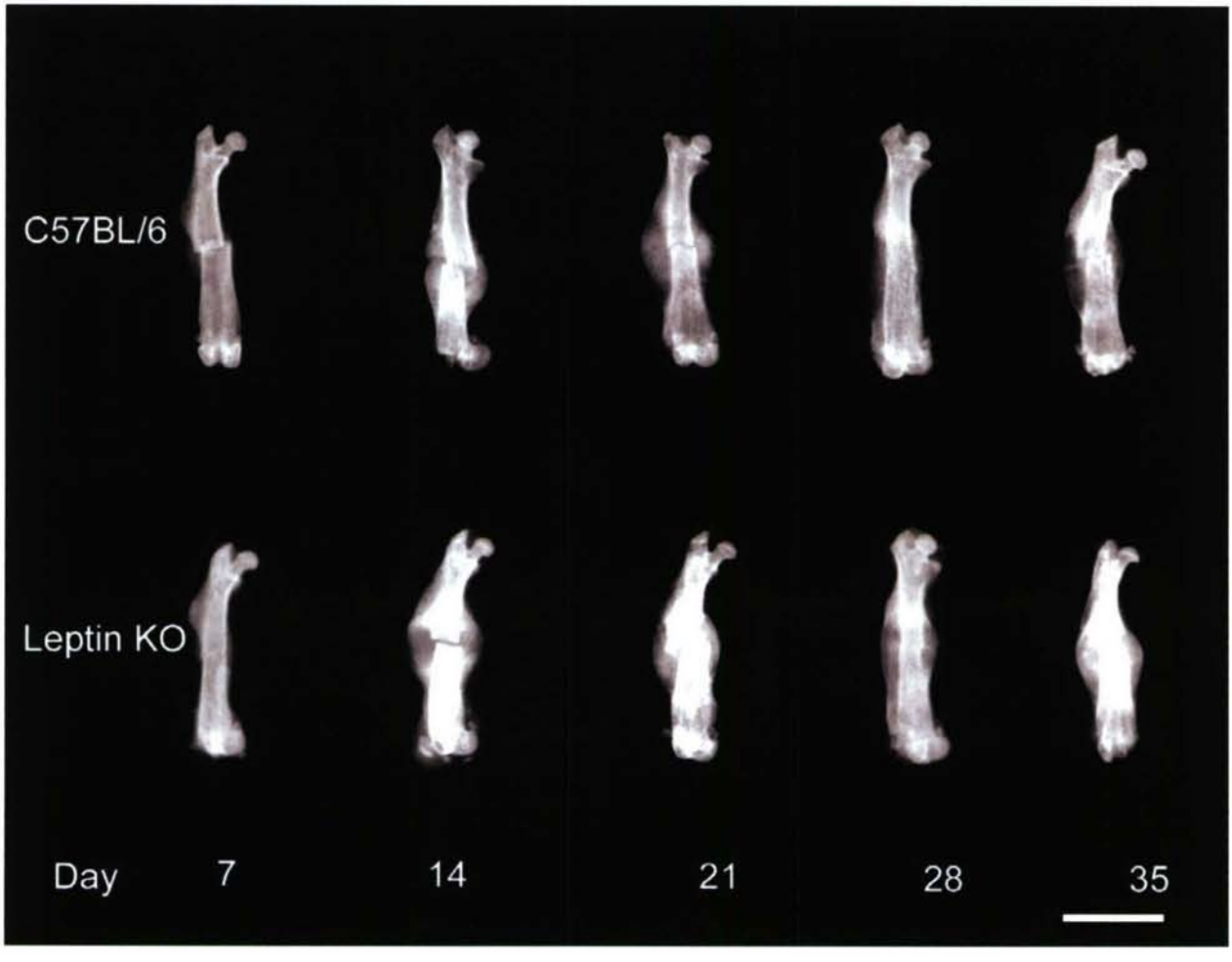

Figure 5. X-ray photograph of healing mouse fractured right femurs in leptin knockout (KO) mice compared with C57BL/6 wild-type mice at 7, 14, 21, 28, and 35 days post-fracture. The X-ray contains representative femur fractures from 6 male leptin knockout mice were compared with 4 male control mice at each post-fracture time. The development of the mineralized (hard) callus can be monitored from its early stages, at 7 days, through its maximum, at 14 to 21 days, and into remodeling to cortical bone at 28 days. Each stage has characteristic features for comparison to impaired fracture repair. Healing is defined as that point when the bony tissue of the hard callus bridges the fracture gap, usually after 28 days in the mouse; remodeling to cortical bone continues after this time, eventually resolving the fracture callus. Scale bar = 5 mm.

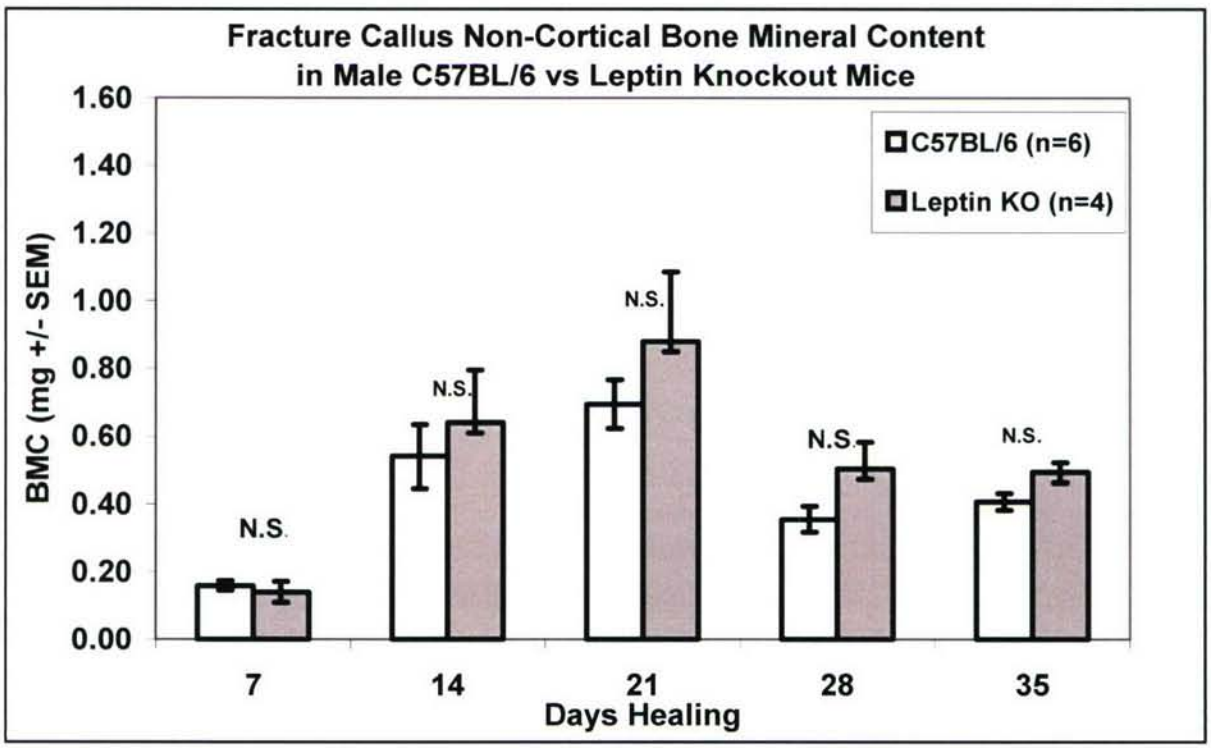

Figure 6. Bone mineral content after femoral fracture in male leptin knockout (KO) and C57BL/6 wildtype control mice. This profile of the bone mineral content during healing is typical of normal fracture healing.

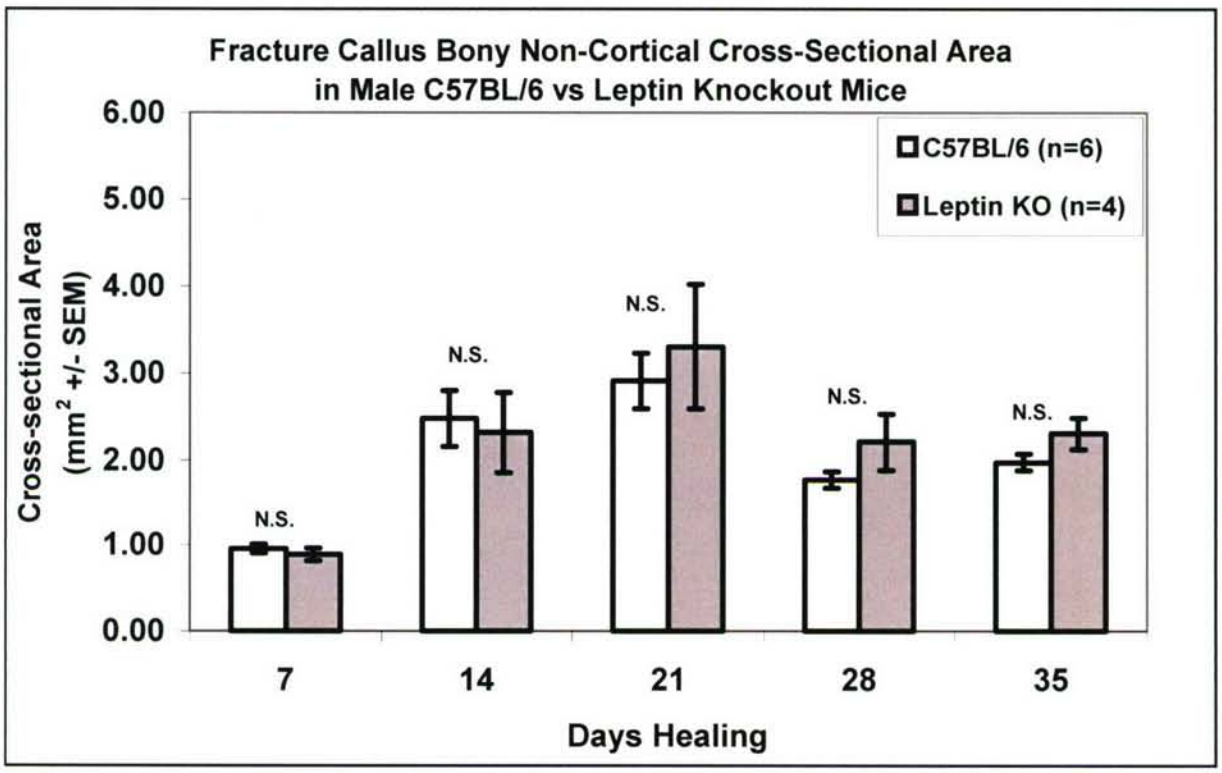

Figure 7. Cross-sectional area of the bony fracture callus after femoral fracture in male leptin knockout (KO) and C57BL/6 wildtype control mice. This profile of this area during healing is typical of normal fracture healing.

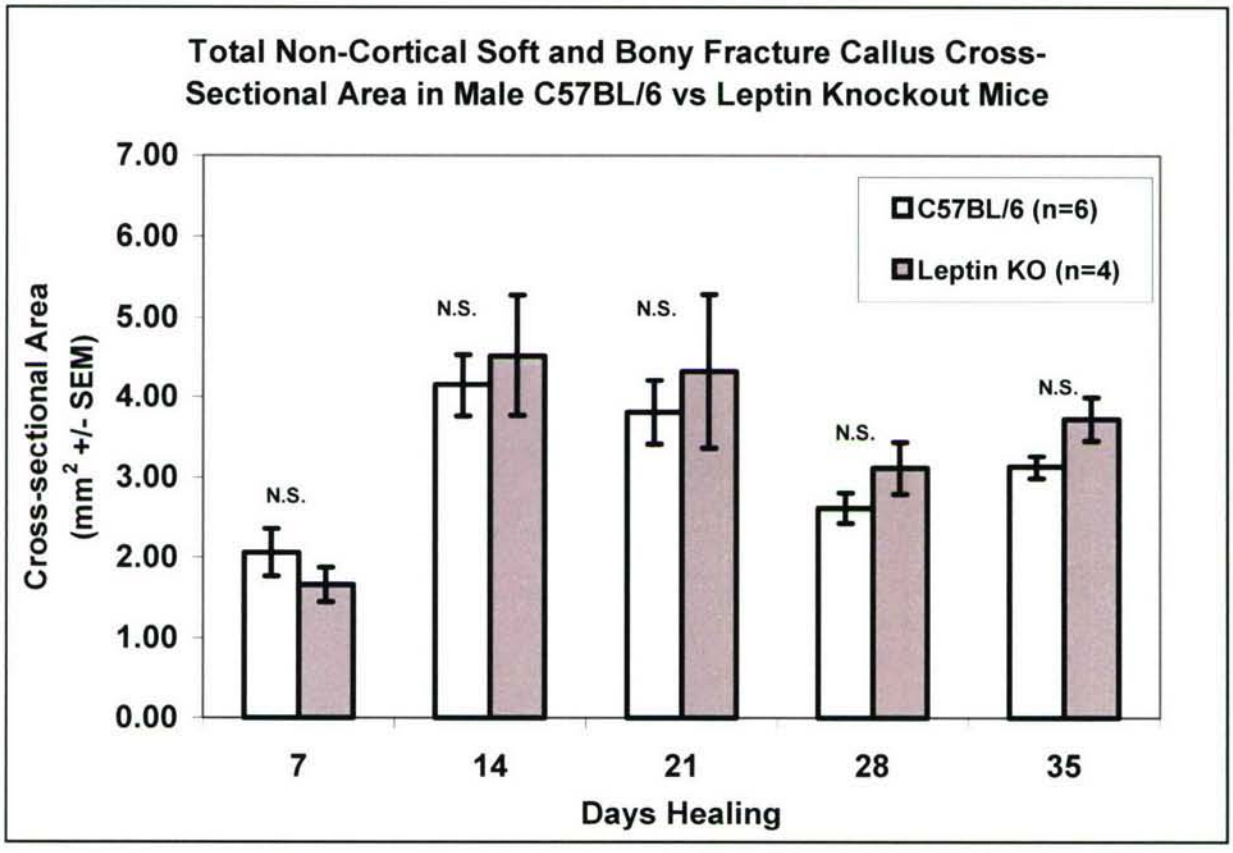

Figure 8. Cross-sectional area of the total fracture callus (soft and bony tissue) area after femoral fracture in male leptin knockout (KO) and C57BL/6 wildtype control mice. This profile of this area during healing is again typical of normal fracture healing.

The pQCT data for each of the 5 post-fracture healing times was collected in the leptin knockout and C57BL/6 mice. As observed in the X-ray, the bone mineral content of this low-density callus bone peaked at 14 and 21 days, and then declined upon remodeling later in healing. Based upon the numbers of animals examined to date, at no time during healing did the leptin knockout mice display any significant changes in the bone content or cross-sectional area of the bony tissue or total tissue. The different phases of callus development that are manifested in these callus parameters were therefore normal during fracture healing in this knockout mouse strain. The leptin knockout mice probably had additional conditions, such as diabetes, that contributed to fracture healing. If micro-CT analysis becomes available, leptin knockout fracture calluses will be examined to obtain a higher resolution measurement of healing.

Unfortunately, there was a higher than expected mortality in leptin knockout mice after surgery, and more than 50% of the mice often died due to difficulties following surgical anesthesia. We are modifying the anesthesia by incorporating an isofluorane anesthesia procedure to minimize mortality. The leptin knockout mice also bred more slowly than expected, limiting the total number of homozygous mice to 15 that entered the fracture repair study. Breeding sufficient numbers of this mouse proved to be difficult due to litter mortality. The mothers often ignored or cannibalized the pups, especially if they were the first litter. Surprisingly, the yield of homozygote knockouts, expected to be approximately 25% of the litter,

was found by genotyping to be much lower. This analysis is currently being completed with additional animals.

Additional Findings in the Leptin Knockout Mice

As initially considered in the mechanical loading studies conducted on the tibias, measurement of the unfractured contralateral bones of male leptin knockout mice in the fracture study revealed surprising changes in femur size relative to male wild-type mice and female leptin knockout and wild-type mice. We pursued this investigation. To determine whether leptin differentially affects bone formation in males and females, we compared body characteristics and several parameters of bone size in male and female knockout mice with male and female mice of its wild-type C57BL/6 background strain.

1. The initial phenotypic comparison of body weight, total body fat and total lean body mass was performed on male and female mice at 10 weeks of age. Each study group contained at least 12 animals.
2. Bone parameters in male and female mice were then compared at 12 weeks of age. The midpoint of the femoral diaphysis was analyzed by peripheral quantitative computerized tomography (pQCT). The periosteal circumference (PC), endosteal circumference (EC) and total bone mineral density (BMD) total bone mineral content (BMC) using an analysis threshold of 630-630. pQCT measurements of the trabecular bone area used an analysis threshold of 570-214. Each study group contained more than 11 animals.
3. Gender-specific differences in bone mass and size also implicate the sex steroid hormones in bone metabolism (17). To determine whether a reduction in androgen levels might explain the effect of leptin deficiency on bone size, the circulatory levels of androgen and estrogen in male and female leptin knockout mice were also assessed. Each study group contained more than 18 animals.

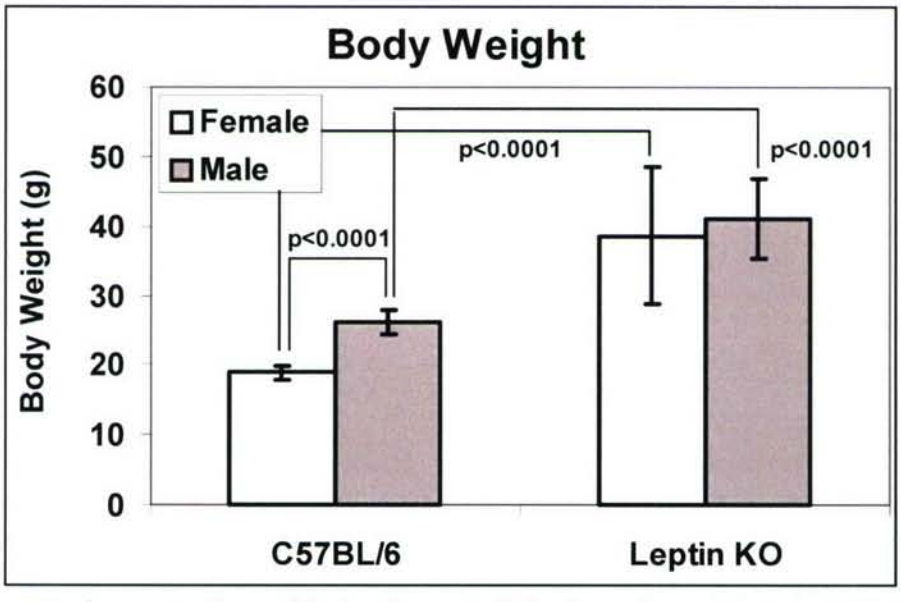

Figure 9. Phenotypic comparison of body characteristics in male and female leptin knockout (KO) and C57BL/6 wild-type mice: body weight. Values are expressed as mean +/- Standard Error of the Mean (SEM). Statistical analysis was performed by two-way ANOVA with a post-hoc Newman-Kuels Test. Differences were deemed significant at $p<0.05$.

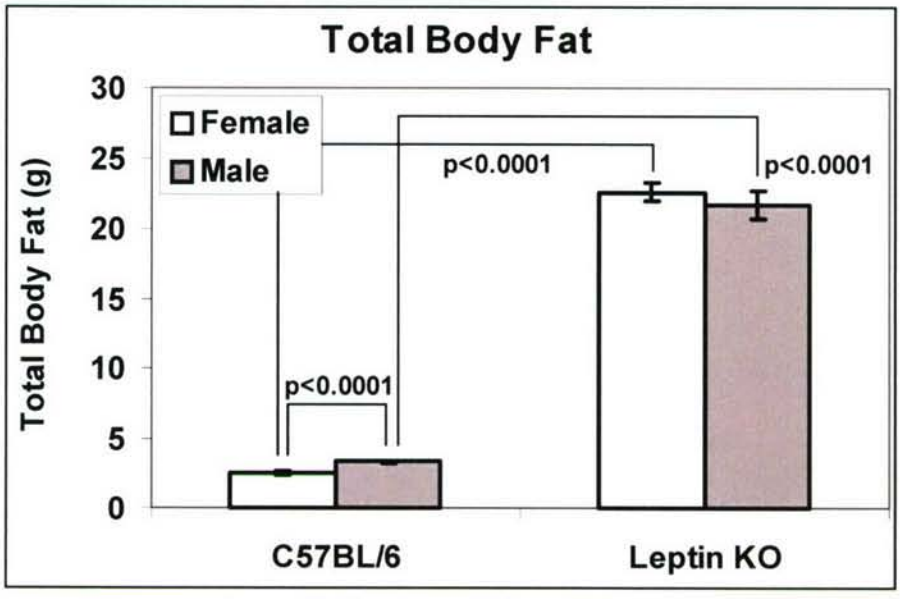

Figure 10. Phenotypic comparison of body characteristics in male and female leptin knockout (KO) and C57BL/6 wild-type mice: <u>total body fat</u>. Values are expressed as mean +/- Standard Error of the Mean (SEM). Statistical analysis was performed by two-way ANOVA with a post-hoc Newman-Kuels Test. Differences were deemed significant at $p<0.05$.

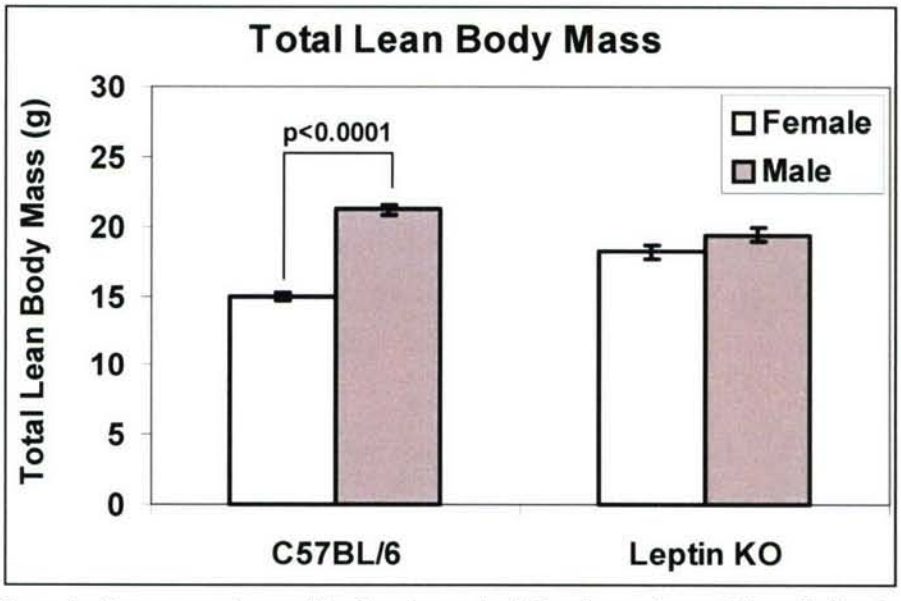

Figure 11. Phenotypic comparison of body characteristics in male and female leptin knockout (KO) and C57BL/6 wild-type mice: <u>total lean body mass</u>. Values are expressed as mean +/- Standard Error of the Mean (SEM). Statistical analysis was performed by two-way ANOVA with a post-hoc Newman-Kuels Test. Differences were deemed significant at $p<0.05$.

The results from Figures 9, 10 and 11 indicate that the expected significant differences in the body weight, total body fat and total lean body mass between male and female C57BL/6 mice were not observed between male and female leptin knockout mice. Sex-specific body characteristics were therefore lost in the obese male mouse, and leptin deficiency interfered with

androgen-related effects on bone formation in male leptin knockout mice. This effect reduced male characteristics of lean body mass and body fat to those of female mice. The femurs of leptin knockout male and female mice were then compared with those of C57BL/6 male and female mice to further characterize sex-specific differences that might contribute to bone formation or repair. Several femoral parameters were examined by pQCT measurements at the femoral midshaft. Statistical analysis was performed by two-way ANOVA with a post-hoc Newman-Kuels Test. Differences were deemed significant at $p<0.05$.

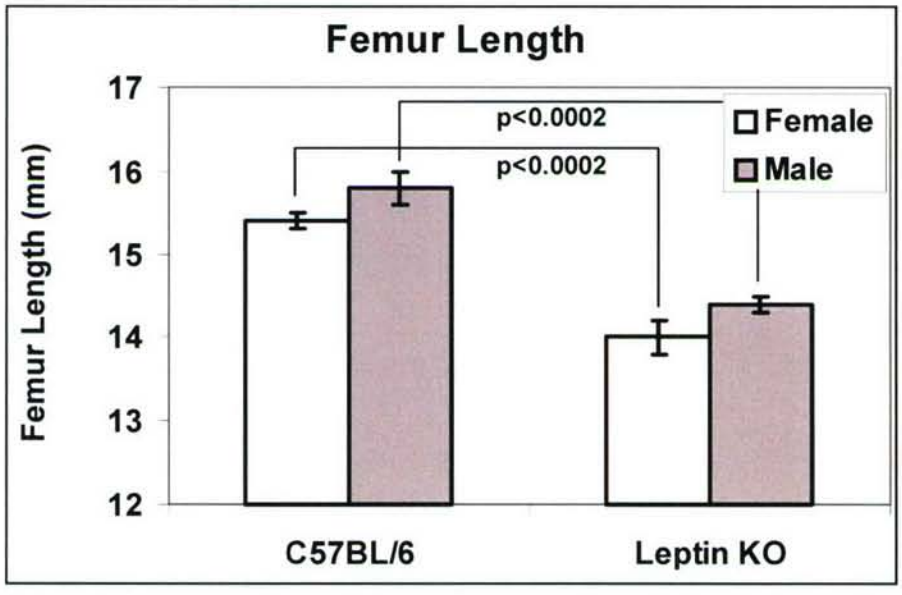

Figure 12. Phenotypic comparison of bone size in male and female leptin knockout (KO) and C57BL/6 wild-type mice: femur length. Values are expressed as mean +/- Standard Error of the Mean (SEM).

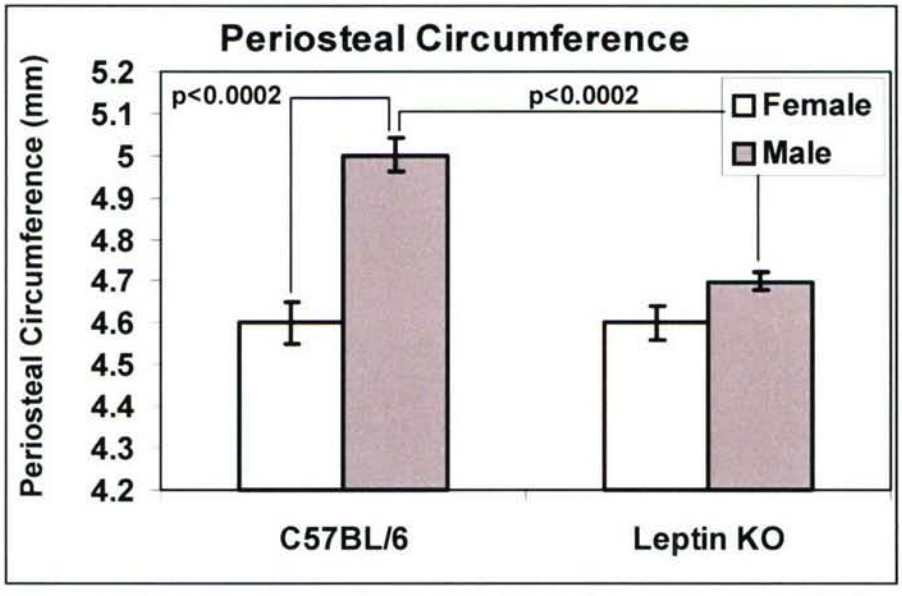

Figure 13. Phenotypic comparison of bone size in male and female leptin knockout (KO) and C57BL/6 wild-type mice: femoral periosteal circumference. Values are expressed as mean +/- Standard Error of the Mean (SEM).

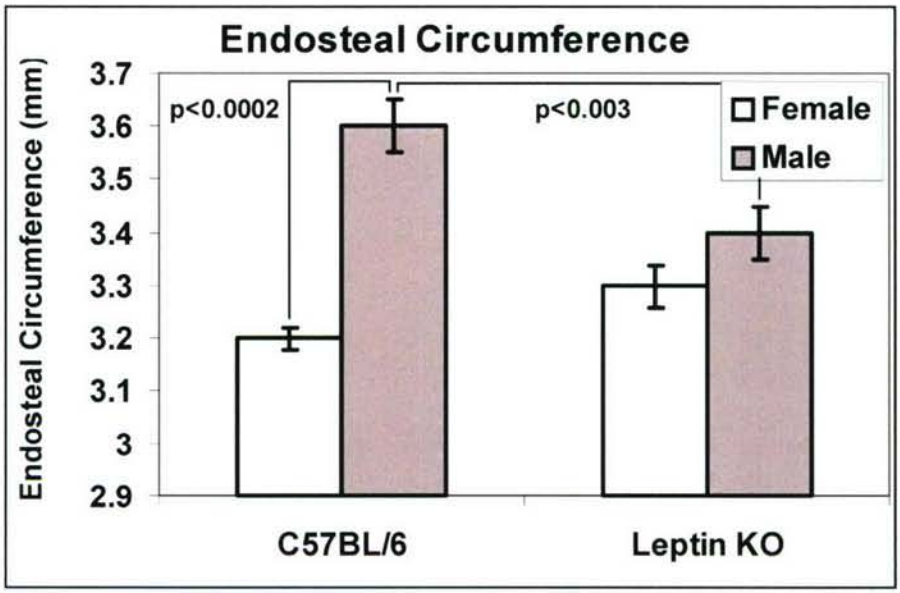

Figure 14. Phenotypic comparison of bone size in male and female leptin knockout (KO) and C57BL/6 wild-type mice: femoral endosteal circumference. Values are expressed as mean +/- Standard Error of the Mean (SEM).

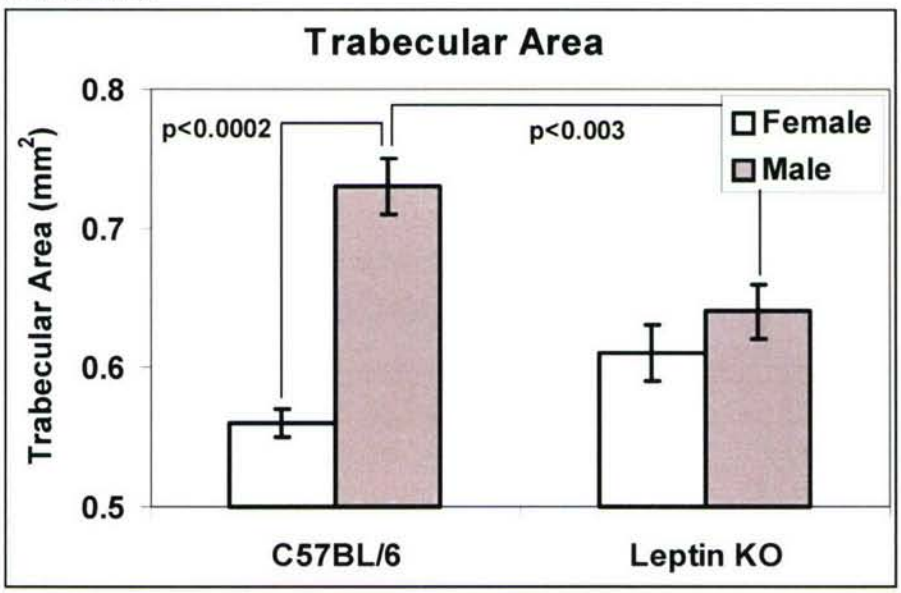

Figure 15. Phenotypic comparison of bone size in male and female leptin knockout (KO) and C57BL/6 wild-type mice: femoral cross-sectional trabecular area. Values are expressed as mean +/- Standard Error of the Mean (SEM).

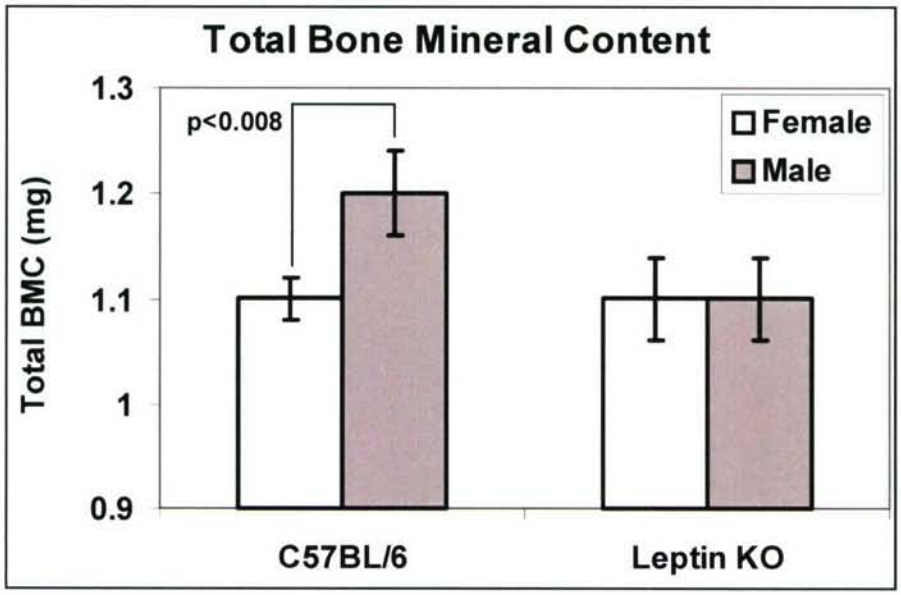

Figure 16. Phenotypic comparison of bone size in male and female leptin knockout (KO) and C57BL/6 wild-type mice: total femoral bone mineral content. Values are expressed as mean +/- Standard Error of the Mean (SEM).

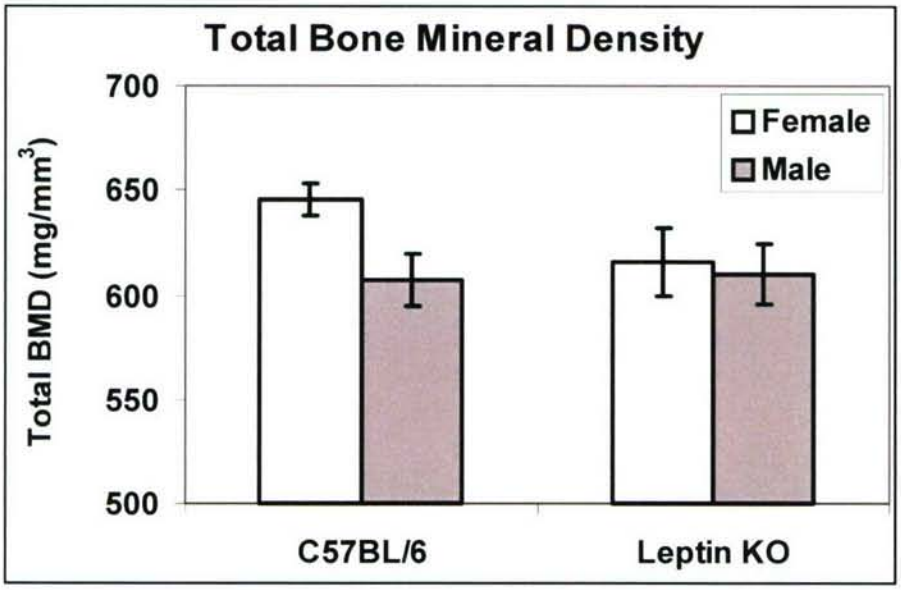

Figure 17. Phenotypic comparison of bone size in male and female leptin knockout (KO) and C57BL/6 wild-type mice: total femoral bone mineral density. Values are expressed as mean +/- Standard Error of the Mean (SEM).

A comparison of the femoral measurements between mouse strains and genders established that several parameters of the femur were also altered in male leptin knockout mice (Figures 12 to 17). Significant differences in the periosteal circumference, endosteal circumference and trabecular bone area between male and female C57BL/6 mice were not observed between male and female leptin knockout mice (Figures 13 to 15). The total bone mineral content was also significantly reduced in male leptin knockout mice (Figure 16). There was no significant

difference in the total bone mineral densities between male and female leptin knockout mice (Figure 17); because the total bone mineral content of each was reduced in males, this observation suggested a coordinated reduction of several parameters of bone formation in male leptin knockout mice. The exception was the femur lengths, which were the not significantly different between males and females of either strain (Figure 12). We conclude that leptin deficiency in the male mouse resulted in a loss of several sex-specific differences in bone size that might be attributable to androgen effects on bone formation.

The circulatory levels of androgen and estrogen in male and female leptin knockout mice were also measured to establish whether the effect of leptin deficiency on bone size was the result of a reduction in androgen levels (Figure 18). Mouse sera were collected from the retro-orbital venous plexus under general anesthesia, and serum testosterone and estradiol were determined using the respective ^{125}Iodine radioimmunoassay (RIA) kits.

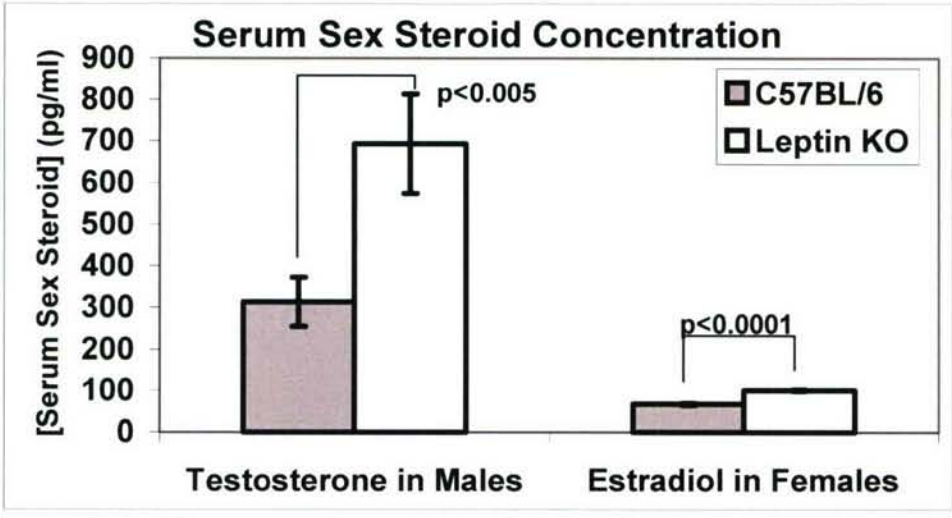

Figure 18. Comparison of serum sex hormone levels in leptin knockout (KO) and C57BL/6 wild-type male and female mice. Values are expressed as mean +/- Standard Error of the Mean (SEM). Statistical analysis was performed by two-way ANOVA with a post-hoc Newman-Kuels Test. Differences were deemed significant at $p<0.05$.

Androgen action is primarily anabolic, while the estrogens act mainly through the suppression of resorption. The sex hormones are also influenced by body fat accumulation and distribution (reviewed in 18), which suggests interactions with regulators of body fat, such as leptin. The significantly higher serum testosterone levels in male leptin knockout mice as compared to C57BL/6 wild-type mice indicate that the loss of sex-specific characteristics in the body phenotype and bone parameters could not be attributed to a reduction in testosterone levels, but possibly to a defect in testosterone signaling. Estradiol levels were significantly higher in leptin knockout female mice, but the similarities in the body characteristics and femoral bone parameters between the C57BL/6 and leptin knockout female mice suggest that the effects observed in males were not estrogen-related. We are currently examining androgen receptor expression and function in the leptin knockout mouse to test the hypothesis that androgen signaling is defective in the absence of leptin. Because of obvious implications for the interactions of bone size, obesity and sex hormone effects, we will continue to investigate this phenomenon in leptin knockout mice.

Bax Knockout Mice

To date, 9 homozygous mice at the age of 12 weeks have been used for fracture repair study and analyzed by X-ray (Figure 19) and pQCT. The X-rays at 14 and 28 days healing appeared to show a more robust bony callus, which was further examined by pQCT measurements of these fractures (Figures 20, 21, 22).

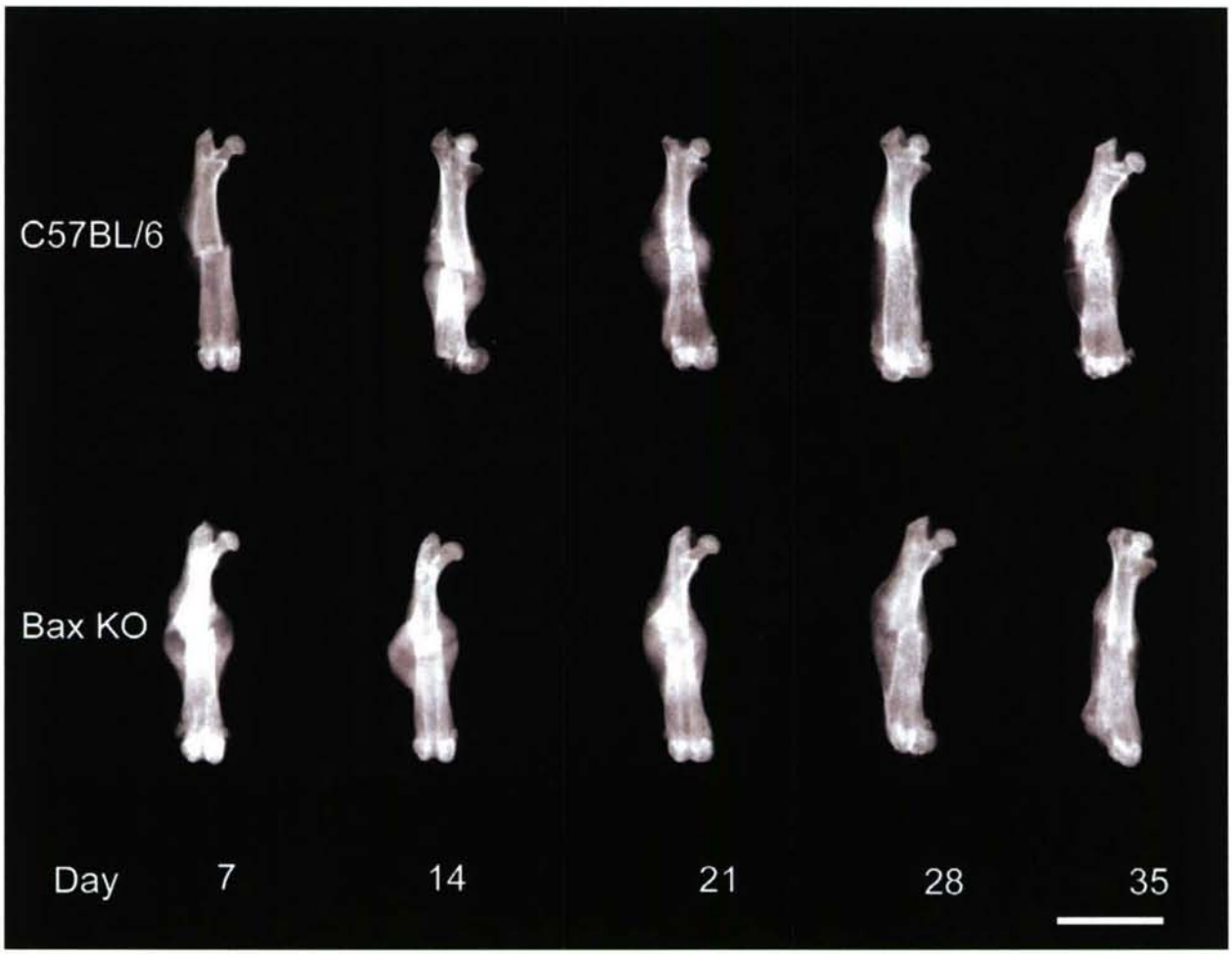

Figure 19. X-ray photograph of healing mouse fractured right femurs in Bax knockout (KO) mice compared with C57BL/6 wild-type mice at 7, 14, 21, 28, and 35 days post-fracture. The X-ray contains representative femur fractures from 6 male Bax knockout mice were compared with 6 or 7 male control mice at each post-fracture time. The C57BL/6 fractures are the same as those used in the leptin knockout mouse X-ray comparison. As with the leptin knockout mice, the development of the mineralized (hard) callus in Bax knockout mice can be monitored from its early stages, at 7 days, through its maximum, at 14 to 21 days, and into remodeling to cortical bone, at 28 days. Scale bar = 5 mm.

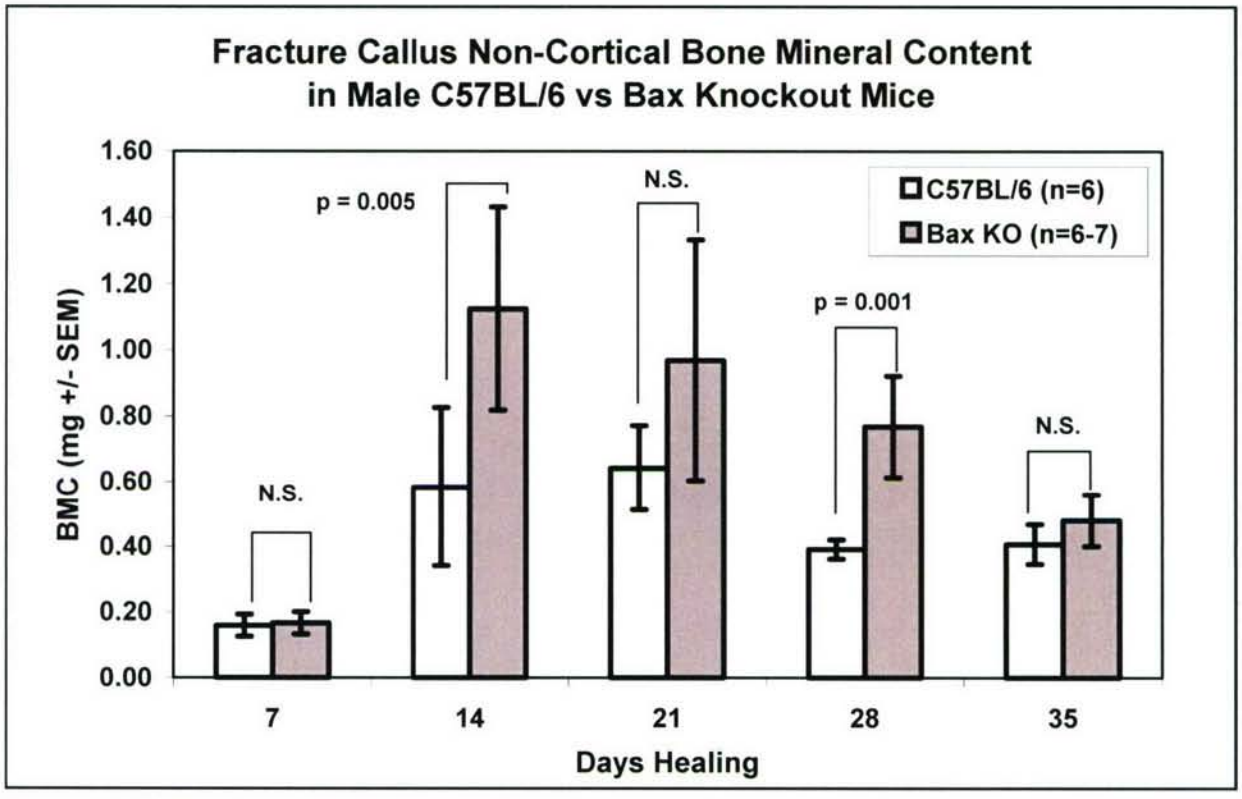

Figure 20. Bone mineral content after femoral fracture in male Bax knockout (KO) and C57BL/6 wild-type control mice. The bone mineral content of the fracture callus was significantly different at 14 and 28 days healing.

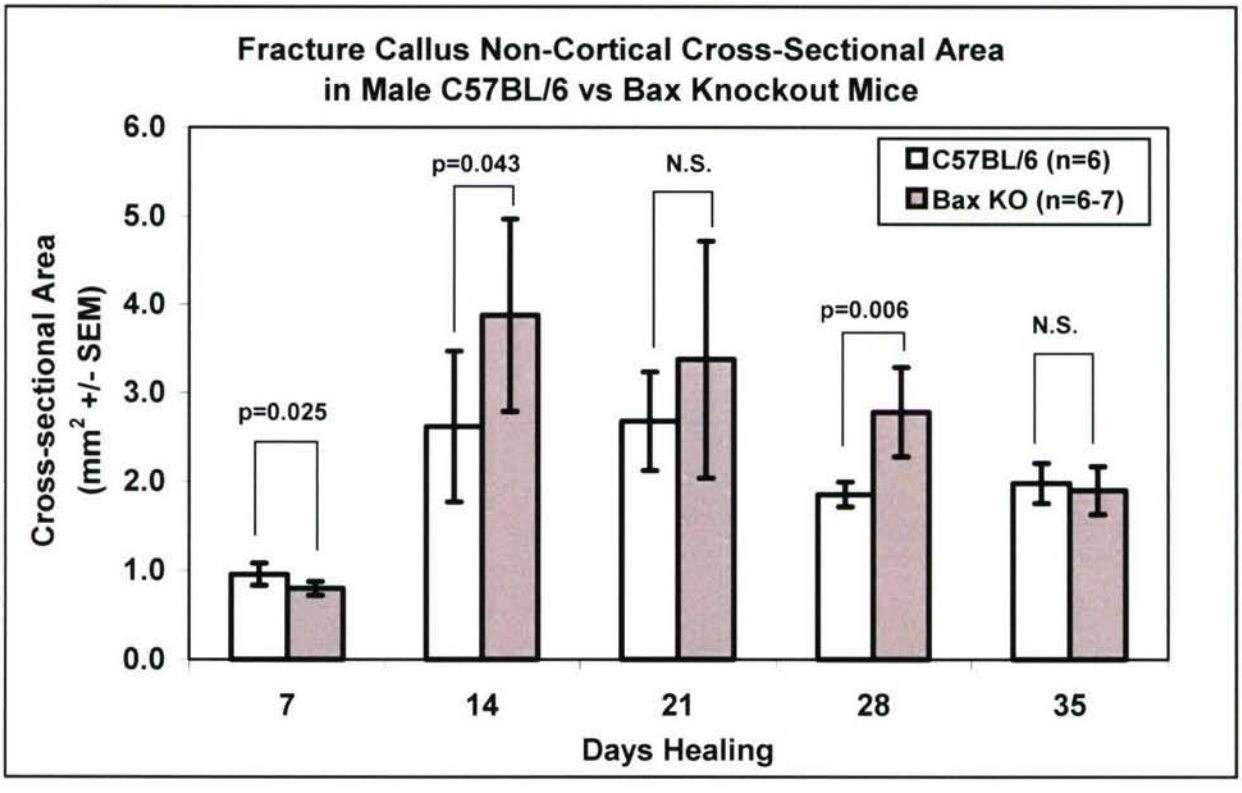

Figure 21. Cross-sectional area of the bony fracture callus after femoral fracture in male Bax knockout (KO) and C57BL/6 wildtype control mice. As with the bone mineral content, the cross-sectional area of bony tissue was significantly different at 14 and 28 days healing. However, it was also significantly different during early fracture healing, at 7 days.

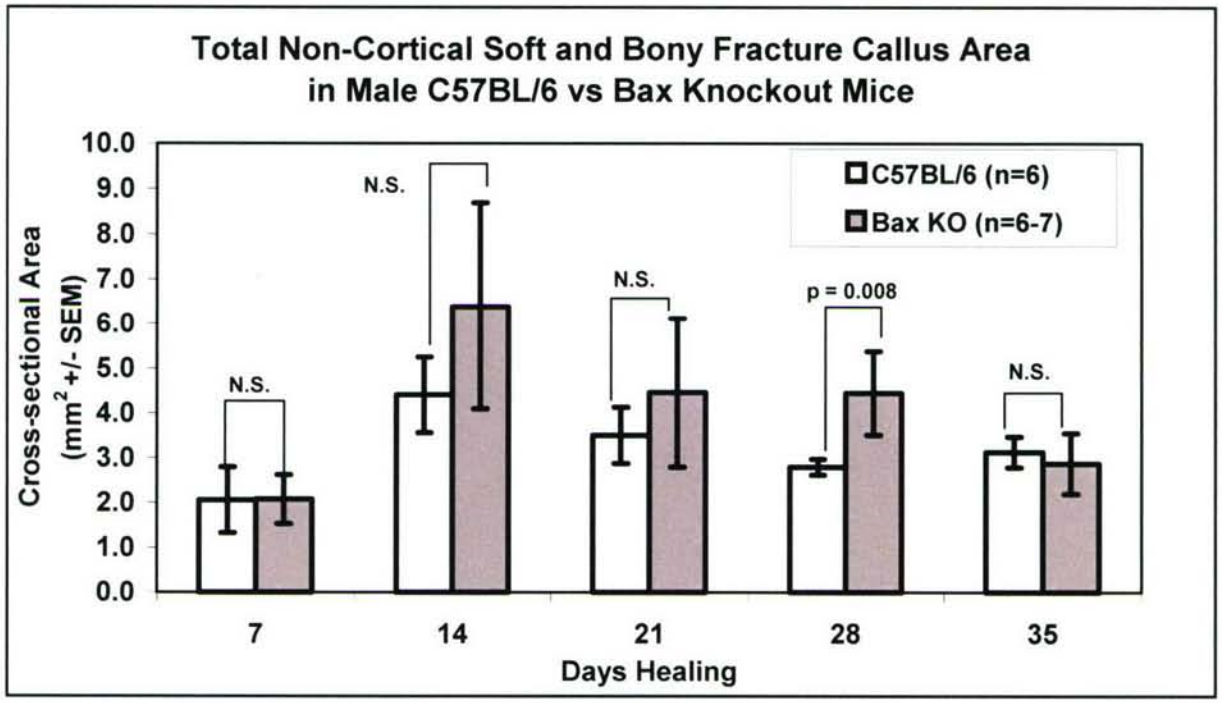

Figure 22. Cross-sectional area of the total fracture callus (soft and bony tissue) area after femoral fracture in male leptin knockout (KO) and C57BL/6 wildtype control mice. In contrast to the hard callus measurements of Figures 19 and 20, the total callus area was significantly different only at 28 days healing, indicating a persistence of soft tissue in the fracture callus of the Bax knockout mice.

From the pQCT results of Figures 20 and 21, it is evident that the Bax knockout mice develop hard callus areas with significant differences during early (7 and 14 days) and later (28 days) fracture healing. The bone mineral content of the Bax knockout fractures is significantly greater than the control fractures at 14 and 28 days. This observation suggests normal soft callus formation with reduced apoptosis in early healing (14 days) prolongs osteoblast function and increases bone formation, but slower remodeling later in healing (28 days) reduces the removal of hard callus bone. This observation is visible in the X-ray of the slightly more mineralized Bax knockout callus at 14 and 28 days post-fracture (Figure 19). The conclusion remains consistent with our hypothesis that the absence of Bax gene expression might reduce apoptosis and both increase bone formation and reduce bone remodeling. More knockout mice are being analyzed to confirm whether the bone mineral content is observed throughout fracture healing might be explained by an inhibition of Bax-mediated apoptosis, but these results confirm those of the first year of the study.

As with the mechanical loading studies, the Bax mouse fracture project is improving as breeding improves and more Bax knockout mice become available. Initially, this knockout strain displayed litter mortality similar to the leptin knockout mouse, with a high proportion of pups either neglected or cannibalized. However, at this time the problem has improved, probably because the mothers have become more experienced with additional litters.

Serpine Knockout Mice

The serpine knockout mouse fracture study has suffered from delayed acquisition and breeding, but several litters of pups are currently approaching the appropriate 12-week age for fracture analysis, which is expected to be completed in the next two months. Fracture studies have begun and the initial harvest of 4 fractures at 14 days healing examined by X-ray (Figure 23).

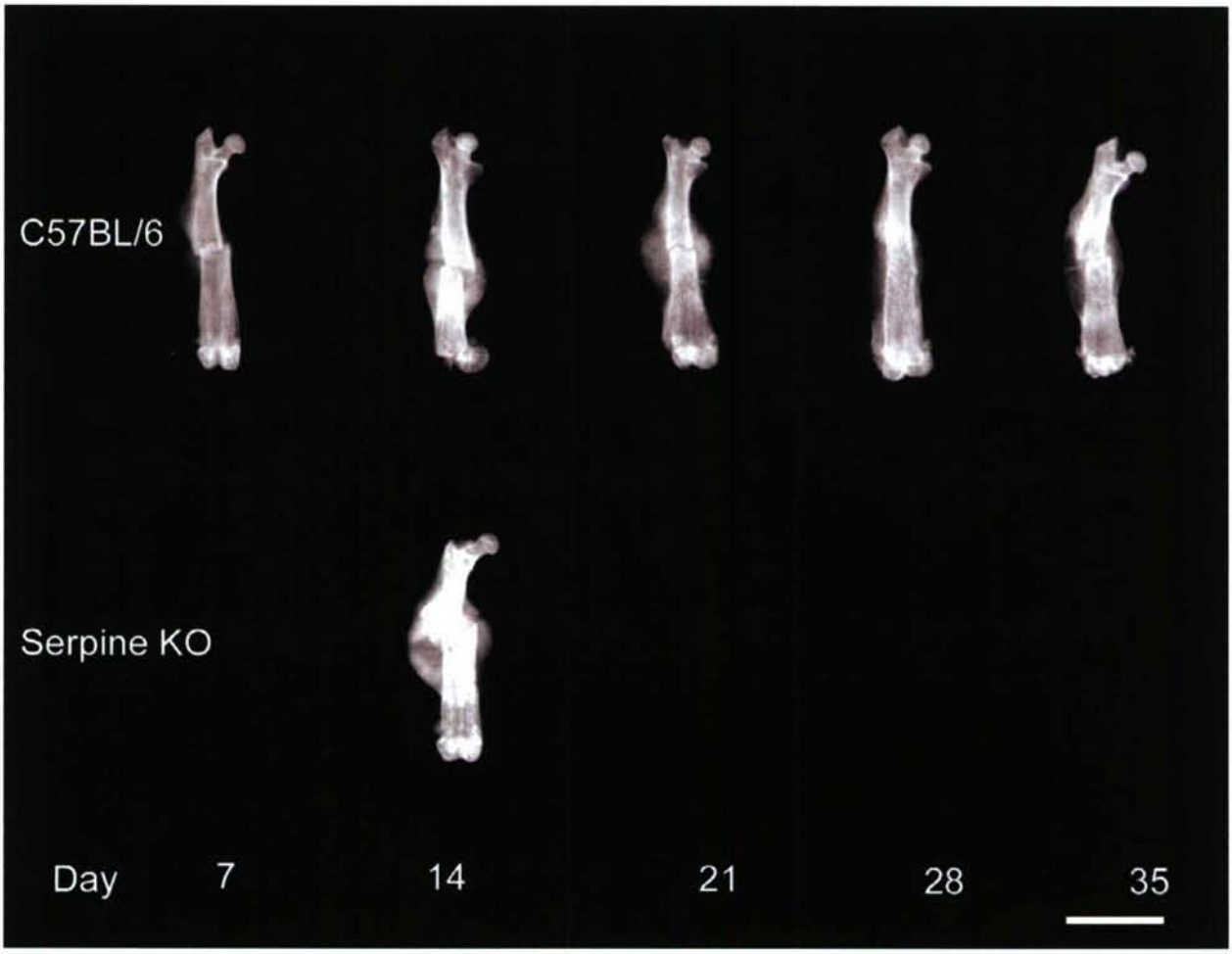

Figure 23. X-ray photograph of healing mouse fractured right femurs in Serpine knockout (KO) mice compared with C57BL/6 wild-type mice at 14 days post-fracture. The X-ray contains representative femur fractures from the 4 male Serpine knockout mice available to date that were compared with 6 or 7 male control mice at each time. The C57BL/6 fractures are the same as those used in the leptin knockout mouse X-ray comparison. As with the other strains of knockout mice, the development of the mineralized (hard) callus will be monitored throughout healing, as more of these mice become available. Scale bar = 5 mm.

X-ray examination of the 14 day fracture calluses available for the serpine knockout fractures harvested to date reveals a robust mineralized callus. X-ray examination and pQCT measurements of additional fracture calluses as they become available could demonstrate variations in healing due to serpine deficiency.

Histological comparisons of the C57BL/6 wild-type control mice and leptin and Bax knockout fractures throughout healing failed to show any observable differences in the fracture histology (Figure 24). Histology at each of the 7, 14, 21, and 28 day post-fracture time points examined was highly similar. Any differences in fracture histology due to knockout gene deficiencies were not of sufficient magnitude to allow quantification by histomorphometry. Variations in healing, as defined by differences the time required or tissues present for bridging of the fracture gap, were not evident. We will continue to pursue histology, but micro-CT examination, which was not possible due to instrument difficulties, presents a much better option for identifying subtle changes in fracture repair.

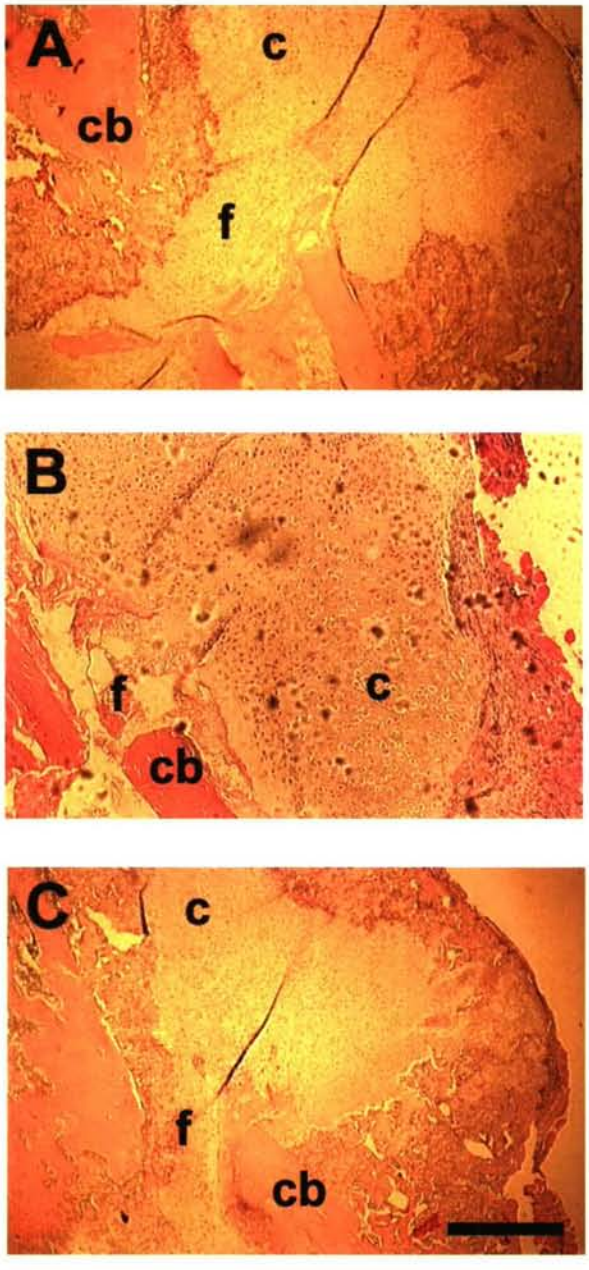

Figure 24. Hematoxylin and eosin stains of fracture callus sections at 14 days healing. (A) C57BL/6 wild-type control mouse, (B) leptin knockout mouse, (C) Bax knockout mouse. The cortical bone (cb), cartilage (c) and the fracture (f) are visible in each panel. Healing is typical of normal fracture repair in the mouse. The gap will eventually bridge by 28 days healing. Scale bar = 0.50 mm.

Specific Objective 2: to apply microarray technology to study gene expression in the fracture tissues of the one strain of knockout mice that exhibited the greatest phenotypic differences in fracture healing.

This study used whole genome microarray gene analysis to identify the genes expressed in fracture repair of the Bax knockout mouse femur at 14 days healing, when the pQCT data indicated that the Bax knockout fracture callus contained more lower-density (non-cortical) bone in the fracture callus than the wild-type C57BL/6 wild-type control. This observation suggested that the midpoint of fracture healing displayed higher bone formation as a result of the reduced apoptosis produced by the Bax deficiency. Additionally, this stage was prior to the 21 day to 28 day period of healing when the Bax fracture callus again displayed more lower-density bone than the wild-type control mice, and suggested that reduced apoptosis from Bax deficiency slowed remodeling of the fracture callus. This healing time in this knockout mouse presented the greatest differences in bone formation in fracture healing relative to the control mice fractures, as well as a time prior to other potential differences Bax callus remodeling after 21 days healing. The repertoire of expressed genes regulating these two processes would be expected to differ greatly from controls at this time, so the Bax knockout 14 day fracture callus was chosen for an analysis of global gene expression in fracture repair.

Total RNA was compared by microarray analysis of 14 day fracture calluses from 5 individual male Bax knockout mice and 5 individual C57BL/6 knockout mice. The individual pairs of samples were hybridized and analyzed separately. The RNA from each fracture callus was labeled with Cy3 or Cy5 dye and hybridized to our in-house mouse gene chip that contained approximately 28,000 unique mouse gene targets. Analysis was performed using (Agilent) Genespring software and changes in expression between the Bax knockout fracture callus and the C57BL/6 callus deemed significant at $p<0.05$.

Findings:

An examination of the differences in global gene expression in the 14 day fracture calluses revealed that 5,458 genes displayed significant changes in expression (Table 2). Approximately 15% were unknown genes or expressed sequence tags (ESTs), indicating that a large portion of the molecular regulation of fracture repair remains to be elucidated. Surprisingly, in contrast to other fracture microarray studies, where most genes are up-regulated, approximately equal numbers of known and unknown genes were up-regulated and down-regulated. This difference might be caused by Bax-related apoptotic interactions with other pathways of fracture repair.

Table 2. Summary of Bax Knockout Fracture Microarray Gene Expression Changes 14 Days Healing			
Expression Change (P<0.05)	**Known Genes**	**Unknown Genes**	**Total**
Up-regulated in Bax Knockout	**2234**	**409**	**2643**
Down-regulated in Bax Knockout	**2459**	**356**	**2815**
Total	**4693**	**765**	**5458**

An examination of the Bax-related genes revealed that several of the gene products that Bax interacts with displayed significant changes in gene expression (Table 3). These genes included

Table 3. Bax-Related Genes with Significant Changes in Expression (P<0.05) in Bax Knockout Fractures at 14 Days Healing					
Gene Name	Accession	**Expression Fold-Change**	P-value	Description	Gene Ontology Classification Cellular Component
Pdcd6	NM_011051	**3.99**	0.01	Programmed cell death 6/ALG2	
Bcl2	NM_009741	**2.48**	0.01	B-cell leukemia/lymphoma 2	mitochondrial membrane
Bcl7a	NM_029850	**2.34**	0.01	B-cell CLL/lymphoma 7A	
Biklk	NM_007546	**2.32**	0.02	Bcl2-interacting killer-like	mitochondrial membrane
Bcl6b	NM_007528	**2.03**	0.04	B-cell CLL/lymphoma 6, member B	nucleus
Bcl11b	NM_021399	**1.50**	0.03	B-cell leukemia/lymphoma 11B	nucleus
Bcl2a1b	NM_007534	**1.46**	0.04	B-cell leukemia/lymphoma 2 related protein A1a	
Bcl3	NM_033601	**0.85**	0.04	B-cell leukemia/lymphoma 3	nucleus
Bnip3l	NM_009761	**0.80**	0.01	BCL2/adenovirus E1B 19kDa-interacting protein 3-like	mitochondrial membrane
Zrfp7	XM_135065	**0.74**	0.32	Zinc ring finger 7	nucleus
Caspase 8	NM_009812	**0.66**	0.01	Cysteine protease death initiator	
Bad	NM_007522	**0.56**	0.04	Bcl-associated death promoter	mitochondrion

Table 4. Changes in Expression of Some Major Growth Factor Gene Families in Bax Knockout Fractures at 14 Days Healing				
Growth Factor/Cytokine Gene	**Accession**	**Expression**		**Functions**
		Fold-Change	**P-Value**	
Fibroblast Growth Factors (FGF)				
FGF7	NM_008008	11.89	0.004	wound epithelialization
FGF18	NM_008005	0.57	0.026	morphogenesis
FGF20	NM_030610	6.65	0.002	morphogenesis
FGF Receptor 2	NM_201601	3.95	0.037	FGF7 receptor, proliferation & osteogenesis
FGF Receptor 3	NM_008010	0.48	0.047	chondrogenesis, osteogenesis
Transforming Growth Factors (TGF)				
TGF-B3	NM_009368	0.19	0.049	pleiotrophic
TGF-B Receptor 2	NM_009371	0.03	0.001	TGF-B receptor, pleiotrophic
TGF inducing early response 2	NM_178357	6.57	0.006	TGF-induced transcription factor
TGF inducing early response 3	MMU275989	2.45	0.367	TGF-induced transcription factor
Bone Morphogenetic Proteins (BMP)				
BMP Receptor 1-B	NM_007560	0.06	0.183	BMP receptor, osteogenesis
BMP Receptor 2	NM_007561	0.04	0.010	BMP receptor, osteogenesis
Noggin	NM_008711	0.68	0.001	BMP inhibition
Smad 2 homolog	NM_010754	0.16	0.049	BMP signal transduction
Interleukins (IL)				
IL-1 member 6	NM_019450	4.08	0.023	inflammation

IL-1 receptor-associated protein	NM_008364	5.60	0.044	inflammation
IL-13 receptor alpha-1	NM_133990	4.71	0.034	adherence, anti-inflammatory
IL-18 receptor-associated protein	NM_008365	3.35	0.025	inflammation
IL18 binding protein	NM_010531	3.32	0.004	inflammation

Table 5. Changes in Expression of Hox and Hox-Related Genes in Bax Knockout Fractures at 14 Days Healing

Growth Factor/Cytokine Gene	Accession	Expression		Functions
		Fold-Change	P-Value	
Hox Genes				
Hox-B2	NM_134032	7.21	0.010	developmental transcription factor
Hox-B3	NM_010458	1.50	0.005	developmental transcription factor
Hox-B5	NM_008268	1.76	0.001	developmental transcription factor
Hox-B8	NM_010461	0.08	0.050	developmental transcription factor
Hox-D3	NM_010468	0.62	0.001	developmental transcription factor
Hox-Related Genes				
Shox-B2	NM_013665	3.18	0.008	transcription factor, short stature
Ehox	NM_021300	8.96	0.007	ES-derived transcription factor

several Bcl genes, including Bcl-2. Bax binds and inhibits Bcl-2, thereby promoting apoptosis (reviewed in 19). Bcl-2 up-regulation in the absence of Bax inhibition would be expected to inhibit apoptosis. Few other mitochondrial apoptotic genes displayed differences. Bad, which binds Bcl-XL and which might be expected to compensate for Bax deficiency through an up-regulation in expression, was in fact down-regulated almost two-fold. However, the expression of Biklk (Bik-like), another mitochondrial apoptotic regulator that binds and inhibits both Bcl-2 and Bcl-XL (20), was up-regulated, suggesting that its expression compensated for the absence of Bax in promoting apoptosis and reduced the severity of the Bax knockout phenotype and its effect on fracture healing.

The expression of the major growth factor gene families (Table 4) displayed some differences from other microarray studies of rodent fracture healing (21), The fibroblast growth factor (FGF)-7 gene and various mediators of inflammation have been previously associated with fracture repair and were significantly up-regulated in the Bax knockout fracture. However, there was also a tendency toward the expression of morphogenetic and pleiotrophic genes (FGF20, TGFB-induced 2, TGF-B-induced 3), and away from expression of the osteogenic genes (the BMP family), which implies that the altered regulation of apoptosis in the Bax knockout mice had affected morphogenetic gene expression. Consistent with this observation, several Hox genes and Hox-related genes, notably orthologs and paralogs of Hox-B3, displayed significant changes in gene expression in the knockout mice (Table 5). The Hox gene cluster is critical in the regulation of pattern formation during embryonic morphogenesis (reviewed in 22), and Hox gene expression could regulate altered apoptosis in Bax knockout fracture healing, in combination with FGF and TGF genes (Table 4). Apoptotic events in fracture repair might therefore be very complex and involve the regulation of pattern formation. We will confirm the expression of these genes with using an independent measurement method, such as real-time PCR, and further investigate regulatory gene expression the apoptotic pathways of fracture repair. This study offers an excellent opportunities to elucidate the molecular mechanisms by which apoptosis regulates fracture repair.

Key Research Accomplishments:

1) The mechanical loading model of skeletal exercise and the femoral fracture model of bone repair have been developed and applied to knockout mouse studies. These models have been used to study the functional significance of genes of interest in commercially available strains of knockout mice.
2) Two of the three proposed knockout strains of mice (leptin and Bax) have been phenotypically analyzed by the mechanical loading model. Because of misidentification of the third mouse knockout strain (longjohn) and the difficulty in breeding the leptin knockout mice, the Technical Objective was not completed. These two problems have been corrected.
   a) The molecular marker and microarray analysis of the loaded leptin knockout bones is currently underway.
   b) Additionally, sufficient numbers of the serpine knockout mouse strain that was substituted for the longjohn knockout mouse in these studies are approaching analysis at this time.
3) Two of the three proposed knockout strains of mice (leptin and Bax) have been phenotypically analyzed by the fracture repair model. Because of misidentification of the third mouse knockout strain (longjohn), the difficulty in breeding leptin knockout mice and

their unexpected fracture surgery mortality, the Technical Objective was not completed. These problems have been corrected.

a) Sufficient numbers of the serpine knockout mice strain that was substituted for the longjohn knockout mouse in these studies are approaching or have begun fracture analysis at this time.
b) The molecular marker and microarray analysis of the Bax knockout mouse has been completed and suggests several regulatory pathways for study of the molecular regulation of fracture repair or gene candidates for fracture therapy.

Reportable Outcomes

Xing W., Baylink D.J., Kesavan C., Chadwick R.B., Hu Y. and Mohan S. Global Gene Expression Analysis in the Bones Reveals Involvement of Several Novel Genes and Pathways in Mediating an Anabolic Response of Mechanical Strain in Mice. J Cell Bio (Submitted), 2005

Rundle C.H., Wang H., Yu H., Chadwick R.B., Tesfai J., Lau K-H.W., Mohan S., Ryaby J.T., and Baylink D.J. Microarray analysis of fracture repair identifies the homeodomain transcription factor Prx-2 and other genes that imply similarities between bone repair and scarless fetal tissue healing. Transactions to the 51st Annual meeting of Orthopaed Res Soc abstract # 361, 2005

Rundle C.H., Wang X., Wergedal J.E., Srivastava A.K., Davis E.I., Lau K-H.W., Mohan S., and Baylink D.J. Loss of sex-specific differences in bone size in leptin-deficient (ob/ob) mice. Transactions to the 52nd Annual meeting of Orthopaed Res Soc (in press), 2006

Rundle C.H., Wang H., Yu H., Chadwick R.B., Davis E.I., Wergedal J.E., Lau K-H.W., Mohan S., Ryaby J.T., and Baylink D.J. Microarray analysis of gene expression during the inflammation and endochondral bone formation stages of rat femur fracture repair. Submitted to Bone, in revision, 2005

Wang X., Rundle C.H., Srivastava A., Tesfai J., Davis E.I., Wergedal J.E., Lau K.H-W., Mohan S. and Baylink D.J. Loss of sex-specific difference in bone size in leptin knockout mice. 27th Annual Meeting of the American Society for Bone and Mineral Research, Nashville, TN, 2005

Conclusions

1) The development and optimization of models for exercise (mechanical loading) and bone repair (fracture) in knockout mice allowed the analysis of the functional significance of genes of interest for bone formation in each case.
2) Based upon the numbers of animals analyzed to date, X-ray and pQCT data suggest that leptin influences bone formation in mechanical loading but that Bax expression produces no significant effect.
3) Based upon the numbers of animals analyzed to date, X-ray and pQCT data suggest that Bax influences callus bone formation in earlier fracture repair and callus remodeling in later fracture repair. Several thousand genes exhibit changes in expression in Bax knockout fractures at 14 days healing. Leptin either produces no significant effect on fracture repair or its effects are masked by other physiological conditions in the leptin knockout mouse.

References

1. Mackelvie KJ., McKay HA., Petit MA., et al. (2002). Bone mineral response to a 7-month randomized controlled, school-based jumping intervention in 121 pre-pubertal boys: Associations with ethnicity and body mass index. J. Bone Miner. Res 17:834-844.
2. Kodama Y., Dimai HP., Wergedal J., et al. (2000). Exercise and mechanical loading increase periosteal bone formation and whole bone strength in C57BL/6J mice but not in C3H/Hej mice. Calcif. Tissue Int. 66:298-306.
3. Ducy P., Amling M., Takeda S., et al. (2000). Leptin inhibits bone formation through a hypothalamic relay: A central control of bone mass. Cell 100:197-207.
4. Steppan CM., Crawford DT., Chidsey-Frink KL., et al. (2002). Leptin is a potent stimulator of bone growth in ob/ob mice. Regulatory Peptides 92:73-78.
5. Matkovic V., Ilich JZ., Skugor M., et al. (1997). Leptin is inversely related to age at menarche in human females. J. Clin. Endocrinol. Metab. 82:3239-3245.
6. Takeda S., Elefteriou F., Levasseur R., et al. (2002). Leptin regulates bone formation via the sympathetic nervous system. Cell 111:305-317.
7. Lee, Y-J., Park, J-H., Ju, S-K., et al. (2002). Leptin receptor isoform expression in rat osteoblasts and their functional analysis. FEBS Letters 528:43-47.
8. Knudson CM., Tung KSK., Tourtellotte WG., et al. (1995). Bax-deficient mice with lymphoid hyperplasia and male germ cell death. Science 270:96-98.
9. Mocetti P., Silvestrini G., Ballanti P., et al. (2001). Bcl-2 and Bax expression in cartilage and bone cells after high-dose corticosterone treatment in rats. Tissue & Cell 33:1-7.
10. Hock, JM., Krishnan, V., Onyia, JE., et al. (2001). Osteoblast apoptosis and bone turnover. J. Bone Miner. Res. 16:975-984.
11. Xing, L. and Boyce, BF. (2005). Regulation of apoptosis in osteoclasts and osteoblastic cells. Biochem. Biophys. Res. Commun. 328:709-720.
12. Collen, D. and Lijnen, HR. (1991). Basic and clinical aspects of fibrinolysis and thrombolysis. Blood 78:3114-3124.
13. Carmeliet, P., Kiekens, L., Schoonjans, L., et al. (1993). Plasminogen activator inhibitor-1 gene-deficient mice. I. Generation by homologous recombination and characterization. J. Clin. Invest. 92:2746-2755.
14. Suda, M., Ogawa Y, Tanaka K., et. al. (1998). Skeletal overgrowth in transgenic mice that overexpress brain natriuretic peptide. Proc. Natl. Acad. Sci USA 95:2337-2342.
15. Yasoda A., Ogawa Y., Suda M et al. (1998). Natriuretic peptide regulation of endochondral ossification. J. Biol. Chem. 273, 11695-11700.
16. Bonnarens, F. and Einhorn, TA. (1984). Production of a standard closed fracture in laboratory animal bone. J. Orthop. Res. 2:97-101.
17. Nelson, DA., Simpson, PM., Johnson, CC., et al. (1997). The accumulation of whole body skeletal mass in third- and fourth-grade children: Effects of age, gender, ethnicity and body composition. Bone 20:73-78.
18. Thomas, T. and Burguera, B. (2002). Is leptin the link between fat and bone mass? J. Bone Miner. Res. 9;1563-1569.
19. Willis, S., Day, CL., Hinds, MG., et al. (2003). The Bcl-2-regulated apoptotic pathway. J. Cell Science 116:4053-4056.
20. Coultas, L., Bouillet, P., Stanley, EG., et al. (2004). Proapoptotic BH-3-only Bcl-2 family member Bik/Blk/Nbk is expressed in hematopoietic and endothelial cells but is redundant for their programmed death. Mol. Cell. Biol. 24:1570-1581.

21. Hadjiargyrou, M., Lombardo, F., Zhao, S., et al. (2002). Transcriptional profiling of bone regeneration: Insight into the molecular complexity of wound repair. J. Biol. Chem. 277:30177-30182.
22. Deschamps, J. and van Nes, J. (2005). Developmental regulation of the Hox genes during axial morphogenesis in the mouse. Development 132:2931-2942.

B. GENE THERAPY PROJECTS
Project 6: Systemic Gene Therapy For The Skeleton

Introduction

For this project, we propose to develop and test the efficacy of a mouse model for systemic gene therapy for massive skeletal tissue damage by means of hematopoietic stem cell (HSC) transplant. For this model, we will determine the skeletal marrow tissue and non-skeletal sites of engraftment, the quantity of short-term and long-term bone formation achieved, and the effect of the age of the recipient mice on the bone formation response. To our knowledge, our studies will be the first to use transplantation of transduced HSCs to deliver gene therapy to induce bone formation. These studies will focus on the induction of bone formation for massive skeletal injury. However, there is evidence that HSCs have the plasticity to regenerate other tissue types. Therefore, a successful HSCs-delivered gene therapy strategy for bone injury could be adapted to treat other damaged tissues, such as skin and muscle that are likely to be sustained along with massive skeletal injury, by the insertion of tissue-specific promoters to drive the therapeutic gene.

Body

1. Technical Objectives

Our technical objectives for the current reporting period (year 2) were to continue and complete engraftment studies and optimize our gene therapy murine model.

Technical Objective 1: To complete studies to determine the skeletal marrow and non-skeletal sites of engraftment in recipient mice after transplant with donor HSCs, we will:

1) Transplant GFP-expressing HSCs derived from transgenic mice into myelosuppressed recipient mice and assess the short-term (8 weeks), mid-term (6 months) and long-term engraftment (1 year) in the skeletal marrow and non-skeletal sites. Engraftment efficiencies will be quantitated by measuring the percentage of GFP-expressing cells in the peripheral blood and bone marrow of the recipient mice using flow cytometry.
2) Assess the pluripotent ability of the engrafted donor cells to produce mature hematopoietic lineages (T-cell, B-cell, neutophil/granulocyte/monocyte and erythroid) by using lineage-specific immunostaining and FACs analysis of the recipients' peripheral blood.
3) Detection of donor cells in non-skeletal tissues will be accomplished by frozen sectioning of the heart, lungs, liver and spleen of the recipients and fluorescent microscopic observation.

Technical Objective 2: To complete studies to assess and quantitate the short-term and long-term bone formation achieved in mice following transplantation with HSCs transduced to express a growth factor gene, we will:

1) To transduce HSC-enriched cells with an HIV-based vector expressing the BMP 2/4 gene under the control of the CMV promoter. Transgene expression will be assessed using immunohistochemical staining of the transduced cell cultures and Western blot analysis of the conditioned media
2) Transplant the transduced donor cells via tail vein into myelosuppressed recipient mice and evaluate bone formation after 8 weeks, 6 months and 10 months. Bone formation will be evaluated by measuring serum osteocalcin and alkaline phosphatase. Bone density and

cortical thickness in the host animals will also be assessed by faxitron X-ray and pQCT analysis.

NOTE: Technical Objective 3 revision was approved in June, 2005.

Revised Technical Objective 3: To explore the possible mechanism(s) for why transplantation of HSC-enriched cells transduced to express BMP4 did not induce bone formation as expected.

1) To determine if silencing of the BMP2/4 transgene occurs, we will transplant donor Sca-1^+ cells transduced to express BMP 2/4 (or marker control gene) into myelosuppressed recipient mice and evaluate transgene expression at 8 weeks and 6 months post transplant, transgene expression will be evaluated by real time RT-PCR in RNA extracts and PCR in DNA extracts
2) To determine if BMP2/4 interferes with engraftment of Sca-1^+ cells, we will transduce Sca-1^+ cells transduced to express BMP 2/4 (or marker control gene) and transplant at 4 cell doses (500, 5000, 50,000 or 500,000 cells/recipient) into myelosuppressed recipient mice and evaluate engraftment at 4, 6, 8, 10 and 16 weeks.
3) To determine if BMP2/4 induces Sca-1^+ cell differentiation into hematopoietic lineages, we will transduce Sca-1^+ cells transduced to express BMP 2/4 (or marker control gene) and transplant at 4 cell doses (500, 5000, 50,000 or 500,000 cells/recipient) into myelosuppressed recipient mice and evaluate the percentage of various hematopoietic lineages (T-lymphocytes, B-lymphocytes, monocytic and erythroid) at 4, 6, 8, 10 and 16 weeks. Hematopoietic lineage will be assessed by immunostaining and FACs analysis.

2. Progress on Technical Objectives

Technical Objective 1

Specific Objective 1: To transplant GFP-expressing HSCs derived from transgenic mice into myelosuppressed recipient mice and assess the short-term (8 weeks), mid-term (6 months) and long-term (1 year) engraftment in the skeletal marrow and non-skeletal sites. The Sca-1 molecule has been implicated as a marker for hematopoietic stem cell (HSCs). In year 1, Sca-1^+ cells isolated from TgN-GFP donor mice were transplanted into recipient mice, and skeletal marrow and non-skeletal sites were analyzed for engraftment at various time points post-transplant. The donor TgN mouse is a transgenic strain transduced to produce the GFP marker gene. Use of this donor strain allows for the tracking of donor cells *in vivo* after transplantation. In year 2, we have initiated repeat experiments to confirm our results from the first year. For these studies, we enriched cells from the TgN donor mouse strain for stem cells by using a positive selection for cells expressing the Sca-1 surface molecule. Our original method, which has been established in our laboratory, employed Sca-1 specific antibody magnetic microbead conjugates for isolation of Sca-1 positive cells. However, due to a nationwide unavailability of Sca-1 specific antibody-magnetic microbead conjugates from the manufacturer (Miltenyi Biotech), we had to develop a new method of Sca-1 cell isolation (secondary antibody method). We first tested the efficiency of this method in parallel with the original method (primary antibody method). Figure 1 is a diagram of the Sca-1 enrichment scheme describing the primary and secondary antibody enrichment methods.

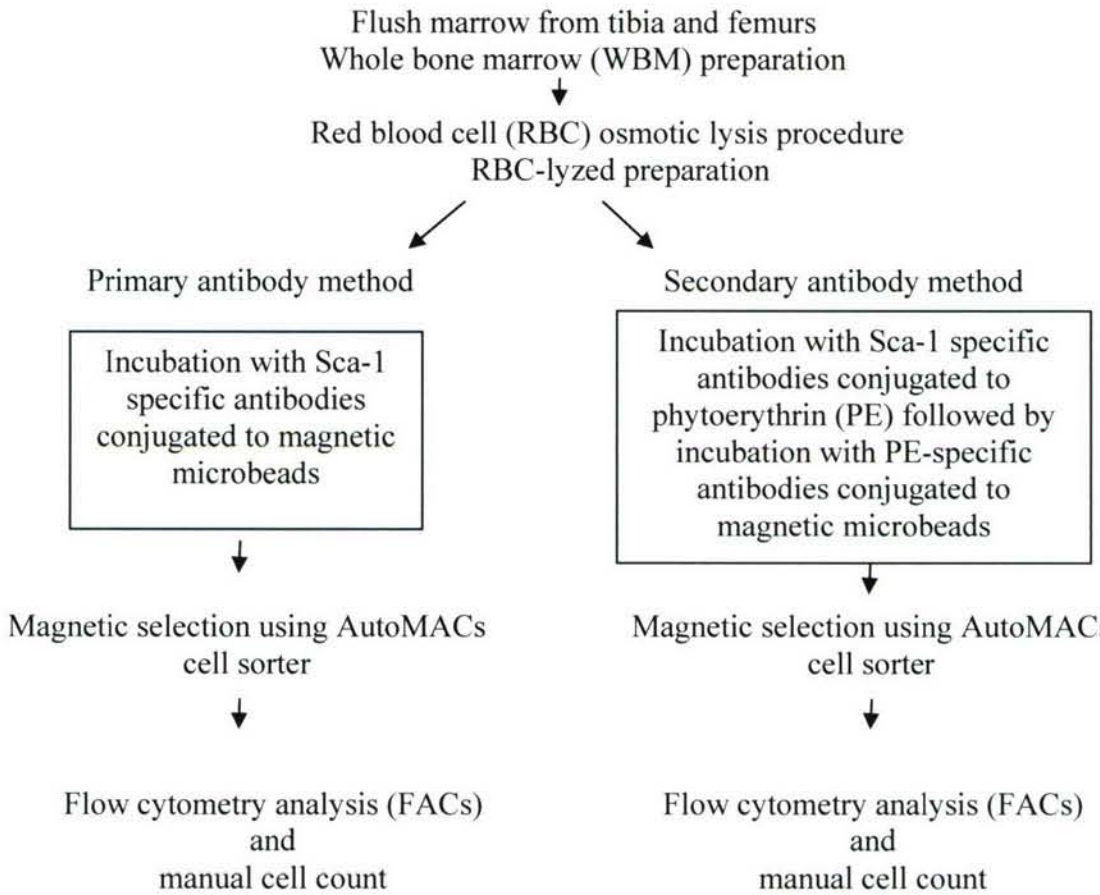

Figure 1: Sca-1 Enrichment Scheme

Briefly, whole bone marrow cells were harvested by flushing tibiae and femurs with PBS using a 26g needle and syringe. Erythrocytes were removed by osmotic lysis using a solution of 155 mM NH_4Cl, 10mM $KHCO_3$ and 110μM Na_2EDTA, followed by rinsing with PBS. After osmotic depletion of erythrocytes (RBC-lyzed), the cell preparation was divided in half. One half was enriched for Sca-1 cells by the primary antibody method by incubating the cells with Sca-1 specific antibody-magnetic microbead conjugates. The other aliquot of RBC-lyzed cells was enriched using the secondary antibody method by incubating the cells with Sca-1 antibodies conjugated to phycoerythrin (PE) fluorochrome, followed by incubation with a secondary anti-PE antibody conjugated to a magnetic microbead. In separate runs, the mixtures were applied to an automated magnetic separation column (AutoMacs™) according to manufacturer instructions. Figure 2 (below) shows the FACs analysis of cell preparations after each preparation step. Additionally, cell yields of aliquots of the WBM, erythrocyte-lysed, and Sca-1^+ cell-enriched preparations were measured by manual cell count of viable cells as determined by trypan dye exclusion.

Table 1 is a summary of enrichment and viability data of each cell preparation. Recovery was calculated by dividing the total number of cells counted after RBC-lysis and after Sca-1^+ enrichment methods by the total number of WBM cells. Total % Sca-1^+ cells was derived by

adding the upper right FACs quadrant (Sca-1^+/GFP$^-$) plus the upper left FACs quadrant (Sca-1^+/GFP$^+$) from each panel in Figure 2 after adjustment for non-specific binding using a PE conjugated rat isotype control antibody. The fold-increase Sca-1 enrichment was calculated by dividing the percentage of total Sca-1^+ cells at each preparation step by that of the WBM preparation. Recovery of cells was similar between the primary and secondary antibody methods (1.5 vs. 1.9%, respectively). As seen in the far right column of Table 1, the Sca-1 enrichment by the two methods was also similar. The primary antibody method increased the percentage of Sca-1^+ by 19-fold and the secondary antibody method by 14-fold. Furthermore, calculation of the actual number of Sca-1 cells yielded from one donor mouse by multiplying the total cells per donor mouse by % total Sca-1^+ were similar between the primary antibody and secondary antibody methods (1.3 and 1.2 million Sca-1^+ cells, respectively). These data suggest that cell enrichment and viability are comparable between the two methods of enrichment.

We next assessed the ability of cells prepared by each enrichment method to engraft in recipient mice. The Sca-1^+ cells prepared by each method were transplanted (500,000 cells in 25uL normal saline) via retro orbital injection into 14 W41/W41 recipient mice (N = 7 per group). To provide optimal engraftment, prior to transplantation, the recipient mice were sublethally irradiated by single dose (500cGY) total body irradiation. At 6 and 10 weeks post transplantation, peripheral blood was collected from each recipient by tail vein bleed. Engraftment was evaluated by FACs analysis of the percentage of GFP-expression (donor) cells in the peripheral blood samples after red blood cell lysis. A high transplantation success rate was observed with both cell preparations, with all 14 mice showing high engraftment (> 80% donor cells). Figure 3 is a bar graph showing the engraftment expressed as % GFP+ cells in recipient peripheral blood at the two time points. At 6 weeks, high engraftment was observed in both the primary and secondary antibody method (87.5 ± 2.3% and 84.7 ± 1.8%, respectively). This high engraftment was also observed at 10 weeks (90.3 ± 1.4% for the primary antibody method and 91.9 ± 1.2% for the secondary antibody method).

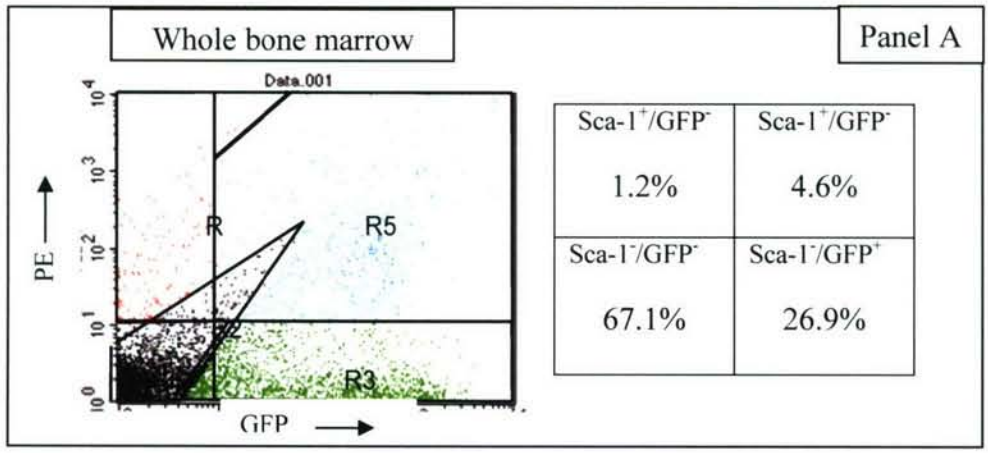

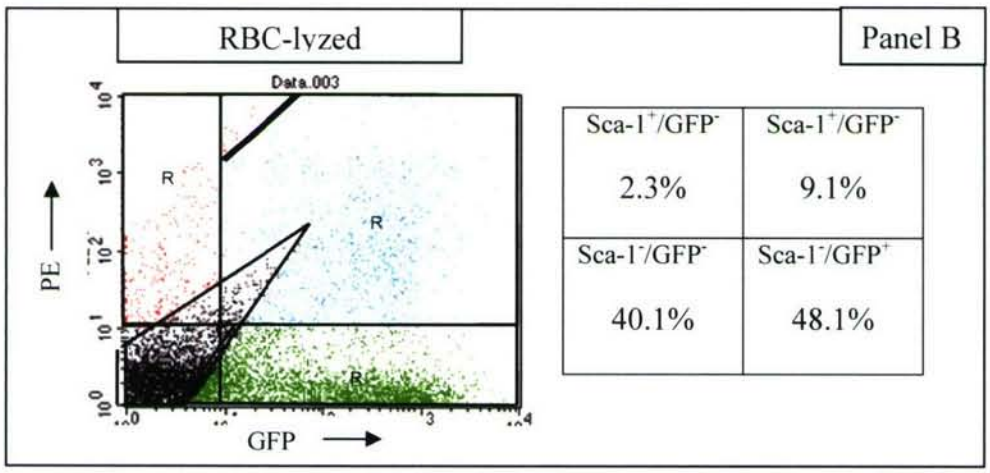

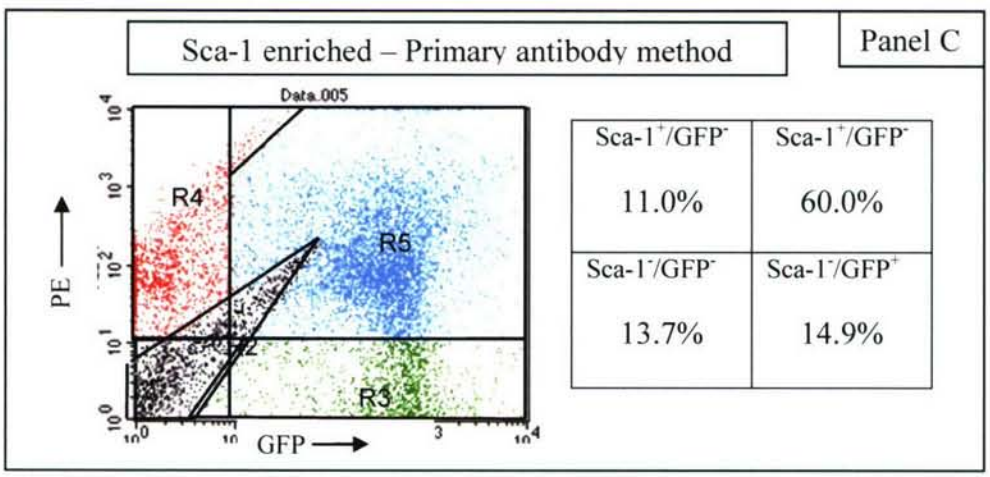

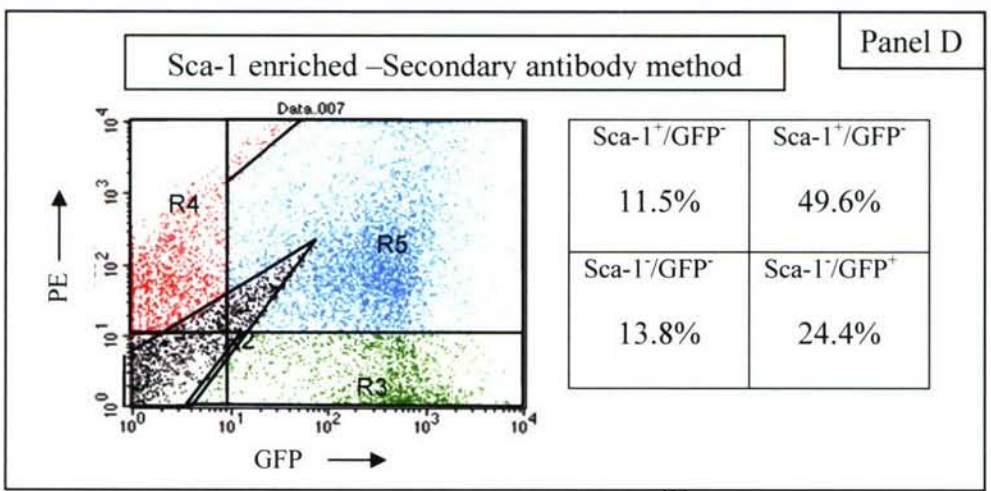

Figure 2: Flow cytometeric (FACs) analysis of cell preparations at each enrichment step. Aliquots of whole bone marrow cells from GFP-transgenic mice before (Panel A) and after (Panel B) RBC-lysis were incubated with PE-conjugated antibodies specific for Sca-1. Half of the RBC-lyzed cell preparation was enriched for Sca-1+ cells by the original method (primary antibody method) and half was enriched by an alternative method (secondary antibody method). Details of the methods are described in the text. Panels C and D show FACs analysis of the primary antibody method and secondary antibody method, respectively. Percentages of cells in each quadrant are displayed in the tables to the right of the FACs analysis graphs in each panel.

Cell counts	Total cells per donor mouse # cells x 10^6	Recovery (%)	% Sca-1^+ and GFP^-	% Sca-1^+ and GFP^+	% Total Sca-1^+	Fold-increase Sca-1 Enrichement
Whole bone marrow	131	-	0.29	3.30	3.59	-
RBC-lysed	47	36	1.38	7.75	9.13	3
Sca-1-enriched (primary antibody method)	1.9	1.5	10.33	58.14	68.47	19
Sca-1-enriched (secondary antibody method)	2.5	1.9	8.63	40.6	49.23	14

Table 1: Cell viability and enrichment cells of each preparation during the enrichment process.

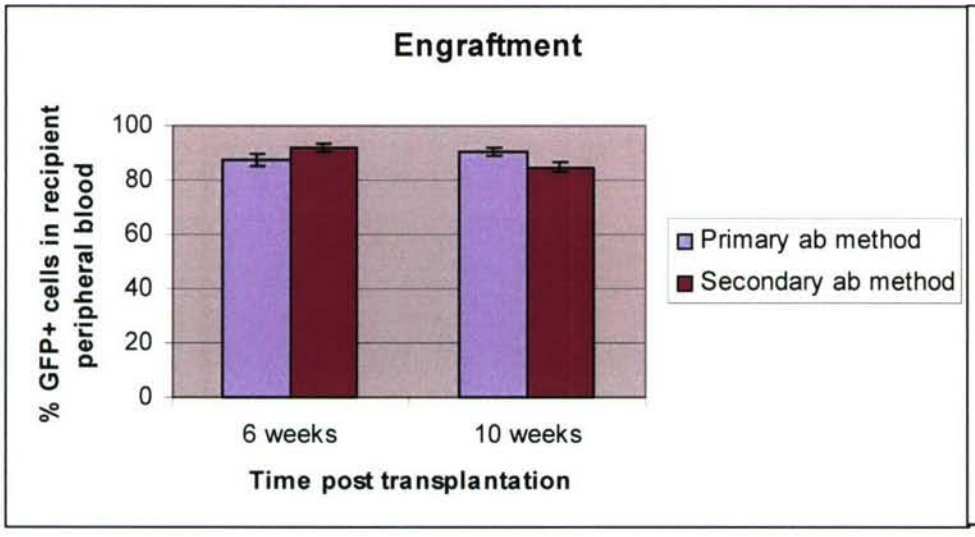

Figure 3: Sca-1^+ cells enriched by the primary and secondary antibody (ab) methods were transplanted via retro orbital injection into 14 sublethally irradiated recipient mice. Peripheral blood was evaluated by FACs analysis for percentage of GFP-expression (donor) cells after red blood lysis.

These results indicate that the two methods of Sca-1+ cell isolation are comparable in cell recovery rates, enrichment and engraftment efficiencies. Therefore, we plan to use the secondary antibody method for future experiments, until the primary antibody conjugated to magnetic beads is commercially available again. Furthermore, these results confirm data collected in our year 1 experiments. As reported in year 1, we achieve consistent recovery rates (2.6%), enrichment (12-fold increase in Sca-1+ cells) and engraftment efficiencies (70-95%) donor cells in peripheral blood of recipients.

Specific Objective 2: To determine the skeletal marrow and non-skeletal sites of engraftment in recipient mice after transplant with donor HSCs, we will assess the pluripotent ability of the engrafted donor cells to produce mature hematopoietic lineages (T-cell, B-cell, neutophil/granulocyte/monocyte and erythroid).

To confirm the results of the experiments performed in year 1, recipient mice in the transplantation experiments described above will be examined for the ability of the engrafted donor cells to produce mature hematopoietic lineages using lineage-specific immunostaining and FACs analysis of the recipients' peripheral blood. These mice have been already been transplanted and these experiments will be performed at 24 and 36 weeks post transplantation.

Specific Objective 3: To determine the skeletal marrow and non-skeletal sites of engraftment in recipient mice after transplant with donor HSCs, we will assess the presence of donor cells in non-skeletal tissues will be accomplished by frozen sectioning of the heart, lungs, liver and spleen of the recipients and fluorescent microscopic observation.

To confirm the results of the experiments performed in year 1, recipient mice in the transplantation experiments described above will euthanized at 52 weeks post transplantation. Skeletal (femurs) and non-skeletal sites (heart, lungs, liver and spleen) will be assessed for the presence of donor cells by frozen sectioning and fluorescent microscopic observation. These mice have been already been transplanted and these experiments will be performed at 52 weeks post transplantation.

Technical Objective 2:

Specific Objective 1:Transduce HSC-enriched cells with an HIV-based vector expressing the BMP 2/4 gene under the control of the CMV promoter and Specific Objective 2: Transplant transduced donor cells via tail vein into myelosuppressed recipient mice and evaluate bone formation after 8 weeks, 6 months and 10 months.

In experiments performed in year 1, we observed that that transplantation of Sca-1^+ cells transduced to express the BMP4 transgene does not result in large increases in bone formation. These results have been confirmed in additional experiments in year 2. For these studies, Sca-1^+ cells from TgN donor mice were isolated and transduced with either a marker gene (b-gal) or BMP2/4 transgene lentiviral based vectors. To explore whether a different bone formation-promoting transgene might increase endosteal bone in our model, we also transduced cells with a viral vector expressing the human growth hormone (hGH). Forty eight hours after transduction, aliquots of 500,000 cells of each preparation were transplanted via retro orbital injection into sublethally irradiated W^{41}/W^{41} recipient mice (N =8 per group). At 6, 8, 11, 14, 16, 20 and 24 weeks post-transplant, engraftment was assessed in the two groups. Peripheral blood was collected from the recipient mice, mononuclear cells were isolated by osmotic lysis and the % of GFP+ cells was determined by FACs analysis. Statistical analysis by one-way ANOVA showed

no significant differences in % GFP+ cells between the groups at any time point (data not shown). We next evaluated bone formation. Mice not surviving the transplantation (N=2) or showing low engraftment (N=4, less than 50% GFP+ cells in peripheral blood) were eliminated from further analysis. At 16 weeks post transplantation, recipient peripheral blood was collected via tail vein bleed and serum was isolated using microtainer specimen tubes. Serum was analyzed for expression of insulin-like growth factor-1 (IGF-1), a surrogate marker for hGH action and skeletal alkaline phosphatase (AP), a bone formation biochemical indicator. Results (mean ± standard deviation) are presented in Table 2. Serum IGF-1 levels in mice transplanted with cells overexpressing hGH (N=5) were significantly higher than those of control mice (N=6) and BMP2/4-transplanted mice (N=7) ($p < 0.01$). There were no significant differences in serum IGF-1 levels in BMP2/4-transplanted mice compared to controls. The increased levels of IGF-1 indicate that we successfully transduced donor cells with the hGH transgene, and achieved transgene expression after transplantation, and that the hGH was functionally active.

Serum AP levels were elevated in the BMP2/4-treated group compared to the control group, but this difference did not reach statistical significance. Surprisingly, serum AP levels in the hGH-treated mice were significantly lower than those of BMP2/4 ($p < 0.05$). The serum AP values for the hGH-treated mice were decreased compared to control mice, but again, statistical significance was not achieved. The reason for this surprising reduction in serum AP in hGH mice is currently under investigation.

Treatment	Serum IGF-1 (ng/ml)	Serum AP (U/L)
b-gal (control)	382 (42)	29 (4)
hGH	545 (71) *†	25 (4) †
BMP	417 (36)	32 (3)

Table 2. Serum biochemical indices of mice transplanted with cells overexpressing b-gal (control), hGH or BMP2/4. Mean ± (standard deviation). * p-value < 0.01 vs., b-gal controls, † p-value < 0.05 compared to BMP2/4 treatment group.

Bone formation parameters [total bone mineral density (BMD), trabecular BMD, cortical BMD, cortical thickness, endosteal circumference or periosteal circumference] of femurs from the 3 groups of mice were determined (Table 3). ANOVA analysis indicated significant differences in 3 parameters: total BMD, trabecular BMD and endosteal circumference. Post hoc analysis using the Tukey HSD test showed that total BMD was significantly lower in mice transplanted with cells overexpressing hGH compared to controls ($p < 0.05$) and to the BMP2/4 group ($p < 0.01$). In contrast, no significant differences were observed in total BMD between the BMP2/4-transplanted mice and controls. Trabecular BMD was elevated in mice in the BMP2/4 treatment group compared to control mice ($p < 0.05$) and hGH treated mice ($p = 0.01$). However, comparison of hGH-treated mice and controls showed no significant difference between the two groups. Endosteal circumference was largest in the hGH group, followed by values for the control mice. Mice transplanted with cells expressing hGH had the highest endosteal circumference and were significantly increased compared to the BMP2/4-treated mice ($p < 0.01$). the enlarged endosteal circumference may indicate an increase in endosteal bone resorption. No difference was observed in endosteal circumference in control mice and those transplanted with cells overexpressing either BMP2/4 or hGH.

Taken together, these data suggest that overexpression of the hGH transgene results in a decrease in bone formation and an increase in endosteal resorption. Parameters in the hGH-transplanted mice showing significant differences from controls (decreased serum AP, decreased

total BMD and increased endosteal circumference) indicate a negative effect on bone formation. Congruent with these results,

	Total BMD	Trabecular BMD	Endosteal circumference
b-gal (control)	0.770 (0.03)	0.266 (0.03)	3.61 (0.25)
hGH	0.687 (0.08)* †	0.234 (0.02)	3.90 (0.05) †
BMP2/4	0.790 (0.04)	0.312 (0.03)* ‡	3.45 (0.24)
ANOVA p-value	0.01	0.0009	0.015

Table 3. pQCT analysis of mice transplanted with cells overexpressing b-gal (control), hGH or BMP2/4. Mean ± (standard deviation). * p-value = 0.05 vs., b-gal controls, † p-value = 0.01 compared to BMP2/4 treatment group, ‡ p-value = 0.01 compared to hGH treatment group.

trabecular BMD in the hGH group was lower than that of controls, although statistical significance was not achieved. In contrast, parameters for the BMP2/4 group suggest a positive effect on bone formation. Trabecular BMD was significantly increased in the BMP2/4-transplanted mice compared to controls, and although not statistically significant, the BMP2/4 mice had higher serum AP, total BMD and smaller endosteal circumference. We acknowledge that these results should be interpreted with caution. Results from experiments performed in year 1, showed no significant differences in bone formation parameters between controls and BMP2/4-treated mice. We suspect that the reason for this discrepancy may be the wide variation in transplantation success and engraftment efficiencies in the year 1 experiments. At that time, we were employing the tail vein injection method as a means of intravenously delivering cells. With this method, we had a transplant success of approximately 50%, with engraftment efficiencies ranging from 5% to 70%. In year 2, we began using retro orbital injections as the injection technique which greatly improved our success rate (83%) and engraftment efficiency (70-90%). In the future, we plan on repeating this experiment using the retro-orbital injection method. An alternative explanation for why no bone formation changes were noted in year 1 experiments is that the transgene expression levels in the recipient mice may be widely variable and/or at a dose too low to elicit statistically significant measurable differences. To explore this possibility, we plan on determining transgene transduction levels (DNA incorporation) and expression levels (RNA) in mononuclear blood cells samples of recipient mice using real time PCR and RT-PCR assays. Finally, although BMP4 is a well-established promoter of bone formation in many animal models, it is possible that overexpression of this protein may adversely affect stem cell engraftment and/or hematopoietic differentiation. Therefore, we also plan to study engraftment kinetics and hematopoietic differentiation in future work.

In February, 2005 we submitted new technical objectives that propose to explore mechanisms that may interfere with bone formation induction with overexpression of BMP4. In June 2005, we received approval to proceed with the revised Technical Objectives.

Technical Objective 3:

Specific Objective 1: To determine if silencing of the BMP2/4 transgene occurs we will, Transplant donor Sca-1$^+$ cells transduced to express BMP 2/4 (or marker control gene) into myelosuppressed recipient mice and evaluate transgene expression at 8 weeks and 6 months

post transplant. Transgene expression will be evaluated by real time RT-PCR in RNA extracts and PCR in DNA extracts. Mice have been transplanted and analyses of these experiments will be performed as described.

Specific Objective 2: To determine if BMP2/4 interferes with engraftment of Sca-1$^+$ cells, we will transduce Sca-1$^+$ cells transduced to express BMP 2/4 (or marker control gene) and transplant at 4 cell doses (500, 5000, 50,000 or 500,000 cells/recipient) into myelosuppressed recipient mice and evaluate engraftment at 4, 6, 8, 10 and 16 weeks. Mice have been transplanted and analyses of these experiments will be performed as described.

Key Research Accomplishments

1) We have repeated enrichment experiments and confirmed that we can consistently achieve high enrichment of Sca-1$^+$ cells. This is in spite of a change in technique that was necessary due to difficulty in obtaining reagents from the manufacturer.
2) We have repeated engraftment experiments and confirmed that we can consistently achieve high transplantation success (83%) and high, stable engraftment of Sca-1$^+$ cells (70-90%) in the skeletal tissues of recipient mice for up to 40 weeks using the retro orbital injection method.
3) We have repeated transduction experiments using the BMP2/4 transgene and confirmed that we can successfully transduced Sca-1$^+$ cells using a retroviral-based vector. We have also transduced cells using a retroviral-based vector that overexpresses an alternative transgene, the human growth hormone (hGH). Elevated expression of a surrogate protein (IGF-1) observed in the serum of recipient mice transplanted with hGH-transduced cells indicates successful *in* vivo engraftment and transgene expression.
4) We have repeated transplantation experiments using the BMP2/4 transgene. Results from year 2 experiments suggest that overexpression of BMP2/4 may result in small increases in bone formation. However, in initial experiments performed in year 1, no changes in bone formation were observed. As a result, we are repeating these experiments again. Furthermore, we have modified our technical objectives to explore possible explanations for the minimal response observed.
5) We have demonstrated that Sca-1$^+$ cells retrovirally transduced to express hGH result in decreased bone formation in recipient mice.

Reportable Outcomes

None

Conclusions

In our systemic gene therapy subproject, we can achieve consistently high yields of highly enriched hematopoietic progenitor cells from donor mice. Transplantation of these cells into preconditioned recipient mice results in consistently high, stable engraftment in the skeletal tissues, with minimal engraftment in non-skeletal tissues of the recipient animal. We have successfully transduced the hematopoietic progenitor cells using retroviral-based vectors which overexpress BMP2/4 or hGH. Transplantation with donor cells retrovirally transduced to express BMP4 or hGH did not produce large increases in bone formation in recipient mice as expected. Therefore, as a means of improving our gene therapy model, we have revised our technical objectives to explore the potential mechanism(s) of action that may explain these results.

Project 7: Study Of Synergistic Growth Factors In Skeletal Gene Therapy

Introduction

Skeletal gene therapy utilizing osteogenic growth factors has shown promising results in our laboratory and others (1,2). Recent studies have strongly suggested that the effect of a single growth factor on the healing of skeletal injuries can be considerably enhanced by combination with a second growth factor (3). Thus, there is a strong rationale for the development of combination therapies that employ two or more therapeutic genes acting synergistically to promote healing of skeletal injuries. Accordingly, the overall goal of this project is to develop safe and effective combination *ex vivo* gene transfer-based therapies to deliver two or more osteogenic genes for repair of skeletal injuries. This approach will involve transplantation of primary bone marrow stromal cells transgenically engineered to express two or more osteogenic genes at appropriate concentrations to the skeletal injury site to promote healing of bone defects. The immediate objective is to identify the appropriate combination of osteogenic genes and their optimal concentrations. Specifically, the current project sought to evaluate the therapeutic potential of primary bone marrow-derived stromal cells overexpressing two osteogenic genes (Cox-2 and VEGF) in a mouse calvarial critical size defect model.

Body

1. Technical Objectives

The following specific objectives were proposed for the first year (year 1) of the project:

1) To prepare MLV-based retroviral vectors expressing the Cox-1 and VEGF genes, and to characterize transgene expression levels following transduction of primary bone marrow derived stromal cell cultures (MSCs) *in vitro*.

2) To evaluate the impact of transplantation of MSCs expressing Cox-1 and VEGF on the rate and quality of healing of critical-sized mouse calvarial defects *in vivo*.

The specific objectives for the current reporting year (year 2) are:

3) Optimize the dose and time of growth factor combinations with regard to bone formation time and bone quality

4) Initiate studies aimed at determining the molecular mechanism of bone formation by osteogenic growth factors

This report focuses on our progress made towards Specific Objectives of the current reporting year (year 2). However, to facilitate the understanding of the reader of our progress report, we will also briefly summarize our progress made towards the proposed work of year 1 in this report. Our results thus far support the notion that this novel therapeutic approach is technically feasible and can significantly improve bone regeneration in a mouse calvarial model. On the other hand, our results also disclose potential problems with ex vivo Cox-2 gene transfer-based therapy for healing calvarial bone defects. Nonetheless, our findings may yield information relating to the mechanism of Cox-2 action *in vivo* with respect to bone healing.

2. Progress on Technical Objectives

A. Summary of Progress for year 1

Specific Objective 1: To prepare MLV-based retroviral vectors expressing the Cox-1 and VEGF genes, and to characterize transgene expression levels following transduction of primary bone marrow derived stromal cell cultures (MSCs) in vitro.

1. Optimization of cell culture conditions for mouse bone marrow derived stromal cells.

Our initial approach was to use a cell type that has been previously used successfully as donor cells to promote bone growth in ex vivo gene transfer-based therapies. Of the three cell types (skin fibroblasts, skeletal muscle-derived myoblasts, and bone marrow-derived stromal cells) that have been used successfully as donor cells in *ex vivo* skeletal gene therapy applications, we chose to utilize bone marrow-derived stromal cells (MSCs) in these experiments because of our previous success in healing critical bone defects in a rat calvarial model using an *ex vivo* gene therapy strategy that employed MSCs (1). During the past year, we found that mouse MSCs grow best in alpha-MEM containing 15% fetal bovine serum. Under these cell culture conditions, mouse MSCs exhibit a doubling time of 24 to 48 h, and can be continuously passaged for 8 –12 weeks without a significant loss in their proliferative capacity. This is sufficient to produce enough cells for *ex vivo* gene therapy applications. Therefore, this cell culture condition was adopted for use in our subsequent experiments.

2. Construction of MLV-based retroviral vectors expressing the VEGF and Cox-2 genes.

We chose VEGF and Cox-2 genes as the test genes because these two genes have been shown to have both osteogenic and angiogenic effects and because angiogenic action, in addition to osteogenic action, is necessary for a complete bone healing. We chose MLV-based vectors for our work because we have extensive experience with these vectors (4) and because these vectors have been shown to effectively transduce proliferating rat and human MSCs. An MLV-based vector containing the 165 amino acid form of human vascular endothelial growth factor (VEGF-A_{165}) (5) was constructed as described previously (4). Expression of the VEGF gene is under control of a constitutively active CMV promoter in an MLV-based retroviral expression plasmid. Similarly, an MLV-based retroviral expression containing the human Cox-2 (Cyclooxygenase 2; Prostaglandin H synthase) was also prepared by the same approach (4). The 72-kDa Cox-2 gene product catalyzes the first step in the biosynthesis of prostaglandins: the conversion of arachidonic acid to prostaglandin H_2 (6). The biological activity of recombinant Cox-2 has been verified in the rat femoral fracture model (7). An MLV retroviral vector expressing human bone morphogenetic protein 4 (BMP-4) was included in our experiments as a positive control to which the therapeutic efficacy of VEGF and Cox-2, either alone or in combination, is compared. In this construct (designated BMP2/4), the signal sequence of the BMP-4 gene is replaced by a signal sequence from the BMP-2 gene. The MLV retroviral vector expressing BMP2/4 has been described previously (4) and has been shown to completely heal critical-sized calvarial defects in a rat model (1). All MLV (MFG-based) retroviral vectors used in this study were grown and titered by the Vector Support Service at the MDC as described previously (4).

3. Characterization of recombinant growth factor expression in transduced primary mouse MSCs *in vitro*.

Mouse MSCs were transduced with MLV-based retroviral vectors according to a 2- or 3-hit (transduction) protocol established by the MDC Vector Support Service Facility. Briefly, cells were plated in 6-well dishes to 50-70% confluency, and then incubated 2 or 3 times over 24 hrs or 36 hrs with a recombinant MLV vector at a dose of 10 – 20 infectious retroviral particles per

cell. This 2- or 3-hit protocol over 24 to 36 hrs ensures that cells are actively proliferating and undergo at least one cell division in the presence of the retroviral vector, which is necessary for the reverse transcribed retroviral DNA genome (carrying the growth factor transgene) to enter the nucleus of the host cell for stable integration into the host genome. Experiments performed with MLV vectors expressing the reporter genes beta-galactosidase (□Gal) or enhanced green fluorescent protein (GFP) demonstrated that transduction efficiencies by this approach frequently exceed 90% of the MSC target cell population under these conditions.

Expression levels of recombinant Cox-2 and BMP2/4 protein in transduced MSCs were examined by Western blots and quantitated by densitometric analysis of the specific protein bands. The production of recombinant Cox-2 levels by the transduced cells reached a relatively high level of 600 – 1200 ng/10^6 cells, whereas that of recombinant BMP2/4 was expressed at levels of 100 – 200 ng/10^6 cells 7 days after transduction. Recombinant VEGF expression levels were measured by ELISA and found to be secreted at a rate of 250 to 500 ng/10^6 cells/24 hrs 7 days after transduction.

Although recombinant growth factor expression was maintained for several weeks after retroviral transduction, growth factor production levels by the transduced cells were found to decrease at different rates for each of the three recombinant proteins. Over a 4-week period in continuing cultures, Cox-2 and BMP2/4 levels produced by the transduced cells declined by 90% from their initial values, whereas that of VEGF production decreased by only 40%. Interestingly, □Gal and EGFP expression was reduced by only 20% over this same period of time. It remains to be determined whether this time-dependent decline is caused by selective gene silencing or by a decrease in the relative numbers of transduced MSCs expressing the transgene (e.g., due to growth arrest or apoptosis of cells expressing high levels of the recombinant growth factor protein) or both. Work is under way to address these possibilities.

Specific Objective 2: To evaluate the impact of transplantation of MSCs expressing Cox-1 and VEGF on the rate and quality of healing of critical-sized mouse calvarial defects in vivo.

1. Establishing a mouse calvarial model for *ex vivo* skeletal gene therapy.

The critical sized calvarial defect model was used because we have good experience with the rat calvarial defect model and because we have shown that the rat calvarial defect model can be used to demonstrate the bone healing effects of BMP4 (1). A bone defect is defined to be of critical size if healing does not occur spontaneously over an extended period of time. Such defects are ideal for testing the growth promoting activity of novel therapeutic modalities such as growth factor gene therapy. A widely used model in bone biology is the rodent calvarial defect, which involves the creation of a circular defect in the center of the parietal bone. Without treatment, calvarial defects do not heal over a period of up to 12 weeks (8). However, treatment with an appropriate growth promoting modality can effect complete healing within 3-4 weeks (1). A main attraction of this model is the easy management of the surgical site. Unlike defects involving limbs or the spinal column, no stabilization is required because this site does not bear any load. Test substances can easily be inserted into the defect and are held tightly in place after suturing of the skin.

During the initial phase of healing of calvarial defects, osteoblasts at the margin of the defect proliferate rapidly, migrate a short distance towards the center of the wound and establish mineralization of the matrix along the wound periphery. This activity is stimulated by growth and differentiation factors that are released locally. Failure to close the critical size defect is thought to result from a deficiency in the level or persistence of local growth factor production

(6). Calvarial defects therefore provide an ideal model in which to test the effectiveness of gene therapy strategies aimed at increasing local growth factor production through transplantation of cells transduced *ex vivo* with recombinant retroviral vectors.

While we have extensive experience in the rat calvarial defect model, we had little experience in the mouse calvarial defect model. Consequently, an important initial goal in this study was to successfully establish a mouse calvarial defect model. The move from a rat model to a mouse model will allow us to take advantage of the availability of a large number of transgenic and knockout mouse strains in which the impact of growth factor gene therapy on molecular mechanisms governing bone regeneration can be studied. In the first year we have successfully established the methodologies needed to create a 5 mm diameter critical-sized defect in mouse calvariae using a diamond-based dental burr. Careful handling of the instrument is required to avoid damaging the highly vascularized dura mater, which can cause excessive blood loss and death of the animal.

Preliminary experiments were conducted with MSC that had been transduced to express either growth factor genes or reporter genes used as controls. These experiments indicated that the mouse calvarial defect model is suitable to the strategy of developing novel growth factor therapies. The progress of these experiments is the focus of this report and is described in detail in the following section.

B. Summary of Progress for the current reporting year (year 2).

Specific Objective 3: Optimize the dose and time of growth factor combinations with regard to bone formation time and bone quality.

1. Analysis of the impact of *ex vivo* gene therapy strategies on the rate and quality of healing of critical-sized mouse calvarial defects.

In our initial experiments, bone formation was assessed 14 d post-transplantation of 1 x 10^6 transduced mouse MSCs cultured overnight on a gelatin matrix scaffold designed to fit the size of the critical defect. Primary murine MSCs were transduced with recombinant MLV vectors expressing either Cox-2, VEGF, BMP2/4 (positive control), or GFP (negative control) and expanded in culture for 14 to 21 days before being applied to the gelatin matrix scaffold. Bone formation was assessed 14 d post-transplantation into the calvarial defect of recipient mouse of the same strain using X-ray densitometry and histology.

As expected, there was no increase in bone density in the defects transplanted with the control cells expressing GFP. In contrast, significant increases in bone density were evident in all defects treated with BMP2/4 expressing MSCs. Surprisingly and intriguingly, transplantation of Cox-2 expressing MSCs resulted in no increase in bone density relative to GFP treated controls. In addition, no increase in bone formation was evident in defects treated with VEGF-expressing cells. However, there was evidence of increased blood vessel formation in this group of animals indicating that sufficient amounts of functional recombinant VEGF was being expressed over the course of these experiments. Conversely and surprisingly, there was no evidence for an increase in angiogenesis in animals treated with Cox-2 expressing cells.

Histological analysis confirmed the results of our bone density analysis. Staining for the bone formation marker alkaline phosphatase was strong throughout the entire defect in animals treated with recombinant BMP2/4 expressing cells, whereas all other experimental groups displayed only weak alkaline phosphatase staining, if at all, along the old bone and at the edge of the defects. Consistent with alkaline phosphatase staining, von Kossa staining for calcium deposits showed increased mineralization in BMP2/4 treated animals. No mineralization was

evident in any of the other experimental groups. Interestingly, in addition to increased blood vessel formation, critical defects treated with VEGF expressing cells also contained more soft tissue in the area of the defect. This was not observed in defects treated with Cox-2 or GFP expressing cells. The absence of a bone formation response with VEGF was not unexpected as it had been shown that VEGF, while able to enhance the bone formation potential of BMP-4, was actually inhibiting bone formation when administered alone (3). While there are many reports showing osteogenic activity of VEGF, it may only be active in conjunction with other factors regulating skeletal healing, such as BMPs.

The absence of an increase in bone formation in Cox-2 treated defects was surprising in view of the many reports that have demonstrated the osteogenic action of Cox-2 and its essential role in bone fracture healing (9). Since the recombinant Cox-2 protein produced by our construct was functional in the fracture repair model and *in vitro* (7), the lack of an angiogenic effect suggests that Cox-2 recombinant protein was not expressed during the test period or was not expressed at sufficient amounts to produce a biological effect. However, experiments utilizing Cox-2 as a therapeutic gene in a femur fracture model have shown that significant increases in

Figure 1: Cross-Section of Calvarial Defect 4 weeks after Implant. Calvariae were dissected after 4 weeks and photographed after coronal sectioning. Arrows mark the edges of the 5-mm defects that were implanted with 1 x 10^6 cells. Shown are representative examples of implant groups that obtained βGal control cells (A) and BMP-4 producing cells (B). Implants containing 4:1 mixture of Cox-2 and VEGF transduced cells (C) and 4:1 mixture of BMP and Cox-2 cells (D) are also shown.

bone formation do not occur until 14 to 21 days post-treatment (7). Thus, an alternative possibility is that there was not sufficient time in our experimental design to allow the Cox-2 transgene to promote bone formation.

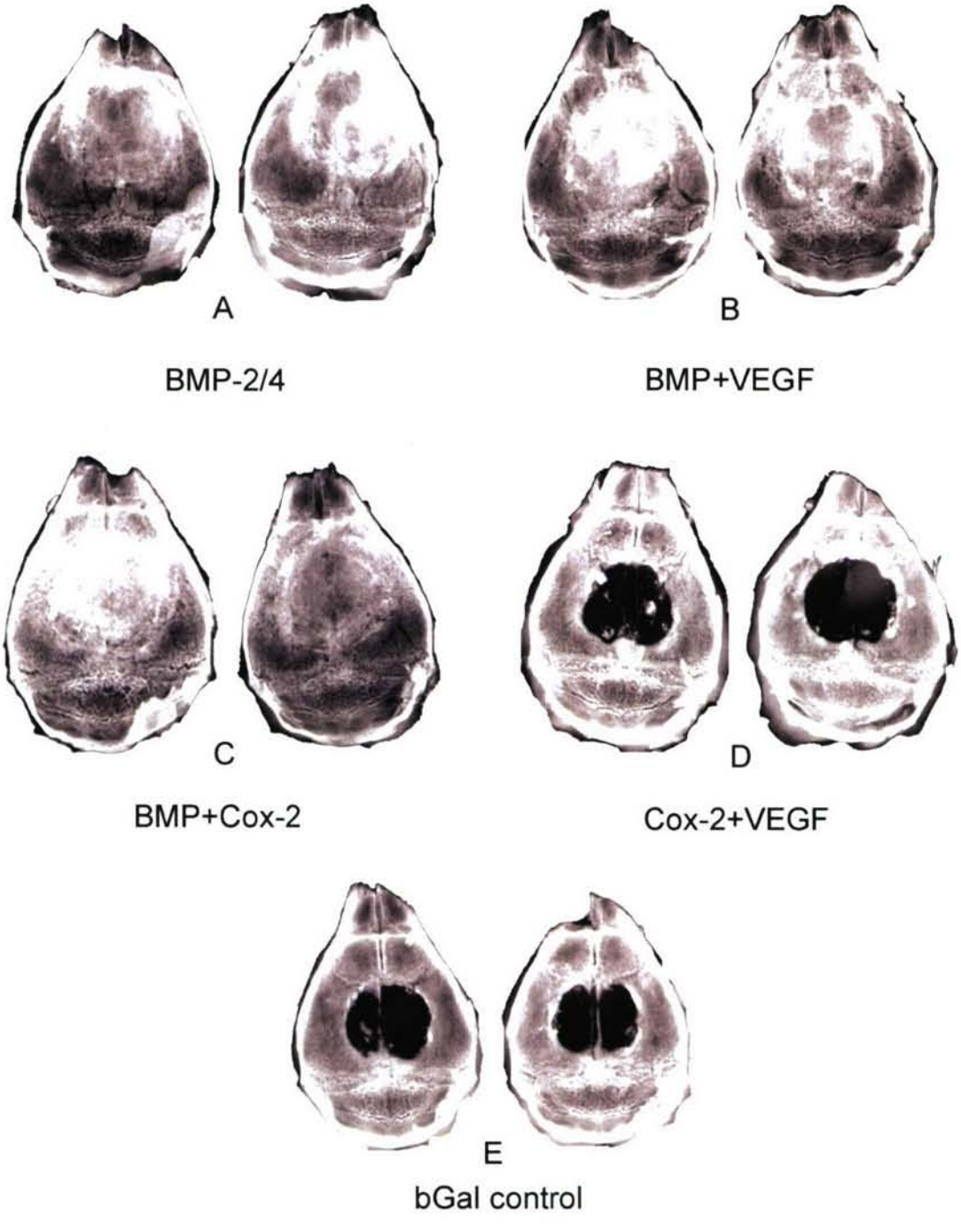

Figure 2: Digital X-Ray Images of Calvarial Defect Model. Shown are 2 representative examples from implant groups that obtained a total of 1 x 10^6 gene-modified mouse bone marrow stromal cells. Group A was implanted with BMP-cells only, and group E with βGal control cells only. Mixtures in a 4:1 ratio were implanted in groups B-D, namely BMP (8 x 10^5) plus VEGF (2 x 10^5) in B, BMP (8 x 10^5) plus Cox-2 (2 x 10^5) in C, and Cox-2 (8 x 10^5) plus VEGF (2 x 10^5) in D.

To address the alternative possibility that longer Cox-2 treatment may be needed for enhanced calvarial healing, a second experiment was performed in which bone formation was evaluated 4 weeks post-transplantation with MLV vector transduced MSCs expressing appropriate growth factor genes. The experimental design was as follows:

1. BMP2/4 alone (positive control);
2. β-Gal alone (negative control);
3. BMP2/4 + VEGF (4:1 mixture);
4. BMP2/4 + Cox-2 (4:1 mixture); and
5. Cox-2 + VEGF (4:1 mixture).

Each of these experimental groups consisted of 5 animals. Each of these animals was implanted with 1 x 10^6 MLV-transduced MSCs on a gelatin matrix as described above. Animals were sacrificed 4 weeks post-transplantation and calvariae were analyzed for bone formation by X-ray densitometry and histology.

Similar to the results seen after 2 weeks of treatment, substantial bone formation was seen in defects treated with MSCs expressing BMP2/4 alone. The extent of bone formation was much more pronounced at this later time point, as evidenced by the calvarial cross sections shown in Figure 1. Defects implanted with BMP2/4 expressing cells exceeded the thickness of the original bone several fold (panels B and D). Soft X-ray imaging indicated that all defects treated with cells expressing BMP2/4 had completely healed by 4 weeks post-transplantation (Figure 2, panels A, B, and C). On the other hand, no significant increase in bone formation was evident in defects treated with cells expressing Cox-2 and VEGF cells (4:1 ratio) (Figure 1, panel C and Figure 2, panel D) relative to negative control animals treated with cells expressing □Gal (Figure 1, panel A and Figure 2, panel E).

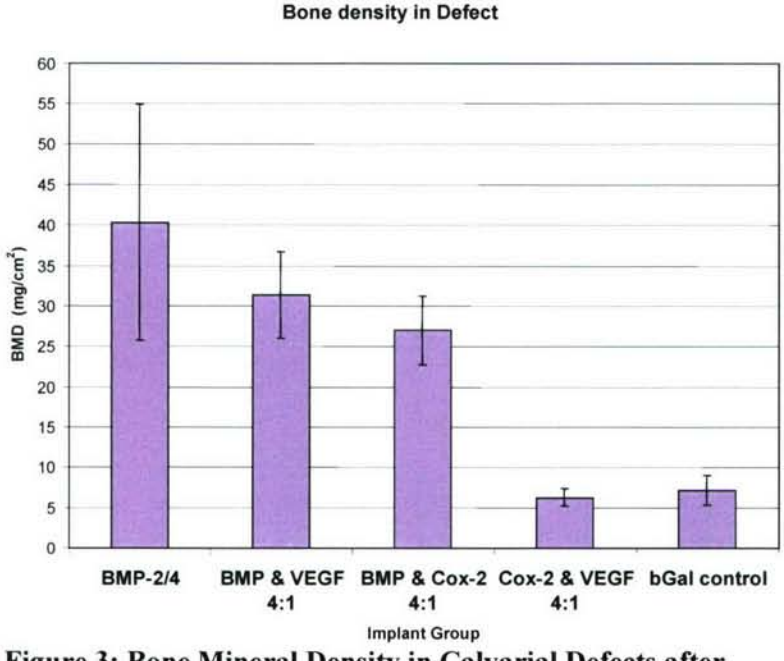

Figure 3: Bone Mineral Density in Calvarial Defects after Implanting with Marrow Stromal Cells. Calvariae were dissected 4 weeks after implant of cells as described in the text. Implant groups contained the modified stromal cells that were described in Figure 2. Bone mineral density (BMD) was measured by dual-energy X-ray absorptiometry (DEXA) using a PIXImus soft-X-ray densitometer (Lunar, Madison WI) and analysis software version 1.46 provided by the manufacturer. Values are average (± SD) from 4 animals for each group.

As shown in Figure 3, quantitative densitometry indicated that the highest bone mineral density (BMD) was reached in the group with BMP-4 cells alone, at 159% (± 57%) of control values.

Implants with mixtures of BMP2/4 +VEGF (123% ± 57%) or BMP2/4 + Cox-2 (107% ± 17%) were slightly lower. Implants with mixtures of MSCs expressing BMP2/4 and VEGF (123% ± 57%) or Cox-2 (107% ± 17%) produced slightly lower BMDs, a finding that is in line with the 20% lower number of BMP2/4 cells implanted in these mixed groups. Aside from increased bone formation in BMP2/4 treated defects, the only other consistent change seen in this study was an increase in vascular tissue mass in animals treated with cells expressing VEGF (Figure

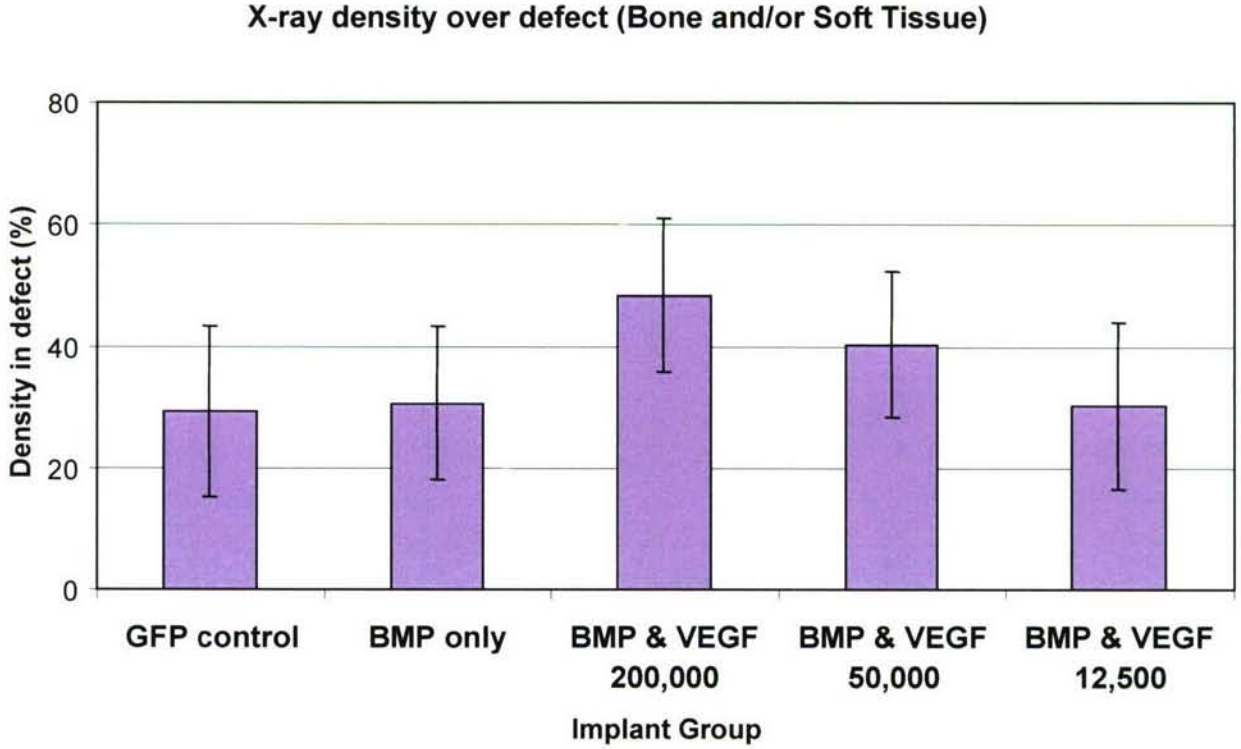

Figure 4: Tissue Density in Calvarial Defects after 4 weeks with BMP and VEGF cells. Calvariae were implanted with 3 x 10^5 growth factor-modified cells and dissected after 4 weeks. X-ray images of the calvariae were taken with a Faxitron MX20 system using Cronex 10T medical X-ray film. Density over the defect area was determined from the film on a low light imaging system (Alpha Innotech) and analyzed with Chemi-Imager 4400 software. Values are average (+/- SD) from 4 animals for each group, which received (from left to right): 3 x 10^5 GFP control cells; 1 x 10^5 BMP plus 2 x 10^5 GFP cells; 1 x 10^5 BMP plus 2 x 10^5 VEGF cells; 1 x 10^5 BMP plus 5 x 10^4 VEGF plus 1.5 x 10^5 GFP cells; 1 x 10^5 BMP plus 5 x 10^4 VEGF plus 1.5 x 10^5 GFP cells; and 1 x 10^5 BMP plus 1.25 x 10^4 VEGF plus 1.875 x 10^5 GFP cells.

1C). However, the presence of VEGF producing cells did not increase bone formation relative to BMP2/4 alone, and the presence of Cox-2 expressing cells had no significant impact on calvarial bone formation when combined with either BMP2/4 or VEGF.

2. VEGF increases soft tissue formation in a dose-dependent manner in the presence of low amounts of BMP.

Because of the strong bone formation response obtained with BMP2/4-cells in the calvarial implants, additional effects by other growth factors may have been masked and thereby may not be readily apparent. We therefore performed several dose-response experiments in the presence of much lower numbers of BMP2/4-cells (1 x 10^5) than are required to elicit complete healing within the standard 4-week observation period (5 x 10^5 to 1 x 10^6). While we found that in the

absence of BMP2/4-cells implanted VEGF cells increase vascularization, but not soft tissue or bone formation (Figure 1), addition of 2 x 10^5 or 5 x 10^4 VEGF cells increased the amount of soft tissue formed after 4 weeks in the presence of 1 x 10^5 BMP cells (Figure 4). The increase in soft tissue density was dose-dependent at the higher VEGF concentration, and had reached background levels with the lowest amount of VEGF cells implanted in this experiment (1.25 x 10^4 cells). While there was no increased formation of mineralized bone in this combination of BMP2/4 and VEGF cells, the increase in soft tissue formation was only seen with the combination of BMP2/4 and VEGF cells, and not with VEGF cells alone (data not shown). These findings do not support a synergistic enhancement between BMP2/4 and VEGF in bone formation at the test doses.

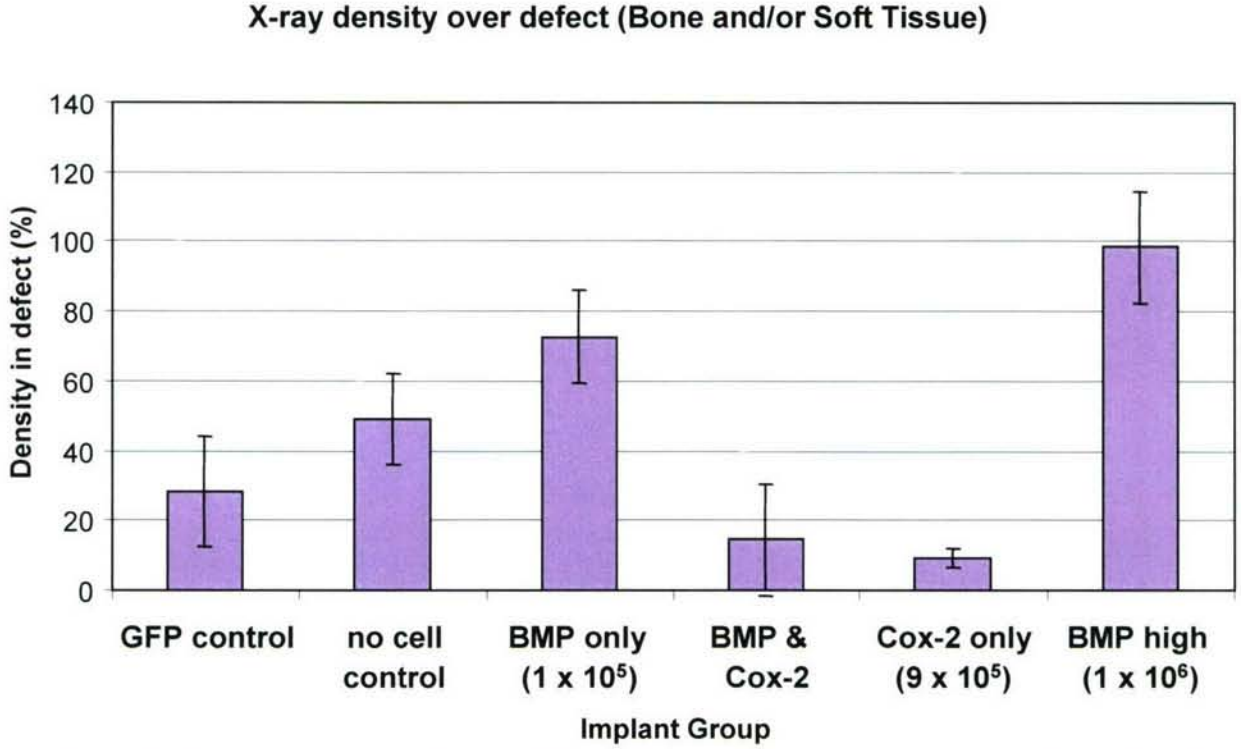

Figure 5: Tissue Density in Calvarial Defects after 4 weeks with BMP and Cox-2 cells. Calvariae were implanted with 1 x 10^6 growth factor-modified cells and density over the defect determined after 4 weeks as described in Figure 4. Implants contained (from left to right): 1 x 10^6 GFP control cells; Gelfoam matrix control with no cells added; 1 x 10^5 BMP plus 9 x 10^5 GFP cells; 1 x 10^5 BMP plus 9 x 10^5 Cox-2 cells; 9 x 10^5 Cox-2 plus 1 x 10^5 GFP cells; and 1 x 10^6 BMP cells. Values are average (+/- SD) from 4 animals for each group

3. Cox-2 reduces soft tissue formation and suppresses BMP-induced bone formation.

As with VEGF, the effect of Cox-2 may have been masked in the presence of high concentrations of BMP2/4 cells that are already eliciting the maximal bone formation response in the defect. Such a situation applies to the experiments previously described in Figs. 1 – 3, where 8 x 10^5 or 1 x 10^6 BMP2/4 cells were implanted, in addition to cells expressing either VEGF or Cox-2. Additional experiments were therefore performed with 1 x 10^5 BMP2/4-cells mixed with 9 x 10^5 Cox-2 or GFP control cells. This low concentration of BMP2/4 cells usually elicits between 15% - 25% of the maximal bone formation response obtained with 1 x 10^6 BMP cells

(Figure 5). Absolute values of bone formation vary between experiments, because the amount of BMP2/4 expression by the transduced mouse MSCs fluctuated considerably between transductions. Differences in titer of the viral preparation used for transduction are one of the primary sources for these experimental variabilities. The small differences in growth rate, which varied between different MSC preparations, passage number, and experimental variation in plating of the cells, could also give rise to substantial differences in the amount of transgene expressed in cells used for implants. Therefore, comparisons between experiments are not always possible (such as the values for 1 x 10^5 BMP cells in Figures 4 & 5) and are best made within experiments using the same cell preparation.

The most striking observation from the experiment shown in Figure 5 is the total suppression of the bone formation response from the low amount of BMP2/4 cells, when combined with a 9-fold excess of Cox-2 modified cells. This observation is very puzzling, as we anticipated that even if Cox-2 had no bone formation effect or enhancing effect in bone formation, Cox-2 should not abrogate the bone formation effects of BMP2/4. The finding that Cox-2 blocked BMP2/4 in stimulating bone formation could be relevant to the molecular mechanism of Cox-2 in the regulation of bone formation. In this regard, the observation that BMP2/4 mRNA levels were reduced in the presence of Cox-2 cells (described in Figure 6 below) might suggest that Cox-2 might have an inhibitory effect on BMP2/4 transgene expression in this experimental model. This might explain the loss of bone formation response of BMP2/4 in the presence of Cox-2. The mechanism of this interaction is currently under investigation. In addition, Cox-2 cells alone also greatly reduce the amount of soft tissue formed in the defect compared to control (GFP) cells. This raises the possibility that high Cox-2 expression might adversely affect the number of transduced cells or the ability of transduced cells to express the transgene.

Specific Objective 4: Initiate studies aimed at determining the molecular mechanism of bone formation by osteogenic growth factors.

1. Background for interaction of Cox-2, VEGF and BMPs.

Cyclooxygenase-2 (Cox-2) is an inducible enzyme that converts arachidonic acid to prostaglandin H_2, which is the precursor of prostaglandin E_2 (PGE_2). Prostaglandins such as PGE_2 are known to participate in inflammatory responses, increase osteoblast activity and new bone formation, and also increase osteoclast activity and subsequent bone resorption. In a recent study, PGE_2 was shown to increase BMP-2 expression in osteoblasts (9). In view of evidence that BMP-2 increases Cox-2 gene expression (10), we postulate that BMP-2, Cox-2, and PGE_2 could form a positive feedback loop that promotes osteoblast proliferation and differentiation. Observations such as these, along with studies of Cox-2 deficient mice, provide strong evidence that Cox-2 and PGE_2 are important mediators of both endochondral and intramembranous bone formation. In fact, in Cox-2 deficient mice, intramembranous bone formation on calvaria was seen to be reduced by up to 60% compared to wild type mice (11). Accordingly, the lack of an increase in bone formation in defects with transplantation of Cox-2 cells is very surprising and puzzling.

The absence of a significant increase in bone formation in our mouse calvarial model following transplantation of Cox-2 expressing cells may be due to a number of factors, including:

1. Insufficient Cox-2 expression and PGE_2 production in transplanted MSCs due to silencing of recombinant Cox-2 expression or cytotoxic effects on MSCs expressing high levels of recombinant Cox-2.
2. The inability of PGE_2 synthesized by transplanted MSCs to influence bone formation due to physical barriers or distance from target cells in the wound site.
3. PGE_2 can only function in an autocrine manner, requiring target cells to be directly transduced with the MLV vector expressing Cox-2.
4. Inhibition of Cox-2 expression (and thereby PGE_2 synthesis) by transduced cells in response to factors secreted during the bone repair process, thereby negating the bone formation effect of Cox-2 expressing MSCs.

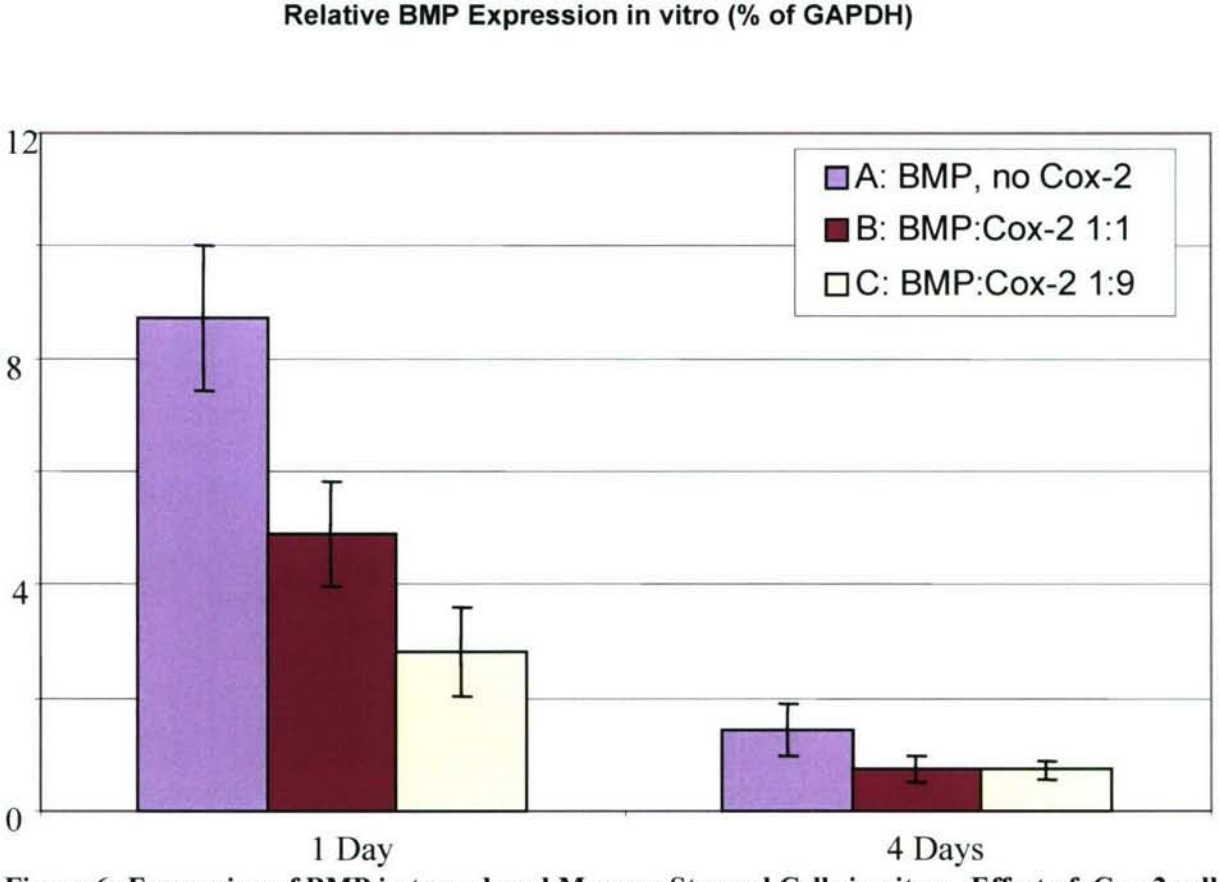

Figure 6: Expression of BMP in transduced Marrow Stromal Cells in vitro – Effect of Cox-2 cells. Gelfoam strips of 5 x 10 mm were loaded with 2 x 10^5 MSC expressing BMP, in combination with Cox-2 cells or with control cells expressing GFP. All Gelfoam strips received a total of 2 x 10^6 cells, and were incubated in wells of 6-well plates containing 2ml of growth medium. After 1d and 4d, strips were briefly washed in PBS, cut in half, and used for isolation of RNA and DNA. RNA was reverse transcribed and analyzed by real-time PCR using specific primers for the human BMP4- transgene. Expression of BMP was calculated relative to GAPDH by using the difference in cycles over threshold, $\Delta C(T)$. Values are average (+/- SD) from 3 Gelfoams, each ran in triplicate on an Opticon real time PCR system (MJ Research), using a QuantiTect Sybergreen PCR kit (Qiagen). Group A received 2 x 10^5 BMP and 1.8 x 10^6 GFP cells. Group B received 2 x 10^5 BMP, 2 x 10^5 Cox-2, and 1.6 x 10^6 GFP cells. Group C received 2 x 10^5 BMP, and 1.8 x 10^6 Cox-2 cells.

Vascular endothelial growth factor (VEGF) is also known to play an important role in bone repair by promoting angiogenesis as well as the recruitment and survival of chondrocytes, osteoblasts, and osteoclasts at the site of injury. VEGF is particularly important for hypertrophic cartilage remodeling and ossification during endochondral bone formation. More recently, VEGF has been shown to be an early mediator of intramembranous bone formation in response to mechanical force (distraction osteogenesis) (12). The absence of a significant increase in bone formation following transplantation with MSCs expressing recombinant VEGF is consistent with the observation by Peng et al. (3) that VEGF alone does not improve bone regeneration in a mouse calvarial model. The absence of a significant increase in bone formation in the presence of both BMP2/4 and VEGF is likely due to the fact that the ratio of BMP2/4 and VEGF expression has not been optimized in our mouse calvarial model.

2. Effect of Cox-2 cells on BMP mRNA *in vitro*.

As indicated earlier, a potential explanation for the observed loss of bone formation in mixtures of Cox-2 cells with suboptimal concentrations of BMP2/4 cells could be due to reduction of BMP2/4 produced by the transduced cells or to loss of BMP2/4 expressing cells in the implant in response to the presence of the Cox-2 or PGE_2. As an initial test of this possibility, an *in vitro* experiment was performed to assess the BMP2/4 and Cox-2 gene expression in gelatin implant matrices containing both cell types. Gene expression was assessed by real-time PCR.

After 1 day and 4 days, total RNA was prepared and the level of BMP-mRNA was determined by Reverse Transcription and quantitative real-time PCR (Figure 6). When expressed relative to the GAPDH reference gene, BMP mRNA levels from 1×10^5 BMP cells on day 1 are reduced by half in the presence of 1×10^5 Cox-2 cells, and are even lower (32%) with 9×10^5 Cox-2 cells, when compared to controls with GFP cells. The latter condition corresponds to that described in Figure 5, where the high Cox-2 cell concentration completely suppressed the bone formation response of the BMP implant. We are currently using the *in vitro* system in order to understand the mechanism of this interaction. If it is found that Cox-2 specifically interferes with BMP expression from our implant cells, this could explain the loss of bone formation in the calvarial implants.

3. Consideration for Future Studies

1. Evidence from studies of Cox-2 effects in a femur fracture model indicate that little or no response is evident over the first 14 d post treatment with Cox-2, but that a significant bone regenerative response is evident after 21 d post-treatment (7). These results suggest that Cox-2 may need to be expressed continuously over a prolonged time period in order to be able to influence bone formation. On the other hand, BMP2/4 may only be required for a brief period, during which the proliferation and differentiation signal has been transmitted to a sufficient number of osteoprogenitor cells in order to assure continued bone formation and closing of the defect.

2. In order to address this question, we will assess the transgene expression levels within the calvarial defect by real-time PCR. Expression levels at 14 and 28 day post-transplantation will be

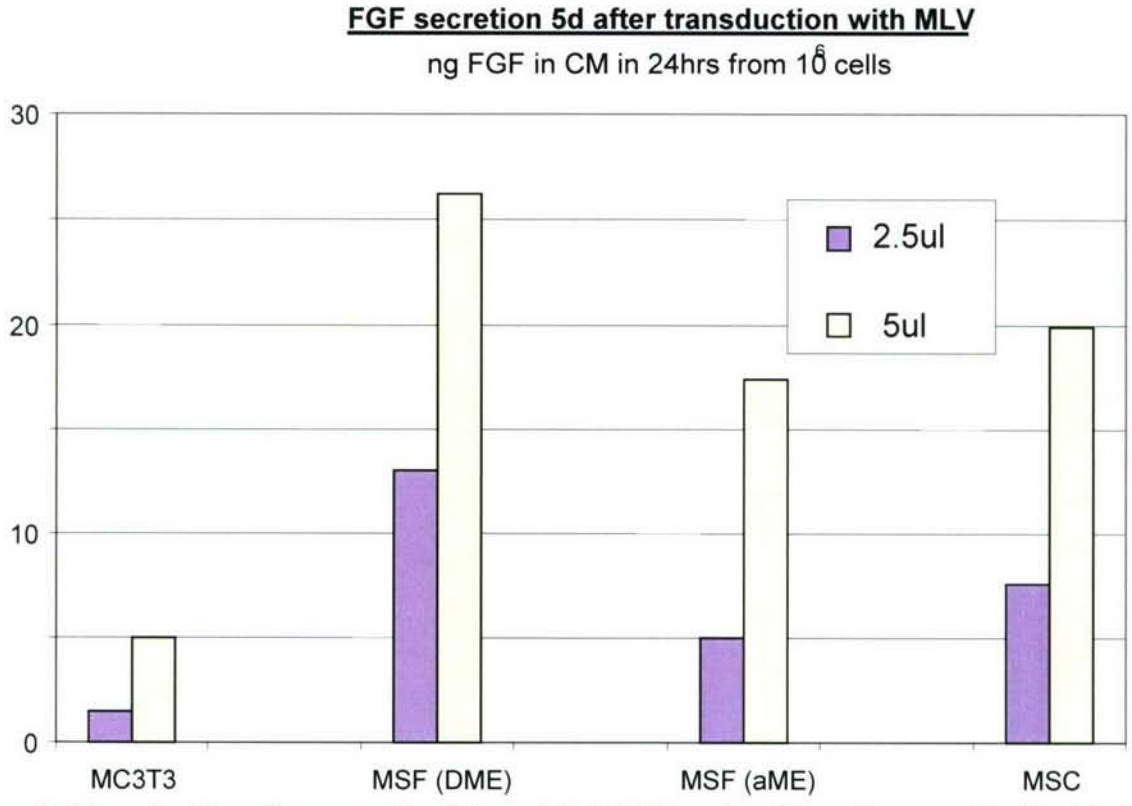

Figure 7: Transduction of mouse cells with modified FGF vector. Normal mouse skin fibroblasts (MSF), stromal cells (MSC) and the osteogenic cell line MC3T3 were plated at a density of 50,000 cells in 6-well plates. After 24h, the cells were transduced with either 2.5 or 5 µl concentrated MLV – preparation in 1.25 ml of growth medium containing 8 µg/ml polybrene. Medium was removed and replaced with fresh virus for a total transduction period of 24 h. Cells were then passaged into 10 cm Petri dishes in standard growth medium (MC3T3 in DMEM, 10% FBS; MSC in αMEM, 15% FBS; MSF was cultured in both media, as indicated in the Figure). Medium was changed on day4 after transduction and collected the next day for measuring the FGF concentration by ELISA (R&D Systems Quantikine kit). Cell numbers were determined and the results expressed as ng of FGF secreted per 1 x 10^6 cells in 24h. Left columns are from 2.5 µl, right coumns from 5 µl viral concentrations.

compared to expression in transplanted cells at time 0 and 2days. This will provide a profile of growth factor expression levels over the course of 28 day post-transplantation that can be related to therapeutic outcomes. Real-time PCR analysis of the persistence of MLV genomic sequences over the course of the experiment will provide a measure of transplanted cell survival and will discriminate between the contribution of gene silencing and cell death to any reduction in growth factor expression. For this purpose, we have designed gene-specific primers and established conditions to measure the presence of transgenes by real time PCR. Experiments are currently in progress aimed at determining the fate of the transplanted cells in the implants by real time PCR and the level and duration of growth factor gene expression by real time RT-PCR. This will be crucial in order to find growth factor combinations that can successfully heal large bone defects.

3. If our experiments indicate that expression of Cox-2 and/or VEGF are not sufficiently high or that expression in the implants declines too fast in order to sustain bone formation, we will explore alternatives that may result in higher activity in implanted cells. Specifically, new implant scaffolds have been described that promote adhesion, growth, and osteodifferentiation of MSCs (13). We will evaluate these newly developed carriers for implantation of our gene-modified cells. Otherwise, if we find that Cox-2 and VEGF, expressed at sufficiently high levels for 2 – 4 weeks in the defect, are not effective in promoting bone healing in combination with each other or with BMP-4, we will explore other osteogenic growth factors such as activin or FGF for synergistic effects in the healing response. In preparation of these experiments, we have transformed various cell preparations with a modified version of basic FGF (FGF-2, Figure 7). This modified FGF gene secretes the growth factor more efficiently than the wild type (14). From these transductions we have prepared both MSC and fibroblast cells that secrete FGF at levels of 20 – 50 ng/ml per $1x10^6$ cells per 24h for extended time periods. These cells will be used in order explore synergistic effects of FGF with other growth factors in the calvarial defect model.

Key Research Accomplishments

1) Cell culture conditions for the growth of mouse bone marrow derived stromal cells (MSCs) have been optimized.

2) MLV-based retroviral vectors expressing recombinant Cox-2 and VEGF have been constructed.

3) MSCs have been shown to be efficiently transduced by MLV-based retroviral vectors, and recombinant Cox-2 and VEGF expression has been verified and quantitated *in vitro* over a 4-week period.

4) Surgical techniques needed to establish the mouse calvarial critical defect model have been developed.

5) Transplantation of MSCs expressing recombinant BMP2/4 alone was shown to result in complete healing of critical sized mouse calvarial defects by 4 weeks post-treatment.

6) Transplantation of MSCs expressing recombinant Cox-2 alone did not promote regeneration of critical sized mouse calvarial defects at either 2 or 4 weeks post-treatment.

7) Transplantation of MSCs expressing recombinant VEGF alone was shown to increase blood vessel formation at 2 and 4 weeks post-treatment, but did not promote bone formation at either time point.

8) Transplantation of mixtures of MSCs expressing recombinant BMP2/4 and VEGF, BMP2/4 and Cox-2, and Cox-2 and VEGF did not produce a significant increase in bone formation at 4 weeks post-treatment relative to the impact that each of these growth factors had alone.

9) VEGF-cells, in combination with suboptimal concentrations of BMP-cells, increase the amount of soft tissue formation in the defect, but do not enhance bone formation over controls.

10) Cox-2 cells in high concentration reduce the amount of soft tissue formation in the defect, and, in combination with suboptimal concentrations of BMP cells, completely abolish the bone formation response.

11) Cox-2 cells in implant matrix incubated in vitro, reduce the production of BMP from mixed-in BMP-cells. This observation could explain the loss of bone-formation response in implants, and the mechanism of this effect is currently under investigation.

Reportable Outcomes

None

Conclusions

1) The results of these studies to date provide good evidence that this novel therapeutic approach is technically feasible and can significantly improve bone regeneration in a mouse calvarial model. Bone marrow derived stromal cells (MSCs) can be grown to sufficient numbers *in vitro* and are efficiently transduced by MLV-based retroviral vectors resulting in sustained expression of the therapeutic transgene.

2) Most importantly, transplantation of MSCs expressing recombinant BMP2/4 was shown to promote complete healing of a critical sized calvarial defect by 4 weeks post-treatment. This result establishes the feasibility of this novel therapeutic approach and demonstrates that all of the critical components of this experimental mouse model for bone regeneration have been successfully established in our laboratory.

3) The absence of a significant increase in bone formation in defects treated with MSCs expressing recombinant Cox-2 was unexpected but raises important questions relating to the mechanism of Cox-2 action *in vivo*. This experimental model will be used to systematically investigate ways to optimize the therapeutic impact of Cox-2, VEGF, and other growth factors on critical sized calvarial bone defects.

References

1. Gysin R, Wergedal JE, Sheng MH-C, Kasukawa Y, Miyakoshi N, Chen S-T, Peng H, Lau K-HW, Mohan S, Baylink DJ. (2002) *Ex vivo* gene therapy with stromal cells transduced with a retroviral vector containing the BMP4 gene completely heals critical size calvarial defect in rats. Gene Ther. 9:991-999.

2. Klamut HJ, Chen S-T, Lau K-HW, Baylink DJ (2004) Progress toward skeletal gene therapy. Crit. Rev. Eukaryot. Gene Expr. 14:89-136.

3. Peng H, Wright V, Usas A, Gearhart B, Shen H-C, Cummins J, Huard J (2002) Synergistic enhancement of bone formation and healing by stem cell-expressed VEGF and bone morphogenetic protein-4. J. Clin. Inv. 110:751-759.

4. Peng H, Chen ST, Wergedal JE, Polo JM, Yee JK, Lau K-HW, Baylink DJ. (2001) Development of an MFG-based retroviral vector system for secretion of high levels of functionally active human BMP4. Mol.Ther. 4:95-104.

5. Tischer E, Mitchell R, Hartman T, Silva M, Gospodarowicz D, Fiddes JC, Abraham JA (1991) The human gene for vascular endothelial growth factor: Multiple protein forms are encoded through alternative exon splicing. J. Biol. Chem. 266:11947-11954.
6. Hla T, Neilson K (1992) Human cyclooxygenase-2 cDNA. Proc. Natl. Acad. Sci. USA 89:7384-7388.
7. Rundle, CH, Strong DD, Chen S-T, Sheng MH-C, Wergedal JE, Lau K-HW, Baylink DJ (2005) Retroviral-based gene therapy with cyclooxygenase-2 promotes the union of bony callus tissues and accelerates fracture healing. Manuscript in preparation
8. Krebsbach PH, Mankani MH, Satomura K, Kuznetsov SA, Gehron Robey P (1998) Repair of craniotomy defects using bone marrow stromal cells. Transplantation 66:1272-1278.
9. Arikawa T, Omura K, Morita I (2004) Regulation of bone morphogenetic protein –2 expression by endogenous prostaglandin E2 in human mesenchymal stem cells. J. Cell Physiol. 200:400-406.
10. Chikazu D, Li X, Kawaguchi H, Sakuma Y, Voznesensky OS, Adams DJM, Hoshio K, Katavic V, Herschman HR, Raisz LG, Pilbeam CC (2002) Bone morphogenetic protein 2 induces cyclo-oxygenase 2 in osteoblasts via a Cbfa1 binding site: Role in effexts of bone morphogenetic protein 2 *in vitro* and *in vivo*. J. Bone Min. Res. 17:1430-1440.
11. Zhang X, Schwarz EM, Young DA, Puzas JE, Rosier RN, O'Keefe RJ (2002) J. Clin. Invest. 110:1405-1415. Cyclooxygenase-2 regulates mesenchymal stem cell differentiation into the osteoblast lineage and is critically involved in bone repair.
12. Carvalho RS, Einhorn TA, Lehmann W, Edgar C, Al-Yamani A, Apazidis A, Pacicca D, Clemens TL, Gerstenfeld, LC. (2004) The role of angiogenesis in a murine tibial model of distraction osteogenesis. Bone 34:849-861.
13. Blum JS, Barry MA, Mikos AG, Jansen JA (2003) *In vivo* evaluation of gene therapy vectors in *ex vivo*-derived marrow stromal cells for bone regeneration in a rat critical-size calvarial defect model. Human Gene Therapy 14:1689-1701.
14. Chen S-T, Gysin R, Baylink D, Lau K-HW (2005) Modification of the Fibroblast growth factor-2 gene led to a marked enhancement in secretion and stability of fibroblast growth factor-2 protein. Manuscript submitted for publication.

Project 8: Nuclear Targeting Of Transposon-Based Plasmid Vectors For Gene Therapy

Introduction

Our primary research objective is to develop improved nonviral plasmid vectors for *in vivo* applications in hard and soft tissues by incorporating into a single vector a nuclear entry sequence to increase transfection efficiency and a transposon to increase long term transgene expression. Plasmid vectors will provide safer, less expensive, and more easily manufactured reagents for gene delivery compared to viral vectors, but, to date, have not been widely used for *in vivo* applications because of several different cellular barriers to *in vivo* transfection and transgene expression. These barriers include plasmid entry into the cell, subsequent entry into the nucleus, and for long term expression, stable transgene integration into genomic DNA. After entering cells, traditional plasmids enter the nucleus during mitosis, so transfection efficiency is dependent on active cell proliferation. We and others have identified nuclear entry DNA sequences, such as the virally derived SV40 DTS, that enhance nuclear entry of plasmid DNA and increase *in vivo* transfection efficiency and transgene expression levels even in non-proliferating cells (1-7). Traditional plasmid DNA integrates into genomic DNA randomly and with low efficiently. To improve efficiency of integration, we have also developed a plasmid vector that expresses a mammalian transposase, *Sleeping Beauty*, (SBT) in addition to the transgene of interest. The transposase facilitates transgene integration into AT-rich regions of genomic DNA, resulting in high levels of long term expression (8). No single plasmid vector has been developed that incorporates both a nuclear entry sequence and transposon with transposase expression. We propose that our enhanced plasmid expression vectors will significantly increase transfection efficiency and transgene integration, resulting in higher levels of long term therapeutic gene expression *in vivo* than are possible with existing nonviral gene therapy vectors. Our studies are designed to prepare novel plasmid vectors with nuclear entry activity, a transposon/transposase and either a marker gene or the BMP-2/4 therapeutic gene. We will show that cells expressing BMP-2/4 from a nonviral vector can produce BMP-2/4 as well as cells expressing BMP-2/4 from an MLV vector. We will show that both vector/cell systems stimulate bone formation *in vitro* and *in vivo*.

Body

1. Technical Objectives

Develop and test a novel nonviral protein expression vector for use in gene therapy. The plasmid will contain DNA sequences to: a) increase movement of the plasmid DNA into the nucleus and thus increase transfection efficiency and expression levels; and b) produce a transposase to increase stable vector DNA integration into genomic DNA, thus increasing long term transgene expression.

Specific objectives for year one that were completed in year two:

1. Insert the nuclear entry sequence from the SV40 DNA virus (SV40 DTS) into different positions of an optimized plasmid vector that can express SBT and a marker gene, Red Fluorescent Protein (RFP).
2. Compare expression levels and longevity of marker genes *in vitro* in rat bone marrow stromal cells (MSCs), and osteoblasts transfected with the SBT/SV40DTS plasmid vectors or transduced with a MLV retroviral reporter gene vector.

3. Prepare SBT/SV40DTS plasmid and MLV retroviral vectors that express human BMP-4, and test BMP-4 short term expression levels in transfected/ transduced rat MSC cultures.

The specific objectives for year two were as follows:

1. Initiate studies to compare effectiveness of SV40DTS/SBT BMP-4 plasmid and MLV BMP-2/4 viral vector in stimulating osteoblast differentiation in cultured rat MSCs and osteoblasts. Differentiation will be assessed by expression of osteoblast specific marker genes and by development of mineralized nodules.

2. Hard tissue model. Initiate studies to compare bone formation induced by rat MSCs transduced *in vitro* with SV40DTS/SBT-BMP-2/4 plasmid or MLV BMP-2/4 viral vectors *in vivo* in a rat subcutaneous implant model.

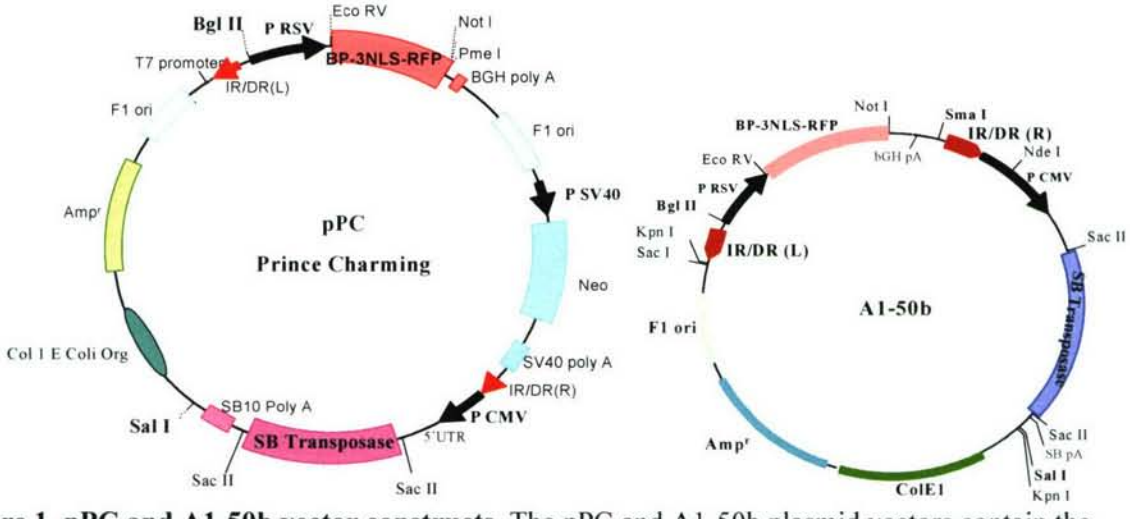

Figure 1. pPC and A1-50b vector constructs. The pPC and A1-50b plasmid vectors contain the Sleeping Beauty (SB)Transposon and transposase (SBT) and a red fluorescent protein (RFP) marker protein with the nuclear localization protein sequence from the IGFBP-3 gene on the amino terminal. When the RFP is expressed, it is localized in the nucleus. The Neomycin resistance gene expression cassette was removed from pPC by PCR to produce A1-50b. Removal of the Neomycin expression cassette reduced the size of the vector by 2 kb and this may be important because smaller DNA vectors transfect cells with more efficiency. Vectors larger than 10 kb do not transfect cells efficiently so reduction in the size of the plasmid will allow the introduction of larger transgenes before the 10 kb size is reached.

2. Progress on Technical Objectives

Summary of progress. In year one, we prepared an optimized pPrince Charming (pPC) vector called A1-50b by PCR that was reduced in size by 2 kb by removing the Neo cassette (Figure 1). We showed that in rat and human osteoblast-like cells the A1-50b vector transfected cells with a higher efficiency than the parental pPC vector (2004 Progress report). We modified the SB transposase expression cassette to further reduce the size of the A1-50b vector.

In year two, we introduced the SV40DTS into the pPC and A1-50b vectors (pPC-SV40DTS and A150b-SV40DTS) and we prepared and tested BMP-2/4 vectors with the parental and

SV40DTS containing plasmids (Tables 1 and 2) by replacing the BP3-NLS-RFP with BMP-2/4. Transfection of rat marrow stromal cells (rMSCs) and rat osteoblasts (rObs) with Effectene (Qiagen) and the pPC-SV40DTS or A150b-SV40DTS vectors resulted in long term expression of nuclear RFP in vitro. After transfection, transgene expression was stable, dividing cells expressed the transgene and colonies of cells expressing the transgene were observed in culture. Transgene expression in some cells continued for two weeks. Long term expression of more than 2-3 days was not seen with vectors that did not have the sleeping beauty transposon system.

Transfection of C2C12 cells with the pA1-50b-BMP-2/4 caused the cells to transdifferentiate and produce ALP activity. Transfection of both the pPC-SV40DTS-BMP-2/4 or the pA1-50b-SV40DTS-BMP-2/4 plasmid vectors stimulated a significant increase in ALP activity in cultured rat osteoblasts.

In year one, we found that BD Biosciences collagen scaffolds treated with fibronectin sustained growth of MLV-GFP transduced rMSCs better than OPLA and ceramic scaffolds *in vitro*. More total RNA was isolated from the collagen scaffold and more osteopontin was produced, reflecting maturation of rMSCs into active osteoblasts. In year two, we reproduced these scaffold studies and studied the ability of scaffolds to support GFP cells *in vivo* in the rat skin implant model. Pleminary data indicated that the collagen matrix supported GFP cells *in vivo* after two weeks. We are continuing to test the OPLA and ceramic scaffolds. We can use the fibronectin coated collagen supports for further studies if the ceramic and OPLA scaffolds do not support cells that express transgene for at least two weeks. The BD Biosciences collagen supports did not invoke an inflammatory response as other collagen matrix supports have.

We have shown that only the BD Bioscience collagen scaffold supports MLV-GFP-rat marrow stromal cell growth for two weeks *in vivo* in the rat implant model. Only the collagen matrix supported GFP cells *in vivo* after two weeks, while the OPLA and ceramic scaffolds did not. We will use the fibronectin coated collagen supports for further studies. The BD Biosciences collagen supports did not invoke an inflammatory response as other collagen matrix supports have.

These experiments validated the use of the skin implant system to compare the ability of rMSCs expressing BMP-2/4 from a retroviral vector and from a plasmid vector to stimulate bone formation, marker gene expression, and histological evidence of matrix deposition.

We are in the process of identifying transfection procedures that will increase transfection efficiencies in rMSCs and rat osteoblasts to 20-50% for the implant studies. The MLV vectors transduce cells with 50-80% efficiency and for *in vivo* comparison, we need sufficient transfection efficiencies to compare cells expressing BMP-2/4. Effectene (Qiagen), Nucleofector (Amaxa) and electroporation protocols are being evaluated in culture systems. rMSCs can be transfected with 5-10% efficiency with Effectene and this was not adequate to stimulate ALP activity *in vitro*. On the other hand, rat osteoblasts were transfected with 25-30% efficiency with Effectene and ALP activity was significantly increased. Because we would like to use both rMSCs and rat osteoblasts for *in vivo* implant studies, we are testing the Nucleofector-based transfection reagents which have resulted in 80-90% transfection efficiencies in similar cells (mouse osteoblasts). When transfection efficiencies of 30-50% or more are obtained in rMSCs or osteoblasts, cells on scaffolds expressing BMP-2/4 from a plasmid will be compared to cells expressing BMP-2/4 from the MLV vector for their ability to stimulate osteoblast marker gene expression *in vitro* and to stimulate bone formation *in vivo*.

Specific Objective 1. Insert the Nuclear Entry Signal from the SV40 DNA virus (SV40 DTS) into different positions of an optimized plasmid vector (A1-50b) that can express the sleeping beauty transposase (SBT) and a marker gene, Red Fluorescent Protein (RFP).

i. Preparation of a clonable SV40 DTS fragment. The 87 bp SV40 DTS (ATGCTTTGCATACTTCTGCCTGCTGGGGAGCCTGGGGACTTTCCACACCCTAACTGACACAC ATTCCACAGCTGGTTGGTACCTGCA) was subcloned into the $pGL3_{Basic}$ and peGFP (Clontech) vectors for other studies. Large quantities of a PCR product with either BglII or Sal I 5' and 3' ends were generated from these templates. We found that blunt end ligation of the small SV40 DTS fragment (as originally proposed) did not work and we subsequently changed to sticky-end ligation with Sal I and BglII overhangs.

ii. Subcloning of the Bgl II-SV40 DTS and the Sal I-SV40DTS into the pPC and A1-50b vectors. After many attempts, we found that we were unable to subclone the blunt or the sticky-ended SV40 DTS fragments directly into the A1-50b vector. We were also unable to sequence the A1-50b vector without devising new sequencing strategies (longer primers at distance from the transposon and higher temperatures), suggesting that the vector had a significant secondary structure. Because of this problem, the SV40 DTS fragments were first subcloned into the pPC vector, which readily accepted the sticky-end DNA fragments, in single or multiple copies. We subsequently removed the Neo Cassette by PCR with Fusion DNA Polymerase (New England Biolabs) and recreated the A1-50b vector with the SV40 DTS. Thus, we have both the pPC and A1-50b constructs with the placement of the SV40 DTS.

The SV40 DTS was placed as a single copy in a forward orientation within the transposon/transgene expression cassette at the Bgl II site in the pPC vector. The pPC vector was reduced in size by PCR to make A1-50b-BglII-SV40DTS. The SV40 DTS was placed into the SalI site in the pPC vector as one, two or three copies. These vectors were reduced in size by PCR to make A1-50b-SalI-SV40DTS (1-3). These vectors are described in Table I.

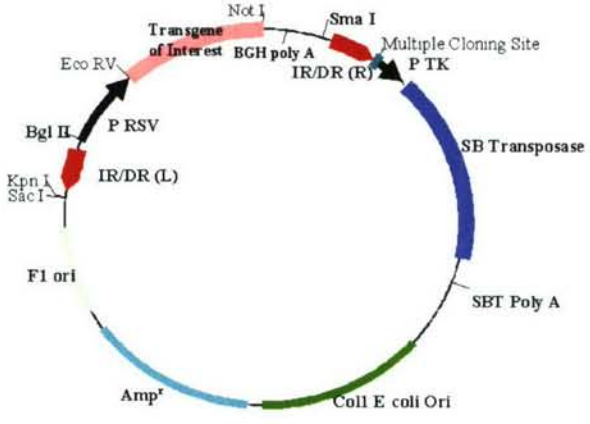

Figure 2. Structure of the A1-50b-TK-SB vector. The 6.38 kb modified pPC vector contains the BP3NLS-RFP expression cassette within the inverted repeats (IR/DRs). Weak constitutive expression of the SB Transposase is driven by the TK promoter. An enhancer can be placed in the multiple cloning site using the unique Nhe I site. A modified Kosak sequence was added to the SB Transposase cDNA to increase protein expression.

While these obstacles significantly slowed our progress, we were able to generate a number of plasmid vectors that could be used for our proposed *in vivo* studies. Table 1

summarizes the plasmid vectors with the nuclear localized RFP marker gene (BP-3NLS-RFP) that are available. We found that the SV40 DTS only in a forward orientation relative to the transgene expression cassette increased transfection efficiency while the reverse orientation suppressed transgene expression.

iii. Introduction of a modified SB Transposase expression cassette in the pPC-vectors. A recent publication (9) indicated that some promoters used to drive SB transposase expression do not function well to provide long term transgene expression in liver tissue. It was found that the relative strength of different promoters expressed in mouse liver did not correlate with the amount of stable transgene expression. Peak levels of long term gene expression were obtained with promoters 30-40 fold less active than the CMV promoter. By correlating the relative strength of the promoter driving transposase production with levels of short term and stable transgene expression, a narrow window of optimal transposase expression could be defined. The investigators concluded that successful *in vivo* transposition may depend primarily on a narrow window of SB transposase concentration obtained shortly after plasmid injection, and that overproduction of transposase can cause inhibition of long term transgene expression (10). The pPC vector was constructed with the CMV promoter to drive SB transposase activity and thus might not be optimal for gene delivery in liver and other tissues. Our original grant was written without this information and we proposed to use the CMV promoter and the EF1α promoter to drive transposase activity. Because of this publication, we have modified this aim to use a promoter that is not expressed as strongly as the CMV promoter so that inhibitory levels of the SB Transposase are not produced in cells after plasmid vector delivery. We wanted to choose a promoter system that we could easily manipulate to alter SB transposase expression levels to be optimum in each cell types and provide for cell specific transgene production. We anticipated that by developing the weakly expressed minimal Thymidine Kinase (TK) promoter together with viral or tissue specific enhancer, we could both modulate the level of transposase expression and also provide for tissue specific expression by using different tissue specific enhancers. Tissue specific expression would also increase the safety of the plasmid vectors developed for clinical use. Thus we have modified our vector design to include the TK promoter in the SB transposase expression cassette and created another set of pPC and A1-50b plasmids. (Table I)

Table 1. Plasmid vectors expressing the nuclear localizing Red Fluorescent Protein (RFP) transgene.

Vector Name	Description of Components	Comments
pPrince Charming (pPC)	RSV promoter driving transgene, SB transposase driven by the CMV promoter, Neo cassette for selection with G418	Harris, et al., 2001
pPC-SalI-SV40 DTS (PSS6B)	RSV promoter driving transgene, SB transposase driven by the CMV promoter, 1 copy of the SV40 DTS in the Sal I site, Neo cassette for selection with G418	The SV40 DTS is in a forward orientation relative to the transgene expression cassette.
pPC-SalI-SV40 DTS rev (PSS6A)	RSV promoter driving transgene, SB transposase driven by the CMV promoter, 1 copy of SV40DTS in Sal I site, Neo cassette for selection with G418	The DTS is in a reverse orientation relative to the transgene expression cassette.
pPC-Bgl II-SV40 DTS	RSV promoter driving transgene, SB transposase driven by the CMV promoter, 1 copy of the SV40 DTS in BglII site, Neo	The BglII site is within the transposon. Long term transgene expression is not

	cassette for selection with G418	affected *in vitro* by SV40 DTS position.
A1-50b	RSV promoter driving transgene, SB transposase driven by the CMV promoter	Shortened pPC by PCR
A1-50b-SalI-SV40 DTS (ASS6B)	RSV promoter driving transgene, SB transposase driven by the CMV promoter	Shortened PSS6B by PCR

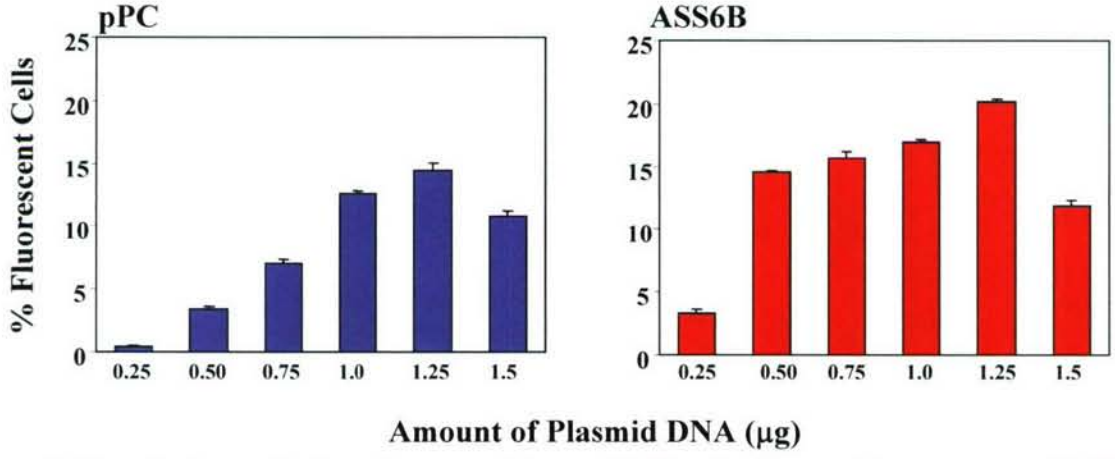

Figure 3. Transient transfection of rat osteoblasts with Sleeping Beauty Transposon and SV40 DTS containing vectors. ROS 17/2.8 cells were transiently transfected with various amounts of plasmid DNA (0.25 μg to 1.5 μg) and fluorescent cell number was evaluated after 48 hours by FACS analysis. Optimal doses were achieved at 1-1.25 μg of DNA. PPC does not have the SV40 DTS while the ASS6B vector does. Both vectors have the SB transposon. In replicate experiments with different lots of Effectene from 5-20% of ROS 17/2.8 cells are optimally transfected.

Specific Objective 2: Compare expression levels and longevity of marker gene expression in vitro in cells transfected with the SBT/SV40DTS plasmid vectors or transduced with a MLV retroviral reporter gene vector for comparison.

We prepared SB transposon vectors with the SV40 DTS either inside or outside the transposon to determine if there were differences in expression. We placed the SV40 DTS in the BglII site (inside the transposon) or in the Sal I site (outside the transposon and transposase expression cassette).

i. Optimizing Doses of plasmid DNA for transfection studies. Optimum doses of pPC and ASS6B DNA were determined in ROS 17/2.8 cells. Cells were plated at 70,000 cells per well in a 6 well plate and from 0.25-1.5 μg of Qiagen purified DNA was added to each well with 5 ul of Effectene, Enhancer and EC Buffer overnight at 37 C in 1 ml of DMEM/10% CS. DNA was removed and media was changed to DMEM/10% CS and 48 hours after transfection, transfection efficiency was analyzed by FACS. The optimal dose of both vectors was obtained at 1.25 μg. Suprisingly, transfection of the pPC vector was more dependent on dosage effects than the ASS6B vector.

ii. Transient transfection with RFP plasmid vectors. We transfected rat osteoblasts (ROS 17/2.8) with additional pPC-SV40 DTS and the A1-50b-SV40 DTS vectors (Table 1) and studied transfection efficiency and longevity of expression. Transient transfection was conducted with

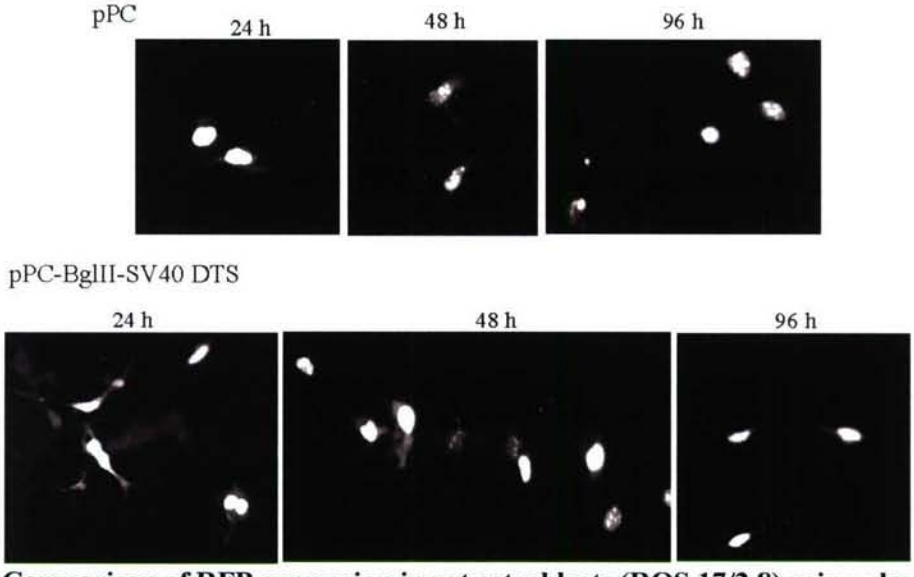

Figure 4. Comparison of RFP expression in rat osteoblasts (ROS 17/2.8) using plasmids with the SB Transposon and with or without the SV40 DTS in the BglII site. One copy of the SV40 DTS was inserted in the pPC vector at the BglII site within the transposon. The SB transposon stimulated long term expression in both types of expression vector with high levels of transgene expression for 96 hours. The placement of the SV40 DTS within the transposon does not disrubt integration and longevity of RFP expression.

Effectene (Qiagen) and 1μg of DNA. We found that RFP expression was maintained in dividing cells and in cells that were cultured for 120 hours (Figure 4 and Figure 5). ROS 17/2.8 cells transfected with peGFP vectors (Clontech), that do not contain the SB Transposon or the SV40 DTS, retained robust GFP expression for only 48 hours (data not shown).

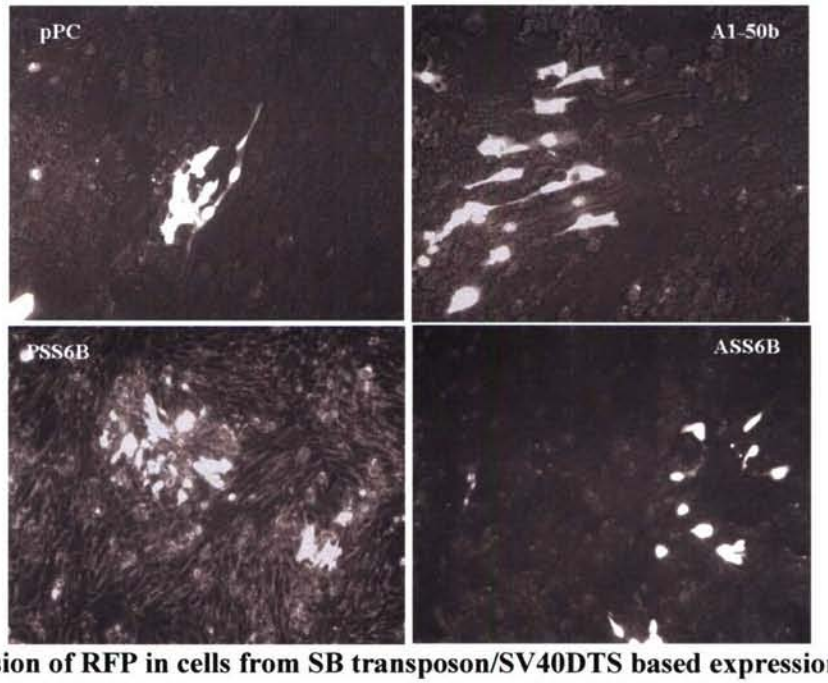

Figure 5. Expression of RFP in cells from SB transposon/SV40DTS based expression vectors with the SV40 DTS in the SalI site after transient transfection. ROS 17/2.8 cells were transfected with 1 μg of PSS6B and ASS6B and Effectene. Five days (120 hours) after transfection, fluorescent cells were characterized by epifluroescent microscopy. Colonies of fluorescent cells formed by five days and were maintained for at least nine to fourteen days in culture (data not shown). This long term expression pattern should provide sufficient transgene expression (BMP-2/4) for *in vivo* experiments.

We next compared transfection efficiencies in the same experiment with pPC, A1-50b, PSS6B and ASS6B to determine if addition of the SV40 DTS to the Sal I site and reduction in plasmid size increased transient transfection efficiency. The DTS placed in either the BglII site (within the transposon) or in the Sal I site (outside the transposon) did not interfere with expression of the transgene. We chose to focus on the plasmids with the SalI insertion in the

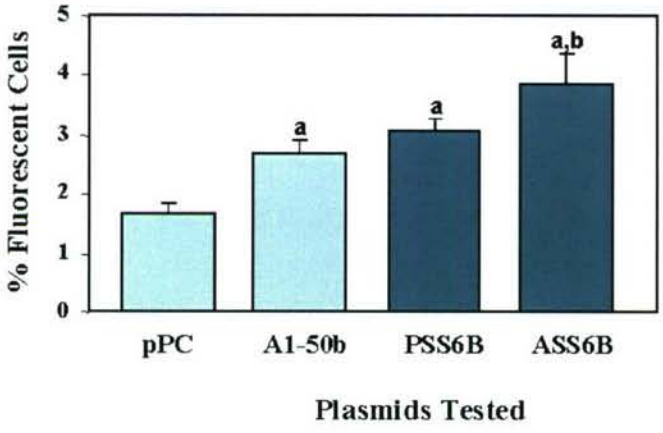

Figure 6.Comparison of transfection efficiency in osteoblsts with the various SB transposon based plasmid expression vectors. ROS 17/2.8 cells were transiently transfected with 1 μg of each plasmid. After 24 hours, FACS analysis was performed to determine transfection efficiency. Two plasmids did not contain the SV40DTS (pPC, A1-50b) and two plasmids contained one copy of the SV40DTS (PSS6B and ASS6B). a, $P < 0.05$ vs. pPC; b, $P < 0.05$ vs. pPC and A1-50b. Values are the mean fluorescent cell number out of 10,000 cells counted from each of six replicate wells $\pm$ S.E.M. Significantly higher transfection efficiencies were obtained with the PSS6B and ASS6B vectors than with the pPC vector that had no SV40 DTS.The smaller ASS6B vector with the SV40 DTS transfected cells with higher efficiency than the larger PSS6B vector but the difference was not significant.

event that transgene expression patterns might be influenced by SV40 DTS location *in vivo*.

We obtained MLV-GFP transduced rat marrow stromal cells and osteoblasts and studied expression of GFP. GFP expression was obtained in 50-80% of cells transduced with MLV-GFP and maintained robust expression for more than ten passages (data not shown). We used these cells to study cell growth and differentiation on BD Biosciences scaffolds presented below.

Specific Aim 3. Prepare SBT/SV40DTS plasmid and MLV retroviral vectors to express BMP-4, and test BMP-4 short term expression levels in transfected/ transduced rat MSC cultures.

i. Preparation of the MLV-BMP-2/4 retroviral vector.We have previously prepared the MLV-BMP-2/4 vectors and reported this in the 2004 progress report. The BMP-2/4 vector has been optimized from BMP-4 secretion.

ii. Preparation of pPC-BMP and A150b-BMP expression plasmids. We have inserted the BMP-2/4 cDNA in place of the BP-3NLS-RFP transgene and made five different SB transposon/SV40 DTS vectors starting with pPC and A1-50b constructs. We have also replaced the CMV promoter with the TK promoter in two additional. Table 2 summarizes the constructs that are available for BMP-4 expression.

Table 2. Plasmid vectors expressing the BMP-2/4 transgene.

Vector Name	Description of Components	Comments
pPC-BMP	RSV promoter driven transgene, SB transposase driven by the CMV promoter, Neo selection expression cassette	
pPC-BMP-SalI-SV40 DTS1 (PBSS6D)	RSV promoter driven transgene, SB transposase driven by the CMV promoter, 1 copy of the SV40 DTS in the Sal I site, neo selection expression cassette	
pPC-BMP-Sal I-SV40 DTS2 (PBSS3C)	RSV promoter driven transgene, SB transposase driven by the CMV promoter, 2 tandem copies of the SV40 DTS in the Sal I site, neo selection expression cassette	
pPC-BMP-Sal I-SV40 DTS3 (PBSS3B)	RSV promoter driven transgene, SB transposase driven by the CMV promoter, 3 copies of the SV40 DTS in the Sal I site, neo selection expression cassette	Transfects cells with the highest efficiency.
A1-50b-BMP-Sal I-SV40 DTS3	RSV promoter driven transgene, SB transposase driven by the CMV promoter, 3 copies of the SV40 DTS in the Sal I site	Derived from PBSS3B Also called ABSS
pPC-BMP-SalI-SV40 DTS3-TK-SB	RSV promoter driven transgene, SB transposase driven by the TK minimal promoter, 3 copies of the SV40 DTS in the Sal I site, neo selection expression cassette	Derived from PBSS3B.
A1-50b-BMP-SalI-SV40 DTS3-TK-SB	RSV promoter driven transgene, SB transposase driven by the TK minimal promoter, 3 copies of the SV40 DTS	Derived from PBSS3B. Stimulates ALP activity as well as PSS3B or

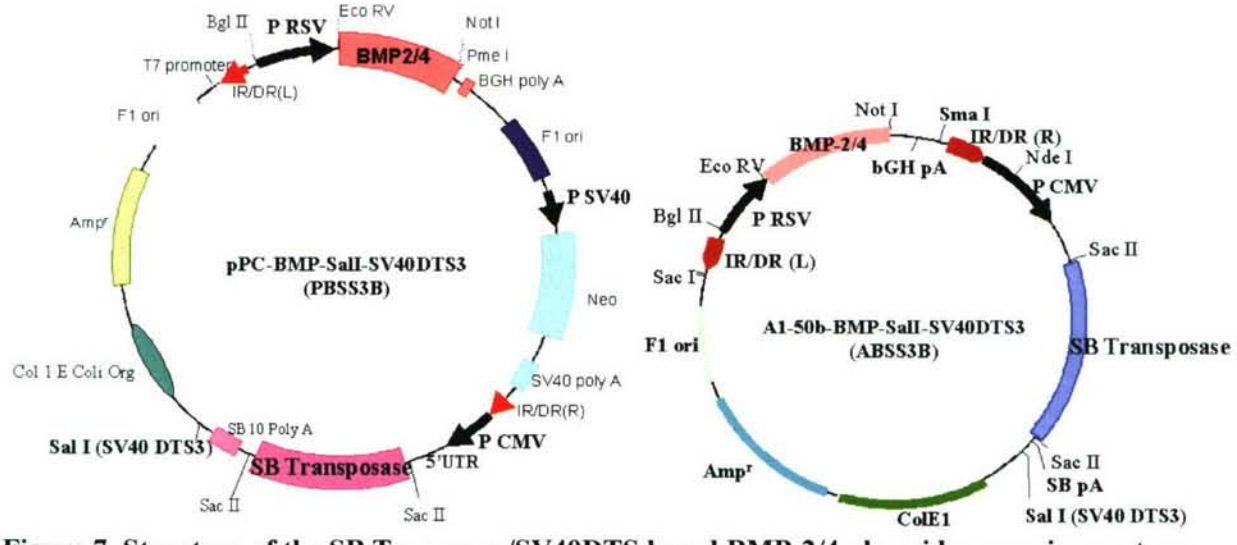

Figure 7. Structure of the SB Transpson/SV40DTS based BMP-2/4 plasmid expression vectors. The human BMP-2/4 cDNA was substituted for the BP-3NLS-RFP cDNA in the pPC and A1-50b vectors. From one to three copies of the SV40 DTS were placed in tandem in the Sal I site.

iii. Testing of the SB-TK vectors. The CMV promoter and long 5'UTR were removed from the PBSS3B vector and the TK-SB transposase cassette with an optimized Kozak sequence (gccgccatgg) was substituted. This reduced the size of the PBSS3B vector by 600 bp. The PBSS3B-TK-SB vector was subsequently reduced in size by PCR to prepare ABSS3B-TK-SB. The ability of the pPC, A1-50b, PSS3B, ASS3B, PSS3B-TK- SB and ASS3B-TK-SB vectors to stimulate osteoblast differentiation were assessed in ROS 17/2.8 cells. Figure 8 illustrates this

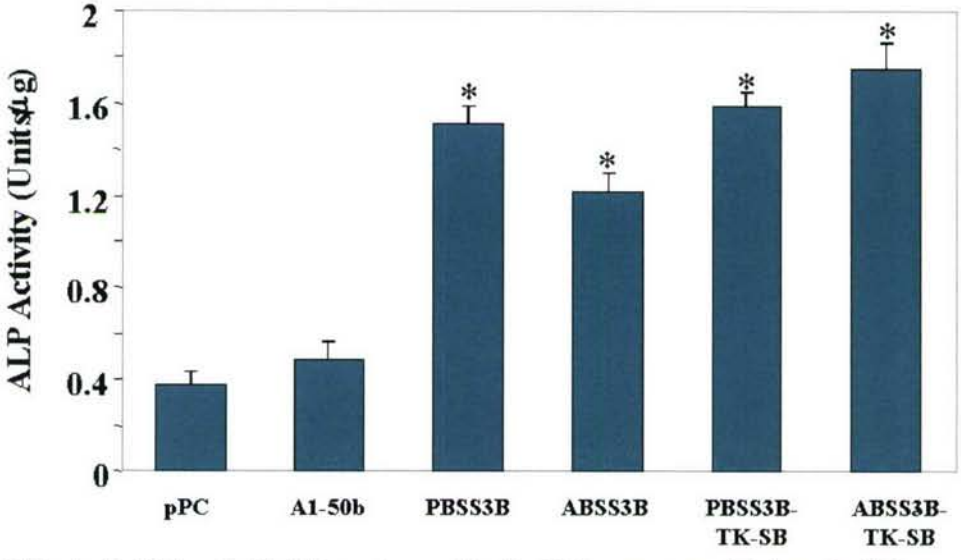

Figure 8. Effect of pPC and A1-50b vectors with the TK promoter driving the SB transposase on ALP activity in osteoblasts. ROS 17/2.8 cells were transiently transfected with 1 µg of each plasmid vector with Effectene. After 48 hours, ALP activity was assessed. Both the pPC and A1-50b vectors with either version of the SB Transposase cassette stimulated ALP activity *in vitro*. The SV40 DTS significantly increased ALP activity. We are in the process of measuring BMP-4 production in cells transfected by these vectors. We will also evaluate these two types of vectors *in vivo* to determine which vector provides maximal bone formation. Values are the mean ± S.E.M of six replicates, *, $P<0.05$ vs. pPC control.

assessment. The PSS3B, ASS3B, PSS3B-TK-SB and ASS3B-TK-SB vectors were found to be superior to the pPC and A1-50b vectors. The PSS3B, ASS3B, PSS3B-TK-SB and ASS3B-TK-SB vectors will be transfected into osteoblasts and marrow stromal cells and evaluated *in vitro* and then the best vector with be used in our *in vivo* implant model. Figure 2 illustrates a generic version of the ABSS3B vector.

iv. Testing the effect of SV40DTS copy number in osteoblasts. ROS 17/2.8 cells were transiently transfected with Effectene and the BMP expressing CMV-based SB-transpoase vectors and ALP activity was assessed after three days. The vectors contained either one, two or three copies of the SV40 DTS in the Sal I site. All of the plasmid vectors tested significantly increased ALP activity. The SV40 DTS significantly increased the amount of ALP activity produced by the osteoblasts with all copies. Three copies of the SV40 DTS increased ALP activity 14 fold and is the superior vector that we will use for *in vivo* studies. We are in the process of performing western blots with BMP-4 specific anibodies to determine if more BMP-2/4 is produced by cells containing the SV40 DTS.

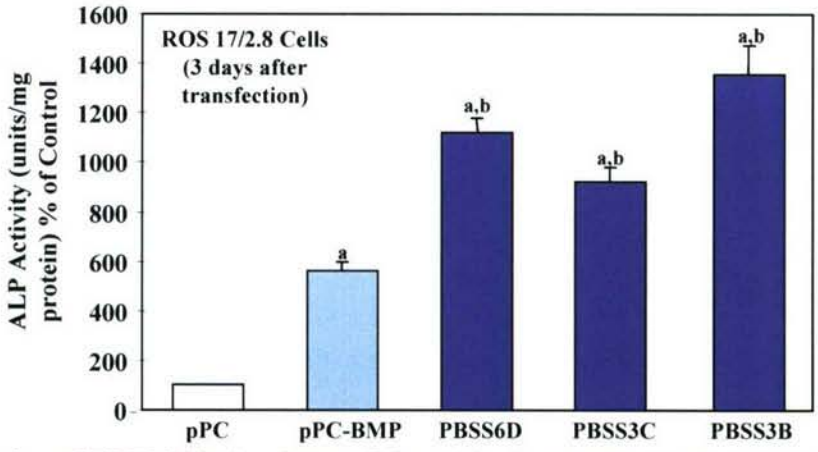

Figure 9. Expression of BMP-2/4 stimulates ALP activity in rat osteoblasts (ROS 17/2.8). ALP activity was evaluated 3 days (72 hours) after transfection with Effectene and 1 μg of each plasmid DNA. Each value is the mean ± S.E.M. of six replicates. a, P<0.05 vs. pPC control; b, P<0.05 vs. pPC-BMP.

v. Testing the effect of SV40 DTS copy number in C2C12 Cells. C2C12 cells are undifferentiated muscle cells that can be reprogrammed to become osteoblasts with BMPs. C2C12 cells were transfected and cultured for 5 days in order to allow development of the osteoblast phenotype. The pPC-BMP2/4 vector did not significantly change ALP activity in C2C12 cells but this vector containing either 1 or 3 copies of the SV40dts (PBSS6B,C or D) increased ALP activity (1.6 and 2 fold) and the osteoblast phenotype. Transfection efficiency in C2C12 cells was 1-2% vs ROS 17/2.8 cells, which transfected at 10-20% efficiency. This difference in transfection efficiency may explain the small increase in ALP activity compared to

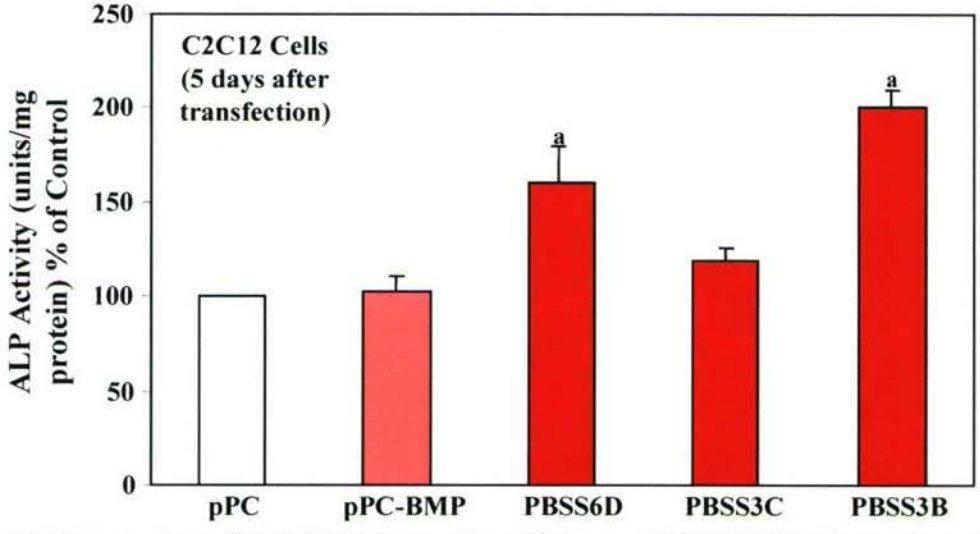

Figure 10. Expression of BMP-2/4 from the pPC based SV40 DTS plasmid vectors. ALP activity was evaluated five days (120 hours) after transfection with Effectene and 1 μg of DNA. Values are the mean ± S.E.M. of 6 replicate samples. a, P <0.05 vs. pPC control. Only vectors containing one or three copies of the SV40 DTS expressed enough BMP-2/4 to stimulate C2C12 cell transdifferentiation.

the increase seen in ROS cells. We will repeat these experiments with nucleofector-based transfections and determine if ALP activity increases with transfection efficiency.

We have transfected rMSCs with the BMP plasmid vectors, however our transfection efficiency with effectene is less than 1% and too low to produce significant BMP. We are testing electroproation conditions and the correct Nucleofector Kits to increase transfection efficiency of rMSCs so that we can do *in vivo* studies with both MSCs and osteoblasts.

vi. Use of Nucleofector reagents to increase transfection efficiency of rMSCs. Amaxa has developed hundreds of cell specific reagents and a special plasmid vector to increase transfection efficiency in almost any cell type. Unfortunately, it is not known which reagent is most effective in rMSCs and each kit is extremely expensive. In preliminary studies, we began with Kit T, which was known to transfect MC3T3 cells with high efficiency (80-90%). rMSCs were electroporated in the presence of the reagent from the T Kit at 120V, 130V, 140V, and 160V and fluorescence was studied by microscopy at 24 hours and by FACS analysis at 48 hours. It was found that over 20% of rMSCs expressed GFP when electroporated at 160V (15 ms), however more than 50% of the cells were killed. This was superior to other conditions which resulted in 8-15% transfection efficiency. We will test the transfection efficiency with other Nucleofector kits and attempt to reach >50% transfection efficiency. The pMAXGFP vector does not contain the SV40 DTS or SB transposon. The SV40 DTS will allow the transfection of nondividing cells

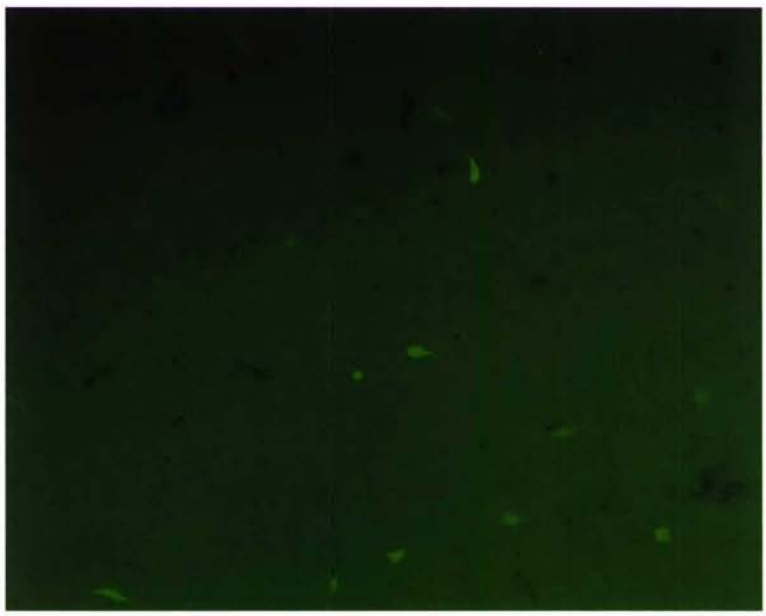

Figure 11. Electroporation of rMSCs with Nucleofector (Amaxa) reagents. rMSCs were electroporated with 2 μg of pMAXGFP at 160V (15 ms) in the Nucleofector T kit reagent and plated in DMEM/10%FBS. Cells expressed GFP at 24 hours after electroporation and at 48 hours 20% of the cells (by FACS analysis) expressed GFP. At 160V, about 50% of the cells were not viable. At lower voltages there was less cell death but only 5-15% transfection efficiency. The fibroblast kit will be tested because others in our laboratory have found that >50% of cells are transfected with this kit

(which is not possible with the pMAXGFP vector) and increase the longevity of transgene expression. The combination of the SV40 DTS/SB transposon based vectors with the Nucleofector reagent and electroporation should make working with cells with plasmids on scaffolds feasible for the implant model.

Specific Objective 4: Initiate studies to compare effectiveness of SV40DTS/SBT BMP-4 plasmid and MLV BMP-2/4 viral vector in stimulating osteoblast differentiation in cultured rMSCs and osteoblasts.

i. rMSC and osteoblast culture and transduction with MLV-GFP vectors. We have prepared and cultured rat bone marrow stromal cells (rMSCs) that express GFP after transduction with the

MLV-GFP viral vector prepared by our Viral Vector Core facility. The cells stably express the GFP marker gene when cultured for several weeks (up to passage 10) as monolayers. These cells also grow on OPLA, ceramic and collagen scaffolds *in vitro* and continue to express GFP.

We have also cultured rat osteoblasts, transduced these cells with the MLV-GFP vector and have begun to grow them on scaffolds. We will test both cell types in our skin implant model.

ii. Growth of rMSCs expressing GFP on scaffolds *in vitro*. We have determined that virally-transduced cells expressing GFP are viable and continue to express GFP when on OPLA, ceramic or collagen scaffolds for up to two weeks in culture (2004 Progress report). We have reproduced these results in year two and found that the cCollagen matrix supports the growth of

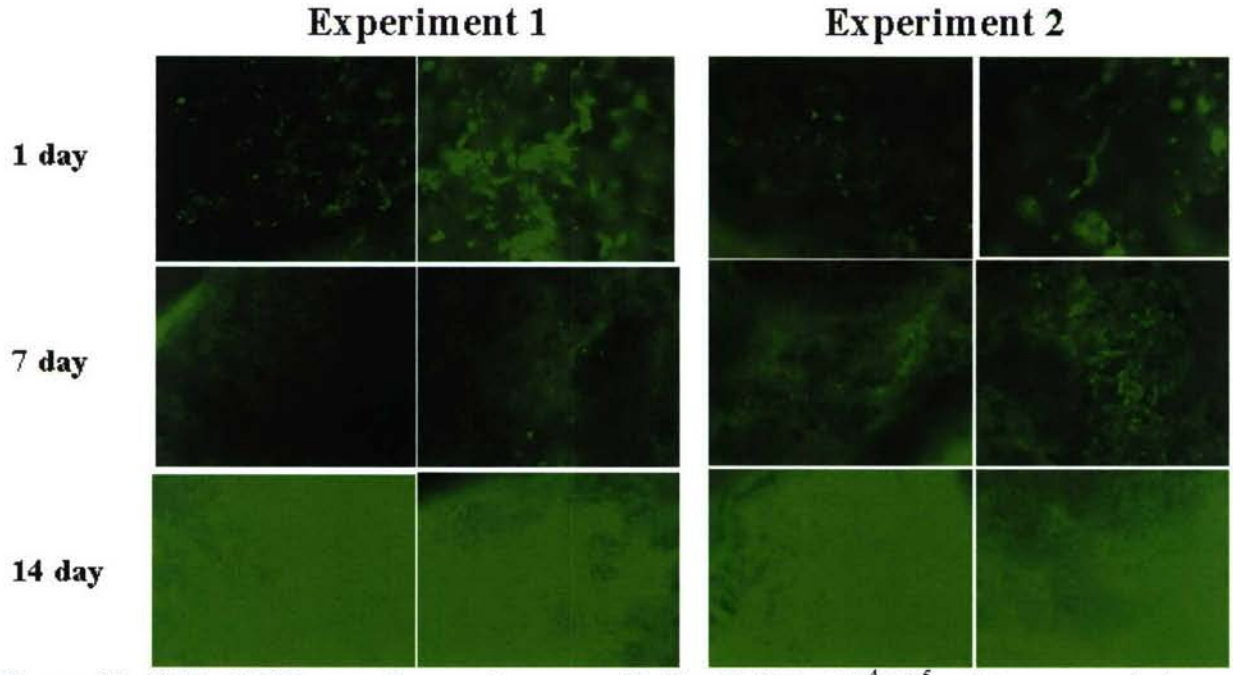

Figure 12. GFP-rMSC growth on collagen scaffolds. RMSCs (10^4-10^5 cells) were seeded on the collagen scaffold coated with fibronectin and cells were observed from 1day to 14 days. For *in vivo* implantation, cells should be grown for two weeks.

more rMSCs than OPLA, particularly when coated with fibronectin. Ceramic supports also supported cell growth and GFP expression as well as collagen again when coated with fibronectin (data not shown). Cells cover the outer scaffold surface and penetrate the scaffold after a few days in culture. For *in vivo* comparison studies (cells expressing GFP or BMP from plasmid or viral vectors), we will electroporate cells and place on the scaffold (collagen and ceramic) for 3-7 days and then implant the scaffold for one and two weeks. Bone formation will then be assessed by histology.

iii. RNA isolation and preparation of cDNA from rat MSCs on scaffolds. RNA was isolated from one 3 mm^3 support chip using the Versagene Kit from Gentra. More RNA was recovered with this kit than with the "Absolutely RNA" kit. cDNA from three separate reactions was

prepared and mixed with 20 ng of total RNA/reaction, 1 ul (5 μM) oligo dt 20 mer primer mix (IDT) and 1 ul of dNTP (10 mM) master mix. RNA was heated to 65 C for 5 minutes and at 4 C for 1 minute before adding 1 ul (200 units) of Superscript III (Invitrogen) reverse transcriptase, 4 ul 5 X first strand buffer mix (250 mM Tris HCl (pH 8.3 at RT), 375 mM KCl, 15 mM $MgCl_2$), 1 ul of 0.1 M DTT and 1 ul of RNAse Out, recombinant RNAse inhibitor (Invitrogen) to a 20 ul total reaction volume. After mixing the solution was incubated at 50 C for 30 minutes and at 70 C for 15 minutes to inactivate the enzyme. After incubating the samples at 4 C for 2 minutes, 1 ul of RNAse H was added and incubation was continued for 20 min at 37 C. cDNA was made in a Minicycler from MJ Research. Samples were removed and stored at –20 C until use.

Table 3. Primer sets developed for Real Time PCR analysis of mRNA levels of osteoblast marker genes.

Gene	Accession #	Primer Sequence	Size of Product	Tm Amplification (^{0}C)
cyclophilin	BC059141	Gcatacaggtcctggcatct gctctcctgagctacagaag	281	56.4
Type Iα2 procollagen 3333-3677	AF121217	gtgtcagcggaggaggctat	344	56.4
Osteopontin	M14656	Gaagaccagccatgagtcaag cttgtcctcatggctgtgtgaa	243	56.4
Alkaline Phosphatase 1737-1960	Y00714.1	Ggattcctgctgccgttgtt gagggactggctgtgactat	223	48
Osteocalcin 123-338	NM_013414.1	cagcgactctgagtctgacaa gtgtccatagatgcgcttgta	215	48

iv. Real-Time PCR assay for osteoblast marker genes. We and others have previously shown that rMSCs that are attached to scaffolds undergo differentiation into mature osteoblasts that produce bone ((15), 2004 progress report). To analyze bone formation from cells attached to the scaffolds or in implants recovered from animals, the mRNA levels of a number of osteoblast marker genes will be analyzed. The osteoblast marker genes will be divided into categories that reflect several stages of differentiation. One gene expressed early in the differentiation process is type I procollagen when preosteoblasts are in the proliferative stage, ALP is expressed at the onset of mineralization, while genes expressed during the later mineralization stage include osteocalcin, and osteopontin. We have tested and validated four osteoblast marker genes for in vitro and *in vivo* testing (Table 3). We reported previously (year 2004 progress report) that the GFP-rMSCs expressed type I procollagen and osteopontin.

Specific Objective 5. Hard tissue model. Initiate studies to compare bone formation induced by rMSCs transduced in vitro with the MLV-BMP2/4 retroviral vector and transfected with the SV40DTS/SB Transposon based plasmid vectors in vivo in a rat subcutaneous implant model.

i. Preparation of rMSC scaffolds. Collagen supports were pre-coated with fibronectin by adding 100 ul of a 100 ug/ml solution to each dry scaffold in wells of a 24 well plate. The scaffold absorbed this solution completely. The scaffolds were incubated 1 hour before adding cells. Cells were trypsinized and filtered through a 40 μM nylon sieve (BD Bioscience) counted and added to each well as 400,000 cells in 1 ml. This number of cells just covered the scaffold. After 3 hours, 1 ml of additional media was added and the cultures were incubated with media changes for 14 days prior to implantation. Scaffolds were moved to new 6 well plates when cells began to populate the bottom of the tissue culture dish. Before implanting, the scaffolds were examined by epifluorescence microscopy and GFP cells were observed on the surface of the scaffold (figure 12).

ii. Rat skin implant surgery. Three Fischer 344 rats, 13 weeks old, were anesthetized with ketamine and xylazine and four 0.8-1.2 cm incisions were made on the shaved back skin. Blunt dissection with a small hemostat was used to create a small pocket to the lateral side of each incision, then one scaffold (containing rMSC-GFP cells) was inserted into the pocket. The incisions were closed with 3 stitches (3-0 non-resorbable) and the rats were allowed to recover in plastic cages on a warm pad before return to normal housing.

iii. Analysis of implanted scaffolds. rMSCs expressing GFP from MLV-GFP vector were implanted on the back of Fischer rats. Initial implant experiments to assess whether the scaffolds and attached cells would induce a significant inflammatory reaction in the host rat tissues were negative. Because syngenic cells were used, a cell rejection raction was not anticipated, but we didi not know what effect the scaffold materials (OPLA, ceramic or collagen), the fibronectin or the fetal bovine serum (form the cultures) would have on the rat tissues. The experiment was designed so that one scaffold was implanted per site, with dulicate scaffolds (one with and one

Figure.13. Analysis of the rMSC-GFP-collagen scaffolds after 14 days *in vivo* in the implant model. Scaffolds were removed and residual GFP positive cells visualized by microscopy. The implants were fixed, sectioned and stained with H&E. Left panel: GFP positive were found on the surface and inside the collagen matrix. Right panel: The scaffold was filled with cells and vessels were found to penetrate the material. Not all of the cells in the scaffold expressed GFP. This could result from transgene silencing or in rMSC cell death.

without fibronectin) per rat.

After 16 days, the rats were euthanized with CO_2 and the implants were dissected out and placed in PBS on ice. There were no indication of an inflammatory reaction in the implant sites.

The implants were fixed in 10% buffered formatin overnight, then processed for paraffin sectioning. Other implants were frozen in the cryostat and sections were made to examine GFP expression in the microscope.

The collagen scaffolds were reduced in size after 16 days (30% of original) suggesting significant resorption of the scaffold material occurred. The collagen scaffolds were also tightly incorporated into the overlying skin dermis layer and had some blood vessel growth. A few GFP positive cells were found on the scaffold surface and inside the scaffold after 14 days (Figure 13).

Key Research Accomplishments

1) We have prepared and tested twelve novel plasmid vectors based on the use of the SV40DTS and the Sleeping Beauty (SB) transposon that can be used for *in vivo* gene delivery and expression. Table 1 and Table 2 describe these plasmid vectors.
2) We found that the vector containing the SB transposon and three tandem copies of the SV40DTS most effectively stimulated RFP and BMP expression to stimulate ALP activity in osteoblasts.
3) We found that manipulation of the SB transposase expression cassette to decrease its size and introduce a multiple cloning site for enhancer addition to provide for tissue specific expression increased ALP activity. It is possible that this vector can be manipulated to optimize SB transposase activity in a cell specific manner by introduction of an enhancer.
4) We have found that Nucleofector (Kit T) transfects over 20% of rMSCs. This may be a sufficient quantity to do *in vivo* studies. We will characterize the fibroblast Nucleofector kit for transfection efficiency before focusing on the T kit.
5) We have demonstrated that plasmid vectors can be expressed at high enough levels after transfection even with low transfection efficiency to transdifferentiate muscle cells and to increase osteoblast activity *in vitro.*
6) We have identified that fibronectin coated collagen matrices containing rMSCs can be used to support cell growth and transgene expression for up to two weeks in a skin implant model to study bone formation.
7) We have shown that rMSCs expressing GFP can be recovered from the collagen matrix after two weeks at the implant site and that the collagen support does not stimulate an inflammatory response.
8) A provisional patent was filed entitled "Methods for Accelerating Bone Repair," describing the use of the SV40DTS/SB Transposon based vectors.

Reportable Outcomes

None

Conclusions

Our preliminary data demonstrate that plasmid vectors with the SV40 DTS and SB transposon have been developed to express GFP and BMP at levels that can transdifferentiate cells *in vitro*. We have identified at least one support material to use *in vivo* for proposed skin implant studies to test our plasmid vectors for at least two weeks. We have procedures in place to determine if our plasmid vectors stimulate bone formation as well as a retroviral vector and we have identified a transfection system to provide enough cells transfected with plasmid for a fair *in vivo* comparison.

References

1. Young JL, Benoit JN, Dean DA 2003 Effect of a DNA nuclear targeting sequence on gene transfer and expression of plasmids in the intact vasculature. Gene Ther 10:1465-70
2. Li S, MacLaughlin FC, Fewell JG, et al. 2001 Muscle-specific enhancement of gene expression by incorporation of SV40 enhancer in the expression plasmid. Gene Ther 8:494-7
3. Dean DA, Dean BS, Muller S, Smith LC 1999 Sequence requirements for plasmid nuclear import. Exp Cell Res 253:713-22
4. Vacik J, Dean BS, Zimmer WE, Dean DA 1999 Cell-specific nuclear import of plasmid DNA. Gene Ther 6:1006-14
5. Wilson GL, Dean BS, Wang G, Dean DA 1999 Nuclear import of plasmid DNA in digitonin-permeabilized cells requires both cytoplasmic factors and specific DNA sequences. J Biol Chem 274:22025-32
6. Dean DA, Byrd JN, Jr., Dean BS 1999 Nuclear targeting of plasmid DNA in human corneal cells. Curr Eye Res 19:66-75
7. Dean DA 1997 Import of plasmid DNA into the nucleus is sequence specific. Exp Cell Res 230:293-302
8. Ivics Z, Hackett PB, Plasterk RH, Izsvak Z 1997 Molecular reconstruction of Sleeping Beauty, a Tc1-like transposon from fish, and its transposition in human cells. Cell 91:501-10
9. Dacic S, Kalajzic I, Visnjic D, Lichtler AC, Rowe DW 2001 Col1a1-driven transgenic markers of osteoblast lineage progression. J Bone Miner Res 16:1228-36
10. Mikkelsen JG, Yant SR, Meuse L, Huang Z, Xu H, Kay MA 2003 Helper-Independent Sleeping Beauty transposon-transposase vectors for efficient nonviral gene delivery and persistent gene expression in vivo. Mol Ther 8:654-65
11. Ohgushi H, Dohi Y, Yoshikawa T, et al. 1996 Osteogenic differentiation of cultured marrow stromal stem cells on the surface of bioactive glass ceramics. J Biomed Mater Res 32:341-8
12. Ito Y, Tanaka N, Fujimoto Y, et al. 2004 Bone formation using novel interconnected porous calcium hydroxyapatite ceramic hybridized with cultured marrow stromal stem cells derived from Green rat. J Biomed Mater Res 69A:454-61
13. Knabe C, Ostapowicz W, Radlanski RJ, et al. 1998 In vitro investigation of novel calcium phosphates using osteogenic cultures. J Mater Sci Mater Med 9:337-45
14. Livingston T, Ducheyne P, Garino J 2002 In vivo evaluation of a bioactive scaffold for bone tissue engineering. J Biomed Mater Res 62:1-13
15. Lennon DP, Haynesworth SE, Young RG, Dennis JE, Caplan AI 1995 A chemically defined medium supports in vitro proliferation and maintains the osteochondral potential of rat marrow-derived mesenchymal stem cells. Exp Cell Res 219:211-22

Appendix –Project 8

Sequences provided for patent:

pPC-Neo-BMP-2/4-Sal I-SV40DTS3 (9726 bp). The Not I and EcoRV site are in bold and frame the BMP-2/4 coding sequence. The BMP-2/4 nucleotide sequence is in italics. The optimized Kozak sequence is underlined. The three copies of the SV40 DTS at the Sal I site are in bold. The Neomycin resistance expression cassette is intact.

```
   1 ggccgctcga gtctagaggg cccgtttaaa cccgctgatc agcctcgact gtgccttcta
  61 gttgccagcc atctgttgtt gtgcccctcc ccgtgccttc cttgaccctg gaaggtgcca
 121 ctcccactgt cctttcctaa taaaatgagg aaattgcatc gcattgtctg agtaggtgtc
 181 attctattct ggggggtggg gtggggcagg acagcaaggg ggaggattgg gaagacaata
 241 gcaggcatgc tggggatgcg gtgggctcta tggcttctga ggcggaaaga accagctggg
 301 gctctagggg gtatccccac gcgccctgta gcggcgcatt aagcgcggcg ggtgtggtgg
 361 ttacgcgcag cgtgaccgct acacttgcca gcgccctagc gcccgctcct ttcgctttct
 421 tcccttcctt tctcgccacg ttcgccggct ttccccgtca agctctaaat cgggggctcc
 481 ctttagggtt ccgatttagt gctttacggc acctcgaccc caaaaaactt gattagggtg
 541 atggttcacg tagtgggcca tcgccctgat agacggtttt tcgccctttg acgttggagt
 601 ccacgttctt taatagtgga ctcttgttcc aaactggaac aacactcaac cctatctcgg
 661 tctattcttt tgatttataa gggattttgc cgatttcggc ctattggtta aaaaatgagc
 721 tgatttaaca aaaatttaac gcgaattaat tctgtggaat gtgtgtcagt tagggtgtgg
 781 aaagtcccca ggctccccag caggcagaag tatgcaaagc atgcatctca attagtcagc
 841 aaccaggtgt ggaaagtccc caggctcccc agcaggcaga agtatgcaaa gcatgcatct
 901 caattagtca gcaaccatag tcccgccccc aactccgccc atcccgcccc taactccgcc
 961 cagttccgcc cattctccgc cccatggctg actaattttt tttatttatg cagaggccga
1021 ggccgcctct gcctctgagc tattccagaa gtagtgagga ggcttttttg gaggcctagg
1081 cttttgcaaa aagctcccgg gagcttgtat atccattttc ggatctgatc aagagacagg
1141 atgaggatcg tttcgcatga ttgaacaaga tggattgcac gcaggttctc cggccgcttg
1201 ggtggagagg ctattcggct atgactgggc acaacagaca atcggctgct ctgatgccgc
1261 cgtgttccgg ctgtcagcgc aggggcgccc ggttcttttt gtcaagaccg acctgtccgg
1321 tgccctgaat gaactgcagg acgaggcagc gcggctatcg tggctggcca cgacgggcgt
1381 tccttgcgca gctgtgctcg acgttgtcac tgaagcggga agggactggc tgctattggg
1441 cgaagtgccg gggcaggatc tcctgtcatc tcaccttgct cctgccgaga aagtatccat
1501 catggctgat gcaatgcggc ggctgcatac gcttgatccg gctacctgcc cattcgacca
1561 ccaagcgaaa catcgcatcg agcgagcacg tactcggatg gaagccggtc ttgtcgatca
1621 ggatgatctg gacgaagagc atcaggggct cgcgccagcc gaactgttcg ccaggctcaa
1681 ggcgcgcatg cccgacggcg aggatctcgt cgtgacccat ggcgatgcct gcttgccgaa
1741 tatcatggtg gaaaatggcc gcttttctgg attcatcgac tgtggccggc tgggtgtggc
1801 ggaccgctat caggacatag cgttggctac ccgtgatatt gctgaagagc ttggcggcga
1861 atgggctgac cgcttcctcg tgctttacgg tatcgccgct cccgattcgc agcgcatcgc
1921 cttctatcgc cttcttgacg agttcttctg agcgggactc tggggttcga aatgaccgac
1981 caagcgacgc ccaacctgcc atcacgagat ttcgattcca ccgccgcctt ctatgaaagg
2041 ttgggcttcg gaatcgtttt ccgggacgcc ggctggatga tcctccagcg cggggatctc
2101 atgctggagt tcttcgccca ccccaacttg tttattgcag cttataatgg ttacaaataa
2161 agcaatagca tcacaaattt cacaaataaa gcatttttt cactgcattc tagttgtggt
2221 ttgtccaaac tcatcaatgt atcttatcat gtctgtaatc aagcttgtgg aaggctactc
2281 gaaatgtttg acccaagtta aacaatttaa aggcaatgct accaaatact aattgagtgt
2341 atgttaactt ctgacccact gggaatgtga tgaaagaaat aaaagctgaa atgaatcatt
2401 ctctctacta ttattctgat atttcacatt cttaaaataa agtggtgatc ctaactgacc
2461 ttaagacagg gaatctttac tcggattaaa tgtcaggaat tgtgaaaaag tgagtttaaa
2521 tgtatttggc taaggtgtat gtaaacttcc gacttcaact gtagggcgag cttgcatgcc
2581 tgcaggtcgt tacataactt acggtaaatg gcccgcctgg ctgaccgccc aacgacccc
2641 gcccattgac gtcaataatg acgtatgttc ccatagtaac gccaataggg actttccatt
2701 gacgtcaatg ggtggagtat ttacggtaaa ctgcccactt ggcagtacat caagtgtatc
2761 atatgccaag tacgcccccc attgacgtca atgacggtaa atggcccgcc tggcattatg
2821 cccagtacat gaccttatgg gactttccta cttggcagta catctacgta ttagtcatcg
2881 ctattaccat ggtgatgcgg ttttggcagt acatcaatgg gcgtggatag cggtttgact
```

2941 cacggggatt tccaagtctc caccccattg acgtcaatgg gagtttgttt tggcaccaaa
3001 atcaacggga ctttccaaaa tgtcgtaaca actccgcccc attgacgcaa atgggcggta
3061 ggcgtgtacg gtgggaggtc tatataagca gagctcgttt agtgaaccgt cagatcgcct
3121 ggagacgcca tccacgctgt tttgacctcc atagaagaca ccgggaccga tccagcctcc
3181 ggactctaga ggatccggta ctcgaggaac tgaaaaacca gaaagttaac tggtaagttt
3241 agtctttttg tcttttattt caggtcccgg atccggtggt ggtgcaaatc aaagaactgc
3301 tcctcagtgg atgttgcctt tacttctagg cctgtacgga agtgttactt ctgctctaaa
3361 agctgcggaa ttgtacccgc ggccgatccg acatcatggg aaaatcaaaa gaaatcagcc
3421 aagacctcag aaaaaaaatt gtagacctcc acaagtctgg ttcatccttg ggagcaattt
3481 ccaaacgcct gaaagtacca cgttcatctg tacaaacaat agtacgcaag tataaacacc
3541 atgggaccac gcagccgtca taccgctcag gaaggagacg cgttctgtct cctagagatg
3601 aacgtacttt ggtgcgaaaa gtgcaaatca atcccagaac aacagcaaag gaccttgtga
3661 agatgctgga ggaaacaggt acaaaagtat ctatatccac agtaaaacga gtcctatatc
3721 gacataacct gaaaggccgc tcagcaagga agaagccact gctccaaaac cgacataaga
3781 aagccagact acggtttgca actgcacatg gggacaaaga tcgtactttt tggagaaatg
3841 tcctctggtc tgatgaaaca aaaatagaac tgtttggcca taatgaccat cgttatgttt
3901 ggaggaagaa gggggaggct tgcaagccga agaacaccat cccaaccgtg aagcacgggg
3961 gtggcagcat catgttgtgg gggtgctttg ctgcaggagg gactggtgca cttcacaaaa
4021 tagatggcat catgaggaag gaaaattatg tggatatatt gaagcaacat ctcaagacat
4081 cagtcaggaa gttaaagctt ggtcgcaaat gggtcttcca aatggacaat gaccccaagc
4141 atacttccaa agttgtggca aaatggctta aggacaacaa agtcaaggta ttggagtggc
4201 catcacaaag ccctgacctc aatcctatag aaaatttgtg ggcagaactg aaaaagcgtg
4261 tgcgagcaag gaggcctaca aacctgactc agttacacca gctctgtcag gaggaatggg
4321 ccaaaattca cccaacttat tgtgggaagc ttgtggaagg ctacccgaaa cgtttgaccc
4381 aagttaaaca atttaaaggc aatgctacca aatactagaa ttggccgcgg ggatccagac
4441 atgataagat acattgatga gtttggacaa accacaacta gaatgcagtg aaaaaaatgc
4501 tttatttgtg aaatttgtga tgctattgct ttatttgtaa ccattataag ctgcaataaa
4561 caagttaaca acaacaattg cattcatttt atgtttcagg ttcaggggga ggtgtgggag
4621 gtttttтcgg atcctctaga **gtcgacatgc tttgcatact tctgcctgct ggggagcctg**
4681 **gggactttcc acaccctaac tgacacacat tccacagctg gttggtacct gcagtcgaca**
4741 **tgctttgcat acttctgcct gctggggagc ctggggactt tccacaccct aactgacaca**
4801 **cattccacag ctggttggta cctgcagtcg acatgctttg catacttctg cctgctgggg**
4861 **agcctgggga ctttccacac cctaactgac acacattcca cagctggttg gtacctgcag**
4921 **tcgac**ctcg agggggggccc ggtacccagc ttttgttccc tttagtgagg gttaatttcg
4981 agcttggcg taatcatggt catagctgtt tcctgtgtga aattgttatc cgctcacaat
5041 tccacacaac atacgagccg gaagcataaa gtgtaaagcc tggggtgcct aatgagtgag
5101 ctaactcaca ttaattgcgt tgcgctcact gcccgctttc cagtcgggaa acctgtcgtg
5161 ccagctgcat taatgaatcg gccaacgcgc ggggagaggc ggtttgcgta ttgggcgctc
5221 ttccgcttcc tcgctcactg actcgctgcg ctcggtcgtt cggctgcggc gagcggtatc
5281 agctcactca aaggcggtaa tacggttatc cacagaatca aaggccgcgt tgctggcgtt
5341 ggggataacg caggaaagaa catgtgagca aaaggccagc aaaaggccag gaaccgtaaa
5401 tttccatagg ctccgccccc ctgacgagca tcacaaaaat cgacgctcaa gtcagaggtg
5461 gcgaaacccg acaggactat aaagatacca ggcgtttccc cctggaagct ccctcgtgcg
5521 ctctcctgtt ccgaccctgc cgcttaccgg atacctgtcc gcctttctcc cttcgggaag
5581 cgtggcgctt tctcatagct cacgctgtag gtatctcagt tcggtgtagg tcgttcgctc
5641 caagctgggc tgtgtgcacg aacccccgt tcagcccgac cgctgcgcct tatccggtaa
5701 ctatcgtctt gagtccaacc cggtaagaca cgacttatcg ccactggcag cagccactgg
5761 taacaggatt agcagagcga ggtatgtagg cggtgctaca gagttcttga agtggtggcc
5821 taactacggc tacactagaa ggacagtatt tggtatctgc gctctgctga agccagttac
5881 cttcggaaaa agagttggta gctcttgatc cggcaaacaa accaccgctg gtagcggtgg
5941 ttttttgtt tgcaagcagc agattacgcg cagaaaaaaa ggatctcaag aagatccttt
6001 gatcttttct acggggtctg acgctcagtg gaacgaaaac tcacgttaag ggattttggt
6061 catgagatta tcaaaaagga tcttcaccta gatcctttta aattaaaaat gaagttttaa
6121 atcaatctaa agtatatatg agtaaacttg gtctgacagt taccaatgct taatcagtga
6181 ggcacctatc tcagcgatct gtctatttcg ttcatccata gttgcctgac tccccgtcgt
6241 gtagataact acgatacggg agggcttacc atctggcccc agtgctgcaa tgataccgcg
6301 agacccacgc tcaccggctc cagatttatc agcaataaac cagccagccg gaagggccga

6361 gcgcagaagt ggtcctgcaa ctttatccgc ctccatccag tctattaatt gttgccggga
6421 agctagagta agtagttcgc cagttaatag tttgcgcaac gttgttgcca ttgctacagg
6481 catcgtggtg tcacgctcgt cgtttggtat ggcttcattc agctccggtt cccaacgatc
6541 aaggcgagtt acatgatccc ccatgttgtg caaaaaagcg gttagctcct tcggtcctcc
6601 gatcgttgtc agaagtaagt tggccgcagt gttatcactc atggttatgg cagcactgca
6661 taattctctt actgtcatgc catccgtaag atgcttttct gtgactggtg agtactcaac
6721 caagtcattc tgagaatagt gtatgcggcg accgagttgc tcttgcccgg cgtcaatacg
6781 ggataatacc gcgccacata gcagaacttt aaaagtgctc atcattggaa aacgttcttc
6841 ggggcgaaaa ctctcaagga tcttaccgct gttgagatcc agttcgatgt aacccactcg
6901 tgcacccaac tgatcttcag catcttttac tttcaccagc gtttctgggt gagcaaaaac
6961 aggaaggcaa aatgccgcaa aaaagggaat aagggcgaca cggaaatgtt gaatactcat
7021 actcttcctt tttcaatatt attgaagcat ttatcagggt tattgtctca tgagcggata
7081 catatttgaa tgtatttaga aaaataaaca aatagggggtt ccgcgcacat ttccccgaaa
7141 agtgccacct gacgcgccct gtagcggcgc attaagcgcg gcgggtgtgg tggttacgcg
7201 cagcgtgacc gctacacttg ccagcgccct agcgcccgct cctttcgctt tcttcccttc
7261 ctttctcgcc acgttcgccg gctttccccg tcaagctcta aatcgggggc tcccttttagg
7321 gttccgattt agtgctttac ggcacctcga ccccaaaaaa cttgattagg gtgatggttc
7381 acgtagtggg ccatcgccct gatagacggt ttttcgccct ttgacgttgg agtccacgtt
7441 ctttaatagt ggactcttgt tccaaactgg aacaacactc aaccctatct cggtctattc
7501 ttttgattta taagggattt tgccgatttc ggcctattgg ttaaaaaatg agctgattta
7561 acaaaaattt aacgcgaatt ttaacaaaat attaacgctt acaatttcca ttcgccattc
7621 aggctgcgca actgttggga agggcgatcg gtgcgggcct cttcgctatt acgccagctg
7681 gcgaaagggg gatgtgctgc aaggcgatta agttgggtaa cgccagggtt ttcccagtca
7741 cgacgttgta aaacgacggc cagtgaattg taatacgact cactataggg cgaattggag
7801 ctcggtaccc tacagttgaa gtcggaagtt tacatacact taagttggag tcattaaaac
7861 tcgtttttca actacaccac aaatttcttg ttaacaaaca atagttttgg caagtcagtt
7921 aggacatcta ctttgtgcat gacacaagtc atttttccaa caattgttta cagacagatt
7981 atttcactta taattcactg tatcacaatt ccagtgggtc agaagtttac atacactaag
8041 ttgactgtgc ctttaaacag cttggaaaat tccagaaaat gatgtcatgg ctttagaagc
8101 tagatctcga tgtacgggcc agatatacgc gtatctgagg ggactagggt gtgtttaggc
8161 gaaaagcggg gcttcggttg tacgcggtta ggagtcccct caggatatag tagtttcgct
8221 tttgcatagg gaggggggaaa tgtagtctta tgcaatacac ttgtagtctt gcaacatggt
8281 aacgatgagt tagcaacatg ccttacaagg agagaaaaag caccgtgcat gccgattggt
8341 ggaagtaagg tggtacgatc gtgccttatt aggaaggcaa cagacaggtc tgacatggat
8401 tggacgaacc actgaattcc gcattgcaga gataattgta tttaagtgcc tagctcgata
8461 caataaacgc catttgacca ttcaccacat tggtgtgcat gaattc**gata** ***tc***gccgcc*at*
8521 *ga*tggtggcc gggacccgct gtcttctagc gttgctgctt ccccaggtcc tcctgggcgg
8581 cgcggctggc ctcgttccgg agctgggccg caggaagttc gcggcggcgt cgtcgggccg
8641 ccctcatcc cagcctctg acgaggtcct gagcgagttc gagttgcggc tgctcagcat
8701 gttcggcctg aaacagagac ccacccccag cagggacgcc gtggtgcccc cctacatgct
8761 agacctgtat cgcaggcact caggtcagcc gggctcaccc gccccagacc accggttgga
8821 gagggcagcc agccgagcca acactgtgcg cagcttccac catgaagaat ctttggaaga
8881 actaccagaa acgagtggga aaacaacccg gagattcttc tttaatttaa gttctatccc
8941 cacggaggag tttatcacct cagcagagct tcaggttttc cgagaacaga tgcaagatgc
9001 tttaggaaac aatagcagtt tccatcaccg aattaatatt tatgaaatca taaaacctgc
9061 aacagccaac tcgaaattcc ccgtgaccag acttttggac accaggttgg tgaatcagaa
9121 tgcaagcagg tgggaaagtt ttgatgtcac ccccgctgtg atgcggtgga ctgcacaggg
9181 acacgccaac catggattcg tggtggaagt ggcccacttg gaggagaaac aaggtgtctc
9241 caagagacat gttaggataa gcaggtcttt gcaccaagat gaacacagct ggtcacagat
9300 aaggccattg ctagtaactt ttggccatga tggccggggc catgccttga cccgacgccg
9361 gagggccaag cgtagcccta agcatcactc acagcgggcc aggaagaaga ataagaactg
9421 ccggcgccac tcgctctatg tggacttcag cgatgtgggc tggaatgact ggattgtggc
9481 cccaccaggc taccaggcct tctactgcca tggggactgc cccttccac tggctgacca
9541 cctcaactca accaaccatg ccattgtgca gaccctggtc aattctgtca attccagtat
9600 ccccaaagcc tgttgtgtgc ccactgaact gagtgccatc tccatgctgt acctggatga
9661 gtatgataag gtggtactga aaaattatca ggagatggta gtagagggat gtgggtgccg
9721 ctga**gc**

A1-50b-BMP-2/4-Sal I-SV40DTS3 (7745 bp). The Not I and EcoRV site are in bold and frame the BMP-2/4 coding sequence. The BMP-2/4 nucleotide sequence is in italics. The optimized Kozak sequence is underlined. The three copies of the SV40 DTS at the Sal I site are in bold. There is no Neomycin resistance expression cassette and a SmaI site (bold) was introduced in its place.

```
   1  ggccgctcga gtctagaggg cccgtttaaa cccgctgatc agcctcgact gtgccttcta
  61  gttgccagcc atctgttgtt gtgcccctcc ccgtgccttc cttgaccctg gaaggtgcca
 121  ctcccactgt cctttcctaa taaaatgagg aaattgcatc gcattgtctg agtaggtgtc
 181  attctattct gggggggtggg gtggggcagg acagcaaggg ggaggattgg gaagacaata
 241  gcaggcatgc tggggatgcg gtgggctcta tggcttctga ggcggaaaga acccgggctc
 301  gaaatgtttg acccaagtta aacaatttaa aggcaatgct accaaatact aattgagtgt
 361  atgttaactt ctgacccact gggaatgtga tgaaagaaat aaaagctgaa atgaatcatt
 421  ctctctacta ttattctgat atttcacatt cttaaaataa agtggtgatc ctaactgacc
 481  ttaagacagg gaatctttac tcggattaaa tgtcaggaat tgtgaaaaag tgagtttaaa
 541  tgtatttggc taaggtgtat gtaaacttcc gacttcaact gtagggcgag cttgcatgcc
 601  tgcaggtcgt tacataactt acggtaaatg gcccgcctgg ctgaccgccc aacgacccccc
 661  gcccattgac gtcaataatg acgtatgttc ccatagtaac gccaataggg actttccatt
 721  gacgtcaatg ggtggagtat ttacggtaaa ctgcccactt ggcagtacat caagtgtatc
 781  atatgccaag tacgcccccc attgacgtca atgacggtaa atggcccgcc tggcattatg
 841  cccagtacat gaccttatgg gactttccta cttggcagta catctacgta ttagtcatcg
 901  ctattaccat ggtgatgcgg ttttggcagt acatcaatgg gcgtggatag cggtttgact
 961  cacggggatt tccaagtctc caccccattg acgtcaatgg gagtttgttt tggcaccaaa
1021  atcaacggga ctttccaaaa tgtcgtaaca actccgcccc attgacgcaa atgggcggta
1081  ggcgtgtacg gtgggaggtc tatataagca gagctcgttt agtgaaccgt cagatcgcct
1141  ggagacgcca tccacgctgt tttgacctcc atagaagaca ccgggaccga tccagcctcc
1201  ggactctaga ggatccggta ctcgaggaac tgaaaaacca gaaagttaac tggtaagttt
1261  agtctttttg tcttttattt caggtcccgg atccggtggt ggtgcaaatc aaagaactgc
1321  tcctcagtgg atgttgcctt tacttctagg cctgtacgga agtgttactt ctgctctaaa
1381  agctgcggaa ttgtacccgc ggccgatccg acatcatggg aaaatcaaaa gaaatcagcc
1441  aagacctcag aaaaaaaatt gtagacctcc acaagtctgg ttcatccttg ggagcaattt
1501  ccaaacgcct gaaagtacca cgttcatctg tacaaacaat agtacgcaag tataaacacc
1561  atgggaccac gcagccgtca taccgctcag gaaggagacg cgttctgtct cctagagatg
1621  aacgtacttt ggtgcgaaaa gtgcaaatca atcccagaac aacagcaaag gaccttgtga
1681  agatgctgga ggaaacaggt acaaaagtat ctatatccac agtaaaacga gtcctatatc
1741  gacataacct gaaaggccgc tcagcaagga agaagccact gctccaaaac cgacataaga
1801  aagccagact acggtttgca actgcacatg gggacaaaga tcgtactttt tggagaaatg
1861  tcctctggtc tgatgaaaca aaaatagaac tgtttggcca taatgaccat cgttatgttt
1921  ggaggaagaa gggggaggct tgcaagccga agaacaccat cccaaccgtg aagcacgggg
1981  gtggcagcat catgttgtgg gggtgctttg ctgcaggagg gactggtgca cttcacaaaa
2041  tagatggcat catgaggaag gaaaattatg tggatatatt gaagcaacat ctcaagacat
2101  cagtcaggaa gttaaagctt ggtcgcaaat gggtcttcca aatggacaat gaccccaagc
2161  atacttccaa agttgtggca aaatggctta aggacaacaa agtcaaggta ttggagtggc
2221  catcacaaag ccctgacctc aatcctatag aaaatttgtg ggcagaactg aaaaagcgtg
2281  tgcgagcaag gaggcctaca aacctgactc agttacacca gctctgtcag gaggaatggg
2341  ccaaaattca cccaacttat tgtgggaagc ttgtggaagg ctacccgaaa cgtttgaccc
2401  aagttaaaca atttaaaggc aatgctacca aatactagaa ttggccgcgg ggatccagac
2461  atgataagat acattgatga gtttggacaa accacaacta gaatgcagtg aaaaaaatgc
2521  tttatttgtg aaatttgtga tgctattgct ttatttgtaa ccattataag ctgcaataaa
2581  caagttaaca acaacaattg cattcatttt atgtttcagg ttcaggggga ggtgtgggag
2641  gtttttttcgg atcctctaga gtcgacatgc tttgcatact tctgcctgct ggggagcctg
2701  gggactttcc acaccctaac tgacacacat tccacagctg gttggtacct gcagtcgaca
2761  tgctttgcat acttctgcct gctggggagc ctggggactt tccacaccct aactgacaca
2821  cattccacag ctggttggta cctgcagtcg acatgctttg catacttctg cctgctgggg
```

2881 **agcctgggga ctttccacac cctaactgac acacattcca cagctggttg gtacctgcag**
2941 **tcgac**ctcga gggggggccc ggtacccagc ttttgttccc tttagtgagg gttaatttcg
3001 agcttggcgt aatcatggtc atagctgttt cctgtgtgaa attgttatcc gctcacaatt
3061 ccacacaaca tacgagccgg aagcataaag tgtaaagcct ggggtgccta atgagtgagc
3121 taactcacat taattgcgtt gcgctcactg cccgctttcc agtcgggaaa cctgtcgtgc
3181 cagctgcatt aatgaatcgg ccaacgcgcg gggagaggcg gtttgcgtat tgggcgctct
3241 tccgcttcct cgctcactga ctcgctgcgc tcggtcgttc ggctgcggcg agcggtatca
3301 gctcactcaa aggcggtaat acggttatcc acagaatcaa aggccgcgtt gctggcgttg
3361 gggataacgc aggaaagaac atgtgagcaa aaggccagca aaaggccagg aaccgtaaat
3421 ttccataggc tccgcccccc tgacgagcat cacaaaaatc gacgctcaag tcagaggtgg
3481 cgaaacccga caggactata aagataccag gcgtttcccc ctggaagctc cctcgtgcgc
3541 tctcctgttc cgaccctgcc gcttaccgga tacctgtccg cctttctccc ttcgggaagc
3601 gtggcgcttt ctcatagctc acgctgtagg tatctcagtt cggtgtaggt cgttcgctcc
3661 aagctgggct gtgtgcacga acccccccgtt cagcccgacc gctgcgcctt atccggtaac
3721 tatcgtcttg agtccaaccc ggtaagacac gacttatcgc cactggcagc agccactggt
3781 aacaggatta gcagagcgag gtatgtaggc ggtgctacag agttcttgaa gtggtggcct
3841 aactacggct acactagaag gacagtattt ggtatctgcg ctctgctgaa gccagttacc
3901 ttcggaaaaa gagttggtag ctcttgatcc ggcaaacaaa ccaccgctgg tagcggtggt
3961 ttttttgttt gcaagcagca gattacgcgc agaaaaaaag gatctcaaga agatcctttg
4021 atcttttcta cggggtctga cgctcagtgg aacgaaaact cacgttaagg gattttggtc
4081 atgagattat caaaaaggat cttcacctag atccttttaa attaaaaatg aagttttaaa
4141 tcaatctaaa gtatatatga gtaaacttgg tctgacagtt accaatgctt aatcagtgag
4201 gcacctatct cagcgatctg tctatttcgt tcatccatag ttgcctgact ccccgtcgtg
4261 tagataacta cgatacggga gggcttacca tctggcccca gtgctgcaat gataccgcga
4321 gacccacgct caccggctcc agatttatca gcaataaacc agccagccgg aagggccgag
4381 cgcagaagtg gtcctgcaac tttatccgcc tccatccagt ctattaattg ttgccgggaa
4441 gctagagtaa gtagttcgcc agttaatagt ttgcgcaacg ttgttgccat tgctacaggc
4501 atcgtggtgt cacgctcgtc gtttggtatg gcttcattca gctccggttc ccaacgatca
4561 aggcgagtta catgatcccc catgttgtgc aaaaaagcgg ttagctcctt cggtcctccg
4621 atcgttgtca gaagtaagtt ggccgcagtg ttatcactca tggttatggc agcactgcat
4681 aattctctta ctgtcatgcc atccgtaaga tgcttttctg tgactggtga gtactcaacc
4741 aagtcattct gagaatagtg tatgcggcga ccgagttgct cttgcccggc gtcaatacgg
4801 gataataccg cgccacatag cagaacttta aaagtgctca tcattggaaa acgttcttcg
4861 gggcgaaaac tctcaaggat cttaccgctg ttgagatcca gttcgatgta acccactcgt
4921 gcacccaact gatcttcagc atcttttact ttcaccagcg tttctgggtg agcaaaaaca
4981 ggaaggcaaa atgccgcaaa aaagggaata agggcgacac ggaaatgttg aatactcata
5041 ctcttccttt ttcaatatta ttgaagcatt tatcagggtt attgtctcat gagcggatac
5101 atatttgaat gtatttagaa aaataaacaa atagggggttc cgcgcacatt tccccgaaaa
5161 gtgccacctg acgcgccctg tagcggcgca ttaagcgcgg cgggtgtggt ggttacgcgc
5221 agcgtgaccg ctacacttgc cagcgcccta gcgcccgctc ctttcgcttt cttcccttcc
5281 tttctcgcca cgttcgccgg ctttccccgt caagctctaa atcgggggct ccctttaggg
5341 ttccgattta gtgctttacg gcacctcgac cccaaaaaac ttgattaggg tgatggttca
5401 cgtagtgggc catcgccctg atagacggtt tttcgccctt tgacgttgga gtccacgttc
5461 tttaatagtg gactcttgtt ccaaactgga acaacactca accctatctc ggtctattct
5521 tttgatttat aagggatttt gccgatttcg gcctattggt taaaaaatga gctgatttaa
5581 caaaaattta acgcgaattt taacaaaata ttaacgctta caatttccat tcgccattca
5641 ggctgcgcaa ctgttgggaa gggcgatcgg tgcgggcctc ttcgctatta cgccagctgg
5701 cgaaaggggg atgtgctgca aggcgattaa gttgggtaac gccagggttt tcccagtcac
5761 gacgttgtaa aacgacggcc agtgaattgt aatacgactc actatagggc gaattggagc
5821 tcggtaccct acagttgaag tcggaagttt acatacactt aagttggagt cattaaaact
5881 cgtttttcaa ctacaccaca aatttcttgt taacaaacaa tagttttggc aagtcagtta
5941 ggacatctac tttgtgcatg acacaagtca tttttccaac aattgtttac agacagatta
6001 tttcacttat aattcactgt atcacaattc cagtgggtca gaagtttaca tacactaagt
6061 tgactgtgcc tttaaacagc ttggaaaatt ccagaaaatg atgtcatggc tttagaagct
6121 agatctcgat gtacgggcca gatatacgcg tatctgaggg gactagggtg tgtttaggcg
6181 aaaagcgggg cttcggttgt acgcggttag gagtcccctc aggatatagt agtttcgctt
6241 ttgcataggg agggggaaat gtagtcttat gcaatacact tgtagtcttg caacatggta

6301 acgatgagtt agcaacatgc cttacaagga gagaaaaagc accgtgcatg ccgattggtg
6361 gaagtaaggt ggtacgatcg tgccttatta ggaaggcaac agacaggtct gacatggatt
6421 ggacgaacca ctgaattccg cattgcagag ataattgtat ttaagtgcct agctcgatac
6481 aataaacgcc atttgaccat tcaccacatt ggtgtgcatg aattc**gatat c**gccgccatg
6541 atggtggccg ggacccgctg tcttctagcg ttgctgcttc cccaggtcct cctgggcggc
6601 gcggctggcc tcgttccgga gctgggccgc aggaagttcg cggcggcgtc gtcgggccgc
6661 ccctcatccc agccctctga cgaggtcctg agcgagttcg agttgcggct gctcagcatg
6721 ttcggcctga aacagagacc caccccagc agggacgccg tggtgccccc ctacatgcta
6781 gacctgtatc gcaggcactc aggtcagccg ggctcacccg ccccagacca ccggttggag
6841 agggcagcca gccgagccaa cactgtgcgc agcttccacc atgaagaatc tttggaagaa
6901 ctaccagaaa cgagtgggaa aacaacccgg agattcttct ttaatttaag ttctatcccc
6961 acggaggagt ttatcacctc agcagagctt caggttttcc gagaacagat gcaagatgct
7021 ttaggaaaca atagcagttt ccatcaccga attaatattt atgaaatcat aaaacctgca
7081 acagccaact cgaaattccc cgtgaccaga cttttggaca ccaggttggt gaatcagaat
7141 gcaagcaggt gggaaagttt tgatgtcacc cccgctgtga tgcggtggac tgcacaggga
7201 cacgccaacc atggattcgt ggtggaagtg gcccacttgg aggagaaaca aggtgtctcc
7261 aagagacatg ttaggataag caggtctttg caccaagatg aacacagctg gtcacagata
7321 aggccattgc tagtaacttt tggccatgat ggccggggcc atgccttgac ccgacgccgg
7381 agggccaagc gtagccctaa gcatcactca cagcgggcca ggaagaagaa taagaactgc
7441 cggcgccact cgctctatgt ggacttcagc gatgtgggct ggaatgactg gattgtggcc
7501 ccaccaggct accaggcctt ctactgccat ggggactgcc cctttccact ggctgaccac
7561 ctcaactcaa ccaaccatgc cattgtgcag accctggtca attctgtcaa ttccagtatc
7621 cccaaagcct gttgtgtgcc cactgaactg agtgccatct ccatgctgta cctggatgag
7681 tatgataagg tggtactgaa aaattatcag gagatggtag tagagggatg tgggtgccgc
7741 tga**gc**

C. SUPPORT SERVICE FACILITIES
Project 9: Administrative Support Service

Introduction

The research proposed in this application will be performed within the Musculoskeletal Disease Center (MDC), which is a large, multi-disciplinary research center consisting of more than 70 scientific and technical staff members, including 15 senior investigators with diverse expertise and research training. Of the 70 staff members, 43, including 13 senior investigators, are currently working on the Army projects. Strong administrative support is needed for organizing, coordinating, facilitating, and monitoring the research supported by the Army projects and is absolutely essential for the success of such a large, dynamic, and expanding research program. Consequently, the primary responsibility of this Administrative Support Service Facility is to support the administrative needs of the investigators supported by this Army grant. Moreover, synergistic interactions and collaborations between the investigators of the Army grant and other investigators of the MDC, as well as other investigators at local academic institutions and research organizations, such as Loma Linda University (LLU), Loma Linda Veterans Association for Research and Education (LLVARE), Loma Linda VA Medical Center, the University of California at Riverside, and City of Hope, would enhance the productivity of the Army projects. Accordingly, the secondary objective of this Administrative Support Service Facility is to provide and stimulate interdepartmental, interdisciplinary, and inter-institutional dialogue and to improve the existing interactions and productivity between various investigators of the local institutions and organizations in musculoskeletal research.

Body

1. Technical Objectives

Technical Objective 1:

Regular weekly or bi-weekly meetings are convened at which our senior investigators (Drs. Mohan, Lau, Strong) discuss scientific issues related to the fulfillment of the specific objectives of all of our Army funded projects. In order to assure that all of the scientific work of our current Army awards remains on track and progress toward meeting the specific objectives of each of our awards is being met, these regular meetings are essential. Our current awards include: DAMD17-99-1-9571; DAMD17-01-1-0744; DAMD17-02-1-0685; and DAMD17-03-2-0021.

Technical Objectives 2 and 3:

Our Administrative Support Staff work with the investigators on these awards to keep them apprised of ongoing budgetary issues; to facilitate supply and equipment purchasing decisions; to order supplies and equipment; to prepare manuscripts for publication; to retrieve journal articles from the library; to prepare paperwork for submission to oversight committees; to organize meetings; to help with recruitment; and to help facilitate the preparation of progress reports. Maintaining a strong administrative support team has been critical to the success of our scientists. During the second year of the award for this project, our scientists have published 13 articles and 24 abstracts. The total number of publications supported for our group since 2000 is 35 plus the 24 abstracts published in the past year.

Technical Objective 4:

Weekly staff meetings are held for all Musculoskeletal Disease Center (MDC) staff. When scientific issues are presented at the MDC staff meetings, these meetings are open to other investigators from Loma Linda University (LLU) as well as other VA and LLVARE investigators. Senior Investigators give talks on new technologies and areas relevant to the Army funded projects. Likewise, MDC investigators are invited to meetings of various research groups at LLU, the City of Hope and, periodically, the University of California Riverside (UCR). We invite expert scientists from other institutions to give talks on issues relevant to our Army funded research. This sharing of ideas with investigators from other institutions has proven to be very important.

Technical Objective 5:
User Committees to evaluate the performance of our Informatics/Microarray, Vector, and Phenotype Core facilities filed their reports to the Acting Chief of the MDC. These committees evaluated the performance of these facilities during the first year of this award. The committees report general, overall satisfaction with the performance of the Core Facilities. Suggestions for improvement included further education of the end-user on the application of the informatics technology. Responses to the suggestions of the respective User Committees follow:

2. Progress on Technical Objectives

Suggestions for Improvement in Phenotype Core

1. The access to some equipment was inadequate according to few investigators; however, this problem was sorted out by maintaining sign up sheets for a month in advance.

   Response: A meeting was held with all users to review usage and ask for cooperation between all users. Because of the heavy useage and because workers schedules change, advance signups do not solve all problems. Equipment frequently stand idle because the individual signed up had a change in schedule. Users were urged to let others know and adjust the signup if they were not going to use the equipment.

2. It is advisable to conduct yearly calibration of Instron Dynatup Mechanical Tester either through yearly service contract or by one time yearly service.

   Response: The Instron has been recalibrated.

3. Although the turn-around time for histology, considering the labor-intensive procedure, was considered satisfactory, the core director may want to look at possibilities to decrease turn around time.

   Response:
   a. With the purchase of a Cryostat, the preparation of frozen sections has become more routine. Frozen sections, while producing poorer cell morphology, require less tissue processing and less turn-around time.
   b.The addition of tissue processor has also eliminated the occasional long delays in preparing bone tissues for paraffin sections.

4. Clean up of data stored in the computers controlling the imaging devices such as Faxitron X-ray, pQCT, and PIXImus could be more frequent to avoid computer crashes.

   Response:
   a. A hard drive has been added to the pQCT to increase data storage capacity and reduce the number of times it is necessary to backup the data.
   b. Users of the PIXImus system have been reminded to transfer their data off the instrument to reduce clogging of the hard drive.

5. A more user-friendly system for computer-based data acquisition of Faxitron X-Ray imaging and Instron Dynamite Mechanical Tester system outputs should be explored to increase productivity.

   Response:
   We are exploring the possibility of updating the software for the Instron Dynamite Mechanical Tester. The updated software appears to automate more functions and would be more user friendly.

6. Several investigators felt that a high-resolution three-dimensional imaging system such as Micro-CT (non-invasive 3D X-ray microscopy) would provide a qualitative improvement in understanding the pathophysiology of skeletal tissue.

   Response:
   In lieu of purchasing an expensive piece of equipment, we have access to a MicroCT scanning through an instrument maintained by the University. The drawbacks of the instrument are the somewhat limited resolution (@ 70 microns) and a fee would be charged for time on the equipment.

Suggestions for Improvement in Informatics/Microarray Core

Recommendations:

Microarray and Informatics Support Services User Committee Report.

It is the committee's view that the Microarray and Informatics Support Service should continue to seek ways to improve the quality and reproducibility of slide printing and analysis at the MDC, and that improvement in these technologies should be communicated to all investigators at the MDC on a regular basis.

The analysis of microarray data is a computationally intensive task that requires state-of-the-art bioinformatics technologies for image analysis, database storage, and the extraction, organization, and interpretation of gene expression data. The committee recognizes that the Microarray and Informatics Support Service can only achieve its goal of providing high quality microarray production and analysis to MDC investigators if it is given access to state-of-the-art hardware (e.g. slide scanners, computers) and software (e.g. GeneSpring). Several users expressed minor concerns relating to their personal capacity to understand and properly apply

these bioinformatics technologies to the analysis of their data sets. The committee recommends that the Microarray and Informatics Support Services expand their efforts to educate MDC investigators in the application of current bioinformatics technologies, perhaps by offering regularly scheduled Microarray Users Group meetings and seminars.

Response:

In response to the committee's recommendations, in the past year the Microarray and Informatics Support Services have improved the training, microarray scanning and computational capabilities of these support services. Following is a summary of these improvements.

Training

Scientists and staff have improved the microarray facility by learning of the latest advancements at conferences in state of the art technologies for microarray expression analysis. The methods learned were incorporated into updating the microarray laboratory's protocols and informatics analysis. Improvements learned at these conferences were communicated and summarized for the staff of the Musculoskeletal Disease Center. Following are conferences attended by staff of the Microarray laboratory in the past year:

1. Latest Technologies and Development Conferences attended by Dr. Subburaman Mohan:
   - The Endocrine Society, 87th Annual Meeting, June 4-7, 2005, San Diego, CA
2. Latest Technologies and Development Conferences attended by Dr. Robert Chadwick:
   - American Association for Cancer Research, 96th Annual Meeting, April 16-20, 2005, Anaheim, CA
3. Latest Technologies and Development Talks given by Dr. Robert Chadwick:
   - Update on genetics and new technologies, a report for the 96th Annual Meeting of The American Association for Cancer Research, May 18, 2005, MDC staff meeting.
4. Latest Technologies and Development Conferences attended by Dr. Liming Bu and Yan Hu:
   - Agilent Technologies Microarray Workshop, University of California, San Diego, October 24-26, 2004, San Diego, CA.

Microarray Scanning

The Microarray Laboratory upgraded its scanning capacity through the purchase of a Axon 4200 Genepix scanner. This scanner can scan a microarray in only four minutes at 10 micron resolution. This is approximately a three fold increase in the scanning speed over our previous scanner (GSI Lumonics 4000).

The quality of an image, and the ability to quantify signals accurately, is determined by the signal-to-noise ratio of the scanner. Signal-to-noise ratio determines the confidence in the accuracy of a signal measurement. As noise increases, the confidence in measuring signals that are near background decreases—the signal gets lost in the noise. In most signal processing applications, the commonly accepted definition for detection limit is a sample with a signal-to-noise ratio of 3. The new scanner has a dynamic range of four orders of magnitude with a minimum signal-to-noise value greater than 3.0. This dynamic range allows us to detect a greater range of expression values with increased confidence in the accuracy of the data.

Computational Capabilities

In the past year, we have increased the density of number of genes and controls spotted on our custom microarrays 2.5 fold (from 15,000 clones 38,467 70mer oligonucleotide probes). This has required us to also increase our computational capabilities in order to analyze this high number of genes. For this purpose, we have purchased a Dell Optiplex SX280 workstation for the institution's informatics analysis. This workstation has over 2.8 GHx CPU, and 2048 megabytes of RAM, an increase of over 3 fold the amount of CPU and memory of our old computers. For archiving our data, we also have purchased two DVD burners with the capacity to archive approximately 5 gigabytes of data on each DVD disk.

For microarray expression analysis, we have upgraded our Genespring software from version 6.0 to version 7.2. GeneSpring 7.2 uses a new way to classify samples from gene expression data - Support Vector Machines (SVMs). An SVM is a learning algorithm that uses prior knowledge of sample classes to identify unknown samples. SVMs avoid several problems associated with unsupervised clustering methods, such as k-nearest neighbors, hierarchical clustering methods and self-organizing maps. These computer and software additions give our researchers more options to determine the optimal methods for performing expression analysis.

Suggestions for Improvement in the Vector Core

Specific objectives for the second year of funding period

- **Specific Objective 1: To assist investigators in the design of and to provide with appropriate research-grade viral or plasmid vectors.**

In the previous review of the Vector Support Service Facility, the reviewers were concerned about the variability of transduction efficiencies between different lots of virus preparations. The reviewers recommended that an additional examination into ways of eliminating viral titer variability and quality could be conducted to increase virus quality. To address these concerns, the viral core started to develop methods to determine the titers of the viral vectors without marker gene. The experiments are in progress. Additionally, we started to pool several lots of viral production together before release them to the end users. This practice may eliminate the possible variation caused by batch differences.

During the past twelve months, the Vector Support Service produced numerous VSV-G pseudotyped MLV vectors and HIV-based vectors for various investigators working on projects supported by the Army. Specifically, 1) in collaboration with Dr. Rundle (sub-project 4), the facility generated various batches of concentrated VSV-G pseudotyped MLV vectors expressing different growth factor or control genes that have been used successfully in animal experiments. These growth factor or control genes included □galactosidase (□-gal), enhances green fluorescent protein (EGFP), basic fibroblast growth factors (FGF-2) and its derivatives, bone morphogenetic protein-4 and its derivatives (BMP-4), growth hormone (GH), and cyclooxygenase (Cox-2). Additionally, we prepared two batched of VSV-G pseudotyped HIV-based vectors with either BMP-4 gene or □-gal gene for Dr. Rundle. He used these vectors to compare the efficacy between MLV-based and HIV-based vectors in his studies. 2) In support of the sub-project 6, the facility generated eleven different batches of HIV-based vectors for use in the study of systemic gene therapy of musculoskeletal diseases. These HIV-based vectors included those expressing □-gal, EGFP, BMP2/4 and GH genes. To ensure the safety of these HIV-based vectors, each HIV-based vector was harvested and concentrated, tested for potential contamination of recombination competent retrovirus (RCR) within the preparation. None of

these HIV-based vector preparations has shown RCR contamination in our assay system. The results have been submitted to and approved by the Biosafety committee and Animal care and use committee. 3) In collaboration with Dr. Gysin (sub-project 7), the facility produced four different batches of concentrated MLV-based vectors, expressing □–gal, BMP2/4, and Cox-2 genes, respectively. These viral vectors were used in Dr. Gysin experiments testing potential synergistic interaction between BMP2/4 and Cox-2 in promoting bone formation in the critical sized calvarial bone defect model. 4) In collaboration with Dr. Strong (sub-project 8), the facility produced three different batches of concentrated VSV-G pseudotyped MLV vectors, expressing □–gal, LMP-HA, and IGFBP6 gene with or without secretion signal, for animal experiments.

- **Specific objective 2: To provide education, tutorials, practical training, technical assistance, and protocols to Investigators for the experimental use of gene transfer vector.**

In the last review, the committee felt that the core director should update investigators in a more widely attended staff meeting regarding new technology and vectors that are available in the Vector Support Service Facility at least every 6 months. Although yearly progress report is available to gene therapy investigators, investigators working on other Army projects would benefit by such a biannual presentation at staff meetings.

With respect to providing education and tutorials to investigators, Dr. Chen (the director of the Vector Support Service) gave three lectures to J.L.Pettis VAMC, Musculoskeletal Diseases Center during the past 12 months. These lectures were designed to educate and tutor Army projects investigators in viral gene transfer technology. Two lectures addressed the safety issues concerning the use of viral vectors in gene therapy. One lecture discussed the current development of viral and non-viral vectors used for musculoskeletal disease gene therapy.

Project 10: Phenotype Support Services

Introduction

The phenotype support service facility is essential for efficient progress in all of the specific projects in this proposal in the molecular genetics division and also in the gene therapy division for a total of eight projects, ranging from clinical projects to projects involving molecular techniques. The assays to be performed in the phenotype support service facility include: 1) total bone density in rodents by pQCT; 2) total skeletal bone density in rodents by dual energy x-ray densitometry (PIXI); 3) bone strength analysis and performance of very precise femoral fracture using the Instron mechanical tester; 4) X-ray imaging by the Faxitron; 5) histological analysis, including quantitative morphology, immunocytochemistry, and fluorescence microscopy; 6) serum and urine chemical assays, including bone markers and IGF assays; and 7) statistical support. It would be difficult for the principal investigator of each of the separate projects to set-up the facilities to perform this large array of routine phenotypic measurements without considerable duplication of effort. Consequently, this phenotypic vector support facility will be highly efficient and cost effective for the proposed specific projects in this grant application. The emphasis in this support service facility will be to perform highly reliable, precise measurements of the phenotype requested. The director of this support facility will keep abreast of new technologies and transfer this information to those principal investigators potentially interested in the corresponding new technology. The director of this support facility will also provide training courses in the various phenotypic measurements made in this support service facility. It is essential for the investigators to have a fundamental understanding of the measurements being made so that they will be aware of the pitfalls and advantages of the application of there techniques. Study design and statistical support will also be provided when requested.

Body

1. Technical Objectives

The major technical objective for this phenotype support service facility will be to receive samples, perform the appropriate measurements on these samples, and then transfer all the data electronically to the corresponding investigator. Specific objectives are:

1. To assist investigators in the design of studies involving given phenotypes.
2. To perform measurements as requested by the investigators on the samples provided.
3. To follow the development of emerging technologies in the literature and at meetings and make recommendations to investigators regarding the possibility of adopting some of these new technologies in the phenotype support service facility.

2. Progress on Technical Objectives

Specific Objective 1. To assist investigators in the design of studies involving given phenotypes.

Subproject 1. Digit tip regeneration.

a. Selection of the appropriate sampling site is always an important aspect of bone histology. Current studies have continued to improve the sampling site selection for the digit wound healing study. Our previous work had used latero-medial sectioning which allowed several digits including cut and uncut digits to be seen on one section. However, it became apparent that the view of the wound-healing site varied with depth of the sectioning. Therefore, optimum depth required different sections for different digits. Consequently, we considered antero-posterior

sectioning (perpendicular to the nail). It was apparent from test sections on normal digits that this orientation of the specimens gave a better view of the bone in the third phalanx and was less sensitive to depth of the section. These advantages offset the disadvantages that only one digit could be viewed at a time and maintaining a consistent orientation was more difficult. With more experience with the new technique, the sampling orientation became more consistent. It was also found that maintaining the paw intact helped to keep the orientation constant. However, partial cutting and removal of the skin proximal to the third phalanx improved the infiltration of fixatives and paraffin.

b. This modified sampling method was used to process samples for the time study of wound healing with multiple inbred strains of mice. The investigators were assisted in interpreting the morphology and cell staining in the wound-healing site. The cell morphology, Hematoxylin-eosin staining and Masson trichrome (collagen) staining helped to identify a sub dermal site with some characteristics of a blastema. These characteristics included mitotic figures, indicating increased cell proliferation, and cells with mesenchymal cell morphology.

c. The investigators were also assisted in testing immunostaining for products of several genes. The protocols, basic staining reagent, the expertise and equipment needed were provided.

Subproject 4.

Transgenic mice to assess gene function in mechanical testing and bone fracture. Transgenic mice with Leptin or Bax gene knockouts are being studied to determine the influence of these genes on mechanical testing and bone fracture. Evaluation of fracture healing is being done by pQCT densitometry and faxitron x-Ray analysis. Because fracture healing involves the addition of a cancellous bone bridge on the periosteal surface, the thresholding parameters in the pQCT analysis need to be adjusted. Parameters that work well with normal bone structure do not distinguish the new bone on the periosteal surface. Furthermore, lowering of the outer threshold value allows determination of the total hard and soft callus. These parameters have been established and are being used to assess the fracture healing in the transgenic mice.

Subproject 6.

a. Green fluorescent protein (GFP) is a fluorescent marker used to label the hematopoietec stem cells. GFP labeled hematopoietic stem cells infused into mice appear in bone marrow and can be detected by GFP fluorescence. The FACS analysis is a sensitive way to detect GFP fluorescence in cell suspensions. Generation of GFP labeled hematopoietic cells in the blood stream or in marrow cell suspensions can be readily detected by FACS analysis. Histological detection of GFP labeled cells appears to be less sensitive. Fluorescence microscopy of bone sections readily detects strongly labeled cells. However, weakly labeled cells are difficult to distinguish from background autofluorescence. Frozen sections are the optimum platform for viewing fluorescence because auto fluoresce is minimized. However, frozen sections do not attach well to the slide. Staining procedures designed to identify the nature of the labeled cells commonly result in distortion and loss of tissue. An alternative approach is to use antibodies to detect GFP. Good antibodies are available for GFP. The methodological details are being adjusted to increase the sensitive of the immunostaining procedure. To compare methodologies, we have devised three approaches for the detection and identification of GFP labeled cells in bone: 1) fluorescence in frozen sections followed by staining for cell identification, 2) Fluorescence in

plastic embedded section (with revised protocol to improve preservation of fluorescence) followed by staining for cell identification, and 3) GFP immunostaining followed by staining for cell identification. These procedures are being compared using samples with a known range of GFP labeled cells. Preliminary results show advantages and disadvantages of each of the three approaches.

b. Progress is continuing on developing methods suitable for identifying osteoblasts expressing green fluorescent protein GFP. One of the needed methodologies is to be able to examine GFP expression and osteoblast markers in the same section. This is needed to confirm that GFP labeled cells that have been introduced in to the animal can develop into osteoblasts. While GFP expressing cells can be identified by immunostaining in paraffin sections, alkaline phosphatase, the most commonly used osteoblast marker, is inactivated by this protocol. We have tested an alternative approach that employs frozen sectioning. The technical difficulty with frozen sections is that they do not attach well to the slides. Attachment needs to be good enough in order to maintain the osteoblasts on the surface of the bone during staining. We have found that mineralized bone matrix does not attach well to the slides and the matrix will move or be lost during staining. Demineralized bone matrix attaches better but still not well enough to have good retention of the samples. Demineralization does decrease alkaline phosphatase activity in the frozen sections, but the activity is still sufficient for osteoblast identification.

In order to improve attachment, we have tested a new cryostat attachment that is a tape transfer system. A transfer tape is placed over the block before the sections are cut. The tape is used to transfer the section to special slides that are coated with unpolymerized plastic. The slide is then flashed with UV light to polymerize the plastic binding the intact section to the slide. Attachment is still variable so that multiple sections must be prepared to find ones that are satisfactory. Attachment to the slide is better with demineralized sections than with mineralized sections.

Another difficulty is balancing the ALP staining with the antibody horse radish peroxidase staining. Neither staining should be too strong or the presence of the second stain will be obscured; and selection of the appropriate color of dye affects the detection of dual staining. An alternate substrate for the DAB used in horseradish peroxidase labeled antibodies (AEC) was tested. The AEC yielded a reddish orange color that lacked the intensity necessary for the dual staining. The brownish color of the product of DAB substrate was better. However, some brown deposits in the normal marrow caused some confusion in the interpretation of the stained sections. These brown deposits were shown to be homosiderine by staining them for iron. The Prussian blue iron stain converted the brown to blue so that it could be distinguished from the brown DAB staining. Thus the combination of red staining (ASTR substrate) for ALP and brown staining (DAB substrate) for GFP antibodies with blue blocking of iron deposits and blue hemetoxylin counterstaining appears to provide the best combination for osteoblast identification.

One additional difficulty remains. Endogenous peroxidase activity in bone is readily blocked in paraffin sections of bone by hydrogen peroxide pretreatment. Endogenous peroxidase activity is much stronger in frozen sections and less sensitive to inactivation by hydrogen peroxide pretreatment. While osteoblasts do not have much endogenous peroxidase, some of the marrow cells have strong peroxidase activity. This activity gives strong marrow cell staining in control sections and complicates the interpretation of staining patterns. Alternative blocking methods for endogenous peroxidase activity are being sought.

Specific Objective 2. To perform measurements as requested by the investigators on the samples provided.

Subproject 1.

Samples of paws from several mouse strains and several time points have been obtained Paraffin sections have been prepared and studied with the various staining methods.

Subproject 4.

a. Bone Sections from Leptin and Bax knockout mice have been prepared and stained. Samples include fractured and unfractured bones at various times after fracture. Samples were demineralizedin EDTA, processed in a tissue processor, embedded in paraffin and sectioned. Sections are stained for H&E, Mason's trichrome, Van Geisens, and Saffranin O. The Saffranin O stained sections were used to follow the development and loss of cartilage during fracture repair. Samples were also evaluated for bone resorption by staining for tartrate-resistant acid phosphatase an osteoclast marker. Tunnel staining is being used to evaluate apoptosis in BAX knockout mice.

b. Bone density and bone geometry measurements have been made by pQCT and Faxitron X-Ray analysis to establish basal values and to follow fracture healing. The instrument threshold settings must be done carefully because of the deposition of low density "woven bone" at the fracture repair site.

Subproject 6.

a. Bone samples from mice treated with GFP labeled hematopoietic stem cells are being processed for histological evaluation in the Phenotyping laboratory. Histological processing includes both frozen and paraffin embedded sections of bone and soft tissues.

b. Bones are also being evaluated for bone formation by analysis of density and geometry by pQCT analysis.

Specific Objective 3. To follow the development of emerging technologies in the literature and at meetings and make recommendations to investigators regarding the possibility of adopting some of these new technologies in the phenotype support service facility.

Subproject 1.

We continue to review the literature and attend presentations related to wound healing. As noted previously we have looked at methods for evaluating basement membrane development in healing fractures. Both the methamine silver (GOYA) method and PAS staining techniques show basement membranes but also stain other membranes. Thus, they are not specific but do give information about the structure.

Development of new technologies.

a. Evaluation of new technologies includes literature review and attending lectures. An evaluation of current methodology was presented at the workshop "non-invasive Assessment of Trabecular Bone Microarchitecture Working Group" given at the American Society of Bone and Mineral Research Meeting in Seattle.

b. MicroCT.

We are continuing to monitor the development of MicroCT equipment. New developments include the addition of bone density determination to the Scanco MicroCT instrument. This is the first instrument to include density measurement to the area measurements. It involves standardizing the beam with phantom standards.

Analytical methods for generating trabecular bone parameters from microCT scans are continuing to evolve. Analytic approaches can sharpen the images obtained and reduce the scan time. This is important for in vivo scanning where radiation exposure is a limiting factor for longitudinal studies. However equipment costs remain high.

c. MRI.

The resolution of microMRI continues to improve and instruments specifically designed for small animals are becoming available.

Project 11: Microarray & Informatics Support Services

Introduction

As a result of the sequencing of the human and mouse genomes, there has been a tremendous increase in the discovery of novel genes with unknown functions. It is therefore important to next interpret and determine the function and genetic pathways of the large amounts of sequence information now available. One powerful method of determining unknown gene function and genetic pathways is by microarray expression profiling. Microarrays (also called DNA chips) are glass or plastic substrates onto which known sequences of DNA have been synthesized or spotted. Fluorescently labeled RNA from different biological samples are hybridized to their complementary sequences on the microarrays. The resulting fluorescent intensities are quantified and data analysis performed to determine expression levels of RNA transcripts. Thus, microarrays allow for the experimental analysis of many genes in a single experiment, and one can compare expression levels of genes over several time-points and different biological or disease conditions. Comparing these expression levels gives clues to gene function and is a very powerful method of discovery. Project 11 of this grant had the goal to upgrade and improve the microarray and informatics support services in the Musculoskeletal Disease Center. Following are the technical objectives:

Body

1. Technical Objectives:

Following are the specific objectives during the second year of the grant period:

Technical Objective 1: To provide technical service.
Technical Objective 2: To provide education.
Technical Objective 3: To update on recent advances.

To achieve the above technical objectives, the following Specific Objectives are proposed during years 1 and 2 of this proposal:

1) To provide technical service, microarray and informatics support service will:
   - i) Prepare cDNA probes for genes related to musculoskeletal tissues
   - ii) Spot cDNA probes on the slides
   - iii) Perform labeling of cDNA, hybridization and detection of labeled probes
   - iv) Develop the informative infrastructure to produce, analyze, interpret and house the information derived from microarray experiments
   - v) Mining of functional and expression data for genes spotted in the slides
   - vi) Identify SNPs for genes involved in the IGF regulatory system using various SNP databases
   - vii) Build maps of genetic loci for ENU mutant and QTL studies and identify overlapping BAC clones for functional testing

2) To provide education, microarray and informatics support service will:
   - i) Train investigators in the preparation of good quality RNA
   - ii) Train investigators in the use of appropriate statistical methods for data analysis

3) To update on recent advances, microarray and informatics support service will:
   - i) Improve spotting and labeling techniques by incorporating latest technology developments in these areas
   - ii) Incorporate new advances in data management and analysis

We have accomplished all of the above specific objectives. Our progress in each of the Specific Objectives is given below.

Progress on Technical Objectives

Technical Objective 1: To provide technical service.

In year two of subproject 11, we have further increased the number and density of genes on our microarrays. To accomplish this, we obtained the MEEBO (Mouse Exonic Evidence Based Oligonucleotide) set from Illumina. The set contains a collection of oligo probes, derived from constitutively expressed exons, allowing interrogation of almost 25,000 mouse genes. The set was designed to enable study of mouse transcription patterns and, as broadly as possible, alternative splicing of genes. An exon-centric design was selected to allow the differentiation of constitutively expressed versus alternatively expressed exons. In addition to the exon-centric probes, the set contains an extensive assortment of controls that facilitate accurate evaluation of expression results. The MEEBO Set contains 38,467 70mer oligonucleotide probes with an amino modification on the 5' end. The amino modification enhances binding efficiency to microarray glass slides. The probes in the MEEBO set are at a final yield of 200pmol each, and delivered in 101 384-well microarray plates. The probes are normalized to have an average melting temperature of 80C, and are designed to minimize cross-hybridization and secondary structure. The set contains a total of 35,302 probes targeting mouse genes. Probes are categorized as follows:

1. Constitutive Exonic Probes (30,125 probes): A probe that will recognize all known transcripts of a gene.
2. Alternatively Spliced / Skipped Exonic Probes (4,201 probes): Probes that will recognize exons that are present in some, but not all, transcripts of a gene.
3. Non Coding RNA Probes (196 probes): Probes recognizing non-protein coding transcripts (ribosomal RNAs, miRNAs).
4. BCR / TCR Genic / Regional Probes (372 probes): Probes recognizing transcripts from genes that undergo somatic rearrangement.
5. Mitochondrial Probes (13 probes): Probes recognizing mouse mitochondrial derived DNA sequences.
6. Transgenic / Cassette Probes (37 probes): Probes recognizing elements commonly used for transgenic constructs (e.g. GFP, YFP).
7. Murine Viral Probes (358 probes): Probes recognizing mouse viral pathogen sequences.
8. Controls. The set contains a total of 3,482 controls. The controls fall into the following categories:
    a) Negative Controls (317 empty wells and 97 probes). Empty wells and 97 random sequences are positioned throughout the set to assist in determining background.
    b) Positive Controls (1,152 probes): Probes recognizing a small subset of mouse transcripts.
    c) Doped (Spike-in) Controls (1,916 probes): Probes recognizing non-mouse sequences that can be spiked into RNA samples.

Mouse Sequence Selection and Probe Design. A systematic methodology was applied to identify the exons, generate all possible 70mer candidate probes, and select the optimal probe from the candidates. The pipeline for sequence selection and probe design included three steps:

1) Collect and curate exon sequences. Supplement as needed with transcript sequences.
2) Design the candidate 70mer probes for exon or transcript sequences. Using ArrayOligoSelector, an open source tool for selecting 70mer oligo probes from a defined set of sequence data, was used to generate a list of candidate probes for each exon or

transcript sequence. Multiple filters including uniqueness, self-binding, complexity, GC, content, and user defined parameters were used to narrow and rank the list of candidate probes.

3) Pick the best probe from the list of candidate probes. Several criteria were used to identify the optimal probe from the list of candidate probes:
    a. Uniqueness: Probes that had binding energies of > -35 kcal / mol for other sequences were preferred.
    b. 3' Proximity: Probes that were less than 1,000 bases from the 3' end of the transcript were preferred.
    c. Constitutive: Probe should be present in all transcripts.

If the above three criteria could not be met, more than one probe would be selected for the exon or transcript sequence.

Technical Objective 2. To provide education.

The new MEEBO microarrays have many additional genes of known and unknown function. Thus, in order to assist researchers in analyzing their microarray data, we have updated the genetic information for each gene and probe spotted on to the microarrays. The following are the Annotation Details for the MEEBO microarrays.

Probe annotation information contains the following data elements:

1. Plate_Name: Contains the name that will appear on the plate label. MCC plates contain mouse probes; non-MCC plates contain controls.
2. Plate_Number: Contains the plate number used to identify which packing box a plate is located.
3. Row: Oligo plate row position.
4. Column: Oligo plate column position.
5. Probe_Name: Contains the oligo name. The following codes can assist with interpreting the oligo name:
6. Rockefeller MouSDB3 constitutive exons / islands (oligo names start with 'scl' followed by a number >0)
7. LocusLink constitutive exons / islands (oligo names start with 'scl0' followed by a number >0)
8. mRNA derived 70mers which may span intron/exon boundaries (oligo names start with 'scl00' followed by a number >0)
9. A collection of alternative spliced / skipped exons generated through extensive curation of published datasets (oligo names start with 'scl000' followed by a number >0)
10. Syntenic orthologs of human loci exhibiting cis-antisense transcription (1).

Microarray Quality Control Improvements. In year two of this subproject, we have also developed new methods of validating microarray manufacture and quality control. Since our new oligo microarrays are single stranded DNA, this necessitated developing new methods to determine the proper quantity of DNA to spot as well as to determine the size, quality and distance between each spot on the microarrays. In order to optimize these parameters, we have begun QCing manufactured slides using fluorescently labeled random nanomer oligonucleotides. These "panomer" oligodeoxynucleotides are random primers that are labeled at the 5' end with either Cy3 or Cy5 dyes. These labeled controls are very useful for assessing microarray spot morphology, hybridization efficiency and channel bleed-through on oligo microarrays. Each lot

of microarrays we manufacture is now QCed using these labeled nanomers. Figure 1 shows images of a microarray that was hybridized with the panomer controls. In the microarray shown, the highest density of genes that could be spotted on to a 1" x 3" glass slide was determined. From this experiment, we determined we could spot a maximum of 40,638 spots.

From the density spotting experiments, we determined the density, pattern and maximum number of spots to use to manufacture the MEEBO mouse microarrays. In summer of 2005, we manufactured the first lot of these microarrays and began the first expression profiling experiments with them. Figure 2 shows data from these first experiments.

Microarray Controls. The Microarray Facility has also three types of controls on to our microarrays; negative controls, positive controls and spike-in controls. The negative controls consist of empty spots which are spotted only with 25% DMSO buffer. The positive controls consist of housekeeping genes that are constitutively expressed in nearly all tissues. The spike-in controls are obtained from Ambion, Inc. and consist of E. coli genes that show no sequence similarity to mammalian genomes. These have been tested experimentally to insure that they do not cross-hybridize to each other or to human and mouse RNA.

Through the use of the spike-in controls, gene expression data can be evaluated by relating experimental data to that obtained from our spike-in control genes of known concentration and ratio. This allows us to evaluate the microarray data quality of each slide. If the spike-in controls give the expected concentrations and expression ratios, this is a good indication that the experimental RNA samples have been labeled and normalized correctly and that correct expression values are being obtained. Table 2 shows the expected ratio values of the spike-in controls. Figure 3 shows experimental results obtained from the spike-in controls.

Conferences and Continuing Education. The methods described are advancements developed as a result of learning of new methods and technologies from networking and scientific conferences attended by scientists in the MDC. Following is a list of conferences attended and talks given by scientists in the MDC. These conferences led to improvement and incorporations of state of the art technologies in the Microarray Laboratory and Informatics Support Services:

Latest Technologies and Development Conferences attended by Dr. Robert Chadwick:

- American Association for Cancer Research, 96th Annual Meeting, April 16-20, 2005, Anaheim, CA

Latest Technologies and Development Talks given by Dr. Robert Chadwick:

- Update on genetics and new technologies, a report for the 96th Annual Meeting of The American Association for Cancer Research, May 18, 2005, MDC staff meeting.

Latest Technologies and Development Conferences attended by Dr. Liming Bu and Yan Hu:

- Agilent Technologies Microarray Workshop, University of California, San Diego, October 24-26, 2004, San Diego, CA

Additional Progress

Scientific collaborations with Dr. Mike Lilly of the Loma Linda University School of Medicine were undertaken investigating isolation of RNA from archival tissue specimens. Since these specimens yield RNA that is of lower quality than flash frozen tissue samples, we are working on developing improved RNA isolation and labeling methods from degraded RNA. If

the methods can be optimized to give consistent and reliable expression results from archival tissue, this will be of great use in proposed future clinical studies.

For isolation of RNA from paraffin embedded tissue we found that the Epicentre MasterPure Nucleic Acid isolation kit gives high yields of RNA. Following is the protocol we currently use:

RNA Isolation from Paraffin Embedded Tissue

1. Cut 10 micron sections from the paraffin embedded tissue.and place the tissue in a 1.5 ml microtube.
2. Deparaffinize the tissue through successive washes of citrosolve (1 ml for 5 min each time), 96% ethanol (1 ml twice for 5 min each time), and 70% ethanol (1 ml once for 5 min).
3. Dilute 2ul of Proteinase K into 300ul of Tissue and Cell Lysis solution for each sample. Resuspend the cell pellet with this Lysis solution and mix thoroughly.
4. Incubate at 65°C for 45min, and vortex every 15min.
5. Place the sample on ice for 5min.
6. Add 150ul of MPC protein Precipitation Reagent to 300ul of lysed sample and vortex the mixture for 10sec.
7. Spin for 10min 4°C at max speed in a microcentrifuge. Transfer the supernant to a clean tube.
8. Add 50ul of MPC protein Precipitation Reagent and repeat above step.
9. Add 500ul isopropanol to the recovered supernatant, invert the tube 30-40 times.
10. Pellet the RNA by centrifugation at 4°C for 10min in a microcentrifuge.
11. Carefully pour off the isopropanol without dislodging the RNA pellet. Remove all of the residual isopropanol with a pipet.
12. Air dry 10-15min.
13. Quantify and determine the quality of the RNA by Agilent Bioanalyzer and Nanodrop UV260 analysis.

If the tissue is frozen, steps one and two of the above protocol are omitted. Frozen tissue RNA gives very high quality RNA as well as high yields. The initial experiments on RNA isolation from paraffin embedded tissue show that the RNA is highly degraded (Figure 4). However, high yields of RNA have been obtained from paraffin embedded tissue.

Using the RNA samples shown in Figure 4, microarray expression profiling was attempted. The frozen RNA sample gave high yields of Cy3 and Cy5 labeled RNA. However, the paraffin RNA sample did not give usable yields of labeled RNA. We believe that this is due to the highly fragmented nature of the paraffin RNA. Microarray labeling protocols use oligo dT for priming and the short fragments of paraffin RNA do not hybridize oligo dT and label efficiently.

Thus, we undertook experiments using realtime PCR expression profiling and initial cDNA synthesis by random decamer priming. We found that expression profiling of paraffin RNA by realtime PCR works well, as long as the RT-PCRs are short (~100 bp). Figure 5 shows an amplification plot from paraffin RNA isolated

Key Research Accomplishments

1) Increased the density of number of genes and controls spotted on custom microarrays 2.5 fold (from 15,000 clones 38,467 70mer oligonucleotide probes).
2) Improved microarray analysis results by the use of Ambion spotting and spike-in controls. These controls have known RNA concentrations and Cy3/Cy5 ratios and their use gives confidence that correct expression results are obtained.
3) Improved quality control of microarray manufacture through the use of Cy3 and Cy5 labeled random nanomers (panomer). These controls allow for the determination of optimal DNA concentration for spotting and grid parameter determination for maximum gene density.
4) Investigated new methods for isolation of RNA from archival specimens (paraffin embedded tissue).
5) Trained multiple investigators in informatics and microarray data analysis.
6) Attended research conferences to learn of latest advances in microarray manufacture and analysis.
7)

Reportable Outcomes

None.

Conclusions

1) The technical objectives (1) To provide technical service; (2) To provide education; and (3) To update on recent advances have been achieved.
2) The microarray and informatics support services have increased throughput and improved microarray expression results in the Musculoskeletal Disease Center.
3) The improvements made to the microarray and informatics support services will expedite and advance research into gene discovery, function and genetic pathway analysis in the MDC.

References

1. Yelin R, Dahary D, Sorek R, Levanon EY, Goldstein O, Shoshan A, Diber A, Biton S, Tamir Y, Khosravi R, Nemzer S, Pinner E, Walach S, Bernstein J, Savitsky K, and Rotman G. "Widespread occurrence of antisense transcription in the human genome." Nature Biotechnology Volume 21(4):379-86 (2003).

Table 1. Annotation information from a small portion of the MEEBO set. Only 12 probes out of 35,302 are shown due to space limitations.

Plate_Name	Plate_Num	Row	Column	Oligo_ID	Probe_Name	LocusLink_ID	Gid	Accession	Symbol	Probe_Sequence	Sequence_ID	Tm	GC	Product
003-MCC	3	A	1	mMC000769	scl44253.13.1_34	218030	GI_27923922	NM_175006	Pou6f2	CCGAGATTGCTGAGAAGCTAAACTACGA CCGGGAAGTAGTTAGAGTTTGGTTCTGC AATAAGAGACAAGC	mSQ000769	76.5	46%	POU domain, class 6, transcription factor 2
003-MCC	3	A	2	mMC000770	scl40603.7.49_6	13494	GI_6681224	NM_007879	Drg1	AGGTGCCTCACTGTGTACCCATCTCTGCT CATCACCGCTGGAATTTTGATGACCTTTT GGAGAAAATCTG	mSQ000770	77.1	47%	developmentally regulated GTP binding protein 1
003-MCC	3	A	3	mMC000771	scl18378.11.1_20	11486	GI_31982514	NM_007398	Ada	AAGCTTCCTCCCAGAGGAAGAGAAGAAG GAACTTCTGGAACGGCTCTACAGAGAATA CCAATAGCCACCA	mSQ000771	77.7	49%	adenosine deaminase
003-MCC	3	A	4	mMC000772	scl41070.6_518	22344	GI_26024204	NM_016686	Vezf1	GTATTAGATAATCTTCAAATCTGACATCCA GCCTGTTATGCTTGCTCTAGGGCTCGCT GCTTGGCCTGCA	mSQ000772	77.1	47%	vascular endothelial zinc finger 1
003-MCC	3	A	5	mMC000773	scl53823.22.1_4	170722	GI_30794231	NM_130888	Nxf7	ATACTCCAACTTCAAGCTTGTCCTTTCTC AAGAGCAGCAAAGAATGGTGCAGGCTTT CTCCACCCAGTCG	mSQ000773	77.7	49%	nuclear RNA export factor 7
003-MCC	3	A	6	mMC000774	scl32668.4.1_181	13170	GI_8393239	NM_016974	Dbp	CCATGGCCAGTGGTCTGGCCAGCTAGGT GCCCGAAGAACGTCATGATGCAGACAAA TACATTTATATTTT	mSQ000774	77.1	47%	D site albumin promoter binding protein
003-MCC	3	A	7	mMC000775	scl40952.3_414	68127	GI_51766405	XM_484073	B230217C12Rik	GGTCACAGTCATTTAAGCGCTACAGCTCT AGTTTATTCCCAGACTGGAAAAGATTTCC TATCTCTTCCCA	mSQ000775	75.3	43%	RIKEN cDNA B230217C12 gene
003-MCC	3	A	8	mMC000776	scl34898.4.1_27	80857	GI_13447395	NM_030610	Fgf20	CTTTTTACCAAGACCAGTAGACCCAGAAA GAGTTCCAGAATTATACAAAGACCTACTG ATGTACACTTGA	mSQ000776	73.6	39%	fibroblast growth factor 20
003-MCC	3	A	9	mMC000777	scl24377.3_47	230119	GI_34328403	NM_173399	Zbtb5	CACAGGGATTCTAACGGGGACTGGGGAC CTGACTTTTGACTTTTAGCCTTAATTCTAG CCCGGCATAATC	mSQ000777	77.7	49%	zinc finger and BTB domain containing 5
003-MCC	3	A	10	mMC000778	scl33120.2.1_47	68992	GI_51763176	XM_133134	Zfp580	GCCACCTGTCGCGGCACCGCGCCACCCA CCGTGCGCGCGCTGGTCCACCTCACACC TGCCCGCTCTGTCC	mSQ000778	88.8	76%	zinc finger protein 580
003-MCC	3	A	11	mMC000779	scl30121.2.1_3	72131			2010310C07Rik	CAAGGGGAGCCTCGACCCTCCAGTCCA AGAGAGAAAGAAGGCAATAACCCTACTCC CAAGAAACAGCAG	mSQ000779	79.4	53%	RIKEN cDNA 2010310C07 gene

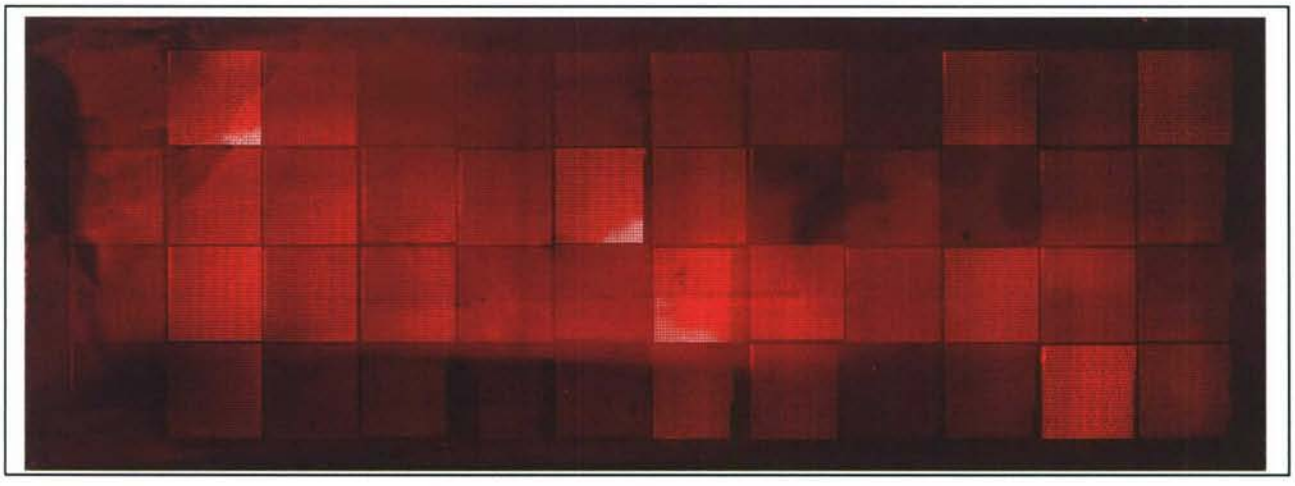

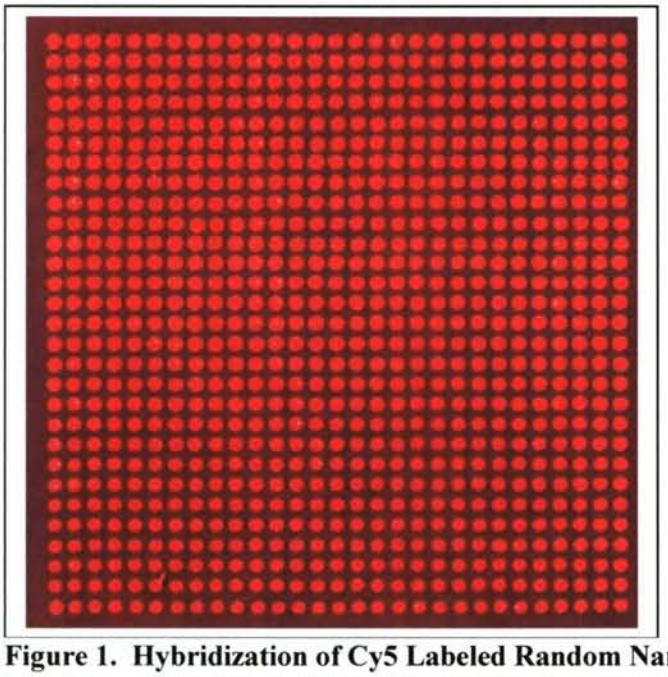

↑ 40,638 oligonucleotide spots printed on to a Corning UltraGap glass slide (above image). There are 48 grids of 841 spots in each grid.

← 841 oligonucleotide spots in a 29 x 29 grid (left image). The spot size of each spot is approximately 100 microns and the distance between each spot is about 25 microns.

Figure 1. Hybridization of Cy5 Labeled Random Nanomers for Microarray Manufacture Quality Control. In the images below 48 tungsten pins were used to stamp oligonucleotides on to a Corning UltraGap glass slide. This corresponds to a total of 40,368 spots on the microarray (29 x 29 grid = 841 spots in each grid. 48 grids x 841 spots = 40, 638 spots).

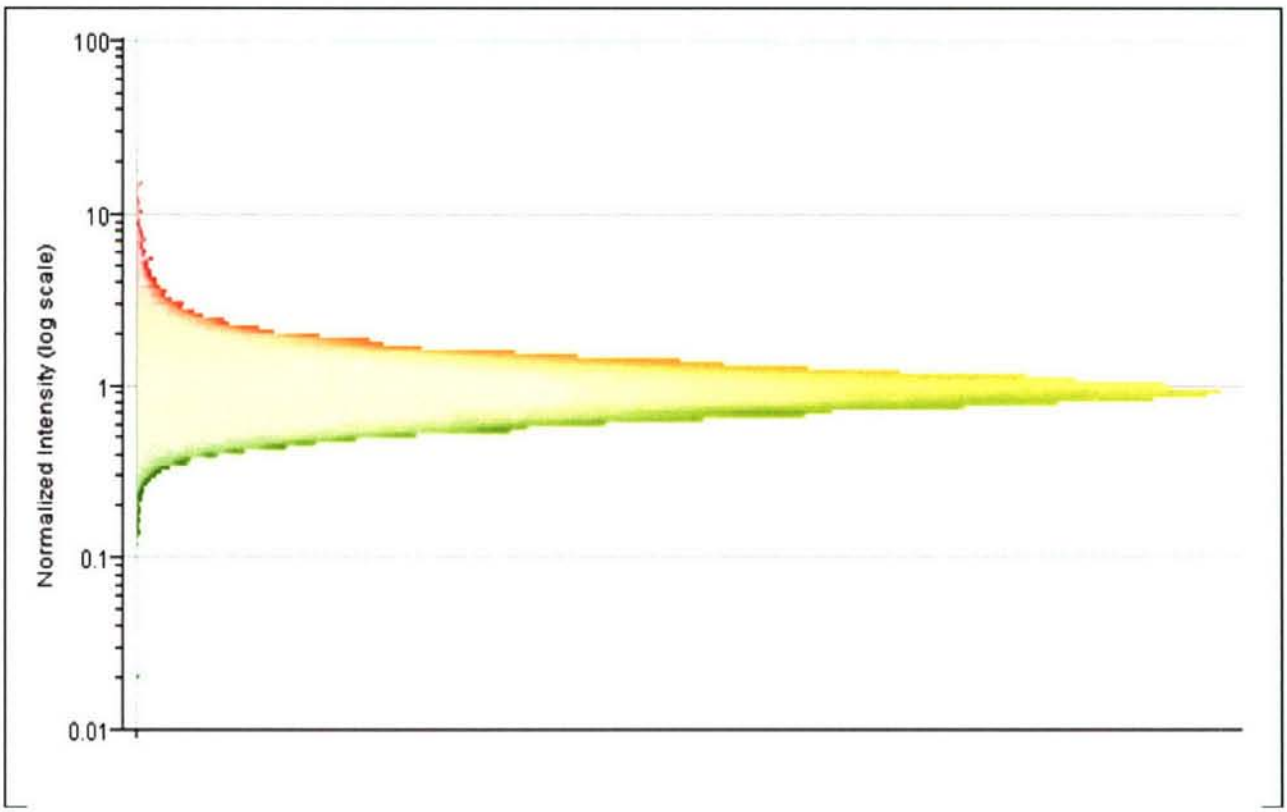

Figure 2. A combined normal plot of 11 microarrays with 38,467 probes each. This corresponds to 423,137 expression values for the 11 microarrays. Note that the data is highly normal and shows little to no skewness, indicating that the data follows Gaussian statistics.

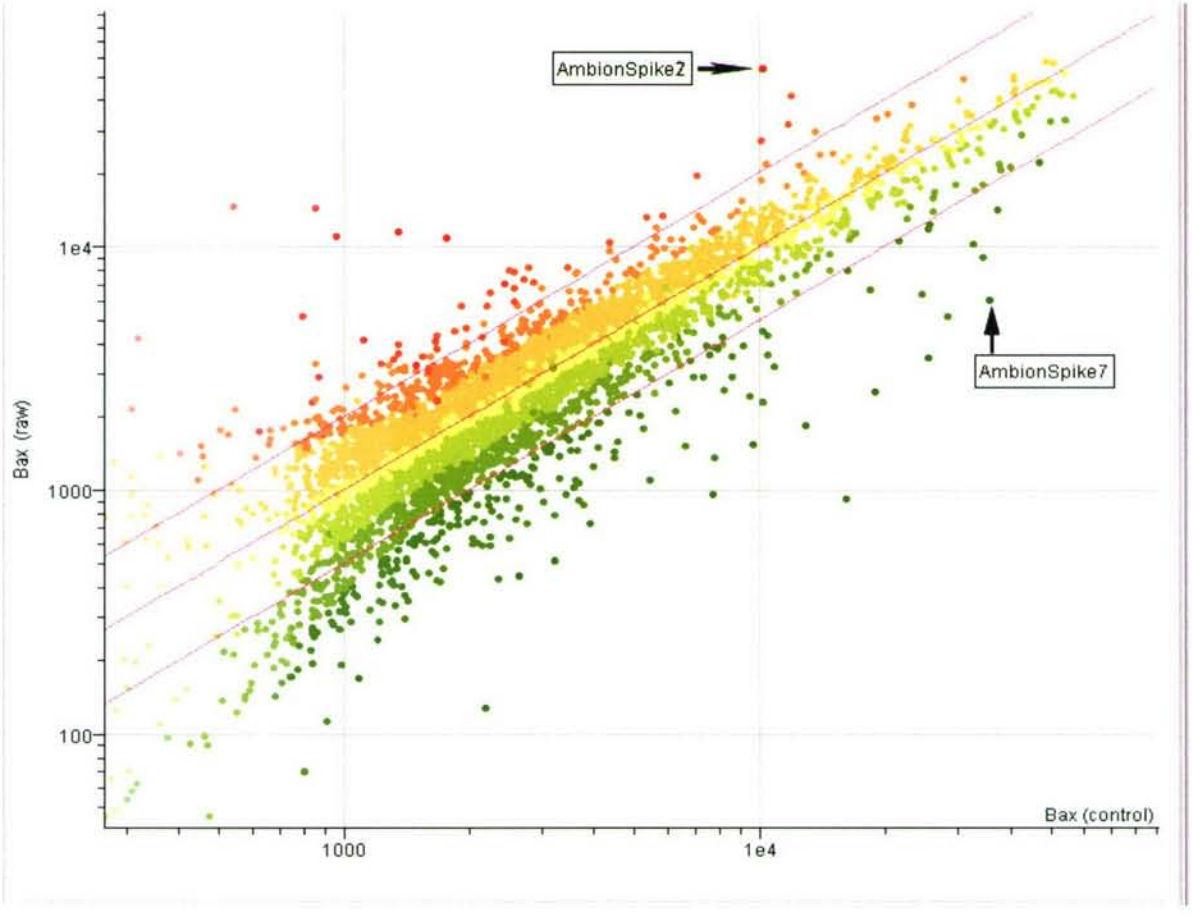

Figure 3. A scatter plot of 11 microarray experiments combined for analysis. The Ambion Spike in controls 2 and 7 are highlighted. Note that they flank the expression data and give approximately the correct expression ratios (10 and 0.1 respectively).

Table 2. The input ratios of the Ambion RNA spikes in the experiment and control samples

	Ambion spike 1	Ambion spike 2	Ambion spike 3	Ambion spike 4	Ambion spike 5	Ambion spike 6	Ambion spike 7	Ambion spike 8
Cy3 channel	2.5	5	0.125	5	0.25	5	1	1
Cy5 channel	2.5	0.5	0.25	1	10	2	10	1
Ratio (Cy3/Cy5)	1	10	0.5	5	0.25	2.5	0.1	1

Figure 4. Comparison of RNA quality obtained from frozen (upper panel) and paraffin embedded (lower panel) tissue. Note the 16S and 28S ribosomal bands present in the frozen tissue RNA. Paraffin tissue RNA yields primarily fragments of only about 100 to 200 bp.

RNA Isolated from Frozen Tissue

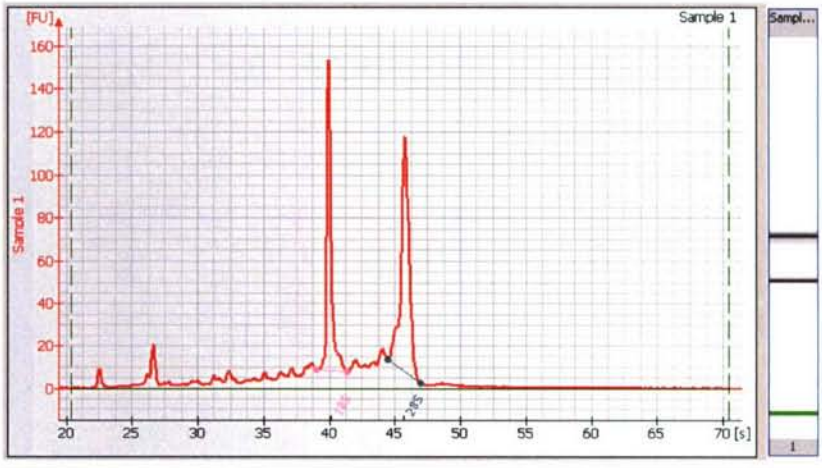

RNA Isolated from Paraffin Embedded Tissue

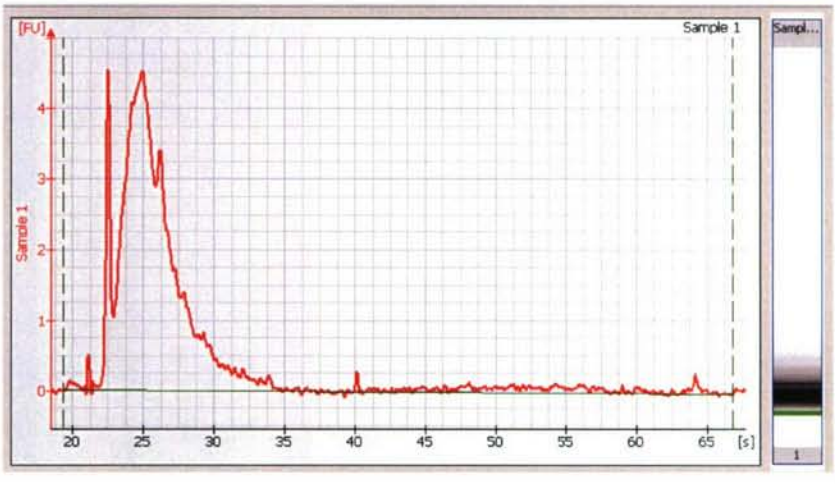

Figure 5. Realtime PCR expression profiling of RNA isolated from paraffin embedded tissue. Expression results from paraffin RNA that are comparable to results obtained from frozen tissue were obtained. For high quality results, it is important to use random priming for cDNA synthesis and that realtime PCR reactions be designed to amplify fragments of less than 200 bp.

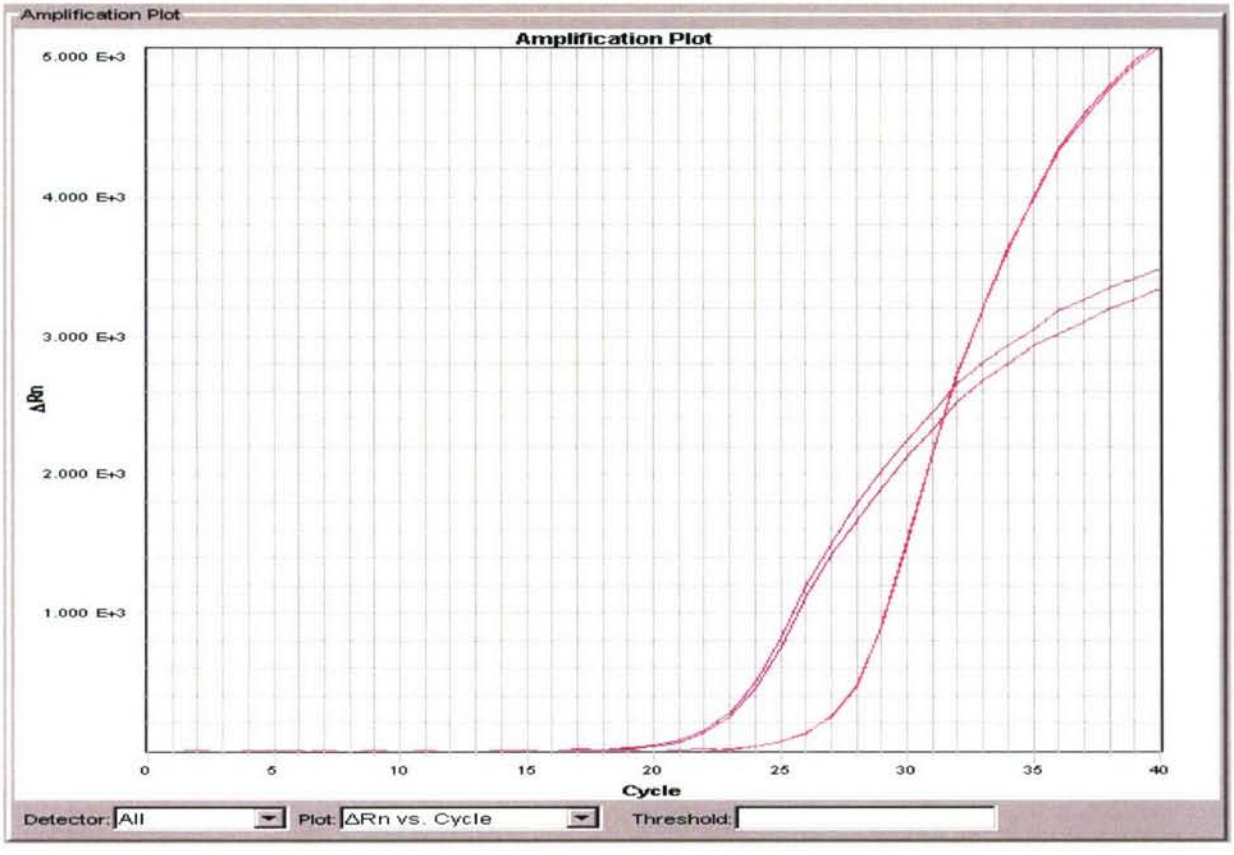

Project 12: Vector Support Service

Introduction

Several sub-projects of this grant involve investigations of gene function and gene therapy. Investigators working on these sub-projects need to use gene transfer technology in their research. Gene transfer uses vectors carrying the gene-of-interest and delivers them to the target cells. Development and design of appropriate vectors require technical expertise. It would be highly efficient and cost-effective to have a centralized Support Service facility within the Musculoskeletal Disease Center to serve these investigators by providing service in vector design and production, education and training, and technical advice in gene transfer technology. Accordingly, the Vector Support Service Facility serves as a dynamic resource for Investigators working on projects funded by the Army. As a result, the emphases of this Support Service focus on development and production of viral vectors, especially retroviral vectors that are based on Moloney murine leukemia virus (MLV) and human immunodeficiency virus (HIV), and non-viral plasmid vectors for gene transfer and to provide training and assistance to investigators with respect to vector development and production.

Body

1. Technical Objectives

There were three specific objectives for this subproject:

1. To serve as a dynamic resource to construct and provide vectors for delivery and expression of appropriate genes for Investigators supported by the Army grant.
2. To serve as an educational resource, providing technical assistance and training to Investigators in the use of viral and non-viral vector gene delivery and gene expression.
3. To improve and expand vector systems available to Investigators as gene transfer technologies advance.

2. Progress on Technical Objectives

Specific Objective 1: To assist investigators in the design of and to provide with appropriate research-grade viral or plasmid vectors.

In the previous review of the Vector Support Service Facility, the reviewers were concerned about the variability of transduction efficiencies between different lots of virus preparations. The reviewers recommended that an additional examination into ways of eliminating viral titer variability and quality could be conducted to increase virus quality. To address these concerns, the viral core started to develop methods to determine the titers of the viral vectors without marker genes. The experiments are in progress. Additionally, we started to pool several lots of viral production together before releasing them to the end users. This practice may eliminate the possible variation caused by batch differences.

During the past twelve months, the Vector Support Service produced numerous VSV-G pseudotyped MLV vectors and HIV-based vectors for various investigators working on projects supported by the Army. Specifically: 1) in collaboration with Dr. Charles Rundle (sub-project 4), the facility generated numerous batches of concentrated VSV-G pseudotyped MLV vectors expressing different growth factor or control genes that have been used successfully in animal experiments. These growth factor or control genes included β–galactosidase (β-gal), enhances green fluorescent protein (EGFP), basic fibroblast growth factors (FGF-2) and its derivatives, bone morphogenetic protein-4 and its derivatives (BMP-4), growth hormone (GH), and

cyclooxygenase (Cox-2). Additionally, we prepared two batched of VSV-G pseudotyped HIV-based vectors with either BMP-4 gene or β-gal gene for Dr. Rundle. He used these vectors to compare the efficacy between MLV-based and HIV-based vectors in his studies. 2) In support of the sub-project 6, the facility generated eleven different batches of HIV-based vectors for use in the study of systemic gene therapy of musculoskeletal diseases. These HIV-based vectors included those expressing β-gal, EGFP, BMP2/4 and GH genes. To ensure the safety of these HIV-based vectors, each HIV-based vector was harvested and concentrated, tested for potential contamination of recombination competent retrovirus (RCR) within the preparation. None of these HIV-based vector preparations have shown RCR contamination in our assay system. The results have been submitted to and approved by the Biosafety committee and Animal care and use committee at the Jerry L. Pettis VAMC. 3) In collaboration with Dr. Reinhard Gysin (sub-project 7), the facility produced four different batches of concentrated MLV-based vectors, expressing β–gal, BMP2/4, and Cox-2 genes, respectively. These viral vectors were used in Dr. Gysin's experiments testing potential synergistic interaction between BMP2/4 and Cox-2 in promoting bone formation in the critical sized calvarial bone defect model. 4) In collaboration with Dr. Donna Strong (sub-project 8), the facility produced three different batches of concentrated VSV-G pseudotyped MLV vectors, expressing β–gal, LMP-HA, and IGFBP6 genes with or without secretion signal, for animal experiments.

Specific objective 2: To provide education, tutorials, practical training, technical assistance, and protocols to Investigators for the experimental use of gene transfer vector.

In the last review, the committee felt that the core director should update investigators in a more widely attended staff meeting regarding new technology and vectors that are available in the Vector Support Service Facility at least every 6 months. Although a yearly progress report is available to gene therapy investigators, investigators working on other Army projects would benefit by such a biannual presentation at staff meetings.

With respect to providing education and tutorials to investigators, Dr. Shin-tai Chen (the director of the Vector Support Service) gave three lectures to the Jerry L. Pettis VAMC Musculoskeletal Diseases Center during the past 12 months. These lectures were designed to educate and tutor Army project investigators in viral gene transfer technology. Two lectures addressed the safety issues concerning the use of viral vectors in gene therapy. One lecture discussed the current development of viral and non-viral vectors used for musculoskeletal disease gene therapy.

Specific Objective 3: To evaluate emerging technologies and develop improved viral and plasmid vectors, as appropriate, for more efficient and effective gene transfer.

a) Development of inducible MLV-based vectors for bone disease gene therapy.

Bone disease gene therapy depends on the expression of growth factors, which can stimulate bone formation, at target sites at the appropriate time. The expression of the growth factor should be turned off when it is no longer necessary. Accordingly, the ubiquitous and unregulated expression of growth factor genes could be a major safety concern. For example, overexpression of BMP2/4 or FGF-2, two potent growth factors for bone formation, could cause serious side effects if their expression is unregulated. Consequently, the Vector Support Service has initiated work on the development of regulatable MLV-based vectors using ligand-inducible promoter. Our initial effort focused on the tetracycline-regulated systems. There are two general types of tetracycline-regulatable systems: 1) TET-ON system in which the expression of the

transgene is enhanced by tetracycline or analogs; and 2) TET-OFF in which the transgene expression is inhibited by tetracyclines. Previously, our laboratory has developed a modified TET-OFF system in MLV-based vector. In this system, a ligand-binding domain of the estrogen receptor was fused to the carboxy terminus of tetracycline activated transcriptional activation (tTA) domain. This modified tetracycline-regulated system was referred to as tTAER. In the tTAER system, the toxicity of the VP16, transacting domain of the tTA, is modulated by the estrogen receptor ligand. The system relies on the removal of tetracycline (TET-OFF) to stimulate the gene expression. This type of tet-off system is difficult to apply to an *in vivo* model since it is very difficult to remove all the tetracycline in short time. Therefore, a system using tetracycline as inducer (TET-ON) will be more appropriated for our applications. In this quarter, we constructed vectors with tet-on regulation system.

In 1995, Gossen et al. reported on the first TET-ON inducible system, rtTA. The gene contains four amino acid exchanges from the parental TET-OFF gene, tTA. The rtTA gene exhibits a reverse phenotype, namely it can turn on the gene expression in the present of ligand (TET-ON). For a kinetic reason, the TET-ON system is often preferable over the TET-OFF system. However, the rtTA system also comes with its own problems. First, it requires very high concentration of ligand (1-2 μg/ml of doxycycline) and this is very difficult to achieve *in vivo*. Second, it exhibits some residual affinity to tetO promoter in absence of ligand, which is recognized as high intrinsic background activity. Therefore, the rtTA system is leaky. Third, the rtTA still contains the VP16 as the transcription activator. In many occasions, it is impossible to generate mouse lines that would produce sufficient amount of rtTA in certain cell types. This may be due to the reduced stability of rtTA and toxicity of VP16. To overcome these problems, in 2000, Urlinger et al. reported a second generation of TET-ON system, rtTA-S2. In this system, the VP16 was replaced with 3 copies of F domain (F domain contains 12 amino acids domain from VP16). In addition, the new system contains four new amino acid exchanged from tTA. Interestingly, there were no overlap in amino acid changes between rtTA and rtTA-S2. The rtTA-S2 is significantly improved from rtTA. It is not as toxic as rtTA and it is not as leaky as the rtTA. Furthermore, in 2004, Das et al. improved the rtTA-S2 by additional amino acid changes. They found three additional mutations at amino acid position 12 (serine to glycine), 84 (phenylalanine to tyrosine) and 209 (alanine to threonine) would further improve the ligand sensitivity and promoter activity of new rtTA-S2. They named the new tet-on system as rtTA-YT (for two mutations at F86Y and A209T from rtTA-S2) and rtTA-GYT (for three mutations at S12G, F86Y and A209T from rtTA-S2). In collaboration with Dr. Das in the University of Amsterdam, we obtained these two doxycycline induced transcriptional factors within this year.

To prepare the TET-ON MLV-based vectors, we used PCR techniques to generate the rtTA-GYT, transcriptional factor genes and subcloned into our pY-based vector (MLV with MFG-like backbone and CMV promoter in the 5' end). Furthermore, we put the reporter gene (EGFP) under the control the tetracycline promoter (tetO) in the same vectors. The diagrams of these vectors are shown in figure 1.

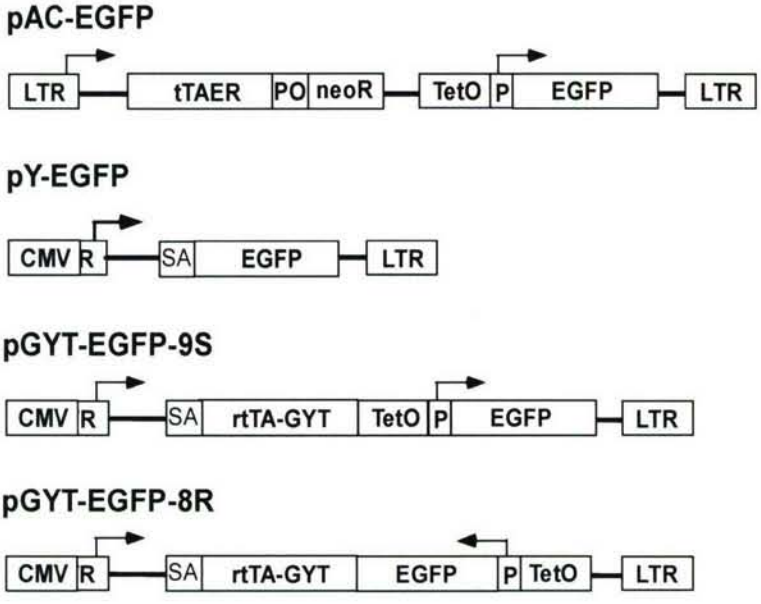

Figure 1. Schematic illustration of TET-OFF and TET-ON MLV-based vectors. The pAC-EGFP is our original TET-OFF system and the pGYT-EGFP is the new TET-ON system. The arrows indicate the direction of the transcription. The only difference between 9S and 8R is the direction of the tetracycline controlled expression unit.

After the construction of the vectors, we generated VSV-G pseudotyped MLV-based vectors by transient transfection in 293T cells. We tittered all the viral vectors in HT1080 cells either in the induction media (+β-est for pAC-EGFP or +Dox for pGYT-EGFP vectors) or suppression medium. Forty-eight hours after transduction, the cells were detached and the fluorescent activities were monitored by FACS techniques. The results were summarized in the Table 1.

Viral Vectors	Types of Media	Viral Titer	Mean Intensity	Fold Induction*
pY-EGFP	Regular	3.3×10^6	282.1	1.0
	+β-est	4.5×10^6	323.1	1.6
	+Doxy	6.2×10^6	340.1	2.3
pAC-EGFP	Regular	5.7×10^4	50.4	1.0
	+β-est	5.3×10^4	103.7	**1.9**
	+Doxy	8.1×10^4	53.6	1.5
pGYT-EGFP-9S	Regular	3.0×10^5	53.2	1.0
	+β-est	7.2×10^5	64.8	2.9
	+Doxy	1.0×10^6	639.4	**39.1**
pGYT-EGFP-8R	Regular	2.7×10^5	28.1	1.0
	+β-est	3.1×10^5	29.2	1.2
	+Doxy	9.7×10^5	138.5	**17.4**

Table 1: Ten μl of viral stocks was used to transduce 2E5 cells of HT1080 in 6-well plates. Forty-eight hr after transduction, the cells were detached and the percentage of GFP positive cells and

the intensity of GFP were determined by flow cytometer. Fold induction is calculated by comparing the value of mean intensity multiple by the percentage of the positive cells. We arbitrarily selected the value from regular medium as 1.

From these results we concluded the new TET-ON system is superior to our original TET-OFF system. First, the viral titer of pGYT-EGFP is higher than pAC-EGFP (compares 1.0 x 10^6 *vs.* 8.1 x 10^4). This may due to the CMV promoter which drives the expression of the genomic RNA of pGYT-EGFP. Second, the expression of pGYT-EGFP is more robust than the pAC-EGFP. Under suppressed condition, pAC-EGFP and pGYT-EGFP9S have the similar back ground, however, under the induced condition, the main intensity of pGYT-EGFP-9S is six times as high (639 *vs.* 103). Furthermore, the pGYT-EGFP-9S expression is even stronger than the pY-EGFP expression (340 *vs.* 639). This is very unusual since the viral promoter of MLV-LTR is very strong. For pGYT-EGFP-8R, we found the viral titer is similar to pGYT-EGFP-9S, but the level of the GFP expression is much less (639 *vs.* 138). Nevertheless, the background GFP expression (under the suppressed condition) is also less when compared with pGYT-EGFP-9S (53 *vs.* 28).

To further demonstrate the function of rtTA-GYT, we transduced the vectors to three different cell lines, 293T, rat marrow stromal cells, and rat skin fibroblast. We measured the expression of marker gene (EGFP) expression under suppressed condition (regular medium) or inducible condition (regular medium plus 1μg/ml of doxycycline). The results are summarized in **Table 2** (below).

	Types of Media	Mean Intensity	Fold Induction*
In 293T cells			
pY-EGFP	Regular	43.1	1.0
	+Doxy	45.6	1.2
pGYT-EGFP-9S	Regular	41.2	1.0
	+Doxy	428.2	**14.9**
pGYT-EGFP-8R	Regular	21.7	1.0
	+Doxy	121.4	**14.1**
In Rat marrow stromal cells			
pY-EGFP	Regular	237.9	1.0
	+Doxy	240.5	1.1
pGYT-EGFP-9S	Regular	66.82	1.0
	+Doxy	1371.7	**20.3**
pGYT-EGFP-8R	Regular	25.7	1.0
	+Doxy	127.2	**26.5**
In Rat skin fibroblasts			
pY-EGFP	Regular	283.9	1.0
	+Doxy	281.6	1.1
pGYT-EGFP-9S	Regular	70.6	1.0
	+Doxy	1532.6	**31.3**
pGYT-EGFP-8R	Regular	47.4	1.0
	+Doxy	179.6	**26.5**

The results shown in Table 2 are consistent with results in Table 1. We can observe a 14-31 fold induction in these cell lines under the inducible condition (1μg/ml of doxycycline). The level of GFP expression of pGYT-EGFP is consistently stronger than that observed in the pY-EGFP vector. The results indicate that the promoter activity of tetO under inducible condition is stronger than MLV-LTR promoter. Based on these data, we chose the new TET-ON system (pGYT-EGFP) as our inducible system and introduced the growth factor genes in this vector.

Previously, we have shown the human bFGF gene can be expressed and secreted by adding a BMP2/4 secretion peptide at the 5'end and replacing the second and third cysteines of bFGF with serine and asparagines, respectively. Using this gene, we demonstrated the FGF can significantly increase the proliferation of the implanted cells *in vivo*. In addition, we also demonstrated mice Sca1 positive cells transduced with bFGF can increase mass amount of bone formation in the marrow cavity after transplanted into a recipient mouse. These data all suggest that bFGF can be a good candidate gene for bone gene therapy. However, the uncontrollable FGF express may also have adverse effects. For example, transplantation of FGFG transduced hematopoietic stem cells (Sca1+ cells) may reduce the marrow space for blood cells and subsequently may have a detrimental effect on the hematopoietic system. We may solve this problem by a controllable expression of FGF. Toward this goal, we constructed a doxycycline inducible FGF vector based on our construct, pGYT-EGFP. The diagram of this vector is shown in figure 2.

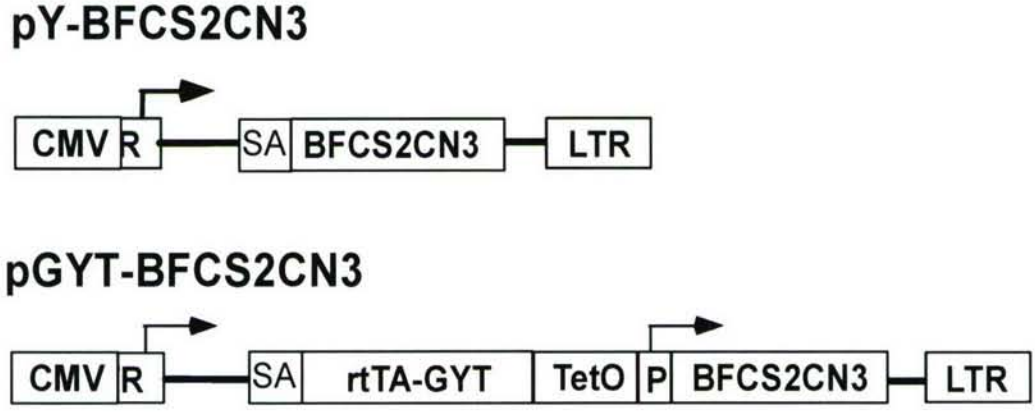

Figure 2. Schematic illustration of tet-on MLV-based vectors. The pY-BFCS2CN3 is our original FGF vector. The expression of the FGF is originated from MLV-LTR promoter after transduction. The pGYT-BFCS2CN3 is the new inducible MLV-based vector. The expression of the FGF gene is from the TetO promoter and it is controlled by doxycycline. The arrows indicate the direction of the transcription.

After the construction of the vectors, we picked two clones of the pGYT-BFCS2CN3 and named them pGYT-BFCS2CN3-18S and pGYT-BFCS2CN3-22S. Based on these two clones, we generated VSV-G pseudotyped MLV-based vectors by transient transfection in 293T cells. We transduced HT1080 cells either in the induction media (+Dox for pGYT-BFCS2CN3 vectors) or suppression medium (regular medium without doxycycline). Forty-eight hours after transduction, the supernatants were harvested. The amount of FGF in the conditional media was determined by ELISA. The results were summarized in the Table 3.

Table 3.

	pY-BFCS2CN3	pGYT-BFCS2CN3-18S	pGYT-BFCS2CN3-22S
Doxycycline (1μg/ml)	**40**	**68**	**84**
Regular	**48**	**2.0**	**4.2**
Fold Induction	**0.8**	**34**	**20**

One hundred μl of viral stocks were used to transduce the duplicated set of HT10080 cells in a 6 well plate containing 2E5 cells per well. After transduction, 1 μg/ml of Doxycycline was added to one set of the wells. Forty-eight hours after transduction, the supernatants were harvested. The amount of FGF in the conditional media was determined by ELISA and presented as ng/ml.

The results shown in Table 3 are consistent with our previous results in marker gene expression. We can observe 20 and 34 fold induction in FGF expression under the inducible condition (1μg/ml of doxycycline) in HT1080. The level of FGF expression of pGYT-BFCS2CN3 is consistently higher than the pY-BFCS2CN3 vector. This result is inline with the marker gene expression in pGYT-EGFP. We conclude that the promoter activity of tetO under inducible conditions is stronger than MLV-LTR promoter in HT1080 cells. Currently, we are studying the inducible gene expression *in vivo*. These studies are in progress.

b) Develop inducible HIV based vectors for expression of therapeutic genes for bone formation and bone repair.

Although, MLV-based vectors have been shown to transduce different cells with high efficiency, it can not transduce non-dividing cell neither to the true hematopoietic stem cell. This shortfall can be overcome by HIV-based vectors. Therefore, an inducible expression of HIV-based vectors would be very important for gene therapy of bone diseases. Based on the construction of inducible-MLV-based vectors, we also constructed several inducible HIV-based vectors. Within this year we incorporated TET-ON systems into our HIV-based vectors. The diagrams of these HIV-based vectors are shown in Figure 3.

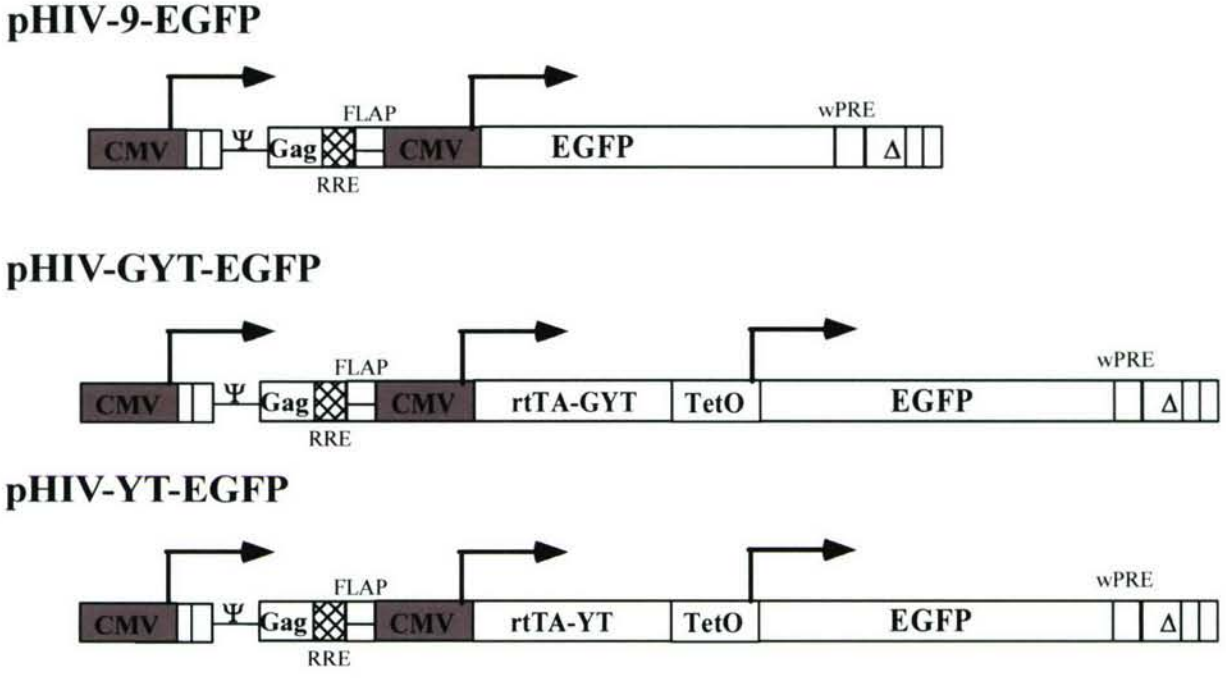

Figure 3. The diagram shows the two inducible HIV-based vectors and they are derived from the pHIV-9-EGFP vector. The EGFP expression is from CMV promote in pHIV-9-EGFP and from TetO promoter in pHIV-GYT-EGFP and pHIV-YT-EGFP.

After the construction of the vectors, we generated VSV-G pseudotyped HIV-based vectors by transient transfection in 293T cells. We tittered all the viral vectors in HT1080 cells either in the induction media (+Dox) or suppression medium (regular medium without doxycycline). Forty-eight hours after transduction, the cells were detached and the fluorescent activities were monitored by FACS techniques. The results were summarized in the Table 4.

Table 4

Viral Vectors	Types of Media	Viral Titer	Mean Intensity	Fold Induction*
pHIV-9-EGFP	Regular	1.01×10^6	998.1	
	+Doxy	1.36×10^6	1044.1	1.41
pHIV-GYT-EGFP	Regular	1.58×10^5	198.1	
	+Doxy	1.64×10^5	506.6	2.65
pHIV-YT-EGFP	Regular	6.80×10^4	207.4	
	+Doxy	1.24×10^5	403.4	3.55

*Fold induction is calculated by comparing the value of mean intensity multiple by the percentage of the positive cells. We arbitrarily selected the value from regular medium as 1.

From these results, we found the viral titer is significantly lower in constructs with the inducible-system (1.36×10^6 vs. 1.64×10^5 and 1.24×10^5). This may be due to the capacity of the foreign gene we have introduced into the HIV-based vectors. We also found the level of EGFP from the CMV promoter is stronger than the inducible promoter (1044.1 vs. 506.6 and

403.4). In addition, the levels of induction (shown as fold induction in table 3) are not as high as those we observed in inducible-MLV-based vectors. Currently, we are investigating the discrepancy of inducible-MLV-based and HIV-based vectors. Before we can find a method to increase the titer or reduce the background, we are not able to apply these vectors *in vivo*.

Key Research Accomplishments

1) Prepared MLV and HIV-based vectors for other sub-projects (sub-projects 4, 6. 7 and 8)
2) Developed TET-ON inducible-retroviral vectors for bone diseases gene therapy

Reportable Outcomes

Publication:

Patents submitted:

1. S. Mohan, K. Lau, S-T Chen, S. Hall and D. Baylink: Systemic and local ex vivo gene therapy of the skeleton with hematopoietic stem cells expressing FGF-2 genes (2005) provisional patent submitted.
2. S. Mohan, K. Lau, C. Rundle, D. Strong, T. Linkhart, S-T Chen and D. Baylink: Molecular and methods (modified Cox-2 alone or with LMP-1, BMP4, FGF2) in gene therapy for skeletal repair using MLV or other viral and plasmid vectors (2005) provisional patent submitted.

Conclusions

1) In collaboration with investigators of other sub-projects of this Army grant, we have generated and provided with the investigators several different batches of MLV and HIV-based vectors for use in their approved projects.

2) We developed an inducible-TET-ON regulatory retroviral vector system. The gene expression of this vector can be modulated by doxycycline. This vector system is essential for skeletal gene therapy and for studying the function of growth factor genes during bone repair.

Appendices

Project One -

Chadwick R.B., Bu L.M., Yu H., Hu Y., Sachdev R., Tan Q.W., Wergedal J.E., Mohan S., and Baylink D.J. Digit Tip Regeneration and Differential Expression Profiling in the MRL Super-Healer Mouse. Wound Healing and Regeneration, Chicago, Illinois, May 2005.

Chadwick R.B., Bu L.M., Yu H., Sachdev R., Tan Q.W., Wergedal J.E., Mohan S., and Baylink D.J. Digit Tip Regeneration and Global Gene Expression Profiling in the MRL Super-Healer Mouse. 26th Annual Meeting American Society of Bone and Mineral Research, Seattle, Washington, October 1-5, 2004

Project 3 -

Xing W., Baylink D.J., Kesavan C., and Mohan S. Transfer of 128-kb BMP-2 Genomic Locus by HSV-Based Infectious BAC Stimulates Osteoblast Differentiation: A Platform for Functional Genomic Studies. ASBMR-2004, 19 suppl 1: S150, 2004

Xing W., Baylink D.J., Kesavan C., and Mohan S. HSV-1 Amplicon-Mediated Transfer of 128 kb BMP-2 Genomic Locus Stimulates Osteoblast Differentiation in vitro. Biochem Biophys Res Commun 319(3): 781-6, 2004

Project 4 -

Xing W., Baylink D.J., Kesavan C., Chadwick R.B., Hu Y. and Mohan S. Global Gene Expression Analysis in the Bones Reveals Involvement of Several Novel Genes and Pathways in Mediating an Anabolic Response of Mechanical Strain in Mice. J Cell Biochem (Submitted), 2005

Rundle C.H., Wang H., Yu H., Chadwick R.B., Tesfai J., Lau K-H.W., Mohan S., Ryaby J.T., and Baylink D.J. Microarray analysis of fracture repair identifies the homeodomain transcription factor Prx-2 and other genes that imply similarities between bone repair and scarless fetal tissue healing. Transactions to the 51st Annual meeting of Orthopaed Res Soc abstract # 361, 2005

Rundle C.H., Wang X., Wergedal J.E., Srivastava A.K., Davis E.I., Lau K-H.W., Mohan S., and Baylink D.J. Loss of sex-specific differences in bone size in leptin-deficient (ob/ob) mice. Transactions to the 52nd Annual meeting of Orthopaed Res Soc (in press), 2006

Rundle C.H., Wang H., Yu H., Chadwick R.B., Davis E.I., Wergedal J.E., Lau K-H.W., Mohan S., Ryaby J.T., and Baylink D.J. Microarray analysis of gene expression during the inflammation and endochondral bone formation stages of rat femur fracture repair. Bone, in Press, 2005

Wang X., Rundle C.H., Srivastava A., Tesfai J., Davis E.I., Wergedal J.E., Lau K.H-W., Mohan S. and Baylink D.J. Loss of sex-specific difference in bone size in leptin knockout mice. 27th Annual Meeting of the American Society for Bone and Mineral Research, Nashville, TN, 2005

DIGIT TIP REGENERATION AND GLOBAL GENE EXPRESSION PROFILING IN THE MRL SUPER-HEALER MOUSE

R. B. Chadwick, L. M. Bu, H. Yu, Y. Hu, R. Sachdev, Q. W. Tan,
J. E. Wergedal, S. Mohan, D. J. Baylink.
Musculoskeletal Disease Center, Loma Linda, CA, USA.

The MRL mouse is the only known strain of mouse that can regenerate cardiac lesions and completely heal ear punches without scarring. To determine if the MRL also has greater regeneration capabilities in amputated digit tips, right paw digit tips of neonatal mice were dissected, with the left front paws as uncut controls. Controls used for regeneration comparison were the DBA, B6, C3H and 129 inbred mouse strains. Consecutive x-ray images were captured of the left and right paws at 0, 7, 14, 21 and 28 days post amputation. MRL mouse digit tips regenerated greater in comparison to all strains tested ($p<0.05$). We next undertook whole genome microarray analysis to identify the genetic mechanisms that contribute to differences in digit tip regeneration. Over 400 genes out of 15,000 were significantly differentially expressed ($p < 0.05$) in MRL and DBA mice at day 4 in comparison to day 0 control tissue. Of these, 170 genes were upregulated and 280 were downregulated in both mouse strains. Pathway analysis reveals that genes in the BMP/TGF pathway are differentially expressed in both mouse strains ($p < 0.05$). Multiple differences between MRL and DBA strains were found in transcription factors that are implicated in gastrulation, including FMN2 and SHRM. Additional differentially expressed genes include NET1 in the WNT signaling pathway. Immunohistochemistry indicates that these proteins are highly expressed in the nuclei of chondrocytes in regenerating digits. We conclude that MRL mice show greater regenerative capacity to heal digit tips and that the increased regenerative capacity of MRL mice may be due to strain specific increased expression of genes involved in the WNT pathway and genes involved in embryonic pattern formation.
Acknowledgments: This work was supported by Assistance Award DAMD17-03-2-0021 and is administered by the US Army Medical Research Activity, 820 Chandler St., Ft. Detrick, MD.

Digit Tip Regeneration and Global Gene Expression Profiling in the MRL Super-Healer Mouse

Robert B. Chadwick, Liming Bu, Hongrun Yu, Yan Hu, Ravneesh Sachdev, Qianwei Tan,
Jon E. Wergedal, Subburuman Mohan, and David J. Baylink.
Molecular Genetics Division, Musculoskeletal Disease Center, Loma Linda, CA.

Abstract: The MRL mouse is the only known strain of mouse that shows complete healing of an ear punch without scarring. Additionally, the MRL mouse can regenerate cardiac lesions. The present study sought to test the hypothesis that the MRL mouse also shows superior regeneration properties in the digit tip amputation model. The control mouse was the DBA mouse that exhibited only moderate healing in ear-punch experiments. Immediately after birth, right paw digit tips of neonatal mice were dissected, with the left front paws as uncut controls. The amount of tissue amputated was measured and consecutive x-ray images were captured of the left and right paws at 7, 14, 21 and 28 days post amputation. Additionally, at four days post dissection, total RNA from the MRL and DBA regenerating digit tips was isolated. Microarray expression profiling was undertaken of this RNA in comparison to RNA from control tissue collected at the time of surgery. At 14 days post amputation both mouse strains were found to regenerate, however the regeneration rate of the MRL digit tips was greater in comparison to the DBA strain ($p=0.016$). Over 500 genes out of 15,000 on the microarray were significantly differentially expressed ($p < 0.05$) in MRL and DBA mice at day four in comparison to control tissue at day zero. Of these, 170 genes were upregulated and 280 were downregulated in both mouse strains. About 50% of these genes represent ESTs and unknown genes. Pathway analysis reveals that genes in the BMP/TGF pathway are differentially expressed in both mouse strains (BMP-1, Actr2, Smad 4, TGFb1i4, Fstl3, Twsg1, TSC22), thus implicating the BMP/TGF signaling pathway in regulation of digit tip regeneration ($p < 0.05$). Multiple differences between MRL and DBA strains were found in transcription factors that are implicated in embryogenesis, including Mesp2 (involved in Notch signaling and somitogenesis, upregulated 2.8 fold), Net1 (highly expressed in neurons and involved in gastrulation, upregulated 1.7 fold), Bola-like transcription factor (upregulated 4.1 fold) and EST Mm. 270291 (DNA binding zinc-finger protein, upregulated 3.0 fold). We conclude that 1) MRL mice show greater regenerative capacity to heal digit tips compared to DBA mice; 2) The BMP/TGF signaling pathway is involved in digit tip regeneration; 3) Increased regenerative capacity of the MRL mouse may be due to strain specific increased expression of transcription factors that function in embryogenesis and development.

Transfer of 128-kb BMP-2 Genomic Locus by HSV-Based Infectious BAC Stimulates Osteoblast Differentiation: A Platform for Functional Genomic Studies

Weirong Xing, David Baylink, Chandrasekhar Kesavan and Subburaman Mohan
Musculoskeletal Disease Center
JL Pettis Memorial Veterans Administration Medical Center, Loma Linda, CA 92357

ABSTRACT

In previous studies, we developed mouse genetic models and discovered genetic components of quantitative trait loci (QTL) on mouse chromosomes that contribute to phenotypes such as bone size, bone density and fracture healing. However, these regions contain dozens of genes in several overlapping bacterial artificial chromosomes (BACs) and are difficult to clone by physical cloning strategies. A feasible and efficient approach of identifying candidate genes is to transfer the genomic loci in BAC clones into mammalian cells for functional studies. In this study, we retrofitted a BAC construct into herpes simplex virus-1 (HSV-1) amplicon and packaged it into an infectious BAC (iBAC) to test gene function in a cell-based system, using a 128-kb clone containing the complete bone morphogenetic protein-2 (BMP-2) as a model. We transduced MC3T3-E1 cells with the iBAC bearing BMP-2 and examined transgene expression and function. Our results have demonstrated that an iBAC can efficiently deliver a BMP-2 genomic locus into preosteoblast cells and express functional BMP-2 protein, inducing a phenotype of cell differentiation, as indicated by an increase in alkaline phosphatase activity (ALP). Therefore, this experimental system provides a rapid, efficient cell-based model of high-throughput phenotypic screening to identify the BAC clones from physically mapped regions that are important for osteoblast differentiation. It also illustrates the potential of iBAC technology in functional testing of single nucleotide polymorphisms (SNP) located in the distal promoter or/and intron regions responsible for low bone density.

INTRODUCTION

Osteoporosis is a common disease characterized by an age-dependent decrease in bone mineral density (BMD) and a microarchitectural deterioration of bone tissue. Although multiple environmental, nutritional and hormonal factors influence the development of osteoporosis, it is clear that the major determinant for the disease is under genetic control. Recently, genome-wide linkage analyses have revealed that the genetic components of quantitative trait locus (QTL) on human chromosomes 1q, 2p, 4p, 11q, and 13q are attributed to BMD. In order to localize chromosomal regions and subsequently identify the genes responsible for skeletal diseases, we have developed mouse genetic models and discovered QTLs on mouse chromosomes that contribute to phenotypes such as bone size and bone density. However, these regions contain dozens of genes and are still difficult to clone by time-consuming, expensive positional cloning strategies. A feasible and efficient approach for identifying candidate genes is to transfer the genomic loci of overlapping bacterial artificial chromosomes (BACs) encompassing the QTL regions into bone cells *in vitro* for a high throughput functional screening.

The delivery of large genomic DNA inserts of BACs into mammalian cells via chemical methods and non-viral vectors, although possible, renders a poor efficiency of gene

transfer. However, the recent advances in the gene therapy field in infectious BAC (iBAC) technology using the herpes simplex virus type 1 (HSV-1) amplicon have made it possible to deliver a genomic locus as large as 150-kb with a high transduction efficiency in most mammalian cells, including dividing and non-dividing cells *in vitro* and *in vivo*. The improved delivery system of the HSV-1 amplicon allows long-term retention and high level of position-independent expression of BAC transgenes. In this study, we chose a BAC clone bearing the bone morphogenetic protein-2 (BMP-2) locus and assembled the genomic DNA as an infectious virion as a model to test the genomic DNA transfer and function.

MATERIALS AND METHODS:

1. **Retrofitting HSV Amplicon into BMP-2 Genomic Locus**

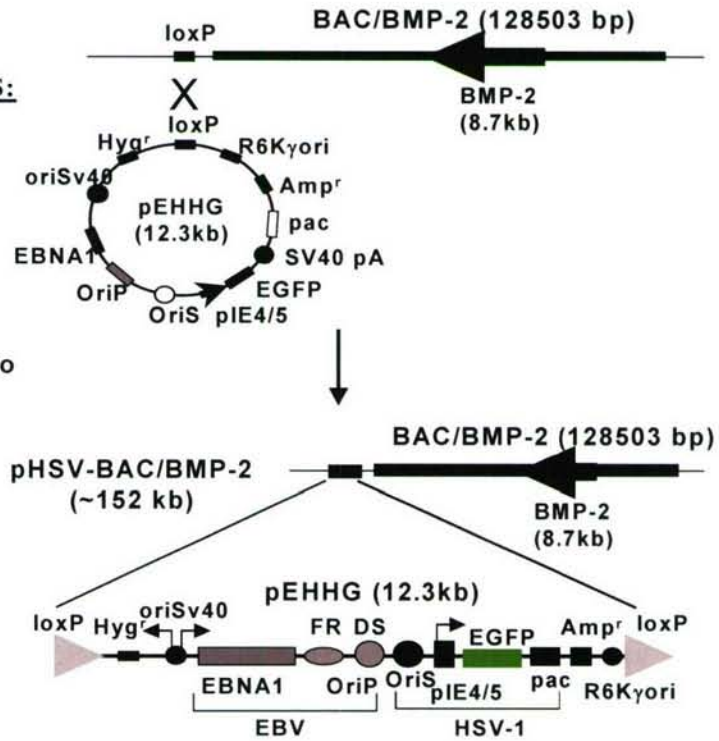

2. **Make Helper Virus-free HSV-1 Amplicon**

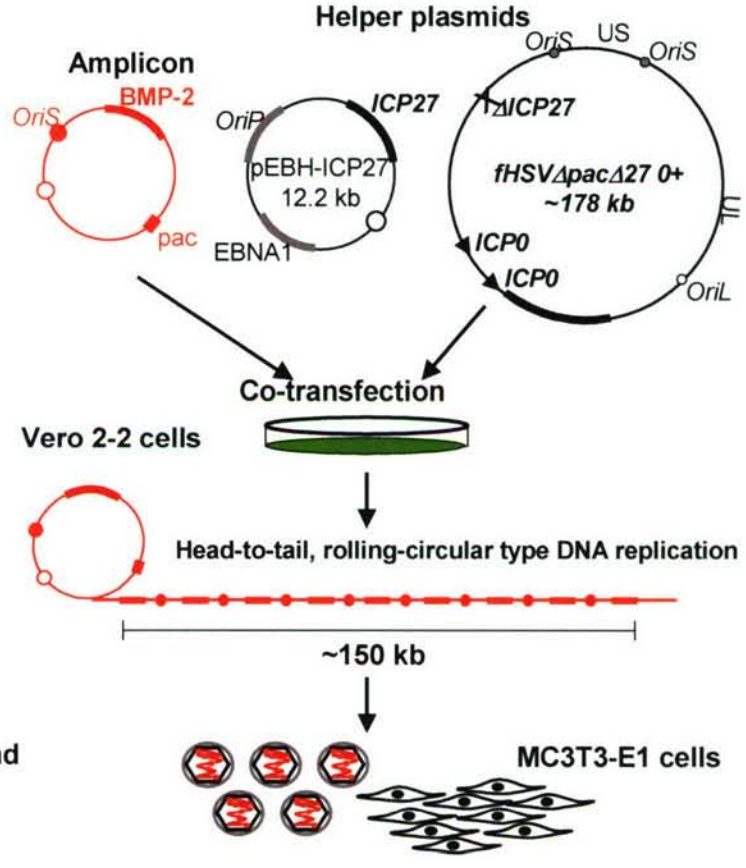

3. **Infect Osteoblast Cells and Examine Phenotypes**

RESULTS

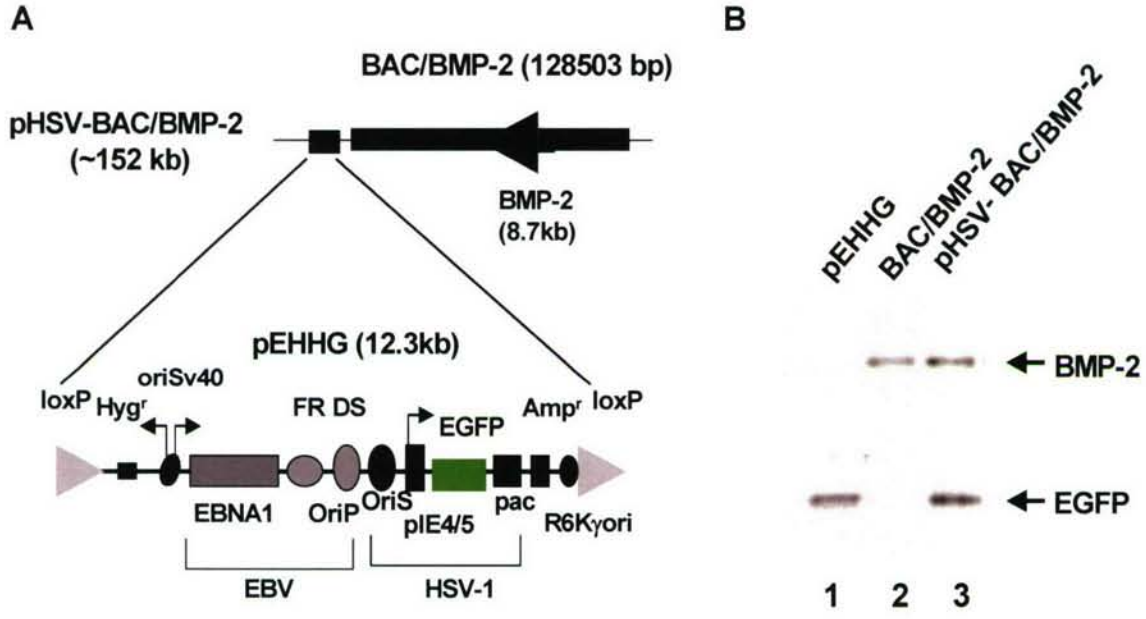

Figure 1. Schematic diagram of infectious HSV-1/BAC/BMP-2 construct. **A**: The retrofitted BAC contains both GFP reporter and BMP-2 genes **B**: Verification of pHSV-BAC/BMP-2 construct by polymerase chain reaction (PCR). Lane 1: pEHHG control; Lane 2: BAC/BMP-2 control; Lane 3: pHSV-BAC/BMP-2 containing both GFP and BMP-2 genes.

Interpretation: HSV amplicon was successfully retrofitted into BMP-2 genomic by homologous recombination in *E. Coli* to generate a BAC construct containing both BMP-2 intact gene and GFP reporter gene.

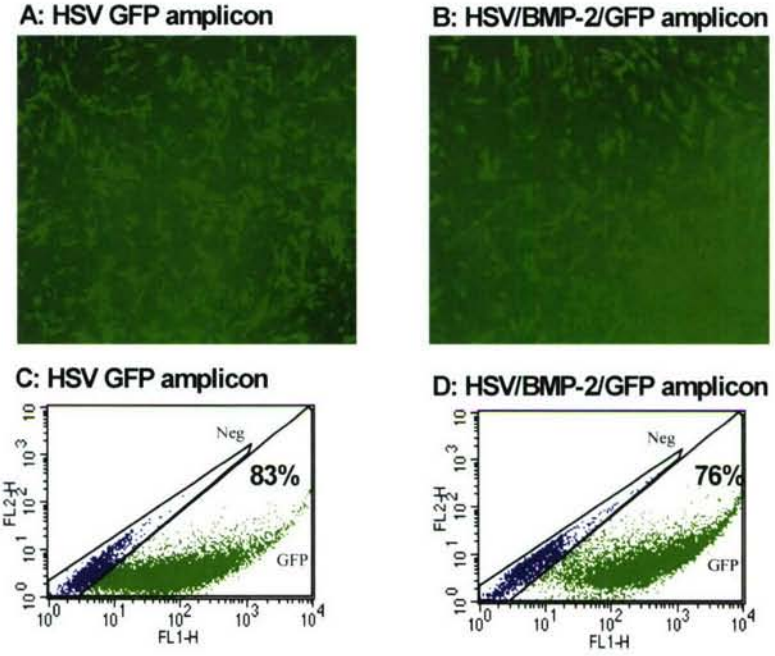

Figure 2. GFP reporter expression in MC3T3-E1 cells transduced with HSV-1 amplicon for 24 hours. **A**: cells transduced with infectious HSV-1 mock amplicon; **B**: cells transduced with infectious HSV-1 amplicon containing a BMP-2 locus; **C**: Flow cytometric analysis in cells infected with HSV-1 mock amplicon containing GFP only; **D**: Flow cytometric analysis in cells infected with HSV-1 amplicon containing GFP and a BMP-2 locus.

Interpretation: Infected MC3T3-E1 cells with HSV virion express GFP. The efficiency of transduction measured by flow cytometer was 83% and 76% in the cells transduced HSV mock virion and HSV virion containing BMP-2, respectively .

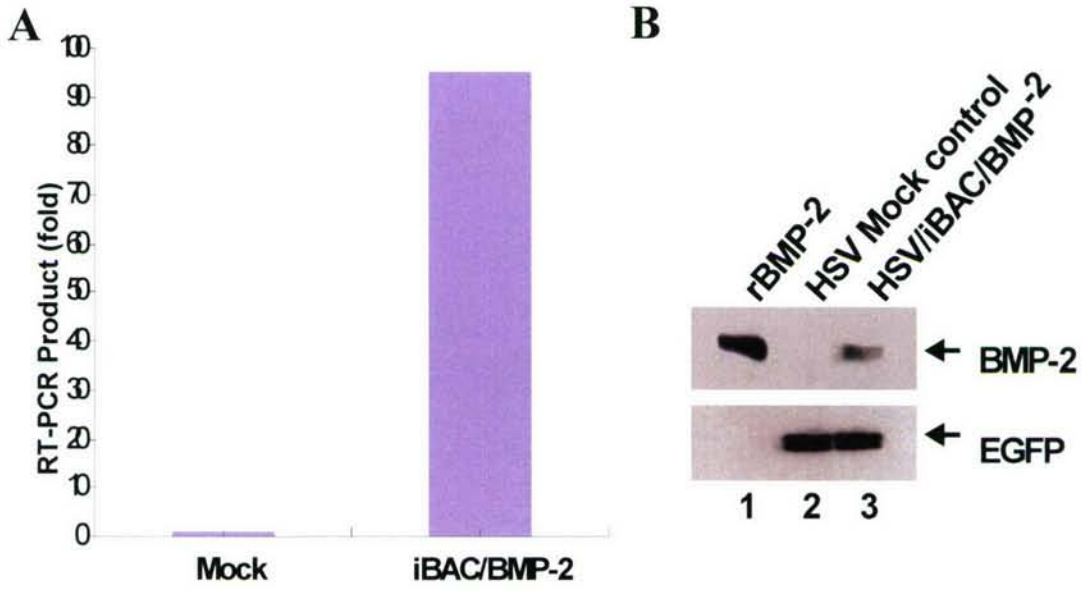

Figure 3. BMP-2 transgene expression in MC3T3-E1 cells. **A**: Real-time PCR data. **B**: Western blot analysis. Lane 1: positive control of recombinant BMP-2 (100 ng); Lane 2: the cells infected with HSV-1 mock amplicon containing GFP only; Lane 3: the cells infected with HSV-1 amplicon containing GFP and a BMP-2 locus.

Interpretation: The cells infected HSV amplicon containing BMP-2 genomic locus express more mRNA than the cells only containing GFP transgene alone (~ 99 fold induction). Western blot analysis detected full length BMP-2 protein.

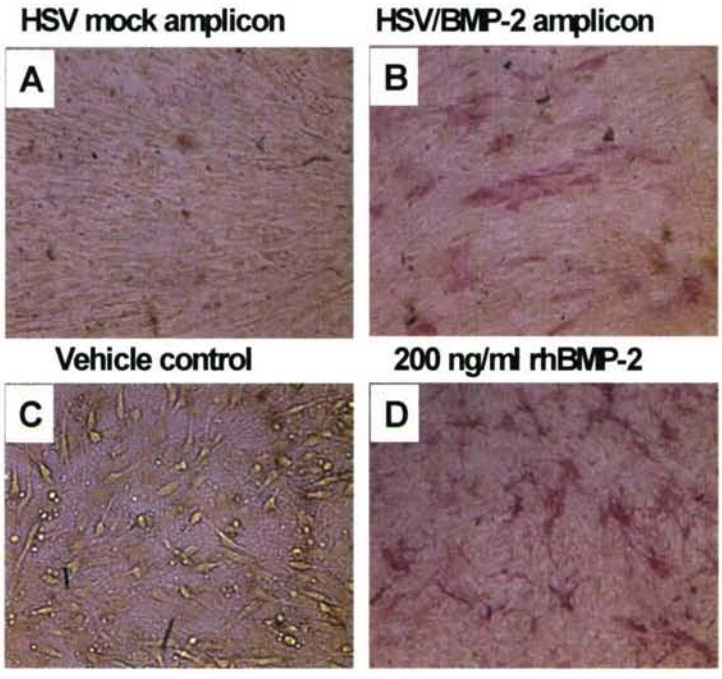

Figure 4: Alkaline phosphatase (ALP) staining of differentiated MC3T3-E1 cells (x 40 images). The cells are differentiated for 9 days and subjected for ALP staining. **A**: the cells infected with HSV-1 mock amplicon; **B**: the cells infected with HSV-1 amplicon containing a BMP-2 locus; **C**: The cells treated with vehicle; **D**: The cells treated with recombinant BMP-2 (200 ng/ml).

Interpretation: Approximately 20% of the osteoblast cells infected with HSV amplicon containing BMP-2 locus were differentiated and exhibited positive ALP-staining. No ALP-positive cells were seen in the control cells infected with HSV mock amplicon or the cells treated with vehicle alone. The cells treated with 200 ng recombinant BMP-2 also induced differentiation in approximately 20% of cells.

CONCLUSIONS

1.We have successfully transferred 128-kb BMP-2 genomic locus into osteoblast cells with high efficiency by utilizing HSV amplicon system.

2.The transgene was retained in osteoblast cells as minichromosomes for a long period of time.

3.The transgene-infected cells expressed functional protein, and induced cell differentiation.

4.The BAC gene transfer provides a rapid and efficient approach for functional testing of candidate genes within the QTL region *in vitro*

ACKNOWLEDGMENTS

This work was supported by Assistance Award No. DAMD17-03-2-0021. The U.S. Army Medical Research Acquisition Activity, 820 Chandler Street, Fort Detrick MD 21702-5014, is the awarding and administering acquisition office. The information contained in this publication does not necessarily reflect the position or the policy of the Government, and no official endorsement should be inferred. All work was performed in facilities provided by the Department of Veterans Affairs.

We are grateful to Dr. Yoshinaga Saeki (the Massachusetts General Hospital, Harvard Medical School, MA) for providing HSV-1 amplicon system and his technical assistance, and Dr. Rozanne Sandri-Goldin (the University of California, Irvine, CA) for her generous gift of a Vero 2-2 cell line.

Available online at www.sciencedirect.com
SCIENCE DIRECT
ELSEVIER
Biochemical and Biophysical Research Communications 319 (2004) 781–786
BBRC
www.elsevier.com/locate/ybbrc

HSV-1 amplicon-mediated transfer of 128-kb BMP-2 genomic locus stimulates osteoblast differentiation in vitro ☆

Weirong Xing, David Baylink, Chandrasekhar Kesavan, and Subburaman Mohan*

Musculoskeletal Disease Center, JL Pettis Memorial Veterans Administration Medical Center, Loma Linda, CA 92357, USA

Received 5 May 2004
Available online 28 May 2004

Abstract

In previous studies, we developed mouse genetic models and discovered genetic components of quantitative trait loci on mouse chromosomes that contribute to phenotypes such as bone size, bone density, and fracture healing. However, these regions contain dozens of genes in several overlapping bacterial artificial chromosomes (BACs) and are difficult to clone by physical cloning strategies. A feasible and efficient approach of identifying candidate genes is to transfer the genomic loci in BAC clones into mammalian cells for functional studies. In this study, we retrofitted a BAC construct into herpes simplex virus-1 amplicon and packaged it into an infectious BAC (iBAC) to test gene function in a cell-based system, using a 128-kb clone containing the complete bone morphogenetic protein-2 (BMP-2) gene. We transduced MC3T3-E1 cells with the iBAC bearing BMP-2 gene and examined transgene expression and function. Our results have demonstrated that an iBAC can efficiently deliver a BMP-2 genomic locus into preosteoblast cells and express functional BMP-2 protein, inducing a phenotype of cell differentiation, as indicated by an increase in alkaline phosphatase activity. Therefore, this experimental system provides a rapid, efficient cell-based model of high-throughput phenotypic screening to identify the BAC clones from physically mapped regions that are important for osteoblast differentiation. It also illustrates the potential of iBAC technology in functional testing of single nucleotide polymorphisms located in the distal promoter or/and intron regions responsible for low bone density.

Keywords: Osteoblast; HSV-1 amplicon; BMP-2; BAC; Gene transfer; Osteogenesis

Osteoporosis is a common disease characterized by an age-dependent decrease in bone mineral density (BMD) and a microarchitectural deterioration of bone tissue with a consequent increase in the risk of developing fragility fractures of the hip, spine, and other skeletal sites [1]. Although multiple environmental, nutritional, and hormonal factors influence the development of osteoporosis, it is clear that the major determinant for the disease is genetic control of BMD, particularly the achievement of peak bone mass at maturity, bone size and structure, and the subsequent rate of bone turnover [2–5]. Recently, genome-wide linkage analyses have revealed that the genetic components of quantitative trait locus (QTL) on human chromosomes 1q, 2p, 4p, 11q, and 13q are attributed to BMD [6–8], while the loci on chromosomes 17q and 19p are responsible for bone size [9]. However, none of the QTLs reported have actually met criteria for genome-wide significance for linkage, and the results are inconsistent due to the great variation between study groups and populations, as well as the possible involvement of different pathways. To localize chromosomal regions and subsequently identify the genes responsible for skeletal diseases, we have developed mouse genetic models and discovered QTLs on mouse chromosomes that contribute to phenotypes such as bone size, bone density, and fracture healing [10–12]. Subsequent analyses of the

☆ *Abbreviations:* BAC, bacterial artificial chromosomes; iBAC, infectious BAC; PAC, P1 artificial chromosomes; HSV-1, herpes simplex virus-1; ALP, alkaline phosphatase; BMP-2, bone morphogenetic protein-2; QTL, quantitative trait loci; MOI, multiplicity of infection; FACS, fluorescence-activated cell sorter; GFP, green fluorescent protein; EBV, Epstein–Barr virus; PCR, polymerase chain reaction.

* Corresponding author. Fax: 1-909-796-1680.
E-mail address: Subburaman.Mohan@med.va.gov (S. Mohan).

0006-291X/$ - see front matter © 2004 Elsevier Inc. All rights reserved.
doi:10.1016/j.bbrc.2004.05.053

congenic mice further confirmed and narrowed the genes of interest to a 3–12.5 centimorgan (cM) region in mouse chromosome 1 [13,14]. However, these regions contain dozens of genes and are still difficult to clone by time-consuming, expensive position-cloning strategies. However, a feasible and efficient approach for identifying candidate genes is to transfer the genomic loci of overlapping bacterial artificial chromosomes (BACs) or P1 artificial chromosomes (PACs) encompassing the QTL regions into bone cells in vitro for a high-throughput functional screening.

The delivery of large genomic DNA inserts of BACs or PACs into mammalian cells via chemical methods and non-viral vectors, although possible, renders a poor efficiency of gene transfer and requires the drug-selection and identification of stably integrated transformants for functional testing [15–17]. However, the recent advances in infectious BAC (iBAC) technology using the herpes simplex virus type 1 (HSV-1) amplicon in the gene therapy field have made it possible to deliver a genomic locus as large as 150-kb with a high transduction efficiency in most mammalian cells, including dividing and non-dividing cells in vitro and in vivo [18–21]. The improved delivery system of the HSV-1 amplicon also contains an EBNA-1 episomal cassette from the Epstein–Barr virus, (EBV) allowing long-term retention and high level of position-independent expression of BAC transgenes as mini-chromosomes in the host cells [20,21]. Therefore, the iBAC offers a rapid and simple method of BAC DNA transfer for functional genomic studies. This system also allows us to test the functional significance of the large number of gene-associated single nucleotide polymorphisms (SNP) located in the regions of the distal promoter or/and introns that could contribute to low bone density [22,23]. In this study, we chose a BAC clone bearing the bone morphogenetic protein-2 (BMP-2) locus and assembled the genomic DNA as an infectious virion as a model to test the genomic DNA transfer and function. Our results indicated that the iBAC could efficiently deliver a BMP-2 genomic locus and express functional protein promoting osteoblast differentiation.

Materials and methods

Vector constructs. The DNA constructs of pCTP-T, pEBHICP27, pEHHG, and fHSVΔ-pac, Δ-27, 0+ were described in detail elsewhere [20,21], and kindly provided by Dr. Yoshinaga Saeki (Massachusetts General Hospital, Harvard Medical School, MA). A BAC clone, RP23-302H4, containing a complete BMP-2 locus was purchased from Invitrogen Life Technologies (Carlsbad, CA).

Cell culture. Vero 2-2 cells (kindly provided by Dr. Rozanne Sandri-Goldin, University of California, Irvine, CA) were routinely maintained in Dulbecco's modified minimal essential medium (Invitrogen) with 10% fetal bovine serum, 100 U/ml penicillin, 100 μg/ml streptomycin, and G486 (500 μg/ml). MC3T3-E1 cells (ATCC, Manassas, VA) were propagated in alpha minimum essential medium (Invitrogen) supplemented with 10% calf serum, 100 U/ml penicillin, and 100 μg/ml streptomycin. The cells were cultured in a humidified 37 °C incubator with 5% CO_2.

Retrofitting of BAC clone. The retrofitting of BAC clone into HSV-1/EBV amplicons was carried out by Cre-mediated recombination in bacterial cells as described previously [21]. Briefly, an aliquot of 35 μl electro-competent cells containing BAC/BMP-2 (RP23-302H4) was mixed with 10 ng each of pEHHG and pCTP-T plasmid DNA, and the mixture was transferred into 0.1-cm gap width electroporation cuvette (Bio-Rad, Hercules, CA). After 5 min incubation on ice, the cells were electroporated with 25 μF at 1800 V using a Gene Pulser (Bio-Rad), then transferred into a 15-ml conical tube containing 500 μl SOC with 20 μg chlortetracycline (Sigma, St. Louis, MO), and incubated at 30 °C with rigorous shaking for 1 h. An aliquot of 100 μl of the bacterial culture was transferred into a new 15-ml tube containing 20 μg/ml chlortetracycline, 100 μg/ml ampicillin, and 20 μg/ml chloramphenicol in 900 μl SOC, and incubated at 30 °C with shaking for another 3 h. Subsequently, 50–100 μl of the bacterial culture was plated on LB plates containing 100 μg/ml ampicillin and 20 μg/ml chloramphenicol, and incubated overnight at 43 °C. DNA of individual clones was purified and verified by polymerase chain reaction (PCR) using specific primers to BMP-2 (forward: 5′-CCTTCGGAAGACGTCCTCAG and reverse: 5′-TCACTCGATTTCCCTCCAGT) and GFP (forward: 5′-TGCCACCTACGGCAAGCTGA and reverse: 5′-CCATGTGATCG CGCTTCTCG) to confirm the correct retrofitted BAC clone.

Packaging HSV-1 amplicon into virion. HSV-1 amplicon was packaged into infectious virion as described previously [21]. Briefly, Vero 2-2 cells (10^6) were plated in a 60-mm dish. After 18 h, the cells were co-transfected with 2.0 μg pHSV-BAC/BMP-2 or pEHHG, 0.2 μg pEBHICP27, and 2 μg fHSVΔ-pac, Δ-27, 0+ using LipofectAMINE Plus (Invitrogen) for 4 h. The cells were scraped into the supernatant 60 h post-infection, frozen and thawed once, sonicated for 1 min, and centrifuged at 3500 r.p.m. for 15 min. The supernatant was then concentrated through a 25% sucrose by ultracentrifuging, and the amplicon pellet was resuspended in Hanks' buffered salt solution. The purified HSV-1 amplicon was titered in Vero 2-2 cells by counting the number of GFP positive cells after 24 h infection. Typically, the titration of HSV-1 amplicon stocks was around 5×10^6–10^7 GFP transducing units/ml.

HSV-1 virion infection, Western blot and FACS analyses. MC3T3-E1 cells were plated in a 6-well plate at a density of 10^5/well. After 24 h, the cells were infected at a multiplicity of infection (MOI) of 5 with HSV-1 amplicon. After 6 h infection, the medium was removed, and fresh medium was added to the cells. The cells were lysed in a lysis buffer containing 50 mM Tris, pH 8.0, 150 mM NaCl, 0.1% SDS, 1% Triton X-100, and 1× Protease Inhibitor cocktail (Sigma) 24 h after infection. An aliquot of 60 μg cellular protein was electrophoresed on a 15% SDS–polyacrylamide gel and transferred to nitrocellulose. The membrane was incubated at 4 °C overnight in a buffer containing 5% dried skim milk, 150 mM NaCl, 50 mM Tris–HCl (pH 8.0), and 0.05% Tween 20. Immunoblotting was performed in the same buffer containing 0.2 μg/ml antibody against BMP-2 or GFP (Santa Cruz, CA) at room temperature for 1 h. Specific proteins were detected using appropriate secondary antibodies and ECL + plus Western blotting detection system (Amersham–Pharmacia Biotech UK Limited, Buckinghamshire, England). The cells in a parallel well were trypsinized 24 h post-infection and analyzed by fluorescence-activated cell sorter (FACS) (BD Biosciences, San Lose, CA) to assess the transduction efficiency [24].

Cytochemical staining for alkaline phosphatase. The cytochemical staining for alkaline phosphatase (ALP) was performed according to the protocol described previously [25]. Nine days after HSV-1 amplicon infection, the MC3T3-E1 cells were washed with PBS and fixed in 0.05% glutaraldehyde at room temperature for 5 min. The cells were then incubated at 37 °C for 30 min in a staining buffer containing 50 mM Tris–HCl, pH 8.6, 100 mM NaCl, 5 mM KCl, 1 mM $CaCl_2$, 1 mM $MgCl_2$, 0.8 mg/ml naphthol AS-TR phosphate, and 0.6 mg/ml

fast red violet LB diazonium (Sigma) in dark, followed by observation without counterstain.

Results and discussion

We searched the GenBank database and identified a mouse BAC library clone containing a complete 8.7-kb BMP-2 genomic DNA locus driven by a 20.5-kb native promoter within a 128.5-kb insert. We chose this clone because it contains a single BMP-2 gene with most, if not all, of the regulatory elements in the promoter, introns, and 3′ non-coding regions that may regulate a physiological gene expression [26,27]. The length of the BAC clone is also within the size limits that the HSV-1 vector can efficiently package into an iBAC [21]. We used a Cre/loxP-based retrofitting method to convert the BAC/BMP-2 with the pEHHG, consisting of HSV-1 amplicon elements, enhanced green fluorescent protein (GFP), EBV episome retention cassette, R6K bacterial replication origin, and a *loxP* site to generate a 152-kb construct of pHSV-BAC/BMP-2 (Fig. 1A) [20,21]. Subsequently, a PCR with specific primers to BMP-2 and GFP was performed to confirm the presence of two genes within a single pHSV-BAC/BMP-2 construct (Fig. 1B). We then packaged the pHSV-BAC/BMP-2 into the iBAC [21] and infected MC3T3-E1 cells to test the transgenes' function (Fig. 2). Twenty-four hours after infection, the GFP reporter gene was expressed in most of MC3T3-E1 cells transduced with either an HSV-1 mock (Fig. 2C) or an HSV-BAC/BMP-2 amplicon (Fig. 2D). Flow cytometry analyses revealed that 84% of the osteoblast cells transduced with HSV-1 mock amplicon expressed GFP (Fig. 2E) and 77% of the cells infected with HSV-BAC/BMP-2 virion were GFP-positive (Fig. 2F). To compare the efficiencies of transduction and transfection, we also transfected MC3T3-E1 cells with pEHHG and pHSV-BAC/BMP-2 (Fig. 1A) using Lipofectamine-Plus. Only less than 5% of MC3T3-

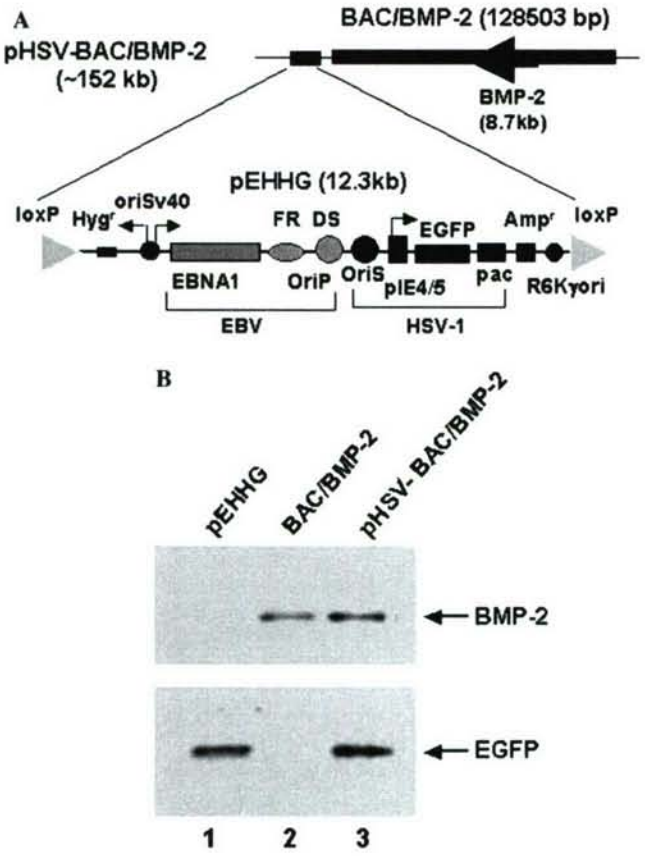

Fig. 1. Schematic diagram of infectious HSV-1/BAC/BMP-2 construct. (A) A detailed structure of retrofitted BAC clone. The retrofitting vector pEHHG containing the HSV-1 amplicon elements (*ori*$_s$ and *pac*) and GFP, the EBV episome retention cassette (*oriP*/*EBNA-1*/*hygr*), the R6K bacterial replication origin, and a *loxP* site is retrofitted into the BAC clone bearing a complete BMP-2 locus by homologous recombination. The retrofitted BAC contains both GFP reporter and BMP-2 genes. (B) Verification of pHSV-BAC/BMP-2 construct by polymerase chain reaction (PCR). Lane 1: pEHHG control; lane 2: BAC/BMP-2 control; and lane 3: pHSV-BAC/BMP-2 containing both GFP and BMP-2 genes.

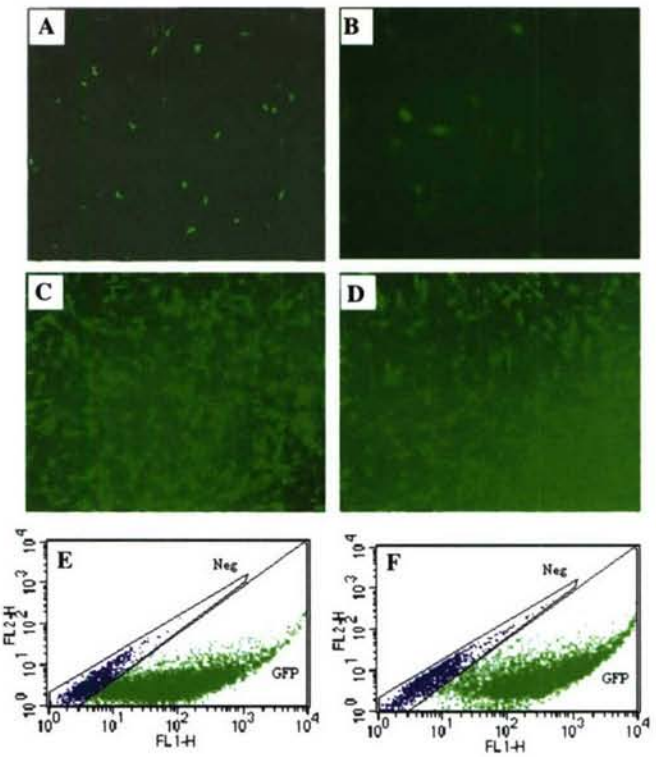

Fig. 2. GFP reporter expression in MC3T3-E1 cells transfected and transduced with HSV-1 amplicon for 24 h (40× images). (A) MC3T3-E1 cells transfected with pEHHG (4 μg) using optimized lipofectamine; (B) MC3T3-E1 cells transfected with pHSV-BAC/BMP-2 (4 μg) using optimized lipofectamine; (C) MC3T3-E1 cells transduced with infectious HSV-1 mock amplicon without BMP-2 genomic locus; (D) MC3T3-E1 cells transduced with infectious HSV-1 amplicon containing a BMP-2 genomic locus; (E) representative data of flow cytometric analysis in MC3T3-E1 cells infected with HSV-1 mock amplicon containing GFP but no BMP-2 genomic locus; and (F) representative data of flow cytometric analysis in MC3T3-E1 cells infected with HSV-1 amplicon containing GFP and a BMP-2 genomic locus.

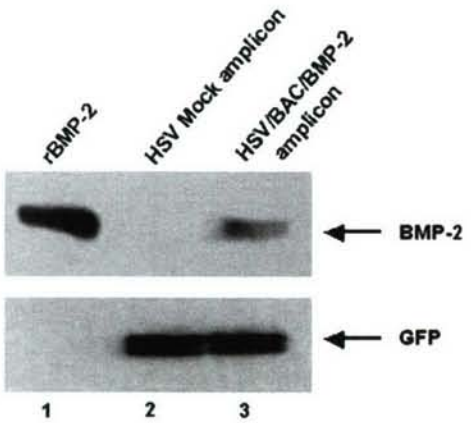

Fig. 3. Western immunoblot analyses of BMP-2 expressed in transduced MC3T3-E1 cells. MC3T3-E1 cells are infected with HSV-1 amplicon for 24 h and harvested for Western blot analysis. An aliquot (60 μg, 10^6 cells) of cellular lysate is separated on 15% SDS–PAGE, transferred to nitrocellulose membranes, and blotted using antibodies against BMP-2 and GFP, respectively. Lane 1: positive control of recombinant BMP-2 (100 ng); lane 2: the cells infected with HSV-1 mock amplicon containing GFP but no BMP-2 genomic locus; and lane 3: the cells infected with HSV-1 amplicon containing GFP and a BMP-2 genomic locus.

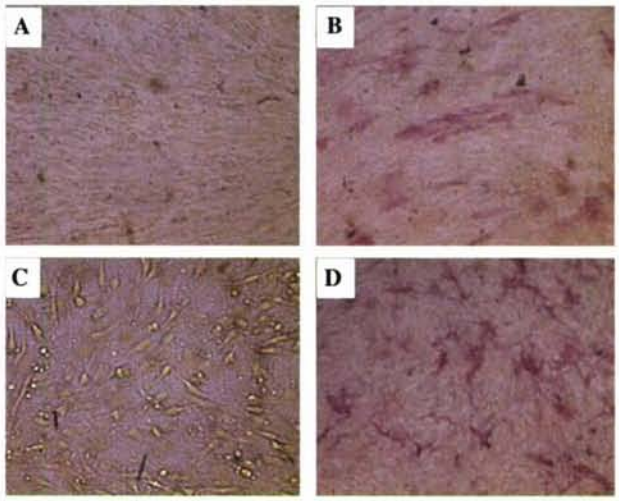

Fig. 4. Alkaline phosphatase (ALP) staining of differentiated MC3T3-E1 cells (40× images). MC3T3-E1 cells are differentiated for 9 days and subjected to ALP staining. (A) The cells infected with HSV-1 mock amplicon without a BMP-2 genomic locus; (B) the cells infected with HSV-1 amplicon containing a BMP-2 genomic locus; (C) negative control of MC3T3-E1 cells treated with vehicle; and (D) positive control of MC3T3-E1 cells treated with recombinant BMP-2 (200 ng/ml).

E1 cells transfected with pHSV-BAC/BMP-2 expressed GFP (Fig. 2A) whereas approximately 10% of the cells transfected with pEHHG turned green (Fig. 2A). Obviously, the efficiency of transduction of BAC-based amplicon was at least 15-fold higher than that of lipid-based transfection (Fig. 2).

The expression of the transgene was examined in cell extract by utilizing Western blot with specific antibodies against BMP-2 and GFP (Fig. 3). The amount of BMP-2 protein was estimated to be 10 ng/10^6 cells based on Western blot analysis (Fig. 3). However, we failed to detect BMP-2 expression in the same number of either native MC3T3-E1 cells or the cells transfected with pHSV-BAC/BMP-2 (Fig. 3 and data not shown). To assess osteoblast phenotype in the cells expressing BMP-2 transgene, we carried out an ALP staining 9 days after transduction (Fig. 4). Like the cells treated with 200 ng/ml recombinant human BMP-2, about 20% of the osteoblast cells were differentiated and exhibited positive ALP-staining (Figs. 4B and D). No ALP-positive cells were seen in the control cells infected with HSV-1 mock amplicon without BMP-2 genomic locus (Fig. 4A) or the cells treated with vehicle alone (Fig. 4C).

In this study, we have demonstrated that the HSV-1 amplicon can efficiently transfer a large piece of genomic locus (Fig. 2), and retain it as episomes in proliferating cells [18]. The GFP gene is consistently active and visible for at least 2 weeks, although the intensity becomes weaker as reported by other investigators [24]. The functional BMP-2 protein in the infected cells was detectable 24 h and even 72 h after infection (Fig. 3 and data not shown) and mediated cell differentiation (Fig. 4) [28]. However, accurate quantification of BMP-2 expression level was impossible because the secreted BMP-2 in the medium was not measured. Nevertheless, the transgene of BMP2 was active and promoted a phenotypic change of targeting cells (Fig. 3, lane 3 and Fig. 4), validating the application of iBAC technology.

In vivo testing of candidate genes in a BAC-based transgenic mouse is time-consuming and expensive, requiring the injection of BAC inserted into fertilized eggs and the examination of mouse phenotypes. Therefore, it would be more efficient to use in vitro cell models via the BAC clone approach to test candidate gene function before introducing in vivo transgenic studies. The studies provided in this manuscript demonstrate that retrofitting of the BAC clone and packaging of the HSV-1 amplicon into infectious virion can be accomplished within 1–2 weeks of work. By utilizing this approach, a candidate gene search in a QTL region is feasible once an appropriate cell model and end points for candidate gene function are determined. In this regard, our data demonstrate that MC3T3-E1 cells can be used as a model for high-throughput phenotypic screening to identify genes important for osteoblast cell differentiation. We have also used this system in C2C12 cells and proved that iBAC containing BMP-2 locus can induce premyoblast dedifferentiation and subsequently commit to osteoblast lineage (data not shown), providing another cell-based model for gene function of dedifferentiation. In addition, BAC or PAC can carry a genomic locus encompassing an intact gene(s) with all regulatory elements including enhancers, suppressors and locus control region that can direct physiological levels of tissue-specific expression for gene therapy. It can also be

manipulated to engineer a deletion, an insertion, and a site-specific mutation in *Escherichia coli* by homologous recombination to mimic natural polymorphisms to test the functional significance of SNPs located in the distal promoter or/and intron regions.

Acknowledgments

This work was supported by Assistance Award No. DAMD17-03-2-0021. The U.S. Army Medical Research Acquisition Activity, 820 Chandler Street, Fort Detrick MD 21702-5014, is the awarding and administering acquisition office. The information contained in this publication does not necessarily reflect the position or the policy of the Government, and no official endorsement should be inferred. All work was performed in facilities provided by the Department of Veterans Affairs. We are grateful to Dr. Yoshinaga Saeki (the Massachusetts General Hospital, Harvard Medical School, MA) for providing HSV-1 amplicon system and his technical assistance, and Dr. Rozanne Sandri-Goldin (the University of California, Irvine, CA) for her generous gift of a Vero 2-2 cell line. We also thank Dr. Shin-Tai Chen, Ms. Mahita Kadmiel, and Mr. Max Davis for their technical assistances of HSV-1 virion purification and FACS analyses (Musculoskeletal Disease Center, JL Pettis Memorial Veterans Medical Center, Loma Linda, CA).

References

[1] D.L. Glaser, F.S. Kaplan, Osteoporosis. Definition and clinical presentation, Spine 22 (1997) 12S–16S.

[2] C.W. Slemenda, J.C. Christian, T. Reed, T.K. Reister, C.J. Williams, C.C. Johnston Jr., Long-term bone loss in men: effects of genetic and environmental factors, Ann. Intern. Med. 117 (1992) 286–291.

[3] C.W. Slemenda, J.C. Christian, C.J. Williams, J.A. Norton, C.C. Johnston Jr., Genetic determinants of bone mass in adult women: a reevaluation of the twin model and the potential importance of gene interaction on heritability estimates, J. Bone Miner. Res. 6 (1991) 561–567.

[4] V. Nicolas, S. Mohan, Y. Honda, A. Prewett, R.D. Finkelman, D.J. Baylink, J.R. Farley, An age-related decrease in the concentration of insulin-like growth factor binding protein-5 in human cortical bone, Calcif. Tissue Int. 57 (1995) 206–212.

[5] D. Baylink, M. Stauffer, J. Wergedal, C. Rich, Formation, mineralization, and resorption of bone in vitamin D-deficient rats, J. Clin. Invest. 49 (1970) 1122–1134.

[6] M.J. Econs, D.L. Koller, S.L. Hui, T. Fishburn, P.M. Conneally, C.C. Johnston Jr., M. Peacock, T.M. Foroud, Confirmation of linkage to chromosome 1q for peak vertebral bone mineral density in premenopausal white women, Am. J. Hum. Genet. 74 (2004) 223–228.

[7] C.M. Kammerer, J.L. Schneider, S.A. Cole, J.E. Hixson, P.B. Samollow, J.R. O'Connell, R. Perez, T.D. Dyer, L. Almasy, J. Blangero, R.L. Bauer, B.D. Mitchell, Quantitative trait loci on chromosomes 2p, 4p, and 13q influence bone mineral density of the forearm and hip in Mexican Americans, J. Bone Miner. Res. 18 (2003) 2245–2252.

[8] F. Wynne, F.J. Drummond, M. Daly, M. Brown, F. Shanahan, M.G. Molloy, K.A. Quane, Suggestive linkage of 2p22-25 and 11q12-13 with low bone mineral density at the lumbar spine in the Irish population, Calcif. Tissue Int. 72 (2003) 651–658.

[9] H.W. Deng, H. Shen, F.H. Xu, H. Deng, T. Conway, Y.J. Liu, Y.Z. Liu, J.L. Li, Q.Y. Huang, K.M. Davies, R.R. Recker, Several genomic regions potentially containing QTLs for bone size variation were identified in a whole-genome linkage scan, Am. J. Med. Genet. 119A (2003) 121–131.

[10] G.L. Masinde, J. Wergedal, H. Davidson, S. Mohan, R. Li, X. Li, D.J. Baylink, Quantitative trait loci for periosteal circumference (PC): identification of single loci and epistatic effects in F2 MRL/SJL mice, Bone 32 (2003) 554–560.

[11] G.L. Masinde, X. Li, W. Gu, J. Wergedal, S. Mohan, D.J. Baylink, Quantitative trait loci for bone density in mice: the genes determining total skeletal density and femur density show little overlap in F2 mice, Calcif. Tissue Int. 71 (2002) 421–428.

[12] W.G. Beamer, C.J. Rosen, R.T. Bronson, W. Gu, L.R. Donahue, D.J. Baylink, C.C. Richardson, G.C. Crawford, J.E. Barker, Spontaneous fracture (sfx): a mouse genetic model of defective peripubertal bone formation, Bone 27 (2000) 619–626.

[13] K.L. Shultz, L.R. Donahue, M.L. Bouxsein, D.J. Baylink, C.J. Rosen, W.G. Beamer, Congenic strains of mice for verification and genetic decomposition of quantitative trait loci for femoral bone mineral density, J. Bone Miner. Res. 18 (2003) 175–185.

[14] W.K. Gu, X.M. Li, B. Edderkaoui, D.D. Strong, K.H. Lau, W.G. Beamer, L.R. Donahue, S. Mohan, D.J. Baylink, Construction of a BAC contig for a 3 cM biologically significant region of mouse chromosome 1, Genetica 114 (2002) 1–9.

[15] R.E. White, R. Wade-Martins, S.L. Hart, J. Frampton, B. Huey, A. Desai-Mehta, K.M. Cerosaletti, P. Concannon, M.R. James, Functional delivery of large genomic DNA to human cells with a peptide-lipid vector, J. Gene. Med. 5 (2003) 883–892.

[16] C. Magin-Lachmann, G. Kotzamanis, L. D'Aiuto, H. Cooke, C. Huxley, E. Wagner, In vitro and in vivo delivery of intact BAC DNA–comparison of different methods, J. Gene. Med. 6 (2004) 195–209.

[17] C. Magin-Lachmann, G. Kotzamanis, L. D'Aiuto, E. Wagner, C. Huxley, Retrofitting BACs with G418 resistance, luciferase, and oriP and EBNA-1-new vectors for in vitro and in vivo delivery, BMC Biotechnol. 3 (2003) 2.

[18] R. Wade-Martins, Y. Saeki, E. Antonio Chiocca, Infectious delivery of a 135-kb LDLR genomic locus leads to regulated complementation of low-density lipoprotein receptor deficiency in human cells, Mol. Ther. 7 (2003) 604–612.

[19] Y. Wang, C. Fraefel, F. Protasi, R.A. Moore, J.D. Fessenden, I.N. Pessah, A. DiFrancesco, X. Breakefield, P.D. Allen, HSV-1 amplicon vectors are a highly efficient gene delivery system for skeletal muscle myoblasts and myotubes, Am. J. Physiol. Cell Physiol. 278 (2000) C619–C626.

[20] R. Wade-Martins, E.R. Smith, E. Tyminski, E.A. Chiocca, Y. Saeki, An infectious transfer and expression system for genomic DNA loci in human and mouse cells, Nat. Biotechnol. 19 (2001) 1067–1070.

[21] Y. Saeki, X.O. Breakefield, E.A. Chiocca, Improved HSV-1 amplicon packaging system using ICP27-deleted, oversized HSV-1 BAC DNA, Methods Mol. Med. 76 (2003) 51–60.

[22] K. Ellnebo-Svedlund, L. Larsson, J. Jonasson, P. Magnusson, Rapid genotyping of the osteoporosis-associated polymorphic transcription factor Sp1 binding site in the COL1A1 gene by pyrosequencing, Mol. Biotechnol. 26 (2004) 87–90.

[23] S.L. Ferrari, D. Karasik, J. Liu, S. Karamohamed, A.G. Herbert, L.A. Cupples, D.P. Kiel, Interactions of interleukin-6 promoter polymorphisms with dietary and lifestyle factors and their association with bone mass in men and women from the Framingham Osteoporosis Study, J. Bone Miner. Res. 19 (2004) 552–559.

[24] R. Nunez, M. Ackermann, Y. Saeki, A. Chiocca, C. Fraefel, Flow cytometric assessment of transduction efficiency and cytotoxicity

of herpes simplex virus type 1-based amplicon vectors, Cytometry 44 (2001) 93–99.

[25] J.E. Wergedal, D.J. Baylink, Characterization of cells isolated and cultured from human bone, Proc. Soc. Exp. Biol. Med. 176 (1984) 60–69.

[26] K.L. Abrams, J. Xu, C. Nativelle-Serpentini, S. Dabirshahsahebi, M.B. Rogers, An evolutionary and molecular analysis of BMP2 expression, J. Biol. Chem. (2004).

[27] L.M. Helvering, R.L. Sharp, X. Ou, A.G. Geiser, Regulation of the promoters for the human bone morphogenetic protein 2 and 4 genes, Gene 256 (2000) 123–138.

[28] D. Noel, D. Gazit, C. Bouquet, F. Apparailly, C. Bony, P. Plence, V. Millet, G. Turgeman, M. Perricaudet, J. Sany, C. Jorgensen, Short-term BMP-2 expression is sufficient for in vivo osteochondral differentiation of mesenchymal stem cells, Stem Cells 22 (2004) 74–85.

Global Gene Expression Analysis in the Bones Reveals Involvement of Several Novel Genes and Pathways in Mediating an Anabolic Response of Mechanical Loading in Mice

Weirong Xing[1], David Baylink[1,2], Chandrasekhar Kesavan[1], Yan Hu[1], Robert Chadwick[1], Susanna Kapoor[1]and Subburaman Mohan[1,2,3,4]
[1]Musculoskeletal Disease Center, JL Pettis Memorial Veterans Administration Medical Center, Loma Linda, CA 92357
[2]Department of Medicine,
[3]Department of Biochemistry,
[4]Department of Physiology, Loma Linda University, Loma Linda, California, USA

Running title: Osteogenic Gene Expression By Mechanical Loading

Address Correspondence to: Dr. Subburaman Mohan
Musculoskeletal Disease Center
Jerry L. Pettis Memorial Veterans Medical Center
Loma Linda, CA 92357
Telephone: 909-825-7084 ext. 2932
Fax: 909-796-1680
E-mail: Subburaman.Mohan@med.va.gov

Keywords:

- **Osteogenesis**
- **Microarray**
- **Mechanical Loading**
- **Bone**
- **Gene expression**

Number of Figures: 3
Number of Tables: 1

Contract grant sponsor: U.S. Army Medical Research Acquisition Activity
Contract grant number: DAMD17-01-1-0744

Abstract

To identify the genes and signal pathways responsible for mechanical loading-induced bone formation, we evaluated differential gene expression on a global basis in the tibias of C57BL/6J (B6) mice after four days of four-point binding. We applied mechanical loads to the right tibias of the B6 mice at 9N, 2Hz for 36 cycles per day, with the left tibias used as unloaded controls. RNA from the tibias was harvested 24 hours after last stimulation and subjected to microarray. Of the 20,280 transcripts hybridized to the array, 346 were differentially expressed in the loaded bones compared to the controls. The validity of the microarray data was established with the increased expression of bone-related genes such as pleiotrophin, osteoglycin, and legumain upon four-point bending and confirmation of increased expression of selected genes by real-time PCR. The list of differentially expressed genes includes genes involved in cell growth, differentiation, adhesion, proteolysis, as well as signaling molecules of receptors for growth factors, integrin, Ephrin B2, endothelin, and adhesion G protein coupled receptor. Pathway analyses suggested that 28 out of the 346 genes exhibited a direct biological association. Among the biological network, fibronectin and pleitrophin function as important signaling molecules in regulating periosteal bone formation and resorption in response to four-point bending. Furthermore, some expressed sequence tags (ESTs) with no prior known function have been identified as potential mediators of mechanotransduction signaling pathways. Further studies on these previously unknown genes will improve our understanding of the molecular pathways and mechanisms involved in bone's response to mechanical stress.

Abbreviations:

AHR: aryl-hydrocarbon receptor; α5β3 integrin: alpha5beta3 integrin; ANXA2: annexin A2; AP-1: activating protein 1; β2M: β-2 microglobulin; COL18A1: Collagen type XVIII alpha 1; Csrp2: cystein and glycine-rich protein 2; CTSD: cathepsin D; EGF: epidermal growth factor; EGFR: EGF receptor; Emp1: epithelial membrane protein 1; ENPP1: ectonucleotide pyrophosphatase/phosphodiesterase 1; Ephb2: ephrin receptor B2; EPS8: EGFR pathway substrate 8; ERK: extracellular signal-regulated kinases; EST: expressed sequence tag; FCGR1A: Fc receptor IgG high affinity I; FGF7: fibroblast growth factor 7; FGFR1: FGF receptor 1; FN: fibronictin receptor; HIF-1A: hypoxia-induced factor1alpha; IER3: immediate early response gene 3; IGF: insulin-like growth factor; IGFBP5: IGF binding protein 5; IGFR: IGF receptor; Itm2a: integral membrane protein 2; Lgmn: legumain; LRR: leucine-rich repeats; MAF: musculoaponeurotic fibrosarcoma oncogene; MAPK: mitogen-activated protein kinase; MMP: matrix metalloproteinase; Npdc1: neural proliferation, differentiation and control gene 1; Ogn: osteoglycin; PCR: polymerase chain reaction; PDGF: platelet derived growth factor; PDGFA: PDGF alpha; PDGFRA: PDGFR alpha; PDGFRB: PDGF receptor beta; Ptn: pleiotrophin; QTL: quantitative trait loci; RGDS: Ral GDP dissociation stimulator; TEP1: telomerase associated protein 1; TIM: tissue inhibitor of metalloprotainase; TNC: Tenascin C; VEGF: vascular endothelial growth factor;

Introduction

It is well established that bone adapts to mechanical loading by adjusting its density, shape, and strength during periods of growth and daily physical activities. Under normal conditions, such as exercise, mechanical loading stimulates bone formation, whereas overloading or unloading may result in unbalanced bone resorption and reduced growth rate [Frost, 1992; Sibonga et al., 2000]. However, the skeletal response to mechanical loading is widely varied in the normal human population [Devine et al., 2004; Rittweger et al., 2005]. For example, some postmenopausal women with severe osteoporosis display a poor anabolic response to mechanical stimuli loaded on their bones, while other patients respond normally to the same degree of mechanical loading [Preisinger et al., 1995; Yamazaki et al., 2004]. A similar variation in anabolic response to mechanical loading has also been observed in some animal models, such as the C57BL/6 (B6) and C3H/HeJ (C3H) mouse strains [Akhter et al., 1998; Pedersen et al., 1999]. We and others have found B6 mice to be more responsive to skeletal loading compared to C3H mice [Akhter et al., 1998; Kodama et al., 1999; Kodama et al., 2000; Robling and Turner, 2002]. In addition, congenic mice of B6.C3H-4T containing a segment of mouse chromosome 4 from the C3H strain in the B6 genetic background were found to be more susceptible to mechanical loading than the B6 mice [Robling et al., 2003]. Together, these studies have confirmed that differential anabolic responses to mechanical loading are, in large part, genetically determined. Therefore, studies to identify the genes and signal transduction pathways involved in bone's adaptive response to mechanical loading are important for the future development of diagnostic markers and/or therapeutic targets for osteoporosis.

In the past few years, studies using *in vitro* culture systems have identified a number of genes susceptible to mechanical force. It has been found that these genes are involved in a number of signaling pathways, including calcium-regulated PI3K-Akt and protein kinase C [Danciu et al., 2003; Pines et al., 2003], growth factor activated extracellular signal-regulated kinases (ERK), prostaglandin synthesis [Kapur et al., 2003] and integrin pathway [Weyts et al., 2002]. While the data generated from these *in vitro* studies have provided important information, one major limitation has been that most of the data obtained were from homogenous osteoblast cells in cell culture systems lacking the vital communications of multiple cell types such as osteocytes and osteoblasts. This is a constraint because bone osteocytes can receive and transmit changes in mechanical forces to other cell types involved in bone remodeling [Ehrlich et al., 2002; Noble et al., 2003; Yang et al., 2005]. In addition, multipotent progenitor cells can also respond to mechanical signals to differentiate toward osteoblast lineage [Estes et al., 2004]. Accordingly, there has been a considerable need for an *in vivo* analysis of gene expression patterns of mechanically-loaded bones compared to unloaded bones that would address these considerations.

Several approaches have been used to identify candidate genes that contribute to phenotypic variation in inbred strains of mice, including quantitative trait loci (QTL), polymerase chain reaction (PCR) differential display, cDNA microarray and high-throughput mutation screening of target region [Doerge, 2002]. Of these techniques, microarray holds a great deal of promise for identifying the genes in question because of its ability to simultaneously characterize the expression levels of many thousands of genes associated with various biological functions and processes using very small

amounts of RNA. This technology has been applied to identify mechanically-induced genes in osteoblast cells exposed to fluid shear stress and has revealed multiple molecular pathways regulating osteogenic gene expression [Kapur et al., 2003]. Therefore, in the present study, we used oligonucleotide microarrays containing over 20,000 probes and evaluated differential gene expression on a global basis in the tibias of female B6 mice after four days of four-point bending. We hypothesized that mechanical activation of one or more sensitive signaling pathways would contribute to the robust increase in new bone formation in response to four-point bending in the female B6 mice.

Materials and Methods

Animals and Materials: Ten week old C57BL/6J female mice were obtained from the Jackson Laboratory and housed at the Jerry l. Pettis Memorial VA Medical Center Animal Research Facility (Loma Linda, CA) under standard approved laboratory conditions with controlled illumination (14 hours light, 10 hours dark), temperature (22^0C) and unrestricted food and water. Studies were performed with the approval of the Animal Ethics Committee of the Jerry L Pettis Memorial VA Medical Center. A mouse development oligonucleotide microarray (22K) slides were purchased from Agilent Technologies, Inc (Mountain View, CA). All probes on the slide were 60 base-pairs in length with sense orientation designed from the National Institute on Aging/National Institute of Health cDNA mouse clone set [Carter et al., 2003]. The designed microarray slides contain a single set of 22,575 spots, of which, 20, 371 are target genes. In addition, the slides also include a total of 1,075 control spots (144 negative controls, 18 corner mark negative controls,196 spike-in probes, 215 staggered start probes, 10 corner mark positive controls and 492 positive control grid). The remaining 1129 spots are blanks. The Cyanine 5-CTP and Cyanine 3-CTP were obtained from PerkinElmer Life Science (Boston, MA).

Mechanical loading *in vivo* and RNA extraction: Mice were externally loaded *in vivo* in a four-point bending device, as described previously [Akhter et al., 1998; Wang et al., 2000]. This model has been used extensively in a number of laboratories for studies on mechanical loading [Cullen et al., 2001; Robling and Turner, 2002; Torrance et al., 1994]. In previous studies, we found that two weeks of four-point bending at 9 N, 2Hz for 36 cycles per day increased total volumetric bone mineral density by 15% in B6 mice

[Kesava, 2004]. In this study, we used four days of loading to minimize the number of genes that change in response to loading-induced bone remodeling. Briefly, the right tibias of the mice were loaded for four days at 9N, 2Hz for 36 cycles per day and the left tibias of the same mice were used as unloaded controls. Twenty-four hours after last stimulation, the mice were sacrificed and the corresponding tibias were removed. The bones were dissected free of soft tissue, flushed with PBS to remove the bone marrow cells and stored in a solution of RNAlater (Ambion, Inc. Austin, TX) at -20^{o}C. To optimally evaluate mechanosensitive genes, only the region of bone that was subjected to four-point bending was used for RNA extraction. We pooled RNA from five loaded or unloaded bones to obtain sufficient RNA for microarray analysis and subsequent real-time PCR work. To generate five pairs of samples, a total of 25 mice were divided into five groups with five mice each. Total RNA was extracted using Trizol (Invitrogen Corporation, Carlsbad, CA), and further cleaned up through RNeasy mini spin columns (Qiagen, Valencia, CA). RNA concentration and integrity were analyzed in an Agilent 2100 Bioanalyzer (Agilent Technologies, Inc.).

Microarray design and hybridization: Probe labeling was performed according to the manufacturer's instructions using Agilent low RNA input fluorescent linear amplification kits (Agilent Technologies, Inc.). Briefly, an aliquot of 2 μg of total RNA was reverse transcribed using a primer containing oligo (dT) and a T7 RNA polymerase promoter. After synthesis of the first and second strands of cDNA, the product was amplified in an *in vitro* transcription reaction in order to generate enough cRNA labeled targets in the presence of cyanine 3- or cyanine 5-labeled CTP. The dye-labeled cRNA was then purified through RNeasy mini spin columns to remove free nucleotides. The cRNA

concentration and dye incorporation were measured using the NanoDrop spectrophotometer (NanoDrop Technologies, Rockland, NE). Hybridization was carried out according to the instructions provided in Agilent oligonucleotide microarray kit (Agilent Technologies, Inc.). Two micrograms of fragmented cyanine 3-labled cRNA of unloaded reference sample was mixed with equal amounts of cyanine 5-labeled cRNA of loaded experimental sample, and the mixture was hybridized to a 22K mouse development oligonucleotide microarray for 17 hours at 60°C at 7 rpm. After hybridization, the slides were dried using a nitrogen-filled air gun, and subsequently scanned using GSI Scanarray 4000 (GSI Lumonics, Inc., Moorpark, CA). The images were analyzed using the ImaGene 5.6 software (Biodiscovery, Inc., El Segundo, CA). The ImaGene software flagged spots with intensities lower than that of the background or spots with aberrant shapes.

Normalization and analysis of microarray data: Expression analysis of the microarray data from five slides was performed using the GeneSpring 6.2 (Silicon Genetics, Redwood City, CA). Local background-subtracted median signal intensities were used as intensity measures, with the data normalized using per spot and per chip intensity/dependent LOWESS normalization [Workman et al., 2002]. Transcripts that passed with flag values "present" in all five replicates and a raw signal greater than the background were targeted for further analyses. In order to minimize the false-positive/negative error rate in our high-density oligonucleotide microarray, we chose a combination of fold change and significant difference to restrict a small gene list [Costigan et al., 2002; Schmalbach et al., 2004]. The transcripts were first scaled to an expression level of 1.5-fold change. The filtered genes (e.g. $\geq$ 1.5-fold) were then further

analyzed utilizing a one-sample Student's t-test with "Benjamini and Hochberg" Multiple Testing Correction [Hochberg and Benjamini, 1990]. Differentially-expressed genes in the loaded bones were defined as those whose normalized average data had a difference of 1.5-fold change or greater with P value < 0.01, compared with the unloaded reference samples.

Identification of signaling pathways. We analyzed the gene list obtained from our microarray analysis using the PathwayAssist software (Stratagene, La Jolla, CA) to identify any specific signaling pathways, gene regulation networks, and protein interaction maps. The PathwayAssist program uses a natural language processor to retrieve information from databases such as PubMed in order to provide direct biological associations.

Real-time PCR: We used reverse transcriptase polymerase chain reaction (RT-PCR) for selected genes to confirm changes in transcription observed in our microarray analysis. Total RNA (2 μg) was reverse-transcribed into cDNA by using a oligo$(dT)_{12-18}$ primer and SuperScript II RNase^{TM} H$^-$ Reverse Transcriptase (Invitrogen). Real-time PCR was carried out in a 96 well plate using a 7700 ABI prism sequence detection system (Applied Biosystems, Foster City, CA). The PCR contained 100 ng of template cDNA, 1x SYBR GREEN master mix (Qiagen) and 100 nM of specific forward and reverse primers in 25 μl volume per reaction. Primers for the housekeeping gene, β-2 microglobulin (β2M), were used to normalize the expression data for each gene. The thermal cycling conditions for real-time PCR were: 10 minutes at 95 °C, followed by 40 cycles of 95 °C for 15 seconds, and 60 °C for 1 minute. Sequences of the primers were: pleiotrophin (Ptn)

(forward 5-gaaaatttgcagctgccttc, reverse 5'-ttcaaggcggtattgaggtc); osteoglycin (Ogn) (forward 5'-tgcaacaggcaattctgaag, reverse 5'-tccttggcagtcagcttttt); legumain (Lgmn) (forward 5'-acctgggtgactggtacagc, revese 5'-gattccttcacgtcgttggt); immediate early response gene 3 (IER3) (forward 5'-tctggtcccgagattttcac, reverse 5'-ctccgaggtcaggttcaaag); β2M (forward 5'-cgagcccaagaccgtctact; reverse 5'-gctatttctttctgcgtgcat); P37nb (forward 5'-aggaggcgttcatttacacg, reverse 5'-gggtttgtatgggaaacacg); neural proliferation, differentiation and control gene 1 (Npdc1) (forward 5'-taggcttcagcgagagatcc, reverse 5'-atggtcaaacagtgggttgc).

Results

Genome-wide expression profiles of mechanically-loaded bones versus unloaded bones. We examined global gene expression profiles in five different RNA pools from loaded and corresponding unloaded bones using an oligonucleotide array consisting of 20, 371 target genes. We found that a total of 20,280 transcripts were hybridized to the array. After an initial filtering of the data, we arrived at an informative data set for further analysis consisting of 19,882 genes which had both passed with flag value "present" in all five replicates and a raw signal greater than the background. Comparison of the gene expression profiles of the loaded and unloaded bones revealed 346 differentially expressed sequences that differed by 1.5-fold or greater with a significance of $P<0.01$ after "Benjamini and Hochberg" multiple testing correction. Table 1 shows a list of differentially regulated genes whose expression levels were either up- or down-regulated at least two-fold and organized in different biological categories. The complete list of 346 differentially regulated genes is provided in the Supplementary Data posted on this Journal's Website.

To determine the validity of our microarray data, we performed various permutation analyses, which include comparisons of 2 loaded samples versus 3 loaded samples, 2 unloaded samples versus 3 unloaded samples, and a pool of 2 loaded plus 2 unloaded versus 3 loaded and 3 unloaded samples. In addition, we also performed sample reproducibility analysis by comparing two normalized samples to three other normalized samples in a two-color system. These analyses revealed that the genes identified in this study cannot be explained on the basis of false discovery rate.

Of the 346 differentially expressed genes/ expressed sequence tags (ESTs) that we have identified, 304 were up-regulated, and 42 were down-regulated. A total of 157 (~46%) of these differentially-regulated genes encode proteins with no characterized function (Figure 1). Interestingly, proteins encoded by some of the genes/ESTs contain functional motifs, such as fibronectin domain, heparin-degrading endosulfatases, tubulin, leucine rich repeats (LRR) and von Willebrand factor type C domain. The remaining 189 known genes encode proteins that could be functionally characterized into 12 categories as assessed by Gene Ontology (GO), including cell growth, differentiation, adhesion, cell cycle, cell death, proteolysis, signaling molecules, transcription regulation, heat shock proteins, cytoskeleton movement and transport (Figure 1). The majority of differentially expressed genes belonged to the signaling molecule category and included growth factor receptors, G-protein coupled receptors, integrin receptors, Ca++ dependent receptor, tyrosine/serine/threonine kinases, intracellular and STAT cascade signaling molecules. The second, third, and fourth largest number of genes were found in cell growth, transport and cell adhesion, respectively. In addition, we also observed increased expression of a number of genes in categories such as transcriptional regulation, proteolysis, cell death, and heat shock proteins in the loaded bones compared to unloaded bones.

Notably, mechanical loading stimulated a large number of genes involved in cell growth, proliferation, and differentiation (Table 1). These genes included growth factors (Ptn, Ogn), receptor tyrosine protein (Ephb2), and oncogenes (leprecan1, Itm2a, Emp1, Csrp2 and Npdc1). In addition to the aforementioned genes, some transcription factors

such as goosecoid and signaling molecules of growth factor receptor pathways, were also identified as promoters of cell growth.

Validation of microarray data. To confirm the expression data from our oligonucleotide microarray studies, we selected five genes differentially expressed between the loaded and unloaded bones and one unchanged gene for quantitative RT-PCR analysis on five pairs of samples. Three of these genes (Ptn, Ogn and Lgmn) have been shown to be involved in the regulation of bone remodeling [Choi et al., 1999; Madisen et al., 1990; Yang et al., 2003]. IER3 has been shown to be an immediate early response gene that regulates cell growth and apoptosis in response to stress [Wu, 2003]. P37nb is a member of leucine-rich repeat protein family with a conserved role in regulation of proliferation, morphology and dynamics of the cytoskeleton, cell adhesion and tissue development [Segev et al., 2004]. Npdc1 is known to be expressed in the brain with an expression that can be coordinated with the regulation of cellular proliferation and differentiation [Evrard et al., 2004]. Based on the above information, we considered the six genes as potential candidates for mechanical signaling pathway. We therefore chose these genes for confirmation by real-time PCR. Consistent with the microarray data, Ptn, Ogn, Lgmn, P37nb and Npdc1 were found by real-time PCR to be expressed at significantly higher levels in the loaded bones. The expression of IER3 was no different between the loaded and unloaded bones, as expected based on our microarray data (Figure 2).

Identification of mechanosensitive signaling pathways involving in anabolic response. To identify potential signaling pathways associated with the skeletal anabolic

response to mechanical loading, we analyzed our microarray expression data using PathwayAssist [Nikitin et al., 2003]. This software comes with a built-in natural language processing module MedScan and a comprehensive database containing more than 150,000 events of regulation, interaction and modification between proteins and cell processes obtained from PubMed which allows it to generate a biological association network (BAN) of known protein-protein interactions. By importing microarray expression data into the BAN, co-expressed genes associated with specific signaling pathways can be identified. In order to characterize signaling pathways involved in response to mechanical loading, we imported 346 differentially expressed genes into the PathwayAssist, and found that 28 of the 346 genes exhibited a direct biological association (Figure 3). This network identified the following genes as coordinately being regulated in response to four-point bending: JUNB, MAF, TIMP1/2, MMP2, $\alpha 5\beta 3$ integrin, FN, TNC, Col18A1, IGFBP-5, EGFR, EPS8, ENPP1, FGF7, FGFR1, PDGFA, PDGFRA/B, PTN, TEP1, CTSD, FCGR1, HIF1A, AHR, ANXA2 and RGDS. Many of these genes represent transcription factors, growth factors and growth factor receptors which have been implicated in regulating the formation and/or activity of bone cells. Some of the genes associated with the network, such as TNC, FN, TIMP1, TIMP2, MMP2, JUNB, and PDGFA, have been also shown to respond to mechanical stress in bone cells *in vitro* [Carvalho et al., 2004; Granet et al., 2002; Hatori et al., 2004; Ponik and Pavalko, 2004]. In addition, it has been shown that the Ptn gene, a ligand for the EGF receptor, is induced in bladder smooth muscle cells in response to mechanical strain [Park et al., 1998]. Thus, a number of genes we have identified in our four-point bending studies in bone are the same genes that have been identified as mechanosensitive genes in

other cell types. Among the 28 genes in the network, fibronectin and Ptn are key signaling molecules that can activate integrin and EGF signaling pathways.

Discussion

The present study is a global microarray analysis of the mouse genome to identify differentially expressed genes in the tibias of female mice after four days of mechanical stimulation *in vivo*. We chose four-point bending as a loading regimen and B6 as our mouse model based on the findings that two weeks of four-point bending with this model caused a dramatic 15% increase in total volumetric bone mineral density and a 40% increase in bone size [Kesava, 2004]. We chose four days of consecutive loading based on the rationale that it leads to activation of important signaling pathways associated with rapid bone remodeling [Raab-Cullen et al., 1994b; Tanaka et al., 2003]. Consistent with the robust bone anabolic response, we identified 346 genes that were differentially expressed in the loaded bones with a 1.5 fold change or greater ($P<0.01$). Some of these genes, such as TIMP1, heat shock proteins, fibronectin, and neuropilin, have been previously implicated in bone's response to mechanical force and in mediating bone remodeling [Park et al., 1999; Shay-Salit et al., 2002; Swartz et al., 2001]. The identification of previously identified mechanosensitive genes and confirmation of microarray data by real-time PCR provided validation of our microarray results.

Previous *in vivo* studies of mechanical loading on rat tibias using a four point bending device revealed dynamic changes of gene expression in periosteal bone cells [Raab-Cullen et al., 1994a; Raab-Cullen et al., 1994b]. In those studies, it was found that transiently stimulated expression of AP-1 proteins within two hours after loading led to increased osteoblast cell proliferation [Raab-Cullen et al., 1994b]. However, the expression of alkaline phosphatase, osteopontin, and osteocalcin, which are typically produced by mature osteoblasts, was reduced [Raab-Cullen et al., 1994b]. The transcripts

of growth factors such as transforming growth factor β (TGFβ) and IGF-I were increased to peak levels after four hours of mechanical loading [Raab-Cullen et al., 1994b]. These studies suggested that acute periosteal response to external mechanical loading was associated with a change in expression of growth factors known to regulate osteoblast cell proliferation. In the present study, we found a moderate induction of AP-1 proteins (e.g. JunB and Maf), IGF-I, IGFBP-5, Ptn, EGF/FGF receptors and other genes related to cell cycle after four-day mechanical loading (Supplementary Data). It should be noted that all of the immediate response genes may not have been identified because the RNA used in this study was extracted 24 hours after the last mechanical load. In addition, our global microarray analysis also revealed that a large number of highly expressed genes which have not been previously implicated in mechanical signaling pathways, such as Ogn, Itm2a, Emp1, leprecan 1 and Npdc1, could act as potential mediators of mechanical stress to promote cell growth.

Our microarray analysis identified 157 previously uncharacterized or unknown genes/ESTs, some containing interesting functional motifs. For example, Csrp2, located on mouse chromosome 10, has a zinc-binding domain present in Lin-11, Isl-1, and Mec-3 (LIM-domain) that can bind protein partners via tyrosine-containing motifs. These proteins have been implicated as key regulators of developmental pathways and it has been proposed that they also regulate cell proliferation and differentiation of vascular smooth muscle cells in response to injuries [Jain et al., 1996; Jain et al., 1998]. We also observed a novel EST (P37nb) with leucine-rich repeats (LRR), a known functional domain present in a number of proteins with diverse functions and cellular locations [Strausberg et al., 2002]. In addition, one recent study found evidence that one of the

LRR proteins, CMF608, a mechanical strain-induced bone-specific protein, is involved in promoting osteochondroprogenitor proliferation [Segev et al., 2004]. Similarly, osteoadherin is another small molecule with LRR that can promote integrin ($\alpha 5\beta 3$)-mediated cell binding in bone tissue [Sommarin et al., 1998]. Our findings suggest that further studies are needed to evaluate whether these ESTs with important functional domains are involved in regulating bone cell proliferation/activity in response to mechanical loading.

In this study, we have confirmed the existence of a direct biological network consisting of the EGF receptor, fibronectin signaling, and proteolysis that are typically involved in bone formation and bone resorption [Anderson et al., 2004; Marie et al., 1990]. Our findings are supported by the fact that expression of PTN, which interacts with the EGF receptor (ErbB1/4), is also stimulated by mechanical stretch in bladder smooth muscle cells [Park et al., 1999]. In addition, it has been reported that over-expression of the PTN protein in osteoblast cells resulted in an increase in cell proliferation and periosteal bone formation [Imai et al., 1998; Tare et al., 2002]. Therefore, the issue of whether or not the elevated expression of PTN and fibronectin are major extracellular mediators of mechanical stress that activate the EGF receptor and integrin signaling pathways that are essential for bone anabolic response in response to mechanical loading requires further study.

Our study also found that several signaling molecules, including adhesion G-protein-coupled receptor 124, chemokine receptor and Eph receptor B2, were modulated by mechanical loading. Of these molecules, it has been previously established that the Eph receptor is localized within the QTL region of mouse chromosome 4 which is

believed to contain mechnosensitive gene(s) [Robling et al., 2003]. In addition, the Eph receptors and their membrane-anchored ephrin ligands are important in regulating cell-cell interactions and communications [Adams et al., 2001]. Targeted disruption of the Eph receptor ligand ephrinB1 in mice has also been reported to cause abnormal cartilage segmentation and the formation of additional skeletal elements, suggesting that ephrinB1 signaling is required for normal morphogenesis of skeletal elements [Compagni et al., 2003]. Our study provides, for the first time, evidence for increased Eph receptor B2 expression in bone cells in response to mechanical loading and establishes the groundwork for further examination of the Eph receptor signaling pathway's role in regulating bone formation.

Our experimental design involved a few waves of mechanical stimulation prior to evaluation of gene expression changes by microarray. Thus, it is possible that some of the genes altered after four days of four-point bending may be bone remodeling-related rather than mechanical responsive genes, and therefore the genes that are directly activated by mechanical stimulation cannot be discriminated. Our analysis also involved using RNA from loading region of bone that included multiple cell types (e.g. osteoblasts, stromal cells, ostocytes and osteoclasts). Thus, we cannot conclude which cell types are contributing to changes in gene expression. Further studies are needed to address this issue.

In conclusion, we have examined the *in vivo* effect of mechanical loading on differentially expressed genes in the whole genome, and identified a number of novel genes/ESTs and pathways that may play important roles in mediating the skeletal anabolic response to mechanical force. Future studies on these unknown genes and signal

molecules will provide a better understanding of the molecular pathways involved in mediating the skeleton's anabolic response to mechanical stress.

Acknowledgments

This work was supported by Assistance Award No. DAMD17-01-1-0744. The U.S. Army Medical Research Acquisition Activity, 820 Chandler Street, Fort Detrick MD 21702-5014, is the awarding and administering acquisition office. The information contained in this publication does not necessarily reflect the position or the policy of the Government, and no official endorsement should be inferred. All work was performed in facilities provided by the Department of Veterans Affairs. We would like to thank Mr. Sean Belcher for his editorial assistance.

References

Adams RH, Diella F, Hennig S, Helmbacher F, Deutsch U, Klein R (2001): The cytoplasmic domain of the ligand ephrinB2 is required for vascular morphogenesis but not cranial neural crest migration. Cell 104:57-69.

Akhter MP, Cullen DM, Pedersen EA, Kimmel DB, Recker RR (1998): Bone response to in vivo mechanical loading in two breeds of mice. Calcif Tissue Int 63:442-9.

Anderson HD, Wang F, Gardner DG (2004): Role of the epidermal growth factor receptor in signaling strain-dependent activation of the brain natriuretic peptide gene. J Biol Chem 279:9287-97.

Carter MG, Hamatani T, Sharov AA, Carmack CE, Qian Y, Aiba K, Ko NT, Dudekula DB, Brzoska PM, Hwang SS, Ko MS (2003): In situ-synthesized novel microarray optimized for mouse stem cell and early developmental expression profiling. Genome Res 13:1011-21.

Carvalho RS, Einhorn TA, Lehmann W, Edgar C, Al-Yamani A, Apazidis A, Pacicca D, Clemens TL, Gerstenfeld LC (2004): The role of angiogenesis in a murine tibial model of distraction osteogenesis. Bone 34:849-61.

Choi SJ, Reddy SV, Devlin RD, Menaa C, Chung H, Boyce BF, Roodman GD (1999): Identification of human asparaginyl endopeptidase (legumain) as an inhibitor of osteoclast formation and bone resorption. J Biol Chem 274:27747-53.

Compagni A, Logan M, Klein R, Adams RH (2003): Control of skeletal patterning by ephrinB1-EphB interactions. Dev Cell 5:217-30.

Costigan M, Befort K, Karchewski L, Griffin RS, D'Urso D, Allchorne A, Sitarski J, Mannion JW, Pratt RE, Woolf CJ (2002): Replicate high-density rat genome

oligonucleotide microarrays reveal hundreds of regulated genes in the dorsal root ganglion after peripheral nerve injury. BMC Neurosci 3:16.

Cullen DM, Smith RT, Akhter MP (2001): Bone-loading response varies with strain magnitude and cycle number. J Appl Physiol 91:1971-6.

Danciu TE, Adam RM, Naruse K, Freeman MR, Hauschka PV (2003): Calcium regulates the PI3K-Akt pathway in stretched osteoblasts. FEBS Lett 536:193-7.

Devine A, Dhaliwal SS, Dick IM, Bollerslev J, Prince RL (2004): Physical activity and calcium consumption are important determinants of lower limb bone mass in older women. J Bone Miner Res 19:1634-9.

Doerge RW (2002): Mapping and analysis of quantitative trait loci in experimental populations. Nat Rev Genet 3:43-52.

Ehrlich PJ, Noble BS, Jessop HL, Stevens HY, Mosley JR, Lanyon LE (2002): The effect of in vivo mechanical loading on estrogen receptor alpha expression in rat ulnar osteocytes. J Bone Miner Res 17:1646-55.

Estes BT, Gimble JM, Guilak F (2004): Mechanical signals as regulators of stem cell fate. Curr Top Dev Biol 60:91-126.

Evrard C, Caron S, Rouget P (2004): Functional analysis of the NPDC-1 gene. Gene 343:153-63.

Frost HM (1992): Perspectives: bone's mechanical usage windows. Bone Miner 19:257-71.

Granet C, Vico AG, Alexandre C, Lafage-Proust MH (2002): MAP and src kinases control the induction of AP-1 members in response to changes in mechanical environment in osteoblastic cells. Cell Signal 14:679-88.

Hatori K, Sasano Y, Takahashi I, Kamakura S, Kagayama M, Sasaki K (2004): Osteoblasts and osteocytes express MMP2 and -8 and TIMP1, -2, and -3 along with extracellular matrix molecules during appositional bone formation. Anat Rec A Discov Mol Cell Evol Biol 277:262-71.

Hochberg Y, Benjamini Y (1990): More powerful procedures for multiple significance testing. Stat Med 9:811-8.

Imai S, Kaksonen M, Raulo E, Kinnunen T, Fages C, Meng X, Lakso M, Rauvala H (1998): Osteoblast recruitment and bone formation enhanced by cell matrix-associated heparin-binding growth-associated molecule (HB-GAM). J Cell Biol 143:1113-28.

Jain MK, Fujita KP, Hsieh CM, Endege WO, Sibinga NE, Yet SF, Kashiki S, Lee WS, Perrella MA, Haber E, Lee ME (1996): Molecular cloning and characterization of SmLIM, a developmentally regulated LIM protein preferentially expressed in aortic smooth muscle cells. J Biol Chem 271:10194-9.

Jain MK, Kashiki S, Hsieh CM, Layne MD, Yet SF, Sibinga NE, Chin MT, Feinberg MW, Woo I, Maas RL, Haber E, Lee ME (1998): Embryonic expression suggests an important role for CRP2/SmLIM in the developing cardiovascular system. Circ Res 83:980-5.

Kapur S, Baylink DJ, Lau KH (2003): Fluid flow shear stress stimulates human osteoblast proliferation and differentiation through multiple interacting and competing signal transduction pathways. Bone 32:241-51.

Kesava CB, D.J.; Wergedal, J.E.; Mohan, S. (2004): Inbred mouse strains exhibit variations in the skeletal adaptive response to 4-point bending: evidence for involvement of different genetic mechanisms. J Bone Miner Res 19:S396.

Kodama Y, Dimai HP, Wergedal J, Sheng M, Malpe R, Kutilek S, Beamer W, Donahue LR, Rosen C, Baylink DJ, Farley J (1999): Cortical tibial bone volume in two strains of mice: effects of sciatic neurectomy and genetic regulation of bone response to mechanical loading. Bone 25:183-90.

Kodama Y, Umemura Y, Nagasawa S, Beamer WG, Donahue LR, Rosen CR, Baylink DJ, Farley JR (2000): Exercise and mechanical loading increase periosteal bone formation and whole bone strength in C57BL/6J mice but not in C3H/Hej mice. Calcif Tissue Int 66:298-306.

Madisen L, Neubauer M, Plowman G, Rosen D, Segarini P, Dasch J, Thompson A, Ziman J, Bentz H, Purchio AF (1990): Molecular cloning of a novel bone-forming compound: osteoinductive factor. DNA Cell Biol 9:303-9.

Marie PJ, Hott M, Perheentupa J (1990): Effects of epidermal growth factor on bone formation and resorption in vivo. Am J Physiol 258:E275-81.

Nikitin A, Egorov S, Daraselia N, Mazo I (2003): Pathway studio--the analysis and navigation of molecular networks. Bioinformatics 19:2155-7.

Noble BS, Peet N, Stevens HY, Brabbs A, Mosley JR, Reilly GC, Reeve J, Skerry TM, Lanyon LE (2003): Mechanical loading: biphasic osteocyte survival and targeting of osteoclasts for bone destruction in rat cortical bone. Am J Physiol Cell Physiol 284:C934-43.

Park JM, Adam RM, Peters CA, Guthrie PD, Sun Z, Klagsbrun M, Freeman MR (1999): AP-1 mediates stretch-induced expression of HB-EGF in bladder smooth muscle cells. Am J Physiol 277:C294-301.

Park JM, Borer JG, Freeman MR, Peters CA (1998): Stretch activates heparin-binding EGF-like growth factor expression in bladder smooth muscle cells. Am J Physiol 275:C1247-54.

Pedersen EA, Akhter MP, Cullen DM, Kimmel DB, Recker RR (1999): Bone response to in vivo mechanical loading in C3H/HeJ mice. Calcif Tissue Int 65:41-6.

Pines A, Romanello M, Cesaratto L, Damante G, Moro L, D'Andrea P, Tell G (2003): Extracellular ATP stimulates the early growth response protein 1 (Egr-1) via a protein kinase C-dependent pathway in the human osteoblastic HOBIT cell line. Biochem J 373:815-24.

Ponik SM, Pavalko FM (2004): Formation of focal adhesions on fibronectin promotes fluid shear stress induction of COX-2 and PGE2 release in MC3T3-E1 osteoblasts. J Appl Physiol 97:135-42.

Preisinger E, Alacamlioglu Y, Pils K, Saradeth T, Schneider B (1995): Therapeutic exercise in the prevention of bone loss. A controlled trial with women after menopause. Am J Phys Med Rehabil 74:120-3.

Raab-Cullen DM, Akhter MP, Kimmel DB, Recker RR (1994a): Periosteal bone formation stimulated by externally induced bending strains. J Bone Miner Res 9:1143-52.

Raab-Cullen DM, Thiede MA, Petersen DN, Kimmel DB, Recker RR (1994b): Mechanical loading stimulates rapid changes in periosteal gene expression. Calcif Tissue Int 55:473-8.

Rittweger J, Frost HM, Schiessl H, Ohshima H, Alkner B, Tesch P, Felsenberg D (2005): Muscle atrophy and bone loss after 90 days' bed rest and the effects of flywheel resistive exercise and pamidronate: Results from the LTBR study. Bone.

Robling AG, Li J, Shultz KL, Beamer WG, Turner CH (2003): Evidence for a skeletal mechanosensitivity gene on mouse chromosome 4. Faseb J 17:324-6.

Robling AG, Turner CH (2002): Mechanotransduction in bone: genetic effects on mechanosensitivity in mice. Bone 31:562-9.

Schmalbach CE, Chepeha DB, Giordano TJ, Rubin MA, Teknos TN, Bradford CR, Wolf GT, Kuick R, Misek DE, Trask DK, Hanash S (2004): Molecular profiling and the identification of genes associated with metastatic oral cavity/pharynx squamous cell carcinoma. Arch Otolaryngol Head Neck Surg 130:295-302.

Segev O, Samach A, Faerman A, Kalinski H, Beiman M, Gelfand A, Turam H, Boguslavsky S, Moshayov A, Gottlieb H, Kazanov E, Nevo Z, Robinson D, Skaliter R, Einat P, Binderman I, Feinstein E (2004): CMF608-a novel mechanical strain-induced bone-specific protein expressed in early osteochondroprogenitor cells. Bone 34:246-60.

Shay-Salit A, Shushy M, Wolfovitz E, Yahav H, Breviario F, Dejana E, Resnick N (2002): VEGF receptor 2 and the adherens junction as a mechanical transducer in vascular endothelial cells. Proc Natl Acad Sci U S A 99:9462-7.

Sibonga JD, Zhang M, Evans GL, Westerlind KC, Cavolina JM, Morey-Holton E, Turner RT (2000): Effects of spaceflight and simulated weightlessness on longitudinal bone growth. Bone 27:535-40.

Sommarin Y, Wendel M, Shen Z, Hellman U, Heinegard D (1998): Osteoadherin, a cell-binding keratan sulfate proteoglycan in bone, belongs to the family of leucine-rich repeat proteins of the extracellular matrix. J Biol Chem 273:16723-9.

Strausberg RL, Feingold EA, Grouse LH, Derge JG, Klausner RD, Collins FS, Wagner L, Shenmen CM, Schuler GD, Altschul SF, Zeeberg B, Buetow KH, Schaefer CF, Bhat NK,

Hopkins RF, Jordan H, Moore T, Max SI, Wang J, Hsieh F, Diatchenko L, Marusina K, Farmer AA, Rubin GM, Hong L, Stapleton M, Soares MB, Bonaldo MF, Casavant TL, Scheetz TE, Brownstein MJ, Usdin TB, Toshiyuki S, Carninci P, Prange C, Raha SS, Loquellano NA, Peters GJ, Abramson RD, Mullahy SJ, Bosak SA, McEwan PJ, McKernan KJ, Malek JA, Gunaratne PH, Richards S, Worley KC, Hale S, Garcia AM, Gay LJ, Hulyk SW, Villalon DK, Muzny DM, Sodergren EJ, Lu X, Gibbs RA, Fahey J, Helton E, Ketteman M, Madan A, Rodrigues S, Sanchez A, Whiting M, Young AC, Shevchenko Y, Bouffard GG, Blakesley RW, Touchman JW, Green ED, Dickson MC, Rodriguez AC, Grimwood J, Schmutz J, Myers RM, Butterfield YS, Krzywinski MI, Skalska U, Smailus DE, Schnerch A, Schein JE, Jones SJ, Marra MA (2002): Generation and initial analysis of more than 15,000 full-length human and mouse cDNA sequences. Proc Natl Acad Sci U S A 99:16899-903.

Swartz MA, Tschumperlin DJ, Kamm RD, Drazen JM (2001): Mechanical stress is communicated between different cell types to elicit matrix remodeling. Proc Natl Acad Sci U S A 98:6180-5.

Tanaka SM, Alam IM, Turner CH (2003): Stochastic resonance in osteogenic response to mechanical loading. Faseb J 17:313-4.

Tare RS, Oreffo RO, Clarke NM, Roach HI (2002): Pleiotrophin/Osteoblast-stimulating factor 1: dissecting its diverse functions in bone formation. J Bone Miner Res 17:2009-20.

Torrance AG, Mosley JR, Suswillo RF, Lanyon LE (1994): Noninvasive loading of the rat ulna in vivo induces a strain-related modeling response uncomplicated by trauma or periostal pressure. Calcif Tissue Int 54:241-7.

Wang Y, Fraefel C, Protasi F, Moore RA, Fessenden JD, Pessah IN, DiFrancesco A, Breakefield X, Allen PD (2000): HSV-1 amplicon vectors are a highly efficient gene delivery system for skeletal muscle myoblasts and myotubes. Am J Physiol Cell Physiol 278:C619-26.

Weyts FA, Li YS, van Leeuwen J, Weinans H, Chien S (2002): ERK activation and alpha v beta 3 integrin signaling through Shc recruitment in response to mechanical stimulation in human osteoblasts. J Cell Biochem 87:85-92.

Workman C, Jensen LJ, Jarmer H, Berka R, Gautier L, Nielser HB, Saxild HH, Nielsen C, Brunak S, Knudsen S (2002): A new non-linear normalization method for reducing variability in DNA microarray experiments. Genome Biol 3:research0048.

Wu MX (2003): Roles of the stress-induced gene IEX-1 in regulation of cell death and oncogenesis. Apoptosis 8:11-8.

Yamazaki S, Ichimura S, Iwamoto J, Takeda T, Toyama Y (2004): Effect of walking exercise on bone metabolism in postmenopausal women with osteopenia/osteoporosis. J Bone Miner Metab 22:500-8.

Yang W, Lu Y, Kalajzic I, Guo D, Harris MA, Gluhak-Heinrich J, Kotha S, Bonewald LF, Feng JQ, Rowe DW, Turner CH, Robling AG, Harris SE (2005): Dentin matrix protein 1 gene cis-regulation: Use In osteocytes to characterize local responses to mechanical loading in vitro and In vivo. J Biol Chem.

Yang X, Tare RS, Partridge KA, Roach HI, Clarke NM, Howdle SM, Shakesheff KM, Oreffo RO (2003): Induction of human osteoprogenitor chemotaxis, proliferation, differentiation, and bone formation by osteoblast stimulating factor-1/pleiotrophin: osteoconductive biomimetic scaffolds for tissue engineering. J Bone Miner Res 18:47-57.

Table 1. Functional categories of selected genes that show expression changes of two-fold (log value) or greater with P value ≤ 0.01 in loaded bones compared to unloaded bones. The genes with fold changes less than 0.5 are identified as down-regulated genes. GenBank accession numbers, chromosomal locations and statistical significance are also listed.

Table 1. Functional categories of selected genes differentially expressed in mechanically loaded bones

Gene	Access No	Description	Change	P Value	Location
Cell Growth/Differentiation					
Ptn	AK011346	Pleiotrophin	4.29	0.0006	6
Ogn	AK014259	Osteoglycin	2.47	0.0040	13
Itm2a	NM_008409	Integral membrane protein 2A	2.85	0.0031	X
Emp1	BC034257	Epithelial membrane protein 1	2.56	0.0015	6
Lepre1	NM_019783	Leprecan 1	2.46	0.0012	4
Tgfbi	XM_122567	Transforming growth factor, beta induced, 68 kDa	2.26	0.0026	13
Pdgfrl	NM_026840	Platelet-derived growth factor receptor-like	2.18	0.0026	13
Morf4l2	NM_019768	Mortality factor 4 like 2	2.04	0.0057	X
Csrp2	NM_007792	Cysteine and glycine-rich protein 2	4.12	0.0013	10 D1
Akr1b7	AK002705	Aldo-keto reductase family 1, member B7	4.72	0.0018	6
Ephb2	BM231330	Eph receptor B2	2.54	0.0048	4 D3
Npdc1	NM_008721	Neural proliferation, differentiation and control gene 1	2.24	0.0093	2 A3
Cell Adhesion					

Col5a1	NM_015734	Procollagen, type V, alpha 1	1.97	0.0011	2
Col6a3	BC005491	Procollagen, type VI, alpha 3	3.36	0.0030	1
Col8a1	NM_007739	Procollagen, type VIII, alpha 1	2.56	0.0018	16 C1
Col14a1	XM_127997	Procollagen, type XIV, alpha 1	2.37	0.0026	15
Col18a1	BC008227	Procollagen, type XVIII, alpha 1	3.40	0.0020	10
PCDH19	XM_033173	Protocadherin 19	2.28	0.0092	X
Lamb1-1	XM_126863	Laminin B1 subunit 1	2.69	0.0011	12
Nid1	NM_010917	Nidogen 1	1.99	0.0042	13
Nrp	AK011144	Neuropilin (an alternate receptor for VEGF-A)	2.13	0.0028	8
ESTs	NM_172399	A930038C07Rik (Fibronectin, type III domain)	2.06	0.0019	6
Fn	XM_129845	Fibronectin receptor	2.58	0.0012	1
Matn2	NM_016762	Mus musculus matrilin 2	2.76	0.0012	15
Loxl3	NM_013586	Lysyl oxidase-like 3	2.14	0.0021	6
Lox	NM_010728	Lysyl oxidase (hydroxylysine residues in collagens)	3.25	0.0042	18
Cell Death					
Gas1	NM_008086	Growth arrest specific 1	2.26	0.0015	13
Bok	BC030069	Bcl-2-related ovarian killer protein	2.48	0.0015	1 D
C1qtnf6	NM_028331	C1q and tumor necrosis factor related protein 6	2.11	0.0015	15 E1
Proteolysis					
Mest	NM_008590	Mesoderm specific transcript	3.05	0.0011	6
Lgmn	NM_011175	Legumain	3.25	0.0030	12 E
Timp1	NM_011593	Tissue inhibitor of metalloproteinase 1	2.46	0.0032	X
Pcolce	NM_008788	Procollagen C-proteinase enhancer protein	2.15	0.0086	5

Serpinb6	NM_009254	Serine (or cysteine) proteinase inhibitor, clade B, member 6a	1.97	0.0039	13
EST	NM_028072	2010004N24Rik (heparin-degrading endosulfatases)	1.95	0.0040	2
Signal Transduction					
Semcap3	NM_018884	SemaF cytoplasmic domain associated protein 3	1.98	0.0023	6
Pdgfrb	NM_008809	Platelet derived growth factor receptor, beta polypeptide	1.97	0.0082	18
EPS8	BC030010	Epidermal growth factor receptor pathway substrate 8	1.98	0.0043	6
Gpr124	NM_054044	Adhesion G protein-coupled receptor 124	1.98	0.0015	8
Entpd2	NM_009849	Ectonucleoside triphosphate diphosphohydrolase 2	2.01	0.0029	2 A3
Scgn10	AK003659	superiorcervical ganglia, neural specific 10 (stathmin-like 2)	2.06	0.0023	3
Dcamkl1	BE824672	Double cortin and calcium/calmodulin-dependent protein kinase-like 1	3.80	0.0038	3
Ania4	NM_021584	Activity and neurotransmitter-induced early gene, similar to CaM-Kinase	2.87	0.0025	Y
Ednrb	AE014177	Endothelin receptor type B	2.91	0.0063	14
Nek6	NM_021606	NIMA (never in mitosis gene a)-related expressed kinase 6	2.14	0.0014	2
Calu	NM_007594	Calumenin (Calmodulin and related proteins, cacium binding)	2.05	0.0100	6
Rcn	NM_009037	Reticulocalbin (Calmodulin and related proteins, cacium binding)	2.31	0.0037	2
D7Ertd671e	XM_133470	DNA segment, Chr 7,Ca2+-binding protein	2.02	0.0023	7
Fstl	NM_008047	Follistatin-like	3.10	0.0018	16
Tax1bp3	NM_029564	Tax1 (human T-cell leukemia virus type I) binding protein 3 (PDZ domain)	1.97	0.0018	11
Il13ra1	NM_133990	Interleukin 13 receptor, alpha 1	2.42	0.0060	X
Ccr5	XM_135269	Similar to C-C chemokine receptor 5, (rhodopsin family)	2.35	0.0015	9 F4
Igsf10	AK018323	Immunoglobulin superfamily, member 10	2.20	0.0020	3D
Transcription Regulation					

Gsc	NM_010351	Goosecoid	2.30	0.0048	12
Ankrd1	BC037138	Ankyrin repeat domain 1 (cardiac muscle)	2.26	0.0099	19 C2
Gli5	BC021517	GLI-Kruppel family member GLI5		0.0094	16
Maged1	NM_019791	Melanoma antigen, family D, 1	2.33	0.0012	X
Mkrn1	NM_018810	Makorin, ring finger protein, 1	0.45	0.0008	6 B1
Heat Shock Proteins					
Hsp25	NM_013560	Heat shock protein, 25 kDa	2.15	0.0062	5
Serpinh1	NM_009825	Serine (or cysteine) proteinase inhibitor, clade H, member 1 (Hsp47)	2.72	0.0023	7 E1
Cytoskeleton Movement					
Tnnt2	NM_011619	Troponin T2, cardiac	3.03	0.0006	1
Cald1	BC015839	Caldesmon 1	2.11	0.0040	7q33
ESTs	NM_023716	2410129E14Rik (tubulin, beta)	2.75	0.0026	13
Tuba1	NM_011653	Tubulin, alpha 1	2.40	0.0006	15
Acta2	NM_007392	Actin, alpha 2, smooth muscle, aorta	1.97	0.0015	19
S100a10	NM_009112	S100 calcium binding protein A10 (calpactin)	2.00	0.0050	3
ESTs	NM_026473	2310057H16Rik (tubulin)	4.69	0.0014	18 E1
Transport					
AI173274	NM_134090	Mus musculus expressed sequence AI173274, mRN	2.33	0.0008	15 E1
Sec23a	AY082671	SEC23A	2.31	0.0039	12
P4hb	XM_126743	PDI, Thbp, ERp59; protein disulfide isomerase;	2.29	0.0017	11 80.0 cM
Slc35f5	NM_028787	Solute carrier family 35, member F5	2.11	0.0057	1

Prl	BC024613	Protein distantly related to to the gamma subunit family	1.97	0.0100	1
Other					
Scr59	BC023432	Spermatogenesis associated, serine-rich 2	2.03	0.0065	15 F1
Ppfibp1	BC035209	PTPRF interacting protein, binding protein 1	2.18	0.0045	6 G3
Fkbp9	NM_012056	FK506 binding protein 9	2.15	0.0015	6
Scd2	NM_009128	Stearoyl-Coenzyme A desaturase 2	2.56	0.0025	19
P37nb	XM_131917	Mus musculus 37 kDa leucine-rich repeat (LRR) protein	3.67	0.0040	5
Fer-1-like 3	XM_148914	RIKEN cDNA 2310051D19 gene, similar to myoferlin isoform b	2.64	0.0039	19
Spon2	NM_133903	Spondin 2, extracellular matrix protein	2.46	0.0012	5
Fkbp11	NM_024169	FK506 binding protein 11 (protein turnover, chaperones)	1.98	0.0080	15
Ms4a6d	NM_026835	Membrane-spanning 4-domains, subfamily A, member 6D	1.96	0.0026	19
Rhced	AF057524	Rhesus blood group CE and D	0.49	0.0052	4
ESTs	BG071710	Mus musculus cDNA clone H3102C09 3', mRNA sequence	0.48	0.0060	9
ESTs	BG071952	Mus musculus cDNA clone H3105A09 3', mRNA sequence	0.43	0.0060	?
ESTs	BG074055	Mus musculus cDNA clone H3130C11 3', mRNA sequence	0.47	0.0047	7
Unknown	BG072471	Mus musculus cDNA clone H3110H06 3', mRNA sequence	0.49	0.0045	3

Legend

Figure 1. Biological functions of the 346 genes differentially regulated between the loaded and unloaded bones. Other selections represent genes involved in protein modification, chaperoning pathways, extracellular matrix biogenesis, hemostasis, metabolism and development. A total of 157 genes/ESTs are yet to be characterized.

Figure 2. Comparison of fold changes in expression for selected genes by microarray and real-time PCR. The results of real-time PCR were normalized to the expression of β-2 microglobulin (β2M) in each sample, and expressed as fold change of the loaded sample over the expression level of the unloaded sample. The data shown are means ± S.D. from 5 replicates. Ptn: pleiotrophin; Ogn: osteoglycin; Lgmn: legumain; IER3: immediate early response gene 3; Npdc1: neural proliferation, differentiation and control gene 1. * represents $P<0.01$ for loaded bones vs. unloaded bones.

Figure 3. Schematic representation of direct biological association of differentially expressed genes involved in bone remodeling. Analysis of a direct biological association of differentially expressed genes is performed using PathwayAssist 2.53 software (Stratagene, La Jolla, CA). Biologically linked proteins indicated by nodes and biological processes are shown in the diagram. An open node represents a gene that is down-regulated in the loaded bones compared to unloaded controls. Solid nodes are genes that are up-regulated in the loaded bones compared to unloaded controls.

Supplementary data. These genes are defined as differentially expressed genes on the basis of our criteria as described in "Materials and Methods" (e.g. relative expression level ≥1.5-fold change, $P<0.01$ with "Benjamini and Hochberg" Multiple Testing

Correction). Fold change of log value presented here is the ratio of gene expression level in the loaded bones to the unloaded controls.

Fig1

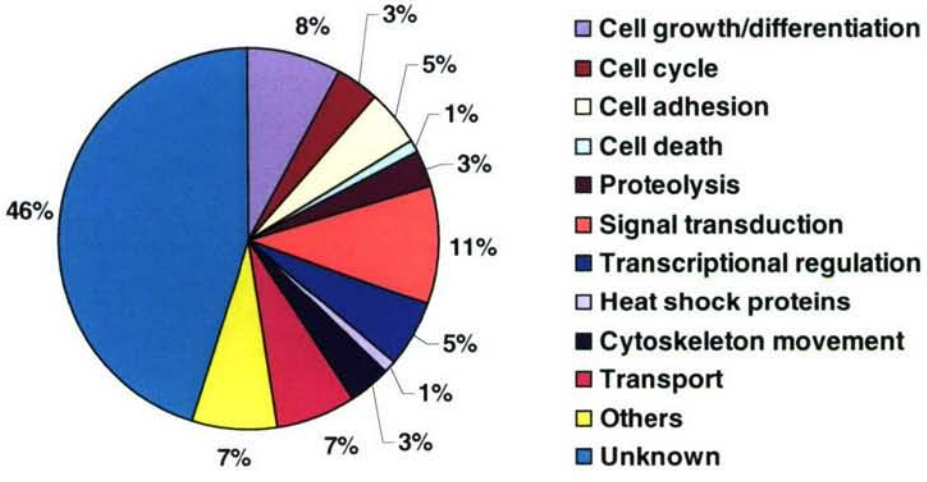
8%
3%
5%
1%
3%
11%
5%
1%
3%
7%
7%
46%
Cell growth/differentiation
Cell cycle
Cell adhesion
Cell death
Proteolysis
Signal transduction
Transcriptional regulation
Heat shock proteins
Cytoskeleton movement
Transport
Others
Unknown

Fig2

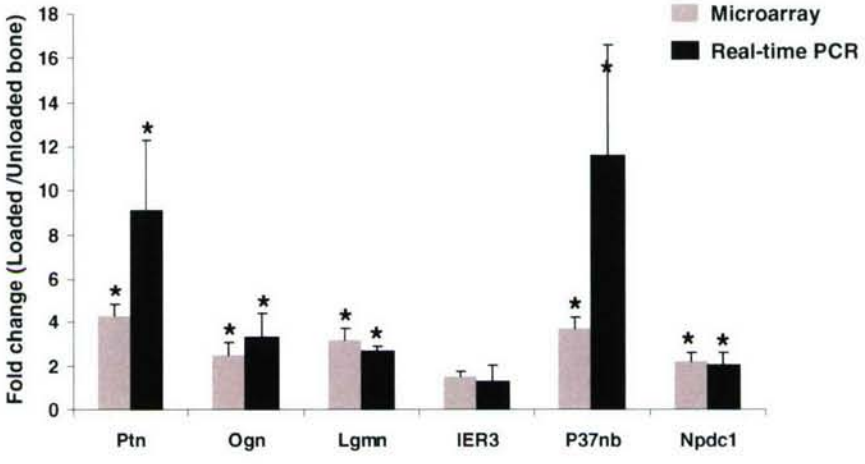
Microarray
Real-time PCR
Fold change (Loaded /Unloaded bone)
18
16
14
12
10
8
6
4
2
0
Ptn
Ogn
Lgmn
IER3
P37nb
Npdc1

Fig3

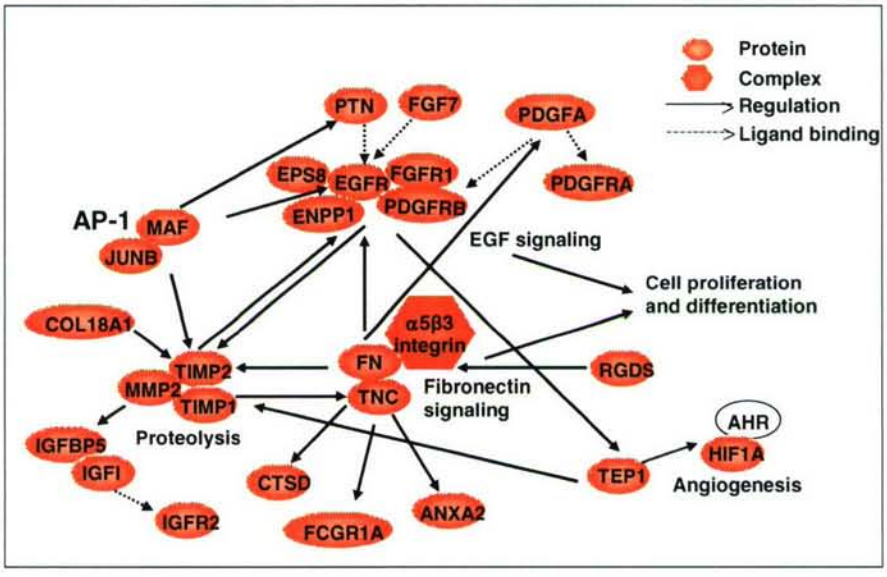
Protein
Complex
Regulation
Ligand binding
PTN
FGF7
PDGFA
EPS8
EGFR
FGFR1
PDGFRA
ENPP1
PDGFRB
AP-1
MAF
JUNB
EGF signaling
Cell proliferation
and differentiation
COL18A1
α5β3
integrin
FN
TIMP2
RGDS
MMP2
TIMP1
TNC
Fibronectin
signaling
AHR
IGFBP5
Proteolysis
HIF1A
IGFI
CTSD
TEP1
Angiogenesis
IGFR2
FCGR1A
ANXA2

Gene Symbol	GenBank Ac	Description	Fold change	P value (MTC)
8430410K20Rik	AK020232	RIKEN cDNA 8430410K20 gene	1.621 (1.341 to 2.158)	0.0100
Igf2r	AK053045	Insulin-like growth factor 2 receptor	1.659 (1.239 to 2.038)	0.0100
B230217N24Rik	AK005396	Microsomal stress 70 protein ATPase core homolog	1.704 (1.373 to 2.361)	0.0100
1110031B06Rik	AK002329	RIKEN cDNA 1110031B06 gene	1.536 (1.32 to 2.051)	0.0100
Prl	AK002424	Clone MGC:25884 IMAGE:4215775	1.969 (1.522 to 3.013)	0.0100
Calu	NM_007594	Calumenin	2.052 (1.413 to 2.84)	0.0100
2310075E07Rik	AK010169	RIKEN cDNA 2310075E07 gene	1.942 (1.41 to 2.71)	0.0099
G431001E03Rik	AK089330	Similar to BA541N10.2 (novel protein) (Fragment)	1.516 (1.282 to 2.024)	0.0099
ADAM	AU020942	Disintegrin and metalloproteinase domain 9	1.537 (1.261 to 1.924)	0.0099
Ankrd1	AK009655	Cardiac responsive adriamycin protein	2.261 (1.573 to 3.689)	0.0099
Mpp6	BG075893	C membrane protein, palmitoylated 6	1.782 (1.265 to 2.238)	0.0095
Basp1	AK011545	22 kDa neural tissue-enriched acidic protein homolog	1.623 (1.204 to 2.016)	0.0094
Gli5	NM_031184	GLI-Kruppel family member GLI5	2.028 (1.402 to 2.763)	0.0094
Nab2	AK034709	Ngfi-A binding protein 2	1.526 (1.127 to 1.717)	0.0094
MAF	AK019255	Avian musculoaponeurotic fibrosarcoma (v-maf)	1.806 (1.397 to 2.356)	0.0093
Npdc1	NM_008721	Neural proliferation, differentiation and control gene 1	2.244 (1.56 to 3.097)	0.0093
Enpp1	AK029600	Ectonucleotide pyrophosphatase/phosphodiesterase 1	1.745 (1.359 to 2.203)	0.0093
4732495E13Rik	AK028196	Similar to chromosome 22 open reading frame 5	1.751 (1.364 to 2.24)	0.0092
PCDH19	AK028278	Similar to: Homo sapiens protocadherin 19	2.281 (1.563 to 3.214)	0.0092
Wnt2	AK012093	Wingless-related MMTV integration site 2	1.937 (1.451 to 2.67)	0.0092
5031439A09Rik	AK019886	RIKEN cDNA 5031439A09 gene	1.917 (1.467 to 2.636)	0.0092
P4ha1	AK030574	Prolyl 4-hydroxylase alpha-1 subunit precursor	1.783 (1.403 to 2.548)	0.0091
Cryac	AK005052	Crystallin, alpha C	1.592 (1.288 to 2.144)	0.0090
Uxs1	AK005536	UDP glucuronic acid	1.878 (1.551 to 2.679)	0.0089
Mod1	AK004980	Malic enzyme, supernatant	1.678 (1.327 to 2.2)	0.0088
Nsg1	AK076451	Neuron specific gene family member 1	1.62 (1.325 to 2.04)	0.0086
Pcolce	NM_008788	Procollagen C-proteinase enhancer protein	2.152 (1.474 to 3.233)	0.0086
Lmna	AK003174	lamin A	1.711 (1.306 to 2.154)	0.0086

Ms4a6b	AK007613	Membrane-spanning 4-domains, subfamily A, member 6B	1.852 (1.469 to 2.79)	0.0086
1700007D05Rik	AK005698	RIKEN cDNA 1700007D05 gene	2.392 (1.503 to 3.373)	0.0086
Sgk	AK043284	Serum/glucocorticoid regulated kinase	1.864 (1.368 to 2.459)	0.0084
Odz3	AK011778	Odd Oz/ten-m homolog 3	1.635 (1.364 to 2.079)	0.0084
D7Wsu86e	AK002742	Expressed sequence on chromosome 7	1.865 (1.362 to 2.348)	0.0083
Anxa8	AK009085	Annexin A8	1.838 (1.481 to 2.516)	0.0083
PFTK1	AK016370	PFTAIRE protein kinase 1	1.586 (1.396 to 2.173)	0.0083
Tcf4	AK014343	Transcription factor 4 (Tcf4)	1.711 (1.391 to 2.379)	0.0083
5730525G14Rik	AK011151	RIKEN cDNA 5730525G14 gene	1.558 (1.268 to 1.971)	0.0082
D15Wsu59e	AK010256	Expressed sequence on chromosome 15	1.541 (1.297 to 1.847)	0.0082
Pdgfrb	AK048486	Platelet derived growth factor receptor, beta polypeptide	1.968 (1.566 to 2.829)	0.0082
Tc10	NM_145491	Ras-like protein	1.611 (1.231 to 2.019)	0.0082
Fgl2	AK009500	Fibrinogen-like protein 2	1.603 (1.358 to 2.111)	0.0082
MGC38539	AK050076	Hypothetical protein MGC38539	1.532 (1.26 to 1.818)	0.0082
D15Ertd366e	BG075908	ERATO Doi 366, expressed on chromosome 15	1.542 (1.223 to 1.824)	0.0080
Des	XM_129882	Desmin	1.502 (1.238 to 1.851)	0.0080
Fkbp11	AK003331	FK506 binding protein 11	1.98 (1.467 to 2.984)	0.0080
Dag1	AK036174	Dystroglycan precursor	1.633 (1.228 to 1.964)	0.0080
MGC37634	NM_145978	Hypothetical protein MGC37634	1.543 (1.287 to 1.931)	0.0080
Cbr2	AK081816	Carbonyl reductase 2	1.782 (1.461 to 2.398)	0.0080
2400003B06Rik	AK010259	RIKEN cDNA 2400003B06 gene	2.068 (1.673 to 3.341)	0.0080
AI643885	AK030762	Large neutral amino acids transporter small subunit	1.548 (1.292 to 1.908)	0.0079
2610311I19Rik	AK007671	RIKEN cDNA 2610311I19 gene	1.743 (1.494 to 2.505)	0.0079
Cai	AK028292	Calcium binding protein, intestinal	1.914 (1.513 to 2.751)	0.0078
Grcb	NM_013534	Gene rich cluster, B gene	1.73 (1.41 to 2.153)	0.0077
0610007N19Rik	AK002304	RIKEN cDNA 0610007N19 gene	1.703 (1.283 to 2.07)	0.0077
Plod2	AK033363	Procollagen lysine, 2-oxoglutarate 5-dioxygenase 2	1.713 (1.394 to 2.354)	0.0077
AW548221	AK019185	Expressed sequence AW548221	1.561 (1.294 to 1.912)	0.0076
Madh1	AK017583	MAD homolog 1	1.67 (1.4 to 2.268)	0.0076
Msr2	AK034125	Macrophage scavenger receptor 2	1.908 (1.34 to 2.523)	0.0076

Eppb9	AK003038	Endothelial precursor protein B9	1.79 (1.433 to 2.429)	0.0075
Nedd4	AK051013	Neural precursor cell expressed, down-regulted gene 4	1.545 (1.253 to 1.856)	0.0073
Ndr4	AK090374	N-myc downstream regulated 4	1.919 (1.49 to 2.546)	0.0071
Zfp52	BG071037	Similar to Zinc finger protein 118	1.761 (1.305 to 2.181)	0.0070
Pdgfra	AK011378	Platelet derived growth factor receptor, alpha polypeptide	1.761 (1.241 to 2.073)	0.0070
Pdk4	AK004543	Pyruvate dehydrogenase kinase, isoenzyme 4	1.618 (1.411 to 2.147)	0.0066
Fcgr1a	AK033874	Fc receptor, IgG, high affinity I	1.757 (1.346 to 2.215)	0.0066
Kdt1	AK040675	HIC protein isoform	1.842 (1.484 to 2.556)	0.0066
Timp2	AK032818	Tissue inhibitor of metalloproteinase 2	1.773 (1.486 to 2.456)	0.0066
2310004K20Rik	AK075863	Differentially expressed sequence	1.862 (1.339 to 2.368)	0.0066
Arl6	AK003778	ADP-ribosylation-like 6	1.923 (1.559 to 2.625)	0.0066
Scr59	AK012237	Serine-rich spermatocytes and round spermatid protein	2.033 (1.427 to 2.696)	0.0065
Ryk	AK076449	Tyrosine-protein kinase RYK precursor	1.645 (1.284 to 1.981)	0.0064
8030445B08Rik	AK031762	Smad ubiquitination regulatory facotr 1	1.519 (1.353 to 1.892)	0.0064
Unknown	BM240601	Unknown	1.631 (1.348 to 1.918)	0.0064
Unknown	BM224845	Unknown	1.777 (1.448 to 2.408)	0.0064
Chl1	AK036295	Close homolog of L1	1.687 (1.253 to 1.928)	0.0064
2310047C17Rik	AK003448	Neuroblast differentiation associated protein AHNAK	1.577 (1.315 to 1.968)	0.0064
Sdnsf	AK033139	Neural stem cell derived neuronal survival protein	1.68 (1.358 to 2.204)	0.0064
MGC38046	AK078473	Hypothetical protein MGC38046	1.682 (1.436 to 2.19)	0.0064
Adamts4	AK028364	Disintegrin and metalloproteinase with thrombospondin motif	1.665 (1.4 to 2.192)	0.0063
ET-B	AK076426	Endothelin receptor type B	2.908 (1.57 to 3.866)	0.0063
Hsp25	AK003119	Heat shock protein, 25 kDa	2.15 (1.668 to 3.24)	0.0062
Il13ra1	AA408993	Interleukin 13 receptor, alpha 1	2.424 (1.781 to 3.437)	0.0060
Sara	AK003538	SAR1a gene homolog	1.529 (1.301 to 1.796)	0.0060
Chsy1	XM_194358	Chondroitin	1.675 (1.386 to 2.069)	0.0060
C1qc	NM_007574	Complement component 1, q subcomponent, c polypeptide	1.627 (1.241 to 1.918)	0.0060
Unknown	BM221100	Unknown	1.612 (1.269 to 1.936)	0.0059
Dkk2	AK028225	Dickkopf homolog 1	1.7 (1.348 to 2.184)	0.0058
Morf4l2	AK075946	MORF-related gene X	2.037 (1.657 to 2.965)	0.0057

Tcf12	AK078415	Transcription factor 12	1.52 (1.291 to 1.873)	0.0057
Slc35f5	AK004892	Solute carrier family 35, member F5	2.114 (1.695 to 3.071)	0.0057
1110020H15Rik	AK003861	RIKEN cDNA 1110020H15 gene	1.667 (1.277 to 1.869)	0.0057
Hspa5	AK004578	Heat shock 70kD protein 5 (glucose-regulated protein, 78kD)	1.5 (1.256 to 1.716)	0.0056
Bicc1	BM217996	Bicaudal C homolog 1	1.788 (1.528 to 2.427)	0.0054
1500032M01Rik	AK050347	Similar to I-beta1,3-N-acetylglucosaminyltransferase	1.527 (1.293 to 1.766)	0.0050
S100a10	NM_009112	S100 calcium binding protein A10 (calpactin)	2.002 (1.392 to 2.399)	0.0050
C730009O10Rik	AK020440	Unknown	1.548 (1.33 to 1.851)	0.0048
Mrc2	AK028157	Mannose receptor, C type 2	1.827 (1.332 to 2.187)	0.0048
Gsc	NM_010351	Goosecoid	2.302 (1.689 to 3.245)	0.0048
2610319K07Rik	AK012054	RIKEN cDNA 2610319K07 gene	1.886 (1.48 to 2.547)	0.0048
Ephb2	AK017630	Ephrin type B receptor 2 precursor	2.543 (1.767 to 3.659)	0.0048
2010209O12Rik	AK008483	RIKEN cDNA 2010209O12 gene	1.718 (1.498 to 2.26)	0.0047
AL024221	AK051349	Expressed sequence AL024221	2.008 (1.624 to 2.663)	0.0047
Col4a2	AK053858	Collagen alpha 2(IV) chain precursor	1.536 (1.268 to 1.812)	0.0047
Ppfibp1	AK003318	PTPRF interacting protein, binding protein 1 (liprin beta 1)	2.176 (1.825 to 3.039)	0.0045
Tsp10	AK030225	Tumor suppressor region 10	1.512 (1.249 to 1.757)	0.0045
AI467484	AK039170	Unknown, LOC226570	1.661 (1.393 to 2.033)	0.0045
2300006M17Rik	AK009034	RIKEN cDNA 2300006M17 gene	1.916 (1.529 to 2.616)	0.0045
Junb	AK006748	Jun-B oncogene	1.671 (1.439 to 2.071)	0.0045
Tram1	AK007839	Tram protein translocating chin associating membrame	1.645 (1.334 to 1.888)	0.0045
5430428G01Rik	AK011733	RIKEN cDNA 5430428G01 gene	1.571 (1.284 to 1.77)	0.0045
Man2a1	AK081775	Mannosidase 2, alpha 1	1.681 (1.438 to 2.125)	0.0044
MGC28917	NM_144839	Hypothetical protein MGC28917	1.834 (1.432 to 2.264)	0.0044
Snx9	AK004449	Sorting nexin 9	1.552 (1.336 to 1.91)	0.0043
Eps8	NM_007945	Epidermal growth factor receptor pathway substrate 8	1.979 (1.459 to 2.564)	0.0043
Igfbp5	AK011683	Insulin-like growth factor binding protein 5	1.586 (1.375 to 1.86)	0.0043
Ptk9	AK077410	Protein tyrosine kinase 9	1.837 (1.564 to 2.463)	0.0042
Unknown	BM120575	Unknown	1.595 (1.387 to 1.935)	0.0042
1810029F08Rik	AK007640	RIKEN cDNA 1810029F08 gene	1.597 (1.401 to 1.982)	0.0042

Nid1	AK041633	Nidogen 1	1.991 (1.57 to 2.474)	0.0042
Lox	NM_010728	Lysyl oxidase	2.68 (1.706 to 3.397)	0.0042
Edg5	AK003144	G protein-coupled receptor EDG-1 like	1.535 (1.359 to 1.815)	0.0041
Unknown	AW542347	Hypothetical 11.0 kDa protein	1.668 (1.371 to 1.964)	0.0041
Ogn	AK014259	Osteoglycin	2.467 (1.728 to 3.357)	0.0040
Il17rl	AK075634	Interleukin 17 receptor-like	1.702 (1.511 to 2.204)	0.0040
AB041545	AK040165	Hypothetical protein	1.545 (1.248 to 1.706)	0.0040
Cald1	AK014755	Caldesmon	2.106 (1.714 to 2.911)	0.0040
2010004N24Rik	AK008108	RIKEN cDNA 2010004N24 gene	1.953 (1.608 to 2.617)	0.0040
Smoc2	AK006809	Secreted modular calcium binding protein 2	1.922 (1.598 to 2.618)	0.0040
AU018702	AK029923	Expressed sequence AU018702	1.565 (1.374 to 1.839)	0.0040
P37nb	BG072784	A 37 kDa leucine-rich repeat (LRR) protein	3.674 (2.582 to 6.443)	0.0040
Serpinb6	AK033731	Serine (or cysteine) proteinase inhibitor, clade B, member 6	1.969 (1.573 to 2.602)	0.0039
E130112L23Rik	AK053592	Unknown LOC268739	1.926 (1.513 to 2.358)	0.0039
Nfix	AK080940	Nuclear factor I/X	1.619 (1.359 to 1.969)	0.0039
Rgds	NM_009058	Ral guanine nucleotide dissociation stimulator	1.66 (1.367 to 1.971)	0.0039
Maoa	AK004337	Amine oxidase	1.578 (1.375 to 1.839)	0.0039
Ifi204	AK042872	Interferon activated gene 204	1.736 (1.442 to 2.13)	0.0039
Sec23a	AK028152	SEC23A	2.306 (1.961 to 3.33)	0.0039
Ubqln2	AK076159	Ubiquilin 2	1.517 (1.372 to 1.78)	0.0039
Fer-1-like 3	AK009153	Fer 1 like protein	2.643 (1.649 to 3.232)	0.0039
IGF-I	AK038119	Insulin-like growth factor 1	1.77 (1.57 to 1.968)	0.0038
Mmp23	NM_011985	Matrix metalloproteinase 23	1.819 (1.376 to 2.071)	0.0038
Dcamkl1	AK013421	Unknown U042427	2.867 (1.815 to 3.827)	0.0038
AA420407	AK036243	Expressed sequence AA420407	1.565 (1.398 to 1.906)	0.0038
Fabp5	AK008782	Fatty acid binding protein 5, epidermal	1.745 (1.493 to 2.196)	0.0038
Sgcb	AK009080	Sarcoglycan, beta (43kD dystrophin-associated glycoprotein)	1.935 (1.702 to 2.65)	0.0038
Adfp	AK002911	Adipose differentiation related protein	1.594 (1.411 to 1.919)	0.0038
Tm4sf8	AK006798	Transmembrane 4 superfamily member 8	1.744 (1.483 to 2.174)	0.0037
Rcn2	AK076153	Reticulocalbin 2	1.721 (1.535 to 2.2)	0.0037

AI838577	AK028767	Unknown	1.917 (1.459 to 2.211)	0.0036
Surf4	AK004691	Surfeit gene 4	2.106 (1.798 to 2.312)	0.0036
8030486F04Rik	AK013118	RIKEN cDNA 8030486F04 gene	1.735 (1.413 to 2.008)	0.0036
AI645720	AK076953	Similar to hypothetical protein FLJ11807	1.774 (1.546 to 2.258)	0.0036
Trim47	BG065693	Tripartite motif protein 47	1.703 (1.454 to 1.959)	0.0035
Tnc	AK040167	Tenascin C	1.522 (1.324 to 1.776)	0.0035
Sart2	AK031737	Squamous cell carcinoma antigen regognized by T cell	2.242 (1.632 to 2.862)	0.0034
Unknown	BG069739	Unknown	1.865 (1.524 to 2.311)	0.0034
EIG180	NM_133237	Ethanol induced gene product EIG180	1.662 (1.363 to 1.974)	0.0034
Arf4	AK002302	ADP-ribosylation factor 4 (Arf4)	1.539 (1.284 to 1.735)	0.0034
Hif1a	AK008499	Hypoxia inducible factor 1, alpha subunit	1.534 (1.282 to 1.682)	0.0033
4930517K11Rik	AK005645	RIKEN cDNA 4930517K11 gene	2.59 (2.118 to 2.988)	0.0033
Cd34	AK044121	CD34 antigen	1.747 (1.447 to 2.029)	0.0033
Cbr1	AK003232	Carbonyl reductase 1	1.505 (1.328 to 1.721)	0.0033
8430408O15Rik	AK018399	RIKEN cDNA 8430408O15 gene	1.507 (1.341 to 1.694)	0.0033
Yap	NM_009534	Yes-associated protein, 65 kDa	1.579 (1.439 to 1.819)	0.0033
Timp1	NM_011593	Tissue inhibitor of metalloproteinase 1	2.459 (1.804 to 3.137)	0.0032
Itm2a	AK014024	Integral membrane protein 2A	2.85 (2.066 to 3.684)	0.0031
Dnajc3	AK004033	DnaJ (Hsp40) homolog, subfamily C, member 3	1.602 (1.372 to 1.806)	0.0031
Zac1	NM_009538	Zinc finger protein regulator of apoptosis and cell cycle arrest	1.722 (1.548 to 2.155)	0.0031
2310022A04Rik	AK007542	HTPAP homolog	1.947 (1.645 to 2.371)	0.0030
Col6a3	BM231452	Type VI collagen alpha 3 subunit	3.359 (2.62 to 4.895)	0.0030
Lgmn	NM_011175	Legumain (Lgmn)	3.245 (2.296 to 4.628)	0.0030
1700020L11Rik	AK005777	RIKEN cDNA 1700020L11 gene	1.811 (1.525 to 2.273)	0.0030
Mfge8	AK087555	Milk fat globule-EGF factor 8 protein	1.544 (1.382 to 1.835)	0.0030
Nox4	AK050371	NADPH oxidase 4	1.726 (1.464 to 2.091)	0.0030
Entpd2	AK002553	Ectonucleoside triphosphate diphosphohydrolase 2	2.007 (1.727 to 2.532)	0.0029
Sec61a	AK007696	SEC61, alpha subunit	1.785 (1.487 to 2.163)	0.0029
Nrp	AK002673	Neuropilin (Nrp)	2.128 (1.697 to 2.575)	0.0028
Tep1	AK087740	Telomerase associated protein 1	1.515 (1.335 to 1.716)	0.0028

Pdgfa	AK017169	Platelet derived growth factor, alpha	1.591 (1.463 to 1.917)	0.0028
Tgfbi	AK084431	Transforming growth factor, beta induced, 68 kDa	2.263 (1.794 to 2.769)	0.0026
Pdgfrl	AK004179	Platelet-derived growth factor receptor-like	2.176 (1.811 to 2.932)	0.0026
1110004G24Rik	AK003420	Ccell growth regulator	1.712 (1.447 to 2.046)	0.0026
Unknown	BG073324	Unknown	1.755 (1.519 to 2.028)	0.0026
9030425E11Rik	AK018527	RIKEN cDNA 9030425E11 gene	1.506 (1.329 to 1.655)	0.0026
Fgf7	AK033934	Fibroblast growth factor 7	1.81 (1.649 to 2.292)	0.0026
2410129E14Rik	NM_023716	RIKEN cDNA 2410129E14 gene	2.745 (1.956 to 3.272)	0.0026
2610001E17Rik	AK009795	RIKEN cDNA 2610001E17 gene	1.782 (1.412 to 1.945)	0.0026
Akr1a4	AK005162	Aldo-keto reductase family 1, member A4	1.748 (1.46 to 1.983)	0.0026
Ms4a11	AK004295	Membrane-spanning 4-domains, subfamily A, member 6D	1.958 (1.588 to 2.269)	0.0026
1200015A22Rik	AK004778	RIKEN cDNA 1200015A22 gene	1.793 (1.533 to 2.158)	0.0026
Col14a1	AK009906	Collagen type XIV	2.368 (1.96 to 3.084)	0.0026
Crip	AK003075	Cysteine rich intestinal protein	1.93 (1.604 to 2.362)	0.0026
2810052M02Rik	AK003809	RIKEN cDNA 2810052M02 gene	1.551 (1.365 to 1.788)	0.0025
Scd2	AK078543	Stearoyl-Coenzyme A desaturase 2	2.564 (1.999 to 3.182)	0.0025
6330577E15Rik	AK004073	RIKEN cDNA 6330577E15 gene	1.902 (1.521 to 2.159)	0.0025
1200007D18Rik	AK003239	RIKEN cDNA 1200007D18 gene	1.523 (1.301 to 1.638)	0.0025
Unknown	BM232043	Unknown	2.576 (2.217 to 3.458)	0.0025
Ania4	BE824672	Activity and neurotransmitter-induced early gene	3.796 (2.759 to 5.606)	0.0025
Cfl2	AK004659	Cofilin 2	1.575 (1.329 to 1.7)	0.0025
2610024B07Rik	AK011524	RIKEN cDNA 2610024B07 gene	1.878 (1.538 to 2.229)	0.0025
Golga3	BM115669	Golgi autoantigen, golgin subfamily a, 3	1.585 (1.393 to 1.831)	0.0025
BC003236	AK029901	Hypothetical protein MGC7720	1.864 (1.54 to 2.163)	0.0025
9530025L16Rik	AK087096	Unknown	1.547 (1.377 to 1.773)	0.0025
Semcap3	AK003849	SemaF cytoplasmic domain associated protein 3	1.979 (1.757 to 2.538)	0.0023
Serpinh1	AK076474	Serine (or cysteine) proteinase inhibitor, clade H, member 1	2.715 (2.29 to 3.882)	0.0023
Nid2	AK004203	Nidogen 2 (Nid2)	1.782 (1.497 to 2.09)	0.0023
DKFZp434H0820	AK033735	Hypothetical protein DKFZp434H0820	1.907 (1.646 to 2.272)	0.0023
D7Ertd671e	AK003918	Expressed sequence (D7Ertd671e)	2.019 (1.559 to 2.247)	0.0023

Scgn10	AK003659	Superiorcervical ganglia, neural specific 10	2.057 (1.577 to 2.33)	0.0023
4930488L10Rik	AK011469	Hypothetical Band 4.1 family containing protein	1.929 (1.75 to 2.437)	0.0023
Elk3	AK052546	ELK3, member of ETS oncogene family (Elk3)	1.571 (1.396 to 1.703)	0.0023
Ifit3	BM119721	Interferon-induced protein with tetratricopeptide repeats 3	1.882 (1.509 to 2.127)	0.0023
AI662855	AK048860	TRF1-interacting ankyrin-related ADP-ribose polymerase	1.506 (1.367 to 1.679)	0.0021
Loxl3	AK030548	Lysyl oxidase-like 3	2.141 (1.807 to 2.474)	0.0021
Unknown	BM117447	Unknown U031412	1.637 (1.419 to 1.827)	0.0021
Bgn	AK086920	Biglycan	1.814 (1.542 to 2.093)	0.0020
Col18a1	AK014292	Procollagen, type XVIII, alpha 1	2.061 (1.827 to 2.536)	0.0020
Igsf10	AK033487	Immunoglobulin and major histocompatibility complex domai	2.2 (1.854 to 2.477)	0.0020
CBP 35	AK008593	Galectin-3	1.73 (1.495 to 1.902)	0.0020
Egfr	AK004883	Epidermal growth factor receptor	1.699 (1.479 to 1.88)	0.0019
A930038C07Rik	AK017759	Fibronectin type III domain containing protein	2.06 (1.733 to 2.524)	0.0019
2310002N04Rik	AK009100	RIKEN cDNA 2310002N04 gene	1.622 (1.419 to 1.807)	0.0019
Mmp2	NM_008610	Matrix metalloproteinase 2	1.585 (1.485 to 1.838)	0.0019
Unknown	BM124490	Unknown	3.032 (2.325 to 4.221)	0.0019
AF506821	AK035655	Hypothetical protein AF506821	1.641 (1.463 to 1.868)	0.0019
Grb10	AK012646	Growth factor receptor bound protein 10	1.735 (1.56 to 1.981)	0.0018
2510001K09Rik	AK010884	RIKEN cDNA 2510001K09 gene	1.779 (1.586 to 2.114)	0.0018
Akr1b7	AK002705	Aldo-keto reductase family 1, member B7	4.723 (3.131 to 6.463)	0.0018
Evi2	AK005353	Hypothetical protein MGC28913	1.773 (1.522 to 2.026)	0.0018
Unknown	AK030674	Unknown	2.47 (2.034 to 3.101)	0.0018
Zfp2	AK030500	Zinc finger protein 2	1.835 (1.669 to 2.136)	0.0018
Ckap4	AK030708	Cytoskeleton associated protein 4	1.827 (1.569 to 2.136)	0.0018
Col8a1	AK018742	Procollagen, type VIII, alpha 1 (Col8a1)	2.555 (2.012 to 3.1)	0.0018
Tm4sf7	AK002709	transmembrane 4 superfamily member 7	1.673 (1.448 to 1.851)	0.0018
Tax1bp3	AK004963	Tax1 binding protein 3 (PDZ domain)	1.967 (1.716 to 2.254)	0.0018
Fstl	AK049440	Follistatin-like (Fstl)	3.101 (2.436 to 4.018)	0.0018
Yap	NM_009534	Yes-associated protein, 65 kDa (Yap)	1.632 (1.51 to 1.881)	0.0017
P4hb	XM_126743	Protein disulfide isomerase precursor	2.291 (1.944 to 2.734)	0.0017

Af1q	AK046005	ALL1-fused gene from chromosome 1q	1.51 (1.373 to 1.665)	0.0015
Anxa5	NM_009673	Annexin A5 (Anxa5)	1.856 (1.634 to 2.107)	0.0015
Slitl2	AK012169	Slit-like 2	1.903 (1.734 to 2.208)	0.0015
Ccr5	NM_009917	CC chemokine receptor-5	2.348 (2.088 to 2.744)	0.0015
Bok	NM_016778	Bcl-2-related ovarian killer protein	2.481 (2.179 to 2.993)	0.0015
Col18a1	AK014292	Procollagen, type XVIII, alpha 1	3.392 (2.702 to 4.344)	0.0015
C1qtnf6	AK012868	C1q and tumor necrosis factor related protein 6	2.112 (1.899 to 2.508)	0.0015
EDG-2, GPCR	AK030330	Endothelial differentiation, G-protein-coupled receptor	1.79 (1.666 to 2.02)	0.0015
Gpr124	AK018412	Adhesion G protein-coupled receptor 124	1.982 (1.823 to 2.413)	0.0015
Unknown	AW554615	Unknown	1.901 (1.728 to 2.168)	0.0015
Lox	NM_010728	Lysyl oxidase (Lox)	3.247 (2.677 to 4.279)	0.0015
6430596G11Rik	AK032559	Hypothetical 24.1 kDa protein	1.618 (1.486 to 1.745)	0.0015
1200007L24Rik	AK004640	RIKEN cDNA 1200007L24 gene	1.62 (1.445 to 1.735)	0.0015
Fkbp9	AK007499	FK506 binding protein -	2.145 (1.738 to 2.365)	0.0015
Clstn1	AK007691	Calsyntenin 1	1.501 (1.411 to 1.641)	0.0015
Vdp	NM_019490	Vesicle docking protein, 115 kDa	1.529 (1.444 to 1.695)	0.0015
Emp1	BM234011	Epithelial membrane protein 1	2.556 (2.242 to 3.246)	0.0015
Gja1	AK011459	Gap junction membrane channel protein alpha 1	1.637 (1.509 to 1.785)	0.0015
Il11ra2	NM_010549	Interleukin 11 receptor, alpha chain 2	1.627 (1.48 to 1.772)	0.0015
Fgfr1	AK028354	Fibroblast growth factor receptor 1	1.628 (1.444 to 1.772)	0.0015
Acta2	AK002886	Actin, alpha 2, smooth muscle, aorta	1.971 (1.74 to 2.278)	0.0015
Farp1	AK034903	Hypothetical 48.4 kDa protein	1.754 (1.574 to 1.942)	0.0015
Nfib	AK030686	Nuclear factor I/B	1.807 (1.546 to 1.986)	0.0015
Sertad4	AK029355	dJ667H12.2.1 (novel protein (isoform 1))	3.411 (2.826 to 4.585)	0.0015
2010004J24Rik	AK019513	weakly similar to ER protein 58	2.161 (1.988 to 2.658)	0.0015
Ctsd	AK089294	Cathepsin D	1.741 (1.527 to 1.913)	0.0015
Rnh1	NM_145135	Ribonuclease/angiogenin inhibitor 1	1.814 (1.623 to 2.026)	0.0015
Gas1	AK081311	Growth arrest specific 1	2.259 (1.973 to 2.779)	0.0015
Nek6	AK004925	NIMA (never in mitosis gene a)-related expressed kinase 6	2.144 (1.904 to 2.442)	0.0014
2310057H16Rik	AK009958	RIKEN cDNA 2310057H16 gene	4.688 (3.504 to 5.818)	0.0014

Pcbp4	AK004580	Poly(rC) binding protein 4	1.536 (1.425 to 1.689)	0.0014
BC027663	XM_150129	Unknown LOC234582	1.871 (1.692 to 2.156)	0.0013
Csrp2	AK003328	Cysteine-rich protein 2	4.123 (3.094 to 5)	0.0013
Anxa2	AK012563	Annexin A2	1.928 (1.751 to 2.212)	0.0013
Rtn4	AK047982	Unknown U012413	1.8 (1.691 to 2.069)	0.0013
Osbpl3	AK004768	Oxysterol binding protein-like 3	1.642 (1.481 to 1.784)	0.0013
Atbf1	AK019957	AT motif binding factor 1	1.605 (1.441 to 1.693)	0.0013
Rex3	AK003429	Reduced expression 3	1.55 (1.438 to 1.687)	0.0013
Unknown	AW539721	Unknown	1.909 (1.75 to 2.165)	0.0012
1110003H02Rik	AK003354	RIKEN cDNA 1110003H02 gene	1.628 (1.548 to 1.747)	0.0012
Fn	AK054456	Fibronectin receptor	2.576 (2.231 to 3.058)	0.0012
Spon2	AW552057	Spondin 2, extracellular matrix protein	2.464 (2.225 to 2.967)	0.0012
Maged1	AK013231	Melanoma antigen, family D, 1	2.334 (2.042 to 2.677)	0.0012
Flnb	AK047011	Filamin A alpha filamin 1 endothelial actin binding protein	1.89 (1.645 to 2.005)	0.0012
Ibsp	NM_008318	Integrin binding sialoprotein (Ibsp)	1.74 (1.639 to 1.934)	0.0012
2310075M15Rik	AK010185	RIKEN cDNA 2310075M15 gene	3.792 (2.917 to 4.36)	0.0012
Matn2	AW546059	Matrilin 2 (Matn2)	2.758 (2.355 to 3.128)	0.0012
Lepre1	AK010578	Leprecan 1	2.461 (2.106 to 2.831)	0.0012
Myo5a	AK002362	Myosin Va	1.747 (1.605 to 1.856)	0.0011
Rcn	AK017494	Reticulocalbin	2.312 (2.006 to 2.603)	0.0011
5730465C04Rik	AK007027	Ribosome binding protein 1	1.625 (1.542 to 1.741)	0.0011
Lamb1-1	AK013952	Laminin beta-1 chain precursor	2.685 (2.243 to 2.984)	0.0011
Mest	NM_008590	Mesoderm specific transcript	3.054 (2.514 to 3.55)	0.0011
Ddah2	NM_016765	Dimethylarginine dimethylaminohydrolase 2	1.614 (1.524 to 1.744)	0.0011
Col5a1	NM_015734	Procollagen, type V, alpha 1	1.968 (1.83 to 2.102)	0.0011
Slc38a4	AK003626	Solute carrier family 38, member 4	1.513 (1.455 to 1.597)	0.0010
AI173274	NM_134090	Expressed sequence AI173274	2.327 (2.035 to 2.479)	0.0008
Unknown	AW552210	Unknown	2.239 (2.046 to 2.388)	0.0006
Tnnt2	NM_011619	Troponin T2, cardiac	3.896 (3.608 to 4.558)	0.0006
Ptn	AK011346	Pleiotrophin	4.287 (3.752 to 4.851)	0.0006

H2-Ke4	AK087839	H2-K region expressed gene 4	1.638 (1.549 to 1.684)	0.0006
Tuba1	BM114503	Tubulin, alpha 1	2.398 (2.194 to 2.567)	0.0006
Copb2	AK088064	Coatomer beta subunit	1.723 (1.655 to 1.832)	0.0006
Macs	AW546394	Myristoylated alanine rich protein kinase C substrate	1.685 (1.59 to 1.775)	0.0006
Parva	AK008197	Parvin, alpha	1.528 (1.475 to 1.583)	0.0006
AU022327	AK044749	Meningioma expressed antogen 6/11	1.655 (1.596 to 1.698)	0.0005
Unknown	CK341862	Unknown	0.584 (0.436 to 0.718)	0.0084
Hipk2	AK013733	Homeodomain interacting protein kinase 2	0.634 (0.483 to 0.717)	0.0079
Unknown	BG069745	Unknown repeat sequence	0.6 (0.463 to 0.706)	0.0079
Ctse	AK040175	Cathepsin E (Ctse)	0.665 (0.575 to 0.765)	0.0079
Ahr	AK014512	Aryl-hydrocarbon receptor	0.627 (0.488 to 0.738)	0.0071
Unknown	AU040533	Unknown	0.521 (0.398 to 0.685)	0.0071
Unknown	CA555984	Unknown	0.642 (0.548 to 0.736)	0.0066
Unknown	AW553679	Unknown U031085	0.624 (0.54 to 0.791)	0.0066
2410008K03Rik	AK010455	weakly similar to GATS protein	0.663 (0.53 to 0.739)	0.0066
Recql4	BM231301	RecQ protein-like 4	0.667 (0.578 to 0.771)	0.0066
2310063P06Rik	AK010031	RIKEN cDNA 2310063P06 gene	0.581 (0.442 to 0.65)	0.0066
AIP-1	AK042878	weakly similar to ARL-6 interacting protein 1	0.58 (0.488 to 0.704)	0.0066
C79127	AK044232	Protein phosphatase 2C alpha isoform	0.626 (0.493 to 0.687)	0.0066
Unknown	BG069399	Uuknown	0.615 (0.502 to 0.711)	0.0066
Unknown	AW541984	Uuknown	0.667 (0.541 to 0.732)	0.0066
Unknown	BG071710	Uuknown	0.481 (0.356 to 0.613)	0.0066
Unknown	BG071952	Uuknown	0.433 (0.328 to 0.627)	0.0066
MGC18873	AK078385	Hypothetical protein MGC18873	0.659 (0.543 to 0.755)	0.0066
Unknown	BM199231	Unknown U023057	0.579 (0.493 to 0.69)	0.0066
Unknown	AU046042	Uuknown	0.558 (0.454 to 0.698)	0.0066
Unknown	C76276	Uuknown	0.661 (0.534 to 0.719)	0.0066
1500001L20Rik	AK005099	Trp-Asp (WD) repeats profile/Trp-Asp (WD) repeats	0.628 (0.547 to 0.768)	0.0066
4432417N03Rik	AK014502	RIKEN cDNA 4432417N03 gene	0.545 (0.434 to 0.649)	0.0057
Maid	NM_010761	Maternal inhibition of differentiation	0.628 (0.534 to 0.716)	0.0056

Rhced	AK079335	Rhesus blood group CE and D (Rhced)	0.491 (0.405 to 0.6)	0.0052
Lipc	NM_008280	Lipase, hepatic	0.639 (0.539 to 0.703)	0.0052
Unknown	AW546550	Unknown	0.528 (0.418 to 0.625)	0.0052
Unknown	BG074654	Uuknown	0.515 (0.452 to 0.677)	0.0052
Spi1-5	AK004999	Serine protease inhibitor 1-5	0.654 (0.582 to 0.722)	0.0052
Hdc	AK076384	Histidine decarboxylase	0.631 (0.537 to 0.721)	0.0052
4933419D20Rik	AK014895	RIKEN cDNA 4933419D20 gene	0.642 (0.579 to 0.751)	0.0052
6720474K14Rik	AK003505	RIKEN cDNA 6720474K14 gene	0.661 (0.576 to 0.727)	0.0052
D930015E06Rik	AK028803	Prokaryotic membrane lipoprotein lipid attachment site	0.649 (0.561 to 0.716)	0.0047
Ris2	AK012041	Retroviral integration site 1 (Ris2), mRNA	0.663 (0.607 to 0.747)	0.0047
Unknown	BG074055	Unknown	0.465 (0.397 to 0.587)	0.0047
Unknown	BG072471	Unknown	0.494 (0.405 to 0.58)	0.0045
Unknown	BM119192	Unknown U011399	0.65 (0.603 to 0.706)	0.0025
Lace1	NM_145743	Lactation elevated 1	0.661 (0.605 to 0.696)	0.0021
AI463083	AK019793	NCK associated protein 1	0.612 (0.577 to 0.678)	0.0021
Vig1	AK010906	Viral hemorrhagic septicemia virus(VHSV) induced gene 1	0.547 (0.495 to 0.589)	0.0017
9030401P18Rik	AK018482	RIKEN cDNA 9030401P18 gene	0.601 (0.564 to 0.639)	0.0009
Mkrn1	AK004225	Makorin, ring finger protein, 1	0.455 (0.419 to 0.487)	0.0008

Microarray analysis of fracture repair identifies the homeodomain transcription factor Prx-2 and other genes that imply similarities between bone repair and scarless fetal tissue healing. CH Rundle, H Wang, H Yu, RB Chadwick, J Tesfai, K-HW Lau, S Mohan, JT Ryaby and DJ Baylink.

Introduction

Tissue healing, including bone repair, involves the complex coordination of gene expression among different gene families. Because many of these genes are also expressed during fetal tissue development and normal fracture repair eliminates scarring, bone repair probably recapitulates at least some aspects of developmental expression pathways. More importantly, bone is one of the very few tissues capable of healing without a scar. However, little is known of the molecular pathways that regulate the regenerative aspects of bone healing.

We hypothesized that the regenerative molecular pathways common in fracture repair and scarless tissue healing could be identified by the analysis of gene expression during fracture healing. The goal of this study was to identify those genes important in regulating the regenerative pathways of bone repair. To identify differentially expressed genes during fracture healing, whole genome expression was performed by microarray analysis of the rat femur fracture during very early healing (day 3) and at the peak of endochondral bone formation (day 11). In our study, we used the appropriate marrow-ablated control diaphyses for comparison with the fractures (see methods). Previous studies used intact bone that included marrow, an approach that compromises differentially expressed genes identified in those studies. Our global analysis using these valid control tissues identified many genes important in fracture repair, but also recognized genes that mediate the scarless repair observed in fetal tissues.

Materials and Methods

Femur fractures were produced in 12-week-old male Sprague-Dawley rats by the three-point bending technique (1). RNA was isolated from the diaphyses at two post-fracture healing times: 3 days (n=5), the inflammation and intramembranous bone formation stages, and 11 days (n=4), the endochondral bone formation stage. Rigorous design of the controls applied the stabilizing Kirschner-wire to both fractured and unfractured control femurs to control for bone formation produced by the K-wire in the marrow, and ablate the marrow equally in fractures and controls. This procedure normalized the contributions of the marrow RNA between fractures and controls.

Microarray analysis was performed using the Agilent low-input labeling system and 20K rat oligomer microarray chip. The low-input system allowed us to use the low RNA recoveries from the control tissues and avoided pooling samples that can conceal individual variations. Lowess normalization and statistical analysis were performed using the Genespring software package. Changes in gene expression at $p<0.05$ were deemed significant.

Results

A microarray analysis that combined the 3 day and 11 day fracture calluses into one group identified 4522 genes with significant changes in expression ($p<0.05$), 33% of which were unidentified genes and ESTs. In agreement with previous microarray studies (3), several growth factor gene families displayed changes in expression, including the IGF-1 ($p<0.004$), FGF ($p<0.016$) and PDGF ($p<0.002$) families.

To test our hypothesis that regenerative molecular pathways are common in fracture repair and scarless tissue healing, we pursued the homeodomain transcription factors, as they are especially important in both development and healing. Consistent with our hypothesis, several homeodomain transcription factor genes showed statistically significant changes in expression during fracture repair. One such transcription factor was Prx-2, a member of the pair-related homeodomain transcription factor family implicated in scarless tissue repair and whose expression was upregulated (3.1-fold, $p<0.009$) at 3 days healing. Several genes that interact with Prx-2 and are involved in fetal scarless healing were also upregulated in fracture healing (Table 1).

Table 1. Genes Expressed in Fracture Repair and in Scarless Healing

Gene	Days Healing	Fold Activation	Function	Fetal Healing (Ref)*
Prx-2	3	+3.1	Txn Factor	(9)
Tenascin-C	3	+1.6	EC matrix	(4, 5)
Fibromodulin	3	+2.4	EC matrix	(8)
TGF-B3	3	+1.5	growth factor	(5)
Mmp-14	11	+1.9	remodeling	(2)

* Gene expression is increased in fetal scarless wound healing.

One possible transcriptional target of Prx-2 is the extracellular matrix gene tenascin-C, upregulated at 3 days healing (1.6-fold, $p<0.024$). Tenascin-C displays colocalized expression with TGF-B3 in scarless wound healing (5) and with Prx-2 and Prx-1 in pulmonary disease (4). The serine protease inhibitor nexin-1, also upregulated at 3 days (1.4-fold, $p<0.049$), has been shown to be a transcriptional target of Prx-2 regulation (7). Although not yet conclusively linked to fetal wound healing, its expression during tissue development (6) suggests that it could also play a role in wound healing through its inhibition of thrombin and tissue plasminogen in the extracellular matrix. Other genes implicated in scarless healing included the previously identified TGF-B3 (1.5-fold, $p<0.001$) at 3 days post-fracture and matrix metalloproteinase-14 (mmp-14; 1.9-fold, $p<0.019$) at 11 days post-fracture. Fibromodulin, an extracellular matrix modulator of TGF-B activity also expressed in scarless fetal wound healing, was upregulated (2.4-fold, $p<0.018$) at 3 days post-fracture. Consequently, our findings support the involvement of Prx-2 in fracture healing and our hypothesis that it shares at least some of the molecular pathways used for scarless healing in fetal tissues.

It should be emphasized that, to our knowledge, Prx-2, fibromodulin and mmp-14 have not been previously reported in microarray studies of fracture repair (3). One of the reasons why we were able to detect changes of these genes in the fracture was probably our use of a K-wire-stabilized unfractured control bone, so that the control marrow and fracture marrow were equally ablated. Because the marrow contains considerable RNA, its ablation in our controls allows for more senstive detection of gene expression in the fracture tissues.

Discussion

Bone is one of the few tissues that can heal without scarring in adult animals. Identifying the genes expressed in fracture repair can therefore suggest applications for scarless healing in other tissues.

Because of their extensively documented regulation during tissue development, the homeodomain transcription factor pathways are obvious candidates for regulation of fetal tissue repair and bone healing. The homeodomain transcription factor Prx-2 and the possible target genes tenascin-C and nexin-1 displayed significant increases in expression early in fracture healing, analagous to their expression observed during the scarless healing of fetal tissues. Prx-2-mediated regulation of these extracellular matrix genes immediately suggests communication with TGF-B3 in scarless wound repair. Such communication could occur through Prx-2-mediated changes in the extracellular matrix, which could bind and alter TGF-B3 availability directly, or modulate latent TGF-binding protein regulation of TGF-B3 availability. The extracellular matrix composition might also affect remodeling genes later in fracture repair. Mmp-14 upregulation is significant in this respect. The genes that modulate scarless fracture healing must require coordination with the molecular pathways of fracture callus maturation in all phases of healing.

It is also apparent that the large number of ESTs identified by our analysis implies that unknown genes play a mjor role in the regulation of fracture repair. This observation strongly suggests that additional genes that coordinate scarless tissue healing could be identified by an examination of bone healing.

In conclusion: 1) using a 20K gene chip and controls that normalized marrow RNA input among multiple replicates at two healing times, we identified 4522 genes with significant changes in expression in fracture tissue; 2) several of the genes identified have been associated with the scarless healing of fetal wounds; among these, the homeodomain transcription factor Prx-2 has not previously been associated with fracture healing. These results demonstrate that fracture repair is similar to fetal tissue development and repair, and that the regenerative qualities of bone repair can be used to elucidate therapies for improved wound healing of skeletal and nonskeletal tissues.

References

1. Bonnerens and Einhorn (1984). J. Orthop, Res. 2:97.
2. Dang et al., (2003). Plastic Reconstructive Surg. 111:2273.
3. Hadjiargyrou et al., (2002). J. Biol. Chem. 277:301277.
4. Jones et al., (2001). Circulation Res. 89:131.
5. Kohama et al., (2002). J. Dent. Res. 81:688.
6. Mansuy et al., (1993). Development 119:1119.
7. Scott et al., (2003). DNA Cell Biol. 22:95.
8. Soo et al., (2000). Am. J. Pathol. 157:423.
9. White et al., (2003). J. Invest. Dermatol. 120:135.

This work was supported by a grant from the US Army.

LOSS OF SEX-SPECIFIC DIFFERENCES IN BONE SIZE IN LEPTIN-DEFICIENT (*OB/OB*) MICE

+*Rundle, C H; *Wang, X; *Wergedal, J E; *Srivastava, A K; *Davis, E I; *Lau, K-H W; *Mohan, S; *Baylink, D J
+*Musculoskeletal Disease Center, J.L. Pettis Veterans Administration Medical Center,
Loma Linda, CA, USA
Charles.Rundle@med.va.gov

Introduction

Leptin is secreted primarily by the adipocytes and has been shown to play an important role in the regulation of food intake and energy expenditure (3). In addition to its adipostatic function, recent studies using transgenic mice deficient in leptin production or its function and in vitro studies on the effects of leptin on osteoblast cells have provided convincing evidence that leptin exerts important effects on skeletal maturation and metabolism (2).

Direct and indirect actions of leptin have been implicated in mediating the effects of leptin on bone metabolism. Anti-osteogenic effects of leptin administration into the cerebroventricular space imply hypothalamic control of signals to osteoblasts and osteoclasts through the sympathetic nervous system (2). The indirect actions of leptin might also involve obesity-induced mechanical loading and/or leptin modulation of hormones, such as insulin (1). It has been suggested that osteoblastic cells might be direct targets for leptin (8). Alternatively, leptin receptor expression on osteoblasts suggests that leptin can directly modulate bone cell metabolism (4).

Gender-specific relationships between fat mass and bone mass (6) and the greater periosteal expansion in the males during puberty implicate androgen effects. There is a positive association between serum leptin levels and whole body bone area (7). Additionally, leptin might act on the periosteal envelope of cortical bone; variations in circulating leptin are involved in genetic variation of hand bone size (6).

We hypothesized that the androgen effect on bone expansion is dependent on leptin function. To test this hypothesis, we compared different parameters of bone size in leptin-deficient (*ob/ob*) mice and corresponding C57BL/6 wild-type mice. We found that gender-dependent differences in bone size were lost in the leptin knockout mice.

Materials and Methods

Leptin knockout and C57BL/6 mice were obtained from the Jackson labs. At least 11 male and female mice were analyzed from each strain at 10 and 12 weeks of age. Mice were analyzed for total body fat and lean tissue mass by dual energy X-ray absorptiometry (DEXA, PIXIMUS™). Bone parameters of femurs from male and female leptin knockout and C57BL/6 mice were analyzed by peripheral quantitative computed tomography (pQCT) at the diaphyseal midpoint. Free serum testosterone and estradiol levels were determined using ^{125}I-radioimmunoassay (RIA) kits. Statistical analysis was performed by two-way ANOVA and Newman-Kuels post-hoc test.

Results

A phenotypic comparison of body weight, body fat and lean body mass in leptin knockout and C57BL/6 mice revealed that the body weights of C57BL/6 male mice were significantly higher than female mice (26.1 vs 18.9 g, $p<0.0001$), but were not different in leptin knockout males and females (41.1 vs 38.5 g). Much of the difference in body weight between strains was due to body fat; it was significantly greater in C57BL/6 males than females (3.4 vs 2.6 g, $p<0.0001$), but not in leptin knockout males and females males and females (21.7 vs 22.7 g). Differences in the lean body mass between C57BL/6 male and female mice (21.2 vs 14.9 g, $p<0.0001$) were not significant between leptin knockout male and female mice (19.4 vs 18.2 g).

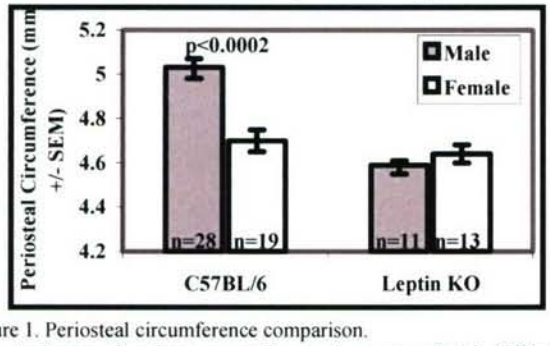

Figure 1. Periosteal circumference comparison.

Androgen functions normally produce sex-related differences several tissues, but sex-related differences were surprisingly absent in the bones of male leptin knockout mice. pQCT measurements of the periosteal circumference (Figure 1) revealed that the differences between male and female C57BL/6 mice (5.0 vs 4.6 mm, $p<0.0002$) were not significant between male leptin and female leptin knockout mice (4.7 vs 4.6 mm). The same was true of the endosteal circumference in C57BL/6 male and female mice (3.6 vs 3.3 mm^2, $p<0.0002$); male and female leptin mice showed no significant differences (3.4 vs 3.3 mm^2). The difference in the trabecular area of the male and female C57BL/6 mice (0.73 vs 0.56 mm^2, $p<0.0002$) was not significant in the leptin male and female knockout mice (0.64 vs 0.61 mm^2). No significant differences were observed in the bone mineral densities between strains or between males and females. There were no significant differences in the bone parameters between C57BL/6 and leptin knockout females.

To determine if the absence of androgen effects could be explained by a lack of testosterone, serum sex hormone levels were examined (Figure 2). Free serum testosterone levels in male leptin knockout mice (313 vs 693 pg/ml, $p<0.005$), were approximately twice the testosterone levels in C57BL/6 mice. Serum estradiol was increased in leptin female mice relative to C57BL/6 female mice (67 vs 100 pg/ml, $p<0.0001$). Our results demonstrate that androgen-specific effects on bone are lost in male leptin knockout mice.

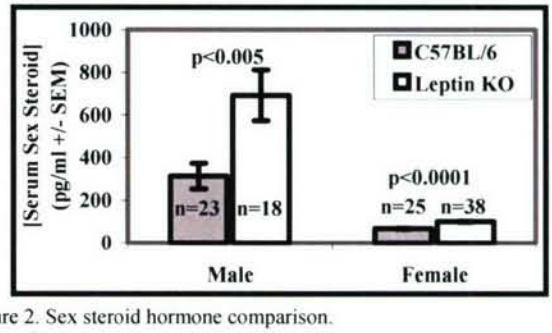

Figure 2. Sex steroid hormone comparison.

Discussion

The femurs of male leptin knockout mice displayed a loss of sex specific characteristics in comparison to the C57BL/6 background strain. Several endochondral bone measurements related to bone size were affected, including the periosteal circumference, a bone parameter affected by androgens.

Leptin is recognized as a key hormone in the regulation of body fat and an important regulator of bone mass. The sex steroids play a critical role in the regulation of bone turnover. There is evidence that testosterone is anabolic and acts primarily through increased bone formation, while estrogen acts primarily through the suppression of bone resorption. Our study is the first to suggest that an interaction, direct or indirect, between leptin and androgen in bone interferes with androgen functions. Other metabolic pathways related to androgen functions, such as the growth hormone axis, could also be affected. The lack of significant differences in the bone parameters between the females of either mouse strain contradicts estrogen-related functions. The elevated concentrations of testosterone in leptin knockout male mice indicate loss of sex-specific effects on bone is not caused by a lack of testosterone production, but might be due to testosterone signaling pathways. The higher variation in the testosterone levels (Figure 2) is highly suggestive of a feedback mechanism. In conclusion, the data is consistent with our hypothesis that androgen effects on bone size are dependent on leptin. Further functional studies of the leptin mechanism are required.

References

1. Bini et al. (2004) Hormone Res. 61:170.
2. Ducy et al. (2000) Cell 100:197.
3. Friedman and Halaas. (1998) Nature 395:763.
4. Iwamoto et al. (2004) Gynecol. Endocrinol. 19:97.
5. Livshits et al. (2003) Osteoporosis Int. 14:476.
6. Nelson et al. (1997) Bone 20:73.
7. Steppan et al. (2000) Reg. Peptides 92:73.
8. Thomas et al. (1999) Endocrinology 140:1630.

Ms # Bone-05-08-00403-R1

MICROARRAY ANALYSIS OF GENE EXPRESSION DURING THE INFLAMMATION AND ENDOCHONDRAL BONE FORMATION STAGES OF RAT FEMUR FRACTURE REPAIR

Charles H. Rundle[a], Hali Wang[c], Hongrun Yu[a], Robert B. Chadwick[a], Emile I. Davis[a], Jon E. Wergedal[a,b], K-H. William Lau[a,b,*], Subburaman Mohan[a,b], James T. Ryaby[c], and David J. Baylink[a,b]

[a] *Musculoskeletal Disease Center, Jerry L. Pettis V. A. Medical Center, Loma Linda, CA 92357,* [b] *Departments of Medicine and Biochemistry, Loma Linda University, Loma Linda, CA 92354, and* [c] *Research and Development, Orthologic Corporation, 1275 Washington St., Tempe, AZ 85281*

* Corresponding Author

Musculoskeletal Disease Center (151)

Jerry L. Pettis V .A. Medical Center

11201 Benton St.

Loma Linda, CA 92357

Tel: 909-825-7084 Ext. 2836

Fax: 909-796-1680

E-mail: William.Lau@med.va.gov

Key Words: Fracture healing; Microarray; Inflammation; Endochondral; Scarless

Abstract

Microarray analysis of gene expression was performed in the healing femur fractures of 13-week-old male rats during the inflammatory stage of repair, at 3 days post-fracture, and the endochondral bone formation stage of repair, at 11 days post-fracture. Multiple replicate pairs of fracture tissues paired with unfractured tissues, and unfractured control bones that had the stabilizing K-wire introduced. This approach normalized the marrow contributions to the RNA repertoire. We identified 6,555 genes with significant changes in expression in fracture tissues at 3 days and 11 days healing. The repertoire of growth factor genes expressed was also surprisingly restricted at both post-fracture intervals. The large number of Expressed Sequence Tags (ESTs) expressed at both post-fracture times indicates that several molecular pathways yet to be identified regulate fracture repair. The number of genes expressed during immune responses and inflammatory processes were restricted with higher expression largely during the early post-fracture analysis. Several of the genes identified in this study have been associated with regulation of cell and extracellular matrix interactions during scarless healing of fetal skin wounds. These observations suggest that these genes might also regulate the scarless healing characteristic of bone regeneration by similar mechanisms.

Introduction

Several million long bone fractures occur annually in the United States, approximately 10% of which display impaired healing [17]. Traditional surgical and non-surgical interventions can facilitate healing, but society would achieve considerable humanitarian and economic benefits from any improvements in fracture treatments. Such improvements would be realized through an understanding of bone repair.

Bone repair requires the regulated expression of diverse families of genes that coordinate complex interactions among various cell types. Endochondral bone repair proceeds through ordered stages of inflammation, intramembranous bone formation, chondrogenesis, endochondral bone formation and finally remodeling [8]. Fracture callus formation eventually results in the bridging of the fracture and the restoration of skeletal integrity. However, bone is unique in that it is one of the very few adult tissues normally capable of healing without a scar, and in this respect bone repair is a truly regenerative process. Although the molecular pathways that regulate bone repair remain largely unknown, studies of gene expression in endochondral bone repair have established that several extracellular matrix components and growth factor gene families that play significant roles in tissue development are also expressed during the different stages of fracture repair [1,2,12,22, reviewed by 5,7]. These observations suggest that the molecular regulation of fracture repair is complex, but probably recapitulates some aspects of skeletal morphogenesis [19]. If developmental genes regulate both fracture repair and bone regeneration, then these pathways can be characterized by identification of the genes expressed during fracture repair.

Microarray analysis of gene expression offers the opportunity for a global survey of gene expression during fracture repair and the elucidation of the molecular pathways of bone

regeneration. Previous examinations of genome-wide gene expression in rodent fracture healing have demonstrated that gene expression in fracture healing is indeed complex, and have also been very helpful in identifying known and novel genes that are expressed in fracture healing and elucidating the molecular pathways of bone repair. These studies have generally examined up-regulated genes from a cDNA-subtracted library [20] throughout normal fracture repair, or up-regulated and down-regulated genes during very restricted periods in normal fracture repair [28] or in restricted repertoires of genes in the normal fracture model [35]. Models of impaired fracture healing [21,33], determinations of response to fracture therapy [46] or alternative bone healing models [38] have also been utilized. Previous studies have generally analyzed pooled RNA samples, an approach that homogenizes individual biological variations. Additionally, microarray analysis usually uses an arbitrary threshold of 1.5- or 2-fold to identify significant changes in gene expression relative to control tissues. Their design has also utilized unfractured control bones without the stabilizing pin, which incorporates the substantial contributions of the marrow component into the RNA repertoire for examination of gene expression from the control bone, but not from the fractured bone. Each of these variables can affect the interpretation of the results.

The objective of this study was to use whole genome microarray gene analysis to identify the genes expressed in fracture repair of the rat femur at two stages: 1) at 3 days, immediately after the inflammatory phase but prior to bone formation, and 2) at 11 days, when intramembranous and endochondral bone formation overlap [8]. However, two important factors distinguish our approach from previous microarray studies using the rodent fracture model. The unfractured femurs used for the control comparison had the stabilizing Kirschner wire introduced into the intramedullary cavity, which controlled for bone formation induced by the pin in the

absence of a fracture, as well as for marrow contributions to the RNA repertoire. We also utilized the Agilent Technologies (Palo Alto, CA) 20,000 gene chip and low-input hybridization system that allowed the examination of gene expression during healing in individual animals without sample pooling, and took biological variation into account. This approach allowed us to apply statistical analysis to corroborate the arbitrary thresholds normally used to define significant changes in gene expression between fractured and unfractured bone. The identification of gene expression changes under these conditions of analysis should provide more accurate insights on the molecular pathways that regulate the bone repair and regeneration, and suggest potential therapeutic pathways to enhance the healing of bone injuries.

Materials and Methods

Femur fractures were produced in 13-week-old male Sprague-Dawley rats (Harlan, Indianapolis, IN) by the three-point bending technique [9]. Thirteen-week-old rats were used in this study, because a) as young adults, these animals had passed the period of most rapid adolescent bone growth that might affect interpretations of gene expression in fracture healing, and b) the fracture healing ability of younger animals is expected to be more effective than older animals. A 1.14-mm diameter stabilizing Kirschner (K)-wire was inserted in both fractured and unfractured control femurs to ablate the marrow equally in each bone. This approach normalized the substantial contributions of the marrow to the fracture RNA repertoire, and controlled for marrow gene expression unrelated to fracture healing and gene expression due to K-wire induction of bone formation in the marrow.

RNA was purified from the fracture diaphyses at two post-fracture healing times: 3 days, between the inflammation and intramembranous bone formation stages, and 11 days, during the

endochondral bone formation stage. These post-fracture times were sufficiently separated to provide an examination of very different stages of bone healing and identify the molecular pathways that regulate each stage. Briefly, the diaphysis was isolated from the fractured femur and from an unfractured control femur with a K-wire at each post-fracture time. The bone was pulverized while cooled with liquid nitrogen, and the RNA isolated using Trizol (Invitrogen, Carlsbad, CA) according to the manufacturer's directions. Total RNA was further purified by RNeasy columns (Qiagen, Valencia, CA) according to the manufacturer's specifications, quantified by Nanodrop (Agilent) and its integrity confirmed by Bioanalyzer (Agilent).

Microarray analysis was performed using the Agilent low-input labeling system and the Cy-5 or Cy-3 labeled RNA applied to the rat 20,000 oligomer microarray chip (Agilent). The low-input system allowed the use of low RNA recoveries from the control tissues, and avoided pooling samples that could conceal individual variations in gene expression. Individual fracture tissues were randomly paired with individual K-wire stabilized but unfractured tissues: 5 pairs of tissues were compared at 3 days healing and 8 pairs of tissues were compared at 11 days healing. Microarray image segmentation analysis was performed using ImaGene software (BioDiscovery, El Segundo, CA), that used an internal statistical analysis of the signal intensity of the spot and immediate surrounding area to flag each spot as present, empty, negative or marginal. Gene expression results were based upon spots flagged as present as well as those flagged as present or marginal. Lowess normalization and statistical analysis were performed using the Genespring software package (Agilent). Changes in gene expression at $p<0.05$ were deemed significant.

Changes in gene expression as determined by microarray analysis were independently confirmed by real-time RT-PCR for selected genes of interest. This confirmation was performed on some of the same fracture tissues that underwent microarray analysis, as well as additional

fracture tissues at 3 and 11 days healing. Total RNA was treated with DNAse I (Invitrogen) and reverse transcribed using the Superscript III kit (Invitrogen) according to the manufacturer's specifications. Real-time RT-PCR was performed on 50 ng of cDNA using gene-specific primers (Integrated DNA Technologies, Coralville, IA) and the Quantitect sybr green detection (Qiagen) as specified by the manufacturer. Real-time PCR was performed on a DNA Engine Opticon thermal cycler (Biorad Laboratories, Hercules, CA) at 45 seconds per step for 35 cycles at annealing temperatures optimized to amplify the gene of interest and the housekeeping gene (Table 1). Each gene of interest was normalized to expression of the housekeeping gene cyclophilin for each fracture tissue.

Results

Microarray analysis of fracture calluses at 3 days and 11 days post-fracture identified 6,555 genes with significant changes in expression ($p<0.05$), 67% (4,873) of which were known genes, and 33% (1,682) of which were unidentified genes and ESTs (Table 2).

An examination of the known genes that were significantly up-regulated or down-regulated revealed that several are associated with fracture healing in previous fracture expression analyses, including several extracellular molecules and members of selected growth factor gene families (Table 3). The increases in expression of these genes corresponded generally to those gene expression changes in previous studies at similar post-fracture healing times, though there were differences in magnitude of expression between studies. The changes in gene expression among other genes did vary between studies; different genes compared well with one study but not with another (data not shown).

A "Gene Ontology" classification [4] of the genes with statistically significant changes in expression was performed for 3 days healing, 11 days healing, and both 3 and 11 days healing (Table 4). Because there were 4,873 known genes with significantly altered expression at $p<0.05$, only those genes with changes in expression at $p<0.0002$ were included. Even at this very high level of statistical significance, this list revealed some TGFβ-related genes, developmental transcription factors, extracellular matrix and adhesion genes, and provided an initial analysis from which to further examine and functionally associate genes with less significant levels of expression.

The up-regulated inflammatory and immune genes were further examined (Table 5). Relatively few inflammatory genes were significantly up-regulated in expression; those that were observed at 3 days post-fracture, corresponding to the established inflammatory phase of fracture repair [8]. B cell, T cell and major histocompatibility genes were notably absent. Members of the complement pathway were present, but the cascade ended before C3a activation, suggesting regulation of innate immunity and the inflammatory response. Relatively few interleukins and Cluster of Differentiation (CD) antigens were represented, and some of those could have non-inflammatory or non-immune functions [24].

To determine whether regenerative molecular pathways are common in fracture repair and tissue development, we examined growth factor genes and transcription factors involved in skeletal development at 3 and 11 days healing (Table 6). Developmental factor and homeodomain transcription factor genes showed statistically significant and greater fold-changes in expression during fracture repair. This analysis included TGF-β3, and the paired box transcription factor Prx-2, not previously described in fracture healing. A further examination of genes related to TGF-β3 and Prx-2 revealed several growth factors and extracellular matrix

genes previously described in studies of scarless wound healing in fetal skin. Real-time PCR measurements of changes in expression of some of these genes generally confirmed their up-regulation in expression during fracture repair, although there was a difference in the magnitude of expression noted for some genes (Table 6).

Discussion

Our global analysis of fracture tissue gene expression recognized many genes important in fracture repair, underscoring the complexity of the fracture repair process (Table 2). The numbers of genes with significant changes in expression at 3 or 11 days indicated that relatively few genes were common to both the inflammatory-intramembranous bone formation and endochondral bone formation stages of fracture repair, and different molecular pathways of gene expression regulate different phases of bone healing. The large number of unknown genes and ESTs identified by our analysis also implies that novel, yet-to-be identified molecular pathways play significant roles in the regulation of fracture repair, and that bone regeneration will need to be characterized by a detailed examination of gene expression in bone healing.

An examination of the known genes that displayed significant changes in expression either up-regulated or down-regulated at 3 and 11 days healing revealed representatives of several growth factor gene families observed in previous studies of gene expression in fracture repair (Table 2). With respect to the collagens and growth factors, we generally found agreement with previous studies [12] and in comparable clusters by [Hadjiargyrou et al [20] and at 3 days post-fracture with the later time point examined by Li et al [28]. Among the growth factors observed at the earliest time point in healing fractures in younger rats [33], only one vascular endothelial growth factor (VEGF) isoform was represented, though the same extracellular matrix

molecules were expressed. Differences in fracture gene expression between studies were common, and it appears that variations in experimental approaches, in addition to biological variation in the regulation of fracture healing, can affect interpretations of gene expression changes.

Several Gene Ontology categories were represented that suggested important regulatory pathways at each time, even at a high level of significance (Table 4). The cell proliferation and protein metabolism categories were well represented at 3 days healing, as required for the subsequent proliferation of periosteal mesenchymal cells of the early soft callus. Several members of the skeletal development, cell adhesion and extracellular matrix categories were present at 11 days healing, consistent with the maturation of the various callus tissues during endochondral bone formation. This classification provided an insight into important molecular pathways of fracture repair that could be further characterized by an analysis of functionally related genes with less significant changes in expression.

Despite the importance of the inflammatory reaction early in fracture healing, the expression of inflammatory genes in fracture healing has not been well characterized. The marrow can be a major source of RNA and inflammatory gene expression resulting from damage produced by K-wire stabilization of the fractured bone. Our fracture controls included the K-wire that ablated the marrow to the same degree as the fracture, normalizing the marrow repertoire to allow for more sensitive detection of inflammatory gene expression in the periosteum, whose vessels constitute the major blood supply to the fracture [11]. Several inflammatory and immune-related genes were observed to be down-regulated in expression at 3 days post-fracture by Li et al [28]. However, conflicting results were presented showing an up-regulation of inflammatory and immune genes in the cDNA-subtracted library microarray analysis performed by

Hadjiargyrou et al. [20], suggesting that the repertoire of expressed genes can be affected by marrow contributions to the fracture model.

In this study, the up-regulation of the platelet-derived growth factor (PDGF) receptor gene implicated PDGF genes during inflammation. The mast cell growth factor, monocyte chemotactic protein 3 [32] and members of the tumor necrosis factor family [15] displayed up-regulated expression, which was higher at 3 days post-fracture (Table 5) and consistent with inflammatory functions in healing. Most notably, in comparison to previous microarray studies [20,28], the T cell receptor, immunoglobulin genes and major histocompatibility genes displayed no significant changes during early and later fracture healing. Though 3 days is probably too early for the adaptive immune response, if immune genes were functional in fracture repair their expression would be observed by 11 days post-fracture. In agreement with previous studies [20], the innate immunity complement genes were up-regulated; however, the complement cascade ceased expression at C3a, the initial immune effector complement component, probably through expression of C3 inhibitors (Table 5). As with growth factor expression, the repertoire of interleukins and CD antigens were similar to other studies with some variations in individual members. The inflammatory mediators interleukin IL-1 [16] and IL-6 [6] and their related components, also observed in other studies, were up-regulated in early fracture healing. Other interleukins and CD antigens were up-regulated later in healing and could be assigned non-inflammatory and non-immune functions. We conclude that marrow gene expression could affect interpretations of microarray analysis in fracture repair.

Bone is the only adult tissue that is capable of healing without scar formation [10], and an examination of fracture gene expression from previous studies (Table 3) in combination with a more detailed analysis of our Gene Ontology list (Table 4) identified growth factors and

developmental genes previously associated with scarless fetal skin repair that might also regulate bone regeneration during fracture healing (Table 6). The genes previously associated with scarless fetal skin wound healing are diverse in function, but those identified to date influence the turnover or adhesion of cells and extracellular matrix components [10]. The genes associated with scarless wound healing and not observed in previous studies might have displayed less dramatic changes in expression that we were able to detect with the statistical approach afforded by the multiple replicates in our study.

Due to their extensively documented regulation during tissue development, the homeodomain transcription factors are obvious candidates for the regulation of bone regeneration. The paired-related homeodomain transcription factor Prx-2 has been previously associated with scarless wound healing [47], and displayed significant increases in expression in fracture healing. Tenascin-C [25] and the plasmin inhibitor protease nexin (PN)-1 [43] have been identified as possible target genes of Prx-2 expression; they also displayed significant increases in expression in fracture healing. Prx-2-mediated changes in the extracellular matrix components through tenascin and PN-1 expression could bind and alter TGF-β3 availability. Consequently, our findings support the involvement of Prx-2 in fracture healing, suggesting a similarity of molecular pathways in both fracture healing and scarless healing in fetal tissues. The expression of the mesenchymal homeodomain transcription factor Meox-2 was also up-regulated during fracture healing. Its role is not well defined, but it has been shown to affect cell migration during developmental somitogenesis [30,48]. Meox-2 expression might therefore regulate bone regeneration by balancing cell adhesion and migration.

Growth factor genes involved in skeletal development and previously associated with scarless fetal wound healing were identified. TGF-β3 gene expression was especially notable in

this respect [27,45], as it was increased 2-fold throughout fracture healing. The TGFs are pleiotrophic growth factors that could exert varied effects on inflammation, proliferation, differentiation and apoptosis in the healing fracture [13]. The TGFs could also be differentially regulated post-transcriptionally by specific extracellular matrix components, such as latent TGF binding protein (LTBP)-1 [39] and fibromodulin [44]. Other growth factor genes expressed in scarless fetal wound healing that were also up-regulated in fracture healing included the angiogenic VEGF-C gene [10] and the apoptosis inhibitor hepatocyte growth factor [37].

The up-regulation of tenascin expression immediately suggested that additional matricellular genes could modulate cell-matrix adhesion and de-adhesion [34]. The expression of the matricellular genes and their respective receptors was up-regulated throughout fracture healing (Table 6). Although only thrombospondin-1 has been associated with fetal wound healing [42], these genes are critical in regulating the cell-matrix interactions implicated in scarless wound healing by other genes expressed in fetal skin repair. The extracellular matrix composition might also affect expression of the remodeling genes, such as matrix metalloproteinase (mmp)-14, observed in both scarless wound healing [14] and during endochondral bone formation in this study.

These results suggest that a similar set of genes that regulate normal tissue healing and scarless wound healing are differentially expressed during the inflammatory and endochondral stages of fracture repair. These include genes that modulate cell-matrix interactions and extracellular matrix organization at different times during healing, such as the matricellular genes. Other genes regulate these genes transcriptionally or post-transcriptionally; examples are Prx-2 and PN-1 inhibition of plasmin [41], and the pleiotrophic effects TGF-β3, which might include the inhibition of inflammation (Fig. 1). The expression of these common genes implies

that the molecular pathways of fracture repair mediate bone regeneration by mechanisms similar to scarless fetal wound healing.

We examined gene expression during the normal repair of a simple femur fracture with the elimination of scar tissue from the healing bone. This model does not address impaired healing, such as fracture non-unions, in which fibrous tissue is retained within the fracture gap without healing of the injured bone. Fracture non-unions can result from several causes beyond the scope of this study, including severe trauma to the bone, often with extensive comminution or a large interfragmentary gap, interruption of the periosteal blood supply and nerves, as well as infection associated with trauma [reviewed in 40]. Nevertheless, even in the absence of very severe trauma, a fracture non-union that results simply from a large interfragmentary gap or excessive motion of the fracture tissues implicates the extracellular matrix as an important mediator of tissue repair.

In conclusion, we identified 6,555 genes with significant changes in expression in fracture tissues at 3 days and 11 days healing using the Agilent rat 20,000 gene chip. Our approach took advantage of multiple replicates of fracture tissues paired with unfractured tissues with the K-wire introduced into the bone to examine gene expression at these critical times of fracture healing. The induction and resolution of the inflammatory phase of early fracture healing is important for the transition from inflammation to repair; it immediately affects the deposition and resolution of the extracellular matrix, and ultimately affects osteogenesis in bone and scar production in injured tissues. A profile of inflammatory gene expression during the early stages of fracture repair identified fewer inflammatory mediators of fracture healing than in previous microarray studies. The intramedullary K-wire also causes intramedullary damage to the bone that might increase osteogenic activity outside of the fracture callus and affect femoral gene

expression during endochondral bone repair. Several of the genes identified during early and later fracture healing have been associated with regulation of the extracellular matrix during scarless healing of fetal skin wounds. A comparison of gene expression in fracture repair by microarray analysis with fetal scarless wound healing would present an ideal opportunity to ascertain additional genes that regulate bone regeneration. The expression of genes that regulate the regenerative qualities of bone repair can be used to elucidate therapies for improved wound healing of both skeletal and non-skeletal tissues.

Acknowledgments

This work was supported in part by Assistance Award No. DAMD17-02-1-0685. The U.S. Army Medical Research Acquistion Activity, 820 Chandler Street, Fort Detrick, MD 21702-5014, is the awarding and administering acquisition office. The information contained in this publication does not necessarily reflect the position or the policy of the Government, and no official endorsement should be inferred. All work was performed in facilities provided by the Department of Veterans Affairs.

References

[1] Andrew JG, Hoyland J, Freemont AJ, Marsh D. Insulinlike growth factor gene expression in human fracture callus. Calcif Tissue Int 1993;53:97-102.

[2] Andrew JG, Hoyland JA, Freemont AJ, Marsh, DR. Platelet-derived growth factor expression in normally healing human fractures. Bone 1995;16:455-60.

[3] Apte SS, Fukai N, Beier DR, Olsen, BR. The matrix metalloproteinase-14 (MMP-14) gene is structurally distinct from other MMP genes and is co-expressed with the TIMP-2 gene during mouse embryogenesis. J Biol Chem 1997;272:25511-17.

[4] Ashburner M, Ball CA, Blake JA, Botstein D, Butler H, Cherry JM, Davis AP, Dolinski K, Dwight SS, Eppig JT, Harris MA, Hill DP, Issel-Tarver L, Kasarskis A, Lewis S, Matese JC, Richardson JE, Ringwald M, Rubin GM, Sherlock G. Gene ontology: tool for the unification of biology. The Gene Ontology Consortium. Nature Genet 2000;25:25-9.

[5] Barnes, GL, Kostenuik PJ, Gerstenfeld LC, Einhorn TA. Growth factor regulation of fracture repair. J Bone Miner Res 1999;14:1805-1815.

[6] Baumann H, Gauldie J. The acute phase response. Immunol Today 1994;15:74-80.

[7] Beasley LS, Einhorn TA. Role of growth factors in fracture healing. In: Canalis E, editor. Skeletal growth factors. Philadelphia, PA: Lippencott, Williams and Wilkins; 2000; 311-22.

[8] Bolander ME. Regulation of fracture repair by growth factors. Proc Soc Exp Biol Med 1992;200:165-70.

[9] Bonnarens F, Einhorn TA. Production of a standard closed fracture in laboratory animal bone. J Orthop Res 1984;2:97-101.

[10] Bullard KM, Longaker MT, Lorenz HP. Fetal wound healing: Current biology World J Surg 2003;27:54-61.

[11] Chanavaz M. Anatomy and histophysiology of the periosteum: Quantification of the periosteal blood supply to the adjacent bone with ^{85}Sr and gamma spectromotery. J Oral Implantol 1995;21:214-19.

[12] Cho T-J, Gerstenfeld LC, Einhorn TA. Differential temporal expression of members of the transforming growth factor B superfamily during murine fracture healing. J Bone Miner Res 2000;17:513-20.

[13] Clark DA, Coker R. Transforming growth factor-β (TGF-β). Int. J. Biochem. Cell Biol 1998;30:293-98.

[14] Dang CM, Beanes SR, Lee H, Zhang X, Soo C, Ting KD. Scarless fetal wounds are associated with an increased matrix metalloproteinase-to-tissue-derived inhibitor of metalloproteinase ratio. Plastic Reconstr Surg 2003;111:2273-85.

[15] Dinarello CA. Proinflammatory cytokines. Chest 2000;118:503-8.

[16] Dinarello CA. The IL-1 family and inflammatory diseases. Clin Exp Rheumatol 2002;20:S1-S13.

[17] Einhorn TA. Enhancement of fracture healing. J Bone Jt Surg 1955;77-A:940-56.

[18] Febbraio M, Hajjar DP, Silverstein RL. CD36: A class B scavenger receptor involved in angiogenesis, athersclerosis, inflammation, and lipid metabolism. J Clin Invest 2001;108:785-91.

[19] Ferguson C, Aplern E, Miclau T, Helms J. Does adult fracture repair recapitulate embryonic skeletal formation? Mech Dev 1999;87:57-66.

[20] Hadjiargyrou M, Lombardo F, Zhao S, Ahrens W, Joo J, Ahn H, Jurman M, White DM, Rubin CT. Transcriptional profiling of bone regeneration. Insight into the molecular complexity of wound repair. J Biol Chem 2002;277:30177-82.

[21] Hatano H, Siegel HJ, Yamagiwa H, Bronk JT, Turner RT, Bolander ME, Sarkar G. Identification of estrogen-related genes during fracture healing, using DNA microarray. J Bone Miner Metab 2004;22:224-35.

[22] Hiltunen A, Hannu TA, Vuorio E. Regulation of extracellular matrix genes during fracture healing in mice. Clin Orthop Rel Res 1993;297:23-7.

[23] Ibelgaufts H. COPE: Horst Ibelgaufts' Cytokines Online Pathfinder Encyclopaedia 2003;www.copewithcytokines.de.

[24] Janeway CA, Jr, Travers P, Walport M, Schlomchik MJ. In: Janeway CA, Jr. editor. Immunobiology: the immune system in health and disease, fifth edition. New York, NY: Garland Publishing; 2001; Appendix 2.

[25] Jones FS, Meech R, Edelman DB, Oakey RJ, Jones PL. Prx1 controls vascular smooth muscle cell proliferation and tenascin-C expression and is upregulated with Prx2 in pulmonary vascular disease. Circulation Res 2001;89:131-8.

[26] Kimball, JW. Biology Pages 2005;users.rcn.com/jkimball.ma.ultranet/BiologyPages/C/Complement.html.

[27] Kohama K, Nonaka K, Hosokawa R, Shum L, Ohishi M. Tgf-β-3 promotes scarless repair of cleft lip in mouse fetuses. J Dent Res 2002;81:688-694.

[28] Li X, Quigg RJ, Zhou J, Ryaby JT, Wang H. Early signals for fracture healing. J Cell Biochem 2005;95:189-205.

[29] Mackie EJ, Halfter W, Liverani D. Induction of tenascin in healing wounds. J Cell Biol 1988;107:2757-67.

[30] Mankoo BS, Skuntz S, Harrigan I, Grigorieva E, Candia A, Wright CV, Arnheiter H, Pachnis V. The concerted action of Meox homeobox genes is required upstream of genetic pathways essential for the formation, patterning and differentiation of somites. Development 2003;130:4655-64.

[31] Mannaioni PF, Di Bello MG, Masini E. Platelets and inflammation: Role of platelet-derived growth factor, adhesion molecules and histamine. Inflamm Res 1997;46:4-18.

[32] Menten P, Wuyts A, van Damme J. Monocyte chemotactic protein-3. Eur Cytokine Net 2001;12:554-60.

[33] Meyer RA, Jr, Meyer MH, Tenholder M, Wondracek S, Wasserman R, Garges P. Gene expression in older rats with delayed union of femoral fractures. J Bone Joint Surg 2003;85-A:1243-54.

[34] Murphy-Ullrich JE. The de-adhesive activity of matricellular proteins: Is intermediate cell adhesion an adaptive state? J Clin Invest 2001;107:785-90.

[35] Nakazawa T, Nakajima A, Seki N, Okawa A, Kato M, Moriya H, Amizuka N, Einhorn TA, Yamazaki M. Gene expression of periostin in the early stage of fracture healing detected by cDNA microarray analysis. J Orthop Res 2004;22:520-5.

[36] Nilsson G, Butterfield JH, Nilsson K, Siegbahn A. Stem cell factor is a chemotactic factor for human mast cells. J Immunol 1994;153:3717-23.

[37] Ono I, Yamashita T, Hida T, Jin HY, Ito Y, Hamada H, Akasaka Y, Ishii T, Jimbow K. Local administration of hepatocyte growth factor gene enhances the regeneration of dermis in acute incisional wounds. J Surg Res 2004;120:47-55.

[38] Pacicca DM, Patel N, Lee C, Salisbury K, Lehmann W, Carvalho R, Gerstenfeld LC, Einhorn TA. Expression of angiogenic factors during distraction osteogenesis. Bone 2003;33:889-98.

[39] Rifkin DB. Latent transforming growth factor-β (TGF-β) binding proteins: orchestrators of TGF-β availability. J Biol Chem 2005;280:7409-12.

[40] Rodriguez-Merchan, EC, Forriol, F. Nonunion: general principles and experimental data. Clin Orthop 2004;419:4-12.

[41] Rossignol P, Ho-Tin-Noe B, Vranckx R, Bouton MC, Meilhac O, Lijnen HR, Guillin MC, Michel JB, Angles-Cano E. Protease nexin-1 inhibits plasminogen activation-induced apoptosis of adherent cells. J Biol Chem 2004;279:10346-56.

[42] Roth JJ, Sung JJ, Granick MS, Solomon MP, Longaker MT, Rothman VL, Nicosia RF, Tuszynski GP. Thrombospondin 1 and its specific cysteine-serine-valine-threonine-cysteine-glycine receptor in fetal wounds. Annu Plast Surg 1999;42:553-63.

[43] Scott KK, Norris RA, Potter SS, Norrington DW, Baybo MA, Hicklin DM, Kern MJ. GeneChip microarrays facilitate identification of Protease Nexin-1 as a target gene of the Prx2 (S8) homeoprotein. DNA Cell Biol 2003;22:95-105.

[44] Soo C, Hu F-Y, Zhang X, Wang Y, Beanes SR, Lorenz HP, Hedrick MH, Mackool RJ, Plaas A, Kim S-J, Longaker MT, Freymiller E, Ting K. Differential expression of fibromodulin, a transforming growth factor-B modulator, in fetal skin development and scarless repair. Am J Pathol 2000;157:423-33.

[45] Soo C, Beanes SR, Hu F-Y, Zhang X, Dang C, Chang G, Wang Y, Nishimura I, Freymiller E, Longaker MT, Lorenz HP, Ting K. Ontogenetic transition in fetal wound transforming growth factor-β regulation correlates with collagen organization. Am J Pathol 2003;163:2459-76.

[46] Wang H, Li X, Tomin E, Doty SB, Lane JM, Carney DH, Ryaby JT. Thrombin peptide (TP508) promotes fracture repair by up-regulating inflammatory mediators, early growth factors, and increasing angiogenesis. J Orthop Res 2005;23:671-9.

[47] White P, Thomas DW, Fong S, Stelnicki E, Meijlink F, Largman C, Stephens P. Deletion of the homeobox gene Prx-2 affects fetal but not adult fibroblast wound healing responses. J Invest Dermatol 2003;120:135-44.

[48] Witzenbichler B, Kureishi Y, Luo Z, Le Roux A, Branellec D, Walsh K. Regulation of smooth muscle cell migration and integrin expression by the Gax transcription factor. J Clin Invest 1999;104:1469-80.

Figure Legends

Fig. 1. A model for bone regeneration regulation by scarless fetal wound healing genes. TGF-β3 exerts pleiotrophic effects, including inhibition of inflammation. Cell motility and cell-matrix adhesion are mediated by the matricellular genes and their receptors, whose digestion by plasmin is inhibited by PN-1.

Table 1. Real-time PCR primers and conditions for the detection of scarless wound healing gene expression.

Target Gene		Primers				
Name	Accession	Position	Direction	Product	Sequence	Annealing Temperature*
Cyclophilin	BC059141	320	Forward	192	5'-GCATACAGGTCCTGGCATCT-3'	
		511	Reverse		5'-TCTTGCTGGTCTTGCCATTC-3'	
Fibromodulin	NM_080698	901	Forward	232	5'-ATGGCCTTGCTACCAACACC-3'	55.2
		1132	Reverse		5'-ATAGCGCTGCGCTTGATCTC-3'	
Meox-2	NM_017149	569	Forward	301	5'-GTCCTGTGCTCCAACTCTTC-3'	53.7
		869	Reverse		5'-GGTCTAGGTTCACCGCTATC-3'	
Mmp-14	NM_031056	966	Forward	330	5'-ACTTCGTGTTGCCTGATGAC-3'	56.5
		1295	Reverse		5'-TGCCATCCTTCCTCTCATAG-3'	
PN-1	NM_012620	2656	Forward	267	5'-CTCCTGGTCAACCACCTTAG-3'	55.4
		2922	Reverse		5'-CCTGTGGTACACGGTGTATG-3'	
Prx-2	NM_238327	432	Forward	227	5'-CTCGCTGCTCAAGTCTTACG-3'	56.2
		658	Reverse		5'-GGCTGTGGTGTAAGCTGAAC-3'	
TGF-β3	BC092195	1067	Forward	194	5'-CAGCATCCACTGTCCATGTC-3'	56.4
		1260	Reverse		5'-GTCGGTGTGGAGGAATCATC-3'	
HAS-1	NM_172323	1543	Forward	219	5'-CTGGCTGCTAACTATGTACC-3'	54.5
		1761	Reverse		5'-TCTGCACAGTCTCCTTACAC-3'	

* Each annealing temperature produces the most efficient amplification of cyclophilin and in the gene of interest.

Table 2. Summary of Fracture Microarray Gene Expression Changes			
Expression Change (P<0.05)	**Known Genes**	**Unknown Genes**	**Total**
3 Days			
Up at 3 days, no change at 11 days	889	215	1104
Down at 3 days, no change at 11 days	1013	388	1401
11 Days			
Up at 11 days, no change at 3 days	904	345	1249
Down at 11 days, no change at 3 days	1206	450	1656
3 and 11 Days			
Up at both 3 and 11 days	354	96	450
Down at both 3 and 11 days	474	181	655
Biphasic			
Up at 3 days, down at 11 days	20	1	21
Down at 3 days, up at 11 days	13	6	19
Total	**4873**	**1682**	**6555**

Table 3. Comparison of selected genes with up-regulated expression in in this study with previous fracture studies

This Study					Previous Fracture Studies
Gene	**Accession**	**Function**	**Fold-Change (P<0.05)**		**Similar Change in Expression**
			3 Days	**11 Days**	
transforming growth factor β-2	BF420705	growth factor	**1.3**	**1.6**	[12]
transforming growth factor β-3	NM_013174	growth factor	**2.4**	**2.0**	[12, 20, 28]
fibroblast growth factor 7	NM_022182	growth factor	**1.3**	NS	[20, 28]
interleukin 6	NM_012589	inflammation	**3.5**	NS	[12, 28]
angiopoietin-2 (like)	NM_133569	angiogenesis	NS	**1.4**	[33]
mesenchymal homeobox-2	NM_017149	transcription factor	**2.5**	**2.8**	[20]
pleiotrophin/OSF-1	NM_017066	several	**2.3**	NS	[20, 28]
frizzled	NM_021266	wnt signaling	**1.5**	**1.5**	[20]
cysteine-rich protein 61	NM_031327	extracellular matrix signaling	**2.6**	**2.8**	[20, 28]
fibronectin	NM_019143	extracellular matrix	**2.4**	**2.1**	[20, 28]
tenascin	BE126741	extracellular matrix	**2.1**	**1.5**	[20, 28]
thrombospondin-2	BF408413	extracellular matrix	**1.7**	**1.8**	[20, 28]
osteonectin/SPARC	NM_012656	extracellular matrix	**1.7**	NS	[20, 28]
aggrecan	NM_022190	extrcellular matrix	NS	**5.1**	[20, 28, 33]
collagen 2α1	AA899303	cartilge maturation	**0.8**	**1.5**	[20, 28, 33]
integrin binding sialoprotein	NM_012587	mineralization	**4.0**	NS	[20, 28]
collagen 5α1	NM_134452	extracellular matrix	**2.4**	**2.1**	[20, 28]
osteocalcin/Gla	NM_012862	mineralization	NS	**2.4**	[12, 20, 28, 33]
protease nexin-1	X89963.1	extracellular matrix protease	**2.1**	**2.1**	[20, 28]

NS: Not Significant

Table 4. Known genes with highly significant (P<0.0002) changes in the expression during fracture healing

Accession	Fold-Change		Gene Description	Gene Ontology Category [4]
	3 Days	11 Days		
BQ209997	**5.02**	**7.80**	similar to Mouse collagenous repeat-containing 26kDa protein (CORS26).	protein metabolism
AA858962	**4.36**	**2.15**	Rat retinol-binding protein (RBP) mRNA, partial cds.	vitamin A metabolism
NM_012587	**3.97**		Rattus norvegicus integrin binding sialoprotein (Ibsp).	extracellular space
BQ211765	**3.49**		Rattus norvegicus DEXRAS1 (Dexras1) mRNA.	signal transduction
BF415205	**2.78**	**6.19**	Rat mRNA fragment for cardiac actin.	actin cytoskeleton
NM_133566	**2.29**	**1.21**	Rattus norvegicus cystatin N (LOC171096).	organogenesis and histogenesis
NM_013104	**1.97**	**4.58**	Rattus norvegicus Insulin-like growth factor binding protein 6 (Igfbp6).	extracellular space
BQ209870	**1.80**	**3.88**	similar secreted modular calcium-binding protein 2 [Mus musculus].	calcium ion binding
CA510266	**1.71**	**1.32**	similar to prefoldin 5; myc modulator-1; c-myc binding protein [Homo sapiens].	regulation of transcription, DNA dependent
NM_012488	**1.55**	**2.53**	Rattus norvegicus α-2-macroglobulin (A2m).	protease inhibitor activity/IL-1, IL-8 binding
BE329208	**1.52**	**1.43**	similar to Cricetulus griseus SREBP cleavage activating protein (SCAP), complete cds.	steroid metabolism
NM_012816	**1.41**		Rattus norvegicus α-methylacyl-CoA racemase (Amacr).	metabolism/peroxisome
NM_057197	**1.40**		Rattus norvegicus 2,4-dienoyl CoA reductase 1, mitochondrial (Decr1).	oxidoreductase
NM_031646	**1.39**		Rattus norvegicus receptor (calcitonin) activity modifying protein 2 (Ramp2).	G-protein coupled receptor signaling
NM_031050	**1.38**		Rattus norvegicus lumican (Lum).	extracellular matrix
NM_017355	**1.27**	**1.24**	Rattus norvegicus ras-related GTP-binding protein 4b (Rab4b).	vesicle-mediated transport
U56859.1	0.90	0.79	Rattus norvegicus heparan sulfate proteoglycan, perlecan domain I (RPF-I), partial cds.	cell adhesion
BF281804	0.85	0.84	similar to solute carrier family 7 member 12; isc-type amino acid transporter 2 [Mus musculus].	amino acid transport
NM_017140	0.85		Rattus norvegicus dopamine receptor D3 (Drd3).	dopamine receptor signaling pathway
BF548886	0.85	0.78	similar to Mouse T-cell antigen receptor α-chain (TCR-ATF2), partial cds.	regulation of transcription, DNA dependent
NM_013029	0.84	0.79	Rattus norvegicus Sialyltransferase 8 (GT3 alpha 2,8-sialyltransferase) C (Siat8c).	amino acid glycosylation
NM_012997	0.82	0.74	Rattus norvegicus Purinergic receptor P2X, ligand-gated ion channel, 1 (P2rx1).	amino acid transport

NM_031725	0.82		Rattus norvegicus secretory carrier membrane protein 4 (Scamp4).	protein transport
AA900738	0.80	0.81	similar to Rat DNA for serine dehydratase.	amino acid metabolism/gluconeogenesis
NM_133322	0.79	0.77	Rattus norvegicus potassium voltage-gated channel, KQT-like subfamily, member 2 (Kcnq2).	synaptic transmission
NM_052801	0.78	0.76	Rattus norvegicus von Hippel-Lindau syndrome (Vhl).	regulation of transcription, DNA dependent/proteolysis & peptidolysis
CB546252	0.78	0.83	similar to zinc finger protein 261; DXHXS6673E [Mus musculus].	nucleus/zinc ion binding
NM_144730	0.78	0.80	Rattus norvegicus GATA-binding protein 4 (Gata4).	regulation of transcription, DNA dependent
NM_030854		**21.97**	Rattus norvegicus chondromodulin-1 (Chm-1).	cell growth and maintenance/proteoglycan metabolism
BF560915		**17.46**	Rattus norvegicus mRNA for collagen α 1 type X, partial.	skeletal development
NM_019189		**13.77**	Rattus norvegicus cartilage link protein 1 (Crtl1).	hyaluronic acid binding
NM_012929		**11.38**	Rattus norvegicus Procollagen II α 1 (Col2a1).	skeletal development
NM_031511		**6.72**	Rattus norvegicus Insulin-like growth factor II (somatomedin A) (Igf2).	development
BQ210664		**5.73**	similar to cartilage intermediate layer protein	unknown
BQ191772		**5.37**	similar to mouse annexin A8.	phospholipid binding
NM_022290		**5.28**	Rattus norvegicus tenomodulin (Tnmd).	collagen maturation
AI576621		**3.73**	similar to Mouse carboxypeptidase X2, complete cds.	protein binding
AA963765		**2.89**	similar to osteoglycin [Mus musculus].	regulation of DNA transcription
BQ200482		**1.41**	similar to Mouse mRNA for acetylglucosaminyltransferase-like protein.	lipopolycaccharide biosynthesis
CB547946		**1.35**	similar to Mus musculus (clone pVZmSin3B) mSin3B, complete cds.	regulation of transcription, DNA dependent
AI059288		0.83	similar to Mouse B-cell activating factor (TNFSF13b, Baff), complete cds.	positive regulation of cell proliferation
CB547491		0.83	similar to Mus musculus very large G protein-coupled receptor 1 (Vlgr1, Mass1), complete cds.	G-protein coupled receptor signaling
CB545755		0.82	similar to RAD54 like (S. cerevisiae) [Mus musculus].	DNA recombination, repair
CB544611		0.82	similar to BACR7A4.19 gene product [Drosophila melanogaster].	G-protein coupled receptor signaling
CB545661		0.81	similar to BC026845_1 Mus musculus, Similar to nucleoporin 133kD, complete cds.	RNA metabolism
AW920271		0.81	similar to mouse cat eye syndrome chromosome region, candidate 5 (Cecr5), complete cds.	metabolim

BQ196556		0.80	similar to nudix (nucleoside diphosphate linked moiety X)-type motif 5 [Mus musculus].	oxidative stress response/DNA repair
AA874884		0.60	Rat heme oxygenase gene, complete cds.	oxidoreductase activity
NM_031740		0.59	Rattus norvegicus UDP-Gal:betaGlcNAc beta 1,4-galactosyltransferase, polypeptide 6 (B4galt6).	glyosphingolipid biosynthesis
NM_053843		0.49	Rattus norvegicus Fc receptor, IgG, low affinity III (Fcgr3).	Immune response

Bold: Up-regulated

Table 5. Up-Regulated Expression in Fracture in Inflammation and Immune Function Genes

Gene		Functions	Fold-Change in Expression ($p<0.05$)	
Description [Reference]	**Accession**		**3 Days**	**11 Days**
Growth Factors				
Platelet-derived growth factor receptor [27]	AA925099	chemotaxis	**2.7**	**1.5**
Monocyte chemotactic protein 3 [28]	BF419899	chemotaxis	**3.3**	**1.6**
Mast cell growth factor/kit ligand [32]	AI102098	stem cell factor, hematopoietic & mast cell growth	**1.3**	**NS**
TNFα/TNFβ [14]	AA819277	inflammation	**NS**	**1.2**
TRAF2	BI282097	TNF inflammation	**1.1**	**NS**
TRAF4	CB546212	TNF inflammation	**1.6**	**NS**
TNF-stimulated gene 6	AF159103.1	TNF inflammation	**1.8**	**1.7**
TGFβ2 [12]	BF420705	inflammation	**1.3**	**1.6**
LTBP1	NM_021587	TGF regulation	**1.9**	**1.5**
TGFβli4	NM_013043	TGF regulation	**1.8**	**1.9**
Interleukins and Related Cytokines (www.copewithcytokines.de)				
IL1 receptor accessory protein [15]	NM_012968	IL1 inflammation	**1.6**	**NS**
IL3 regulated nuclear factor	NM_053727	IL3 MHC, eosinphil, basophil stimulation, apoptosis inhibition	**1.4**	**NS**
IL6 [5]	NM_012589	acute phase protein induction, proliferation	**3.5**	**NS**
IL6 gp130	298242_Rn	IL6 acute phase protein induction	**1.7**	**1.4**
IL6 signal transduction protein	BF398277	IL6 acute phase protein induction	**1.5**	**1.4**
IL11 receptor alpha 1	221254_Rn	IL11 progenitor growth factor, acute phase protein induction	**NS**	**1.3**
IL12 p40 precursor	NM_022611	IL12 hematopoeitic response, adhesion	**NS**	**1.3**
IL18	284329_Rn	T cell activation, hematopoiesis	**1.3**	**NS**
Interferon-γ	NM_138880	immune response	**NS**	**1.4**
Interferon inducible p27-like	NM_130743	immune response	**1.4**	**1.4**
ATP dependent interferon responsive	BG373987	immune response	**NS**	**1.4**
Complement Pathway (users.rcn.com/jkimball.ma.ultranet/BiologyPages/C/Complement.html)				

Complement 1Q binding protein	NM_019259	Complement 4 activation	**1.7**	**NS**
Complement 1R	AA799803	Complement 4 activation	**1.7**	**1.4**
Complement 1S	NM_138900	Complement 4 activation	**2**	**2.6**
Complement 2	NM_172222	Complement 3 activation	**NS**	**1.4**
Complement 4	AI412156	Complement 2 activation	**NS**	**2.3**
Complement H	NM_130409	Complement 3 inhibition	**1.6**	**NS**
Complement I	NM_024157	Complement 3 inhibition	**NS**	**1.1**
CDs (www.immunologylink.com)				
CD14	NM_021744	LPS receptor	**1.4**	**NS**
CD39-like 3	AI070096	ecto-nucleoside triphosphate diphosphohydrolase	**1.5**	**NS**
CD34	AI102873	adhesion, stem cell marker	**1.6**	**1.9**
CD36 [17]	NM_054001	scavenger receptor, inflammation, angiogenesis	**1.6**	**NS**
CD81	NM_013087	T cell stimulation	**1.8**	**2.1**
CD151	NM_022523	adhesion, signaling	**1.4**	**1.3**
CD164	NM_031812	hematopoeitic-stromal interaction	**1.6**	**1.2**

NS: Not Significant

Table 6. Fracture Microarray Genes Associated With Scarless Fetal Wound Healing

		3 Day Expression		11 Day Expression	
		Microarray (P<0.05)	Real-Time PCR	Microarray (P<0.05)	Real-Time PCR
Gene (Function) [Reference]	**Accession**	**Fold-Change**	**Fold-Change[1] (n)**	**Fold-Change**	**Fold-Change[1] (n)**
Homeodomain					
Prx-2 (TGF-β3, PN-1 regulation) [22,43]	BE118447	**4.4**	**2.2 +/- 1.9 (7)**	**2.7**	**2.6 +/- 1.6 (6)**
Meox-2 (cell migration) [44]	NM_017149	**2.5**	**1.7 +/- 0.6 (9)**	**2.8**	**2.5 +/- 1.8 (5)**
TGF-β3-Related [41]					
TGF-β3 (proliferation, differentiation)	NM_013174	**2.4**	**1.7 +/- 0.9 (7)**	**2**	**4.3 +/- 2.0 (8)**
LTBP-1 (TGF-β3 binding)	NM_021587	**1.9**	**ND**	**1.5**	ND
Fibromodulin [23]	NM_080698	**2.3**	**2.1 +/- 1.2 (8)**	**5.2**	**21.0 +/- 13.2 (6)**
Other Growth Factors					
VEGF-C (angiogenesis) [9]	NM_053653	**1.2**	ND	NS	ND
Hepatocyte Growth Factor (anti-apoptosis) [33]	NM_017017	NS	ND	**1.4**	ND
Extracellular Matrix (ECM)					
Fibronectin-1 [25]	NM_019143	**2.4**	ND	**2.7**	ND
Collagen V (α1) (cell spreading) [9]	NM_134452	**2.4**	ND	**2.1**	ND
ECM Matricellular (Adhesion) [30]					
Tenascin [13,25]	BE126741	**2.1**	ND	**1.5**	ND
Calpactin I Heavy Chain (Ten receptor)	NM_019905	**1.9**	ND	NS	ND
Thrombospondin-2	BF408413	**1.7**	ND	**1.8**	ND
Thrombospondin-4	X89963.1	**1.9**	ND	**3.6**	ND
Calreticulin (TSP-receptor)	NM_022399	**1.6**	ND	NS	ND
SPARC	NM_012656	**1.7**	ND	NS	ND
ECM Remodeling					
Protease Nexin-1 (ECM regulation) [36]	X89963.1	**2.1**	**1.1 +/- 0.5 (8)**	**2.1**	**12.3 +/- 6.4 (8)**
Mmp-14 [13]	NM_031056	NS	**1.1 +/- 0.5 (10)**	**2.1**	**4.2 +/- 1.8 (9)**
TIMP-2 (Mmp-14 regulation) [3]	NM_021989	**2.3**	ND	**1.8**	ND

NS: Not Significant; ND: Not Determined; n: number of fractured vs unfractured pairs of tissues in real-time RT-PCR; [1] mean +/- SD.

Figure 1

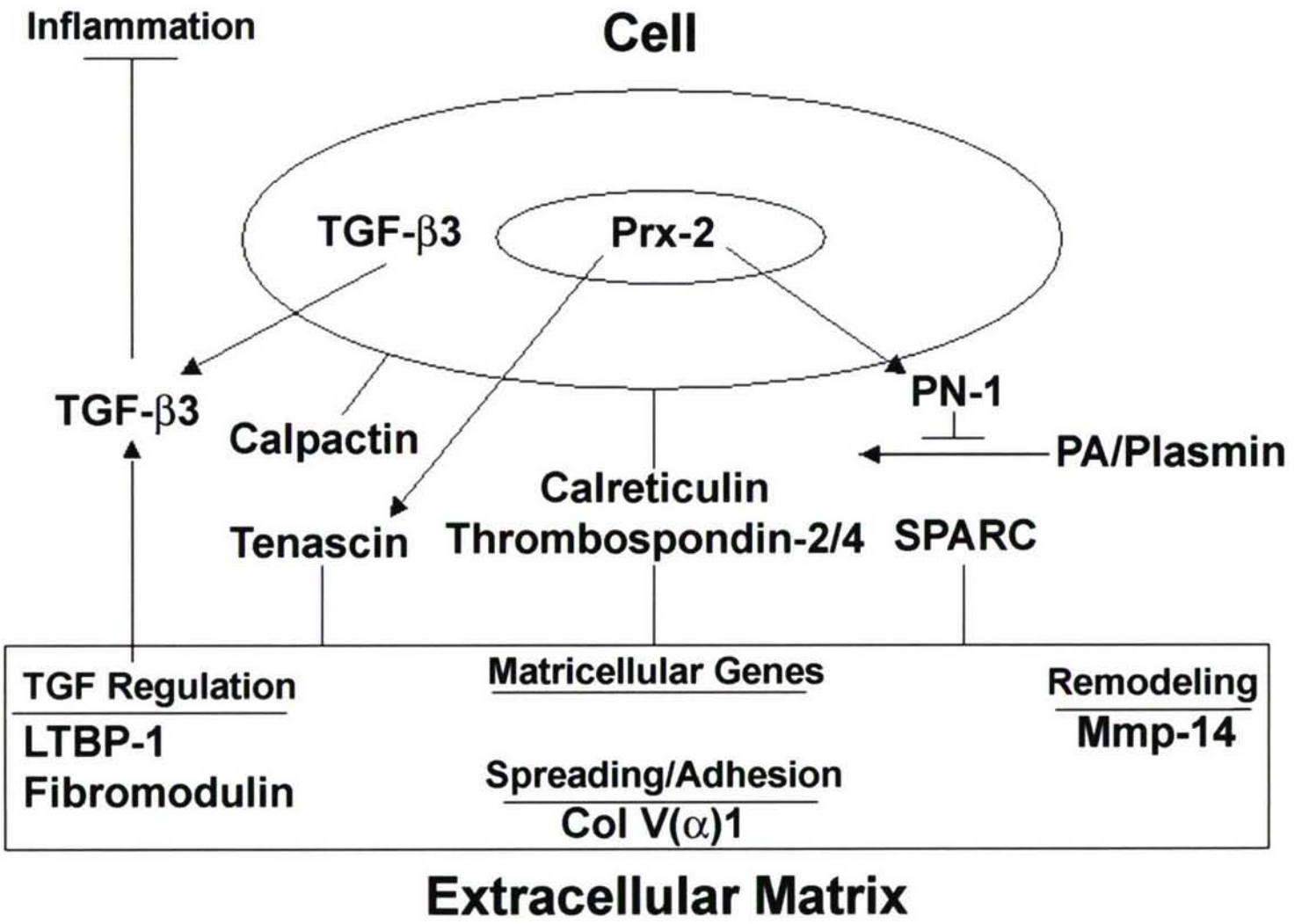
Inflammation
Cell
TGF-β3
Prx-2
TGF-β3
Calpactin
PN-1
PA/Plasmin
Calreticulin
Tenascin
Thrombospondin-2/4
SPARC
TGF Regulation
LTBP-1
Fibromodulin
Matricellular Genes
Spreading/Adhesion
Col V(α)1
Remodeling
Mmp-14
Extracellular Matrix

Loss of Sex-Specific Difference in Bone Size in Leptin Knockout Mice.

X. Wang*, C. H. Rundle, A. Srivastava*, J. Tesfai*, E. I. Davis*, J. E. Wergedal, K. H. W. Lau, S. Mohan, D. J. Baylink. MDC, J.L. Pettis VAMC, Loma Linda, CA, USA.

Presentation Number: SA508

Leptin is an important mediator of body weight and bone metabolism. The obesity of leptin-deficient (*ob/ob*) mice facilitates the study of several fat-related effects of obesity, including hypogonadism. It is well known that the bones of male wild-type mice are larger than female wild-type mice and are the result of androgen actions. Because the effects of androgen and estrogen on bone are mediated in part by different molecular pathways, we asked the question if leptin deficiency exerts differential effects on the bones of male versus female mice.We therefore compared the bones of male and female leptin knockout mice (in C57BL/6 background) with the C57BL/6 wild-type control strain at 10 weeks of age. pQCT measurements in the femoral midshaft using an analysis threshold of 570-214 revealed that the large differences in the periosteal circumference (PC), endosteal circumference (EC) normally observed between male and female wild-type mice were reduced in male leptin knockout mice to values not significantly different from those of female leptin knockout mice (Table 1). The same was true for femur length. Total fat and body weight, as determined by DXA, were not significantly different between male and female leptin knockout mice (Table 1). PC, EC and femur length were not significantly different between female wild-type mice and female leptin mice (Table 1), indicating that the reduction of these parameters in leptin knockout male mice was caused by diminished androgen functions that could be attributed to hypogonadism in leptin knockout male mice. In conclusion, this study suggests that (1) the bone size determination depends on the action of leptin, and (2) the deficiency of leptin action may induce defects in the biological actions of androgen in male mice.

Table 1. C57BL/6-Leptin Knockout Mouse Comparison

Parameter	C57BL/6 Male/Female (%)	Leptin KO Male/Female (%)	C57BL/6 Female/ Leptin KO Female (%)
Femur PC	108.9*	100.0	101.5
Femur EC	110.0*	98.0	94.4
Body Weight	130.0*	101.1	41.3*
Fat	132.9*	95.9	11.4*

* $p<0.006$ by T-test